UNIVERSITÉ DE STRASBOURG

ÉCOLE DOCTORALE des Sciences de la Terre et de l'Environnement

Institut Terre et Environnement de Strasbourg

THÈSE présentée par :

Thifhelimbilu Faith MULABISANA

Soutenue le : **08 décembre 2022**

Pour obtenir le grade de : **Docteur de l'université de Strasbourg**

Discipline/ Spécialité: Géophysique

TITRE de la these

Active Tectonics, Crustal Deformation and Seismotectonic background for a realistic Seismic Hazard Assessment in southern Africa

THÈSE dirigée par :

Mustapha MEGHRAOUI	Professeur, EOST – ITES, Université de Strasbourg
Moctar DOUCOURE	Professeur, University Nelson Mandela
RAPPORTEURS :	
Aurelia HUBERT-FERRARI	Professeur, Université de Liège
Damien DELVAUX	Professeur, Musée Royal d'Afrique Centrale
AUTRES MEMBRES DU JURY :	
Emile OKAL	Professeur, Northwestern University, Illinois
Sophie LAMBOTTE	Docteur, EOST – ITES, Université de Strasbourg
Vunganai MIDZI	Docteur, Council for Geosciences, Pretoria

Résumé

L'objectif de cette thèse est de déterminer l'impact d'un modèle sismotectonique amélioré sur l'évaluation des risques sismiques en Afrique australe. Cet objectif est atteint par la combinaison de plusieurs approches afin d'adopter une stratégie multidisciplinaire permettant d'améliorer notre compréhension de l'occurrence des tremblements de terre dans l'Afrique australe intraplaque. La caractérisation des forts tremblements de terre et des failles dans les régions intraplaques par des études géologiques, géophysiques et de géomorphologie tectonique est bénéfique pour l'amélioration de l'évaluation de l'aléa sismique.

Le premier chapitre décrit la méthodologie de recherche et les étapes suivies pour évaluer la tectonique active, la déformation de l'écorce terrestre et la sismotectonique en Afrique australe afin d'améliorer l'évaluation des risques sismiques. L'Afrique australe appartient au domaine tectonique intraplaque caractérisé par un faible niveau de sismicité et un faible taux de déformation (Stamps et al., 2014 ; Njoroge et al., 2015 ; Saria et al., 2014 ; Johnston, 1996a, 1996b). Cependant, deux tremblements de terre majeurs se sont produits en Afrique australe et ont été choisis comme centre d'intérêt, à savoir les tremblements de terre de Moiyabana en 2017 et de Sainte-Lucie en 1932.

Notre objectif est de mieux comprendre les processus de génération des séismes en Afrique australe intraplaque en utilisant la sismologie en champ proche, la tectonique active, la télédétection (caractéristiques géomorphologiques et InSAR) et l'impact d'une sismotectonique améliorée sur l'évaluation de l'aléa. Wells et Coppersmith (1994) établissent une régression entre la magnitude et la longueur de la rupture en surface, la longueur de la rupture en subsurface, la largeur de la rupture en aval-pendage et la zone de rupture. Aki et Richards (1980) calculent les sources sismiques en fonction de la fonction de la source, de la distance de la station et de la vitesse de l'onde. Hanks et Kanamori (1979) ont corrélé l'ampleur

du moment à partir de la relation entre le moment sismique et la longueur et la zone de la rupture. Johnston (1996a et b) a établi une procédure pour déterminer le moment sismique ainsi que la magnitude du moment pour les données sismiques instrumentales et dérivées de l'intensité dans une région continentale stable.

Les failles actives peuvent être déterminées et caractérisées en cartographiant leurs effets sur les unités quaternaires à l'aide de méthodes telles que la génération de MNE à haute résolution, la géomorphologie tectonique, la paléosismologie, la contribution de l'InSAR à la cartographie des ruptures de surface. Wells et Coppersmith (1994) établissent une régression entre la magnitude et la longueur de la rupture en surface, la longueur de la rupture en subsurface, la largeur de la rupture en aval-pendage et la zone de rupture. Aki et Richards (1980) calculent les sources sismiques en fonction de la fonction de la source, de la distance de la station et de la vitesse de l'onde. Hanks et Kanamori (1979) ont corrélé l'ampleur du moment à partir de la relation entre le moment sismique et la longueur et la zone de la rupture. Johnston (1996a et b) a établi une procédure pour déterminer le moment sismique ainsi que la magnitude du moment pour les données sismiques instrumentales et celles dérivées de l'intensité dans une région continentale stable. La détermination du mécanisme focal pour indiquer les contraintes horizontales et verticales maximales de compression (Zoback et Zoback, 1989 ; Delvaux, 1993 ; Manzunzu et al., 2017) et l'utilisation des informations obtenues sur la cinématique de la faille par l'inversion des contraintes.

La modélisation d'une rupture cosismique est possible à l'aide d'une modélisation prospective et d'une méthode inverse basée sur les paramètres de la rupture de faille pour la composante de glissement de pendage et de glissement de direction de la déformation fragile de l'écorce terrestre. À cette fin, et entre autres méthodes, l'utilisation du code Poly3D considère les surfaces triangulées comme des discontinuités dans un demi-espace linéaire, élastique, homogène et isotrope (Okada, 1985 ; Maerten et al., 2005). D'autres études menées le long de ces failles à l'aide de méthodes géophysiques régionales et terrestres telles que le magnétisme aéroporté, la tomographie de résistivité électrique (ERT) et les profils sismiques de réflexion attestent d'une déformation active. L'application du filtrage de la première dérivée verticale (FVD) sur les données d'intensité du champ magnétique total permet de mettre en évidence les corps les plus étroits, puis de compléter les résultats par des données géophysiques au sol telles que la sismique réflexion et la résistivité pour confirmer la profondeur du déplacement de l'escarpement de la faille.

L'approche de l'évaluation déterministe de l'aléa sismique (DSHA) développe un ou plusieurs séismes de contrôle qui sont prévus comme étant ceux qui produiront le mouvement du sol le plus important sur le site. L'analyse probabiliste des risques sismiques (PSHA) est basée sur la méthodologie classique largement utilisée développée par Cornell (1968), McGuire (1974, 1976) et Der Kiureghian et Ang (1977). Cette technique utilise la plus grande quantité possible de données, combinant des données sismologiques, géologiques et géophysiques pour construire un modèle des processus de production des tremblements de terre. Les études PSHA modernes, qui suivent les idées proposées par Coppersmith et Youngs (1986), Reiter (1991) sont généralement en mesure de traiter ce problème en incorporant dans le modèle ce que l'on appelle un "arbre logique", dans lequel certains paramètres reçoivent une gamme de valeurs possibles avec une attribution subjective de la probabilité de chacune d'entre elles.

Le deuxième chapitre se concentre sur le séisme de Moiyabana (Botswana) de MW 6,5 du 3 avril 2017, qui s'est produit à l'intérieur du continent de la plaque africaine et dans une région sismogénique précédemment considérée comme stable. Notre objectif est de combiner plusieurs approches (enquêtes de terrain et de télédétection) afin d'adopter une stratégie multidisciplinaire pour améliorer notre compréhension de l'occurrence des tremblements de terre dans l'Afrique australe intraplaque.

Le choc principal (25,134 E, 22,565 S ; profondeur 22 ± 3 km) a été suivi par plus de 500 événements de magnitude M ≥ 0,8 enregistrés en avril 2017, y compris la plus grande réplique (MW 4,6 le 5 avril 2017). La structure crustale sous les cratons obtenue à partir des fonctions réceptrices et des stations sismiques à large bande caractérise la profondeur moyenne du Moho à 38 km, ce qui est considéré comme la croûte la plus mince de la région (Nguuri et al., 2001) et peut expliquer l'épaisseur de ~30 km de la couche sismogénique (Midzi et al., 2018). La collision des cratons archéens du Kaapvaal et du Zimbabwe entre 2,7 et 2,6 Ga a conduit à la formation de la ceinture mobile du Limpopo, qui constitue le site du séisme de Moiyabana de 2017 (Roering et al., 1992 ; Brown et al., 2008 ; Begg et al., 2009).

Nous analysons la séquence de la secousse principale et de la réplique sur la base d'un réseau sismique local et des caractéristiques sismotectoniques locales. La plus grande réplique de magnitude MW 4,6 s'est produite à l'ouest de la secousse principale le 5 avril 2017 à une profondeur beaucoup plus faible (~10 km) que la secousse principale. Après la secousse principale, une séquence de répliques a été enregistrée du 8 avril au 29 juin 2017 par un réseau temporaire et montre plus de 900 enregistrements de tremblements de terre. L'enregistrement de la séquence sismique comprend des événements sismiques d'une magnitude aussi faible que ML 0,8 avec une diminution du taux d'occurrence quotidien de 101 à 20 événements sismiques au cours du premier mois d'enregistrement (Midzi et al., 2018). Après le choc principal, la décroissance de la sismicité obtenue à partir du nombre quotidien de répliques est conforme à la loi d'Omori (Utsu et al., 1995). La localisation initiale de la séquence sismique obtenue à l'aide du programme HYPOCENTER modifié (Lienert et al., 1986 ; Lienert et Havskov, 1995) dans le progiciel SEISAN (Ottemöller et al., 2018), montre deux groupes avec une distribution de répliques denses occidentales orientées NNW-SSE et une séquence de répliques orientales orientées N-S mais clairsemées. Afin de fournir une description complète de la distribution des répliques et d'améliorer leur localisation et leur profondeur, les tremblements de terre ont été relocalisés en utilisant une approche de double différence telle que mise en œuvre dans le programme HypoDD (Waldhauser et Ellsworth, 2000).

Les solutions de mécanismes focaux pour 46 répliques sélectionnées ont été calculées sur la base des polarités de premier mouvement de l'onde P (Ross et al., 2018), en utilisant le module FOCMEC dans le progiciel SEISAN (Ottemöller et al., 2018). Les mécanismes focaux des répliques montrent des failles normales et quelques mécanismes obliques (figure 8 et tableau dans SM4). Le choc principal et la plus grande réplique montrent un mécanisme de faille normal, avec des plans nodaux plongeant grossièrement vers le NE et le SE à 41° et 42°, respectivement. Les mécanismes focaux du choc principal et des 45 répliques permettent d'obtenir des informations sur la cinématique des failles grâce à l'inversion des contraintes. Sur les 46 mécanismes focaux (92 plans nodaux) de la base de données, 30 (60 plans nodaux), ainsi que 14 (28 plans nodaux) sont compatibles avec une extension NE-SW en régime de faille normale. L'analyse ultérieure avec 14 mécanismes focaux est effectuée pour tester les résultats après avoir optimisé l'ensemble des données pour une meilleure compatibilité. La plupart des répliques sont caractérisées par un impact moyen NW (340°) avec des plans de faille plongeant vers le NE, ce qui est cohérent avec la distribution des contraintes et l'extension NE-SW. Le mécanisme de faille normale prédominant indique un régime néotectonique en extension dans la zone épicentrale.

La géométrie de la rupture du séisme est contrainte par plus de 900 répliques enregistrées sur une période de trois mois et par l'analyse InSAR des images de Sentinel-1 (orbite ascendante). L'étude InSAR montre des franges avec deux lobes avec un glissement cosismique de 3,86 cm à 5,15 cm sur une déformation de surface allongée NW-SE et longue de 40 km, cohérente avec la localisation du choc principal et le mécanisme de faille normale. La modélisation de la déformation de surface fournit la dimension de la rupture du séisme en profondeur avec un glissement maximal de ~ 50 cm sur un plan de faille orienté à 315°, avec un pendage de 45°, une inclinaison de -80° et avec un Mo de 3,68 x 1018 Nm. Bien que le taux de déformation sismique soit faible, l'occurrence du séisme de Moiyabana en 2017, suivi d'une séquence de répliques dans la ceinture mobile centrale du Limpopo, classe la région intraplaque comme un intérieur de plaque actif.

Le troisième chapitre présente les failles de Tugela et de Greytown dans le Kwazulu-Natal en Afrique du Sud-Est, ainsi que la réévaluation du tremblement de terre de St Lucia MW 6,9 de 1932. Nous effectuons des recherches détaillées sur la sismotectonique et la géomorphologie tectonique de la zone du tremblement de terre de 1932 à St Lucia, dans le but de caractériser les paramètres physiques de la faille sismogénique nécessaires à l'évaluation des risques sismiques dans la région du KwaZulu-Natal (KZN). Le matin du 31 décembre 1932 à 06:31, un tremblement de terre de magnitude MW 6.9 a secoué les habitants du KwaZulu-Natal, en Afrique du Sud. Nous avons relocalisé le tremblement de terre en utilisant les temps d'arrivée répertoriés dans le bulletin du CSI, en suivant la technique de Wysession et al. (1991), qui comprend une estimation d'une ellipse de confiance basée sur un processus de Monte Carlo consistant à injecter un bruit gaussien dans l'ensemble des données. La solution utilise 45 temps d'arrivée P et S et converge vers 29,30°S, 33,04°E, à environ 100 km au SSE des localisations historiques, celle de l'ISC (28,50°S, 32,80°E) étant beaucoup plus proche de la côte, et celle de Gutenberg et Richter (1954) (28,50°S, 32,75°E) représentant peut-être une simple transcription de l'épicentre de l'ISC au quart de degré le plus proche.

Tout d'abord, nous définissons les caractéristiques sismiques et tectoniques des escarpements de faille de Tugela et de Greytown, respectivement orientés E-W et ENE-WSW. L'escarpement de la faille de Tugela est un escarpement orienté EW, qui s'étend sur ~230 km dans le KZN, en Afrique du Sud, et à environ 50 km au sud se trouve l'escarpement de la faille de Greytown, qui mesure ~80 km de long et qui est orienté SW-NE. Nous procédons à la description des marqueurs géomorphologiques des escarpements de faille à l'aide de la géomorphologie tectonique. Des études géomorphologiques tectoniques ont été menées le long de l'escarpement de la faille de Tugela en utilisant le SRTM 1" (Farr et al., 2007) pour identifier les marqueurs géomorphologiques qui ont été affectés par la déformation active le long de la faille. Les preuves de l'activité tectonique le long des failles de Tugela et de Greytown sont clairement visibles avec un mouvement latéral droit illustré par le déplacement des chenaux fluviaux sur plusieurs sites.

D'autres études sur les géométries physiques des failles ont été réalisées à l'aide d'un système de magnétisme aéroporté, de la tomographie de résistivité électrique et de profils de réflexion sismique. D'après l'évaluation qualitative des données existantes, les linéaments sont mal résolus sur les données aéromagnétiques régionales. Des données géophysiques au sol, telles que la sismique réflexion et la résistivité, ont donc été ajoutées pour compléter et confirmer la profondeur du déplacement de l'escarpement de la faille de Tugela. La coupe empilée du point médian commun obtenue le long de la ligne de levé montre six réflecteurs, visibles entre des profondeurs de ~4 m et ~28 m. Les décalages de déformation sont cartographiés à des positions, plongeant verticalement et observés à des distances de ~40 m, ~70 m, ~100 m et ~110 m à des profondeurs de ~8 m à ~28 m.

En outre, nous explorons également l'utilisation du taux de déformation calculé à partir des données GPS obtenues à partir de 14 stations GPS situées dans et autour de la province du KwaZulu-Natal. Nous considérons les stations les plus proches de l'escarpement de la faille de Tugela afin de minimiser l'impact des autres mouvements de faille dans la région. Ainsi, les données des deux stations suivantes au nord et des trois stations au sud de l'escarpement de la faille de Tugela ont été comparées. Cette comparaison indique un mouvement latéral droit le long de l'escarpement de la faille de Tugela, comme le montre la différence de déformation positive du bloc sud par rapport au bloc nord de l'escarpement de la faille de Tugela. La différence de vitesse de déformation entre le nord et le sud de l'escarpement de la faille de Tugela est faible mais perceptible (< 0,1 mm/an), ce qui est habituel en ce qui concerne la vitesse de déformation dans les domaines intraplaques continentaux. Les études de terrain le long des failles, combinées aux études géophysiques et sismotectoniques, conduiront probablement à une réévaluation de l'évaluation des risques sismiques dans la région de KZN.

L'autre partie cruciale de l'évaluation précise de l'aléa sismique est l'évaluation de la contribution de la couche sismogénique dans l'analyse des failles actives. Ainsi, nous profitons ici des résultats des deuxième et troisième chapitres pour déterminer l'épaisseur de la couche sismogénique en Afrique australe afin de compléter notre étude de la couche sismogénique par l'évaluation du D90. L'épaisseur de la couche sismogénique en Afrique australe est dérivée des hypocentres des séismes continentaux intraplaques, combinés à l'analyse des données gravimétriques et magnétiques, et corrélée à l'épaisseur de la croûte. Nous présentons quelques-unes des principales structures tectoniques qui ont pu affecter la composition de la croûte terrestre en Afrique australe. Dans cette étude, nous examinons la couche sismogénique en évaluant la profondeur à laquelle se produisent 90 % des tremblements de terre (D90), en tenant compte des valeurs de profondeur disponibles dans le catalogue de sismicité de l'Afrique australe. La zone sismogénique la plus profonde est située dans la ceinture du Limpopo occidental. Cependant, il est important de souligner que les événements utilisés pour calculer le D90 dans cette région étaient des répliques du tremblement de terre de Moiyabana de 2017. Nous ne pouvons donc pas conclure avec certitude qu'il s'agit bien du D90 de la région si l'on inclut d'autres événements qui ne sont pas des répliques du séisme de Moiyabana de 2017. Par conséquent, nous considérons toutes les sept autres régions comme indiqué dans la figure 5 et le tableau 1. Les régions centrales et méridionales du craton de Kaapvaal ont une couche sismogénique plus épaisse que les cinq autres régions, les deux régions de la ceinture de plissement du Cap étant constituées d'une zone sismogénique mince. La ceinture de plissement du Cap du Cambrien-Ordovicien est la région géologique la plus jeune de cette étude et comprend principalement une épaisseur crustale de 25 à 35 km et une épaisseur sismogénique de 6,5 à 7,4 km.

L'épaisseur de la croûte varie entre 30 et 52 km, de sorte que seuls les 30 % supérieurs de la croûte de l'Afrique australe génèrent 90 % des tremblements de terre. Le craton archéen de Kaapvaal, la région la plus ancienne de la zone d'étude, possède une croûte relativement plus fine, allant de 34 à 42 km au sud, avec de petites poches allant jusqu'à 49 km au nord. La couche sismogénique dans cette région est cependant plus épaisse que dans les régions géologiques plus jeunes. Les ceintures de Namaqua-Natal et de Cape Fold, régions géologiques plus jeunes, ont une épaisseur crustale plus hétérogène, allant de 25 à 50 km, avec une couche sismogénique plus fine de ≤ 12 km. Les valeurs d'épaisseur de la couche sismogénique obtenues dans cette étude indiquent que la croûte supérieure est l'endroit où se produit la libération des contraintes élastiques en Afrique du Sud (de l'Ouest), étant donné que les valeurs d'épaisseur élastique sont supérieures ou égales à l'épaisseur de la croûte (Doucoure et De Wit, 2002). La nature unimodale des valeurs d'épaisseur de la couche sismogénique peu profonde obtenues dans cette étude soutient l'occurrence de ruptures de failles peu profondes et peut donc influencer de manière significative l'aléa sismique de l'Afrique australe.

Le cinquième et dernier chapitre de cette thèse combine des études multidisciplinaires des zones où de grands tremblements de terre se sont produits en Afrique australe, comme discuté dans les chapitres précédents, ainsi que la profondeur sismogénique déterminée dans le quatrième chapitre pour évaluer un risque sismique réaliste à l'échelle régionale. Ceci permet d'atteindre l'objectif de cette thèse qui est de déterminer l'impact d'un modèle sismotectonique amélioré sur l'évaluation de l'aléa sismique en Afrique australe. Nous incluons également des données sur les failles actives et les paramètres sismiques de zones précédemment étudiées telles que la zone active de Ceres dans la province du Cap Occidental (1969, MW 6.3), la région de Kango et Baviaanskloof dans le Cap Oriental, la faille d'Hebron / Dreylingen en Namibie et les failles de Tshipise et Bosbokpoort dans la province de Limpopo. L'intégration et l'interprétation des données compilées ont permis de générer un modèle sismique avec 26 zones sources et sept sources de failles (failles de Kango et Hebron / Dreylingen, Tshipise et Bosbokpoort, Tugela, Greytown et Khurutse). En utilisant les informations disponibles provenant d'études géologiques, paléosismiques, géodésiques et sismologiques, divers paramètres, y compris les paramètres de récurrence (taux de glissement et taux de récurrence de Youngs et Coppersmith (1985)) et les valeurs de Mmax (Wells et Coppersmith, 1994) ont été déterminés pour les quatre failles supposées avoir des preuves fiables de leur capacité.

Comme il n'y a pas de GMPEs qui ont été dérivées spécifiquement pour l'Afrique du Sud, il est nécessaire de développer un modèle / s basé sur l'une des catégories, à savoir :

1. Utilisation d'un ensemble de modèles de mouvement du sol disponibles et attribution d'un poids de probabilité à chaque modèle,

2. Développer une nouvelle relation d'atténuation à partir de données et de modèles de sources sismologiques,

3. Développement d'un modèle composite de mouvement du sol.

Cependant, les accéléromètres n'ont été installés en Afrique du Sud dans les régions aurifères du pays qu'à partir de 2010. Ainsi, le jeu de données existant sur les mouvements du sol ne permet pas aux utilisateurs de dériver un GMPE local en raison du manque de tremblements de terre à fort mouvement. À cet égard, les modèles provenant d'autres régions sont soigneusement sélectionnés et testés pour déterminer s'ils s'adaptent correctement aux données locales.

Des calculs probabilistes classiques de l'aléa sismique ont été effectués à l'aide du logiciel OPENQUAKE développé par la Global Earthquake Model Foundation. Les calculs de l'aléa ont été effectués pour les conditions suivantes, en utilisant un modèle de source sismique caractérisé comme décrit dans les sections ci-dessus :

- Tous les calculs ont été effectués pour une probabilité de dépassement de 10 % en 50 ans (ou une période de retour de 475 ans).
- La magnitude minimale adoptée est Mmin = 5,0, ce qui est cohérent avec la pratique consistant à exclure les événements fréquents et de faible ampleur ayant peu d'importance du point de vue technique.

Les calculs ont été effectués pour trois périodes de réponse cibles, PGA, 0,15s et 2,0s. Toutes les périodes spectrales montrent des valeurs de danger élevées dans les régions des mines d'or, de Koffiefontein et du Cap. La première est principalement influencée par les niveaux de sismicité et les deux dernières régions sont très probablement dues aux forts tremblements de terre enregistrés dans la région et au niveau élevé et continu de la sismicité. Il y a également une influence évidente de la source de la zone MB, qui a enregistré de grands tremblements de terre sur l'aléa pour la partie nord-est du pays, ainsi que des sources de la zone SNAM, principalement en raison de l'essaim d'Augrabies. La forte accélération observée dans la région de KOSH à des périodes plus faibles pourrait être le résultat de séismes modérés peu profonds dans cette zone ainsi que de taux d'activité élevés associés aux séismes liés à l'exploitation minière. L'influence des grands événements dans la partie sud-ouest du pays, dans la province du Cap occidental, est également évidente, principalement en raison des événements modérés à forts et des enregistrements de tremblements de terre plus longs.

La contribution de la sismotectonique du tremblement de terre de Moiyabana et du Kwazulu-Natal, ainsi que la profondeur sismogénique de l'Afrique australe, ont permis

d'obtenir un aléa sismique plus réaliste pour l'Afrique australe. Les changements apportés dans ce nouveau modèle SSC par rapport à la carte précédente (Midzi et al., 2020) sont très importants. Cela prouve l'importance de la sismotectonique dans la région intraplaque de l'Afrique australe. En outre, les GMPE sont également essentiels dans ce travail. Malheureusement, le manque de données sur les mouvements forts dans le pays rend impossible la dérivation d'un modèle spécifique pour l'Afrique du Sud.

Mots-clés : Sismotectonique, tremblement de terre, faille, déformation, choc principal, réplique, failles actives, géomorphologie tectonique, déformation active, profils géophysiques, évaluation des risques sismiques.

Références

Aki K. and P. G. Richards, 1980. Quantitative Seismology, Theory and Methods. San Francisco: Freeman.

Begg G. C., W. L. Griffin, L. M. Natapov, S. Y. O’Reilly, S. P. Grand, C. J. O’Neill, J. M. A. Hronsky, Y. Poudjom Djomani, C.J. Swain, T. Deen & P. Bowden, 2009. The Lithospheric Architecture of Africa: Seismic Tomography, Mantle Petrology, and Tectonic Evolution, Geosphere, 5, 23 – 50.

Brown, R., Gernon, T., Stiefenhofer, J., & Field, M., 2008. Geological constraints on the eruption of the Jwaneng Centre kimberlite pipe, Botswana. J. Volcanol. Geotherm. Res.174 (1), 195–208.

Coppersmith K.J. and R.R. Youngs (1986). Capturing uncertainty in probabilistic seismic hazard assessments within intraplate tectonic environments, Proceedings of the Third U.S. National Conference on Earthquake Engineering, Charleston, 1, 301 – 312.

Cornell C.A. (1968). Engineering seismic risk analysis, Bulletin of the Seismological Society of America, 58, 1583 – 1606.

Delvaux D., 1993. The TENSOR program for paleostress reconstruction: examples from the east African and the Baikal rift zones. EUG VII Strasbourg, France, 4–8 April 1993. Abstract supplement N°1 to Terra Nov. 5: 216.

Der Kiureghian A. and A.H-S. Ang (1977). A fault-rupture model for seismic risk analysis, Bulletin of the Seismological Society of America, 67(4), 1173 – 1194.

Doucouré C. M., M. J. de Wit (2002). Temporal variation in rigidity and mechanical behaviour of old thick continental lithosphere, South African Journal of Geology, 105, 39 – 50.

Farr, T.G., P.A. Rosen, E. Caro, R. Crippen, R. Duren, S. Hensley, M. Kobrick, M. Paller, E. Rodriguez, L. Roth, D. Seal, S. Shaffer, J. Shimada, J. Umland, M. Werner, M. Oskin, D. Burbank, and D. Alsdorf, 2007. The Shuttle Radar Topography Mission, Revision of Geophysics,45, RG2004, doi:10.1029/2005RG000183.

Gutenberg, B., and Richter, C.F., 1954. Seismicity of the Earth and associated phenomena, Princeton University Press, 310 p.

Hanks T.C. and H. Kanamori, 1979. A moment magnitude scale. Journal of Geophysical Research: Solid Earth, 84, 2348 – 2350.

Johnston, A.C., 1996a. Seismic moment assessment of earthquakes in stable continental regions—I. Instrumental seismicity, Geophysics Journal International, 124 (2), 381–414.

Johnston, A.C., 1996b. Seismic moment assessment of earthquakes in stable continental regions—II. Historical seismicity, Geophysics Journal International, 125 (3), 639 – 678.

Lienert B. R., E. Berg & L. N. Frazer, 1986. Hypocenter: an earthquake location method using centered, scaled, and adaptively damped least squares, Bulletin of the Seismological Society of America, 76(3), 771 – 783.

Lienert B. R. and J. Havskov, 1995. A Computer Program for Locating Earthquakes Both Locally and Globally, Seismological Research Letters, 66 (5), 26 – 36.

Maerten, F., Resor, P., Pollard, D., Maerten, L., 2005. Inverting for slip on three-dimensional fault surfaces using angular dislocations, Bulletin of Seismological Society of America, 95 (5), 1654 – 1665.

Manzunzu B., V. Midzi, A. Mangongolo and F. Essrich, 2017. The aftershock sequence of the 5 August 2014 Orkney earthquake (ML 5.5), South Africa, Journal of Seismology, 21, 1323 – 1334.

McGuire R.K. (1974). Seismic structural response risk analysis, incorporating peak response regressions on earthquake magnitude and distance, Massachussets Technical, Department of Civil Engineering, Publication No. 399, p371.

McGuire R.K. (1976). FORTRAN computer program for seismic risk analysis, U.S Geological Survey Open-File Report 76-67, p90.

Midzi V., B. Manzunzu, T. Mulabisana, B.S. Zulu, T. Pule and S. Myendeki (2020). Probabilistic seismic hazard maps for South Africa, Journal of African Earth Sciences, 162.

Midzi V., I. Saunders, B. Manzunzu, M. T. Kwadiba, V. Jele, R. Mantsha , K. T. Marimira, T. F. Mulabisana, O. Ntibinyane, T. Pule, G. W. Rathod, M. Sitali, L. Tabane, G. van Aswegen, & B. S. Zulu, 2018. The 03 April 2017 Botswana M6.5 earthquake: Preliminary results, Journal of African Earth Sciences, 143, 187 – 194.

Nguuri, T. K., Goree, J., James, D. E., Webb, S. J., Wright, C., Zengen, T. G., Gwavava, 0., Snoke, J. A. & Kaapvaal Seismic Group, 2001. Crustal structure beneath southern Africa and its implications for the formation and evolution of the Kaapvaal and Zimbabwe cratons, Geophys. Res. Letters 28, 13, 2501-2504.

Njoroge M., R. Malservisi, D. Voytenko and M. Hackl, 2015. Is Nubia Plate Rigid? A geodetic study of the relative motion of different cratonic areas within Africa, International Association of Geodesy Symposia, p 1-9, doi:10.1007/1345_2015_212.

Okada, Y., 1985. Surface deformation due to shear and tensile faults in a half-space, Bulletin of Seismological Society of America, 75 (4), 1135 – 1154.

Ottemöller, L., Voss, P., Havskov, J., 2018. SEISAN Earthquake Analysis Software for Windows, Solaris, Linux and Macosx. Bergen.

Reiter L., 1991. Earthquake hazard analysis: issues and insights. Columbia University Press.

Roering C., D. D. van Reenen, C. A. Smit, J. M. Barton, J. H. de Beer, M. J. de Wit, E. H. Stettler, J. F. van Schalkwyk, G. Stevens & S. Pretorius, 1992. Tectonic model for the evolution of the Limpopo Belt, Precambrian Research, 55, 539 – 552.

Ross Z. E., M. Meier, & E. Hauksson, 2018. P wave arrival picking and first-motion polarity determination with deep learning, Journal of Geophysical Research: Solid Earth, 123 (6), 5120 – 5129.

Saria E., E. Calais, D.S. Stamps, S. Delvaux and C.J.H. Hartnady, 2014. Present-day kinematics of the East African Rift, Journal of Geophysical Research, 119, doi:10.1002/2013JB010901.

Stamps D.S., L.M. Flesch, E. Calais and A. Ghosh, 2014. Current kinematics and dynamics of Africa and the East African Rift System, Journal of Geophysical Research: Solid Earth, 119, 5161 – 5186, doi:10.1002/2013JB010717.

Utsu T., Ogata, Y., Matsu'ura ; R.S., 1995. The centenary of the Omori formula for a decay law of aftershock activity, J. Phys. Earth, 43, 1-33.

Waldhauser F. & W. L. Ellsworth, 2000. A Double-Difference Earthquake Location Algorithm: Method and Application to the Northern Hayward Fault, California, Bulletin of the Seismological Society of America, 90 (6), 1353 – 1368.

Wells D.L. and K.J. Coppersmith, 1994. New Empirical Relationships Among Magnitude, Rupture Length, Rupture Width, Rupture Area, and Surface Displacement, Bulletin of the Seismological Society of America, 84, 974-1002.

Wysession, M.E., E.A. Okal and K.L. Miller, 1991. Intraplate seismicity of the Pacific Basin, 1913−1988, Pure Applied Geophysics, 135, 261-359.

Youngs R.R. and K.J. Coppersmith, 1985. Implications of fault slip rates and earthquake recurrence models to probabilistic seismic hazard estimates. Bulletin of the Seismological society of America, 75(4), 939 – 964.

Zoback, M.L. and M.D. Zoback, 1989. Tectonic stress field of the continental United States: In Geological Society of America Memoir 172, Chapter 24, 523 – 539.

Résumé

L'objectif de cette thèse est de déterminer l'impact d'un modèle sismotectonique amélioré sur l'évaluation des risques sismiques en Afrique australe. Cet objectif est atteint par la combinaison de plusieurs approches afin d'adopter une stratégie multidisciplinaire pour améliorer notre compréhension de l'occurrence des séismes en Afrique australe intraplaque. La caractérisation des forts séismes et des failles dans les régions intraplaques par des études géologiques, géophysiques et de géomorphologie tectonique, est bénéfique pour l'amélioration de l'évaluation de l'aléa sismique. Le premier chapitre de cette thèse décrit les méthodes adoptées pour étudier la tectonique active, la déformation crustale et la sismotectonique en Afrique australe.

Le premier chapitre décrit la méthodologie de recherche. Le deuxième chapitre présente l’étude du séisme du 3 avril 2017 Mw 6,5, Moiyabana (Botswana) qui s'est produit dans le domaine continental intérieur de la plaque nubienne et dans une région sismogène précédemment considérée comme stable. Nous analysons la séquence de la secousse principale et des répliques sur la base d'un réseau sismique local et des investigations sismotectoniques locales de manière à contraindre la géométrie de la rupture et à la corréler à celle issue de l'analyse InSAR des images Sentinel-1 (orbite ascendante). Les solutions des mécanismes focaux de la secousse principale et des répliques montrent l’existence de deux séquences sismiques avec une prédominance de failles normales orientées NW-SE et à pendage NE et SW. L'inversion des contraintes des mécanismes focaux a produit des résultats qui sont compatibles avec une extension NE-SW sous un régime de faille normale. Bien que le taux de déformation sismique soit de faible niveau, l'occurrence du tremblement de terre Moiyabana de 2017 dans la ceinture mobile centrale du Limpopo classe la région intraplaque comme un intérieur de plaque actif.

Le troisième chapitre se concentre sur la caractérisation des failles de Tugela et Greytown dans le Kwazulu-Natal, en Afrique du Sud, ainsi que sur la ré-évaluation du séisme de 1932 de St Lucia M_W 6.9 (selon ISC). Nous avons effectué des recherches détaillées sur la sismotectonique, couplées à des investigations en géomorphologie tectonique de la zone du séisme de 1932 à St Lucia dans le but de caractériser les paramètres physiques des failles actives nécessaires à l'évaluation des risques sismiques dans la région du KwaZulu-Natal (KZN). Tout d'abord, nous avons identifié les caractéristiques tectoniques des failles Tugela et Greytown, respectivement orientées E-W et ENE-WSW, puis nous procédons à la description des marqueurs géomorphologiques des failles à l'aide de la tectonique quaternaire et la déformation du réseau hydrographique. Nous étudions ensuite la géométrie physique des failles à l'aide de levés magnétiques aériens associés à la tomographie de résistivité électrique et aux profils de réflexion sismique. En outre, nous explorons également l'utilisation de la vitesse de déformation calculée à partir des données GPS. L'intégration de ces études montre des évidences de failles actives avec des décalages latéraux dextres le long des failles de Tugela et Greytown. Les investigations de terrain le long des failles, combinées aux études géophysiques et sismotectoniques, conduisent vers une ré-évaluation de l'aléa sismique de la région du KZN.

L'autre partie de ce travail de thèse est la caractérisation des failles actives et sismogènes par la détermination plus précise de la couche sismogène dans l'analyse de l'aléa sismique. Ainsi, dans le quatrième chapitre, nous examinons l'épaisseur de la couche sismogène pour compléter l'étude de la déformation crustale des régions sud de l'Afrique. Nous étudions l'épaisseur de la couche sismogène en Afrique australe à partir des hypocentres des séismes continentaux intraplaques et nous la corrélons à l'épaisseur de la croûte terrestre. Nous présentons certaines des structures tectoniques majeures qui ont pu affecter la croûte supérieure de la lithosphère. En parallèle, nous étudions la couche sismogène à travers l'évaluation de profondeur à laquelle 90% des séismes se produisent (D90), en considérant les valeurs de profondeur disponibles dans le catalogue sismique du sud de l'Afrique.

Le cinquième et dernier chapitre de cette thèse traite les investigations multidisciplinaires des zones où de grands séismes se sont produits en Afrique australe, tels que présentés dans le premier et le deuxième chapitre, ainsi que de la profondeur sismogène telle que déterminée dans le troisième chapitre pour une évaluation de l'aléa sismique à l'échelle régionale. Nous incluons également dans cette analyse des zones précédemment étudiées telles que la région de Ceres dans la province du Cap occidental, la région de Kango et Baviaanskloof dans le Cap oriental, la faille Hebron / Dreylingen en Namibie et les failles Tshipise et Bosbokpoort dans la province du Limpopo.

Mots-clés : Sismotectonique, séisme, faille, déformation, choc principal, réplique, failles actives, géomorphologie tectonique, déformation active, profils géophysiques, évaluation des risques sismiques.

Summary

The aim of this thesis is to determine the impact of improved seismotectonic model on seismic hazard assessment in southern Africa. This is achieved through a combination of several approaches in order to adopt a multidisciplinary strategy so as to enhance our understanding of earthquake occurrence in intraplate southern Africa. The characterisation of strong earthquakes and faults within intraplate regions through geological, geophysical and tectonic geomorphology studies, is beneficial to the improvement of seismic hazard assessment.

The first chapter describes the research methodology. The second chapter focuses on the 3 April 2017 M_W 6.5, Moiyabana (Botswana) earthquake which occurred in the continental interior of the Nubian plate and in a seismogenic region previously considered as stable. We analyse the mainshock and aftershocks sequence based on a local seismic network and local seismotectonic characteristics so as to constrain the rupture geometry and correlate it to that from the InSAR analysis of Sentinel-1 images (ascending orbit). Focal mechanism solutions of the mainshock and aftershocks display predominance of NW-SE trending and NE dipping normal faulting. Stress inversion of the focal mechanisms produced results that are compatible with a NE-SW extension under normal faulting regime. Although the seismic strain rate is of low level, the occurrence of the 2017 Moiyabana earthquake in the central Limpopo Mobile Belt classifies the intraplate region as an active plate interior.

The third chapter presents the Tugela and Greytown fault in Kwazulu-Natal in Southeast Africa, as well as the reappraisal of the 1932 St Lucia M_W 6.9 earthquake. We perform detailed investigations in seismotectonics and tectonic geomorphology of the 1932 St Lucia earthquake area with the objective of characterising physical parameters of the seismogenic fault necessary for the seismic hazard assessment in the KwaZulu-Natal (KZN) region. First, we delineate the seismic and tectonic characteristics of the E-W and ENE-WSW trending Tugela and Greytown fault scarps, respectively, we proceed with the description of geomorphic markers of fault scarps using tectonic geomorphology, further investigate physical fault geometries using airborne magnetics added with electrical resistivity tomography and seismic reflection profiles. In addition, we also explore using strain rate calculated from GPS data. The integration of these studies shows evidence of active faulting with right lateral offsets along the Tugela and Greytown fault scarps. Field investigations along fault scarps combined with geophysical and seismotectonic studies will likely lead to the re-evaluation of the seismic hazard assessment in the KZN region.

The other crucial part of the accurate assessment of the seismic hazard is evaluating the contribution of the seismogenic layer in the active faulting analysis. Thus, we benefit here from the results of the second and third chapters to determine the thickness of the southern Africa to complete our study of the seismogenic layer. The seismogenic layer thickness within southern Africa is derived from the intraplate continental earthquake hypocentres combined with the gravity and magnetic data analysis and correlate it to the crustal thickness. We present some of the major tectonic structures that may have affected the crustal composition within southern Africa. We investigate the seismogenic layer in this study through the evaluation of depth at which 90% of earthquakes occur (D90), considering the available depth values from the southern African seismicity catalogue.

The fifth and last chapter of this thesis combines multidisciplinary investigations of areas where large earthquakes have occurred in southern Africa, as discussed in the previous chapters, as well as the seismogenic depth determined in the third chapter to assess a realistic seismic hazard at a regional scale. We also include active faulting data and seismic parameters of previously studied areas such as the Ceres active zone in the Western Cape Province (1969, M_W 6.3), the Kango and Baviaanskloof region in the Eastern Cape, Hebron / Dreylingen fault in Namibia and Tshipise and Bosbokpoort faults in the Limpopo province.

Keywords: Seismotectonics, earthquake, fault, deformation, mainshock, aftershock, Active faults, tectonic geomorphology, active deformation, geophysical profiles, seismic hazard assessment.

Acknowledgements

Firstly, I would like to thank my supervisors Prof. Mustapha Meghraoui and Prof. Moctar Doucoure for their invaluable support and guidance throughout the years. Their dedication towards making sure that my PhD research has been a success is beyond measure.

I also would like to thank my mentor Dr Midzi for his support and drive throughout this journey. I would also like to thank my parents for instilling in me the value of excellence, the desire to learn, and for giving me every opportunity. I would like to thank my son for looking up to me and motivating me to work hard so I set a good example for him.

My gratitude also goes to my colleagues at the Council for Geoscience, Brassnavy Manzunzu, Sinovuyo Myendeki, Tebogo Pule, Sbonelo Zulu, Emmanuel Chirenje, Matome Sekiba, Simon Sebothoma, Reuben Mantsha, Vincent Jele and Leonard Tabane. I also would like to thank Campus France, through the French Government and the Council for Geoscience for the financial support and providing me time to work on my studies. I would like to thank all my colleagues who contributed to a successful publication of peer reviewed articles.

Finally, I would like to thank my friends, Fhatuwani Mulaudzi, Rebone Masemola, Hlayisani Baloyi, Mashudu Mamathaba, Katlego Khalo, Andiswa Sidjadu and Busisiwe Sehodi for their continuous support throughout all the stressful days and sleepless nights.

Dedication

I would like to dedicate this PhD thesis to my son, so he learns the benefits of hard work and perseverance. I would also like to dedicate it to all the academics who are living with mental illness, you are seen, valued and worthy. May you continue working hard and taking care of your mental health.

Table of Contents

Introduction

South Africa belongs to the intraplate tectonic domain with crustal and lithospheric structures made of geological shields and cratons where the seismicity is classified as low-level. The occurrence of large ($M_W \geq 6.5$) or moderate ($5 < M_W < 6.5$) earthquakes in such intraplate regions, however, with reduced rate of active deformation may be episodic with a long return period that may reach several thousands of years. Nevertheless, destructive earthquakes are reported in historical and instrumental seismicity catalogue of southern Africa regions.

This thesis dissertation aims at the study of the earthquake geology and seismotectonic background of these regions, including the characteristics of active tectonics and seismogenic layer, the seismic parameters of earthquake ruptures, the long-term (Quaternary) and short-term behaviour of active faulting and their integration into the seismic hazard assessment. Intraplate continental regions are often considered stable due to low level of major earthquakes mostly because their earthquake catalogue is limited in time. So is the intraplate southern Africa being classified as a Stable Continental Region (SCR) where the build-up of tectonic stresses is slow (e.g., < 8 nanostrain/yr.) and hence considered as among the Earth's least seismic active regions (Stamps et al., 2014; Njoroge et al., 2015; Saria et al., 2014; Johnston, 1996a, 1996b). Although the tectonic and seismicity strain rates are rather low (about 1 nanostrain/yr.) in intraplate southern Africa (the seismotectonic characteristics at the continental scale reveal the existence of active zones crossing the presumably stable African shields (Hartnady, 1990; Meghraoui et al., 2016). Large earthquakes do occur in areas with no known major historical earthquakes, surface deformation or strain accumulation, but their sources are poorly known. The short record of instrumental and/or historical seismicity of these regions may preclude the full understanding of their seismogenic characteristics and occurrence rate of large earthquakes.

The collision of the Archean Kaapvaal and Zimbabwe Cratons between 2.7 and 2.6 Ga led to the formation of the Limpopo Mobile Belt (Roering et al., 1992; Brown et al., 2008; Begg et al., 2009). NW-SE trending shear zones within the Limpopo Mobile Belt are well identified by Bouguer anomalies (Ranganai et al., 2002). The Kaapvaal Craton can be subdivided into the Kimberley, Witwatersrand, Pietersburg, and Swaziland Terranes, which were assembled before the extrusion of the Ventersdorp lavas at 2.7 Ga (de Wit et al., 1992). The southern margin of the Kaapvaal Craton is bounded by the ~ 400 km Mesoproterozoic Namaqua-Natal

Belt (Cornell et al., 2006). The Namaqua sector of the Namaqua-Natal Belt is bordered on its north-eastern boundary by the Paleoproterozoic Kheis Mobile belt (de Wit et al., 1992; Cornell et al., 2006; Adams and Nyblade, 2011). The Kheis Mobile Belt was described as a thin-skinned region with east-verging thrust belt characteristics (Cornell et al., 2011). The Pongola rift, situated near the eastern edge of the Kaapvaal Craton, later underwent reactivation as a compressional zone, probably in the late Proterozoic (Johnston et al., 1994). The Neoproterozoic Damara-Katanga Belts bound the north-western margin of the Kaapvaal Craton (Johnston et al., 1994; Adams and Nyblade, 2011). The late Palaeozoic compression formed the Cape Fold Belt, a dominant structural domain along the southern coastal region of Africa (Hälbich, 1983), which extends southwards offshore as far as the Agulhas Bank along the strike slip margin of south-eastern Africa (Tucholke et al., 1981).

Earthquake geology requires multidisciplinary investigations on active zones where large earthquakes have occurred in the past in southern Africa such as near-field seismology, tectonic geomorphology, Quaternary faulting and drainage system, geomorphic analysis of landscapes, shallow geophysics, paleoseismology. Intraplate continental earthquake geology have been assessed in the eastern United States and the New Madrid seismic zone (Hough and Page, 2011; Calais *et al*., 2016), in eastern Canada (Bent, 1994), in Central Europe (Camelbeeck and Meghraoui, 1998), in intraplate India (Rajendran *et al.*, 1996), in Mongolia (Chéry *et al*., 2001), and in Australia (Crone *et al.*, 1997; Clark *et al*., 2008).

With the occurrence of the 2017 Moiyabana earthquake in Botswana, there has come an increasing recognition of the important contribution that active faults (even blind or buried) need to be identified and the hypothesis that southern Africa is a stable continental region needs to be revisited, considering the occurrence of strong earthquakes within the region such as the 1932 M_W 6.9 St Lucia earthquake, 1969 M_W 6.3 Ceres earthquake and 2017 M_W 6.5 Moiyabana earthquake. Even in regions of present-day low to moderate seismicity, large historical earthquakes have caused severe damage [e.g., Boschi et al., 1995; Johnston, 1996]. In such low deformation rate context, it is usually difficult to link the current and past seismic activity with active faults, which hinders our ability to effectively understand the long-term active tectonics and assess seismic hazard. In southern Africa many faults can be classified as blind or buried faults because such active structures are not visible, or because we did not perform enough field investigations little to no surface information that can be used to characterize them. The characterization of these faults became a challenge to realistically being used in studies for the seismic hazard assessment. Currently, the routine methodology in seismic hazard evaluation is to take areal sources for seismic hazard analysis instead of individual faults. The length and related coseismic slip along these faults are not well known and this is a major lack of parameters necessary to determine the largest magnitude any fault is capable of producing.

The seismotectonic characteristics and identification of Quaternary surface faulting in many zones of stable continental regions have led to a better understanding of the seismic activity and relationships to earthquake ruptures (Johnston, 1996a, 1996b; Landgraf et al., 2017). In southern Africa, the link between the instrumental and historical seismic activity with active faults is often difficult due to low seismic strain rate (Andreaoli et al., 1996; Manzunzu et al., 2019). The relatively low level of seismic activity and low deformation rate (< 1 mm/yr; Hartnady, 1990; Malservisi et al., 2013) require an understanding of the long-term active tectonics and recurrence intervals of large and damaging earthquakes. Detailed investigations in tectonic geomorphology and paleoseismology with the objective of seismic and physical characterisation of active faults are pointed out as necessary for the subsequent seismic hazard assessment (Goedhart and Booth, 2016a, 2016b; Meghraoui et al., 2016). Goedhart and Booth (2016a, b) conducted palaeoseismic investigations along the Kango fault and determined a vertical displacement of 2 m with evidence of a paleo-earthquake of magnitude of $6.97 \leq M_W \leq 7.18$.

The recognition and detailed mapping of historical and Quaternary surface faulting in many zones of neotectonic activity have led to recent improvements in the seismic hazard studies (Landgraf et al., 2017). In this thesis dissertation, we explore the impact of improved seismotectonic model on the seismic hazard assessment in southern Africa. A realistic assessment of seismic hazard at a regional scale requires the building of a databank of reliable seismotectonic data, which are used to prepare an accurate seismic source model. The identification and characterisation of active and seismogenic faults for seismic hazard assessment in southern Africa has always been a challenge, as observed in Midzi et al. (1999) hazard assessment conducted with areal sources and Singh et al. (2011) conducting areal seismotectonics. Therefore, we review several seismic hazard studies from Fernández and Guzman (1979); Shapira and Fernández (1989); Midzi et al. (1999); Kijko et al. (2003) and Midzi et al. (2020) along the hazard assessment conducted using a new seismotectonic mode from this study.

We contribute to a realistic seismic hazard assessment in southern Africa through detailed multidisciplinary studies of the 2017 M_W Moiyabana earthquake, 1932 M_W St Lucia earthquake as well as the active faulting in Kwazulu-Natal, and the seismogenic depth in southern Africa. The steps followed in assessing the seismotectonics within intraplate southern African continental region, seismogenic depth within intraplate continental crust and seismic hazard are detailed in the first chapter of the methodology. This is followed by a focus on seismotectonics of the 2017 M_W 6.5 Moiyabana earthquake in chapter 2 as a manuscript published in the Journal of African Earth Science. Furthermore, active faulting characterisation in Kwazulu-Natal, South Africa, and the reassessment of the 1932 M_W 6.9 St Lucia, is discussed in chapter 3 as a manuscript to be submitted to the South African Journal of Geology. In chapter 4, we look at the crustal thickness and seismogenic depth within intraplate southern Africa. And lastly, the new contribution of the seismotectonics and seismogenic depth of southern Africa, to seismic hazard assessment is discussed in chapter 5. Thus, leading to the discussion and conclusion of the thesis in chapter 6.

Chapter 1

Chapter 1: Methodology

In this chapter, we outline the steps taken to assess the active tectonics, crustal deformation and seismotectonics in southern Africa for the improvement of seismic hazard assessment. Southern Africa belong to the intraplate tectonic domain characterized by a low level of seismicity and low strain rate (Stamps et al., 2014; Njoroge et al., 2015; Saria et al., 2014; Johnston, 1996a, 1996b). However, two major earthquakes occurred in southern Africa and were chosen as the focus, namely the 2017 Moiyabana and 1932 St Lucia earthquakes. Our objective is to better understand the earthquake generation processes in intraplate southern Africa using near-field seismology, active tectonics, remote sensing (geomorphic features and InSAR) and the impact improved seismotectonics has on hazard assessment.

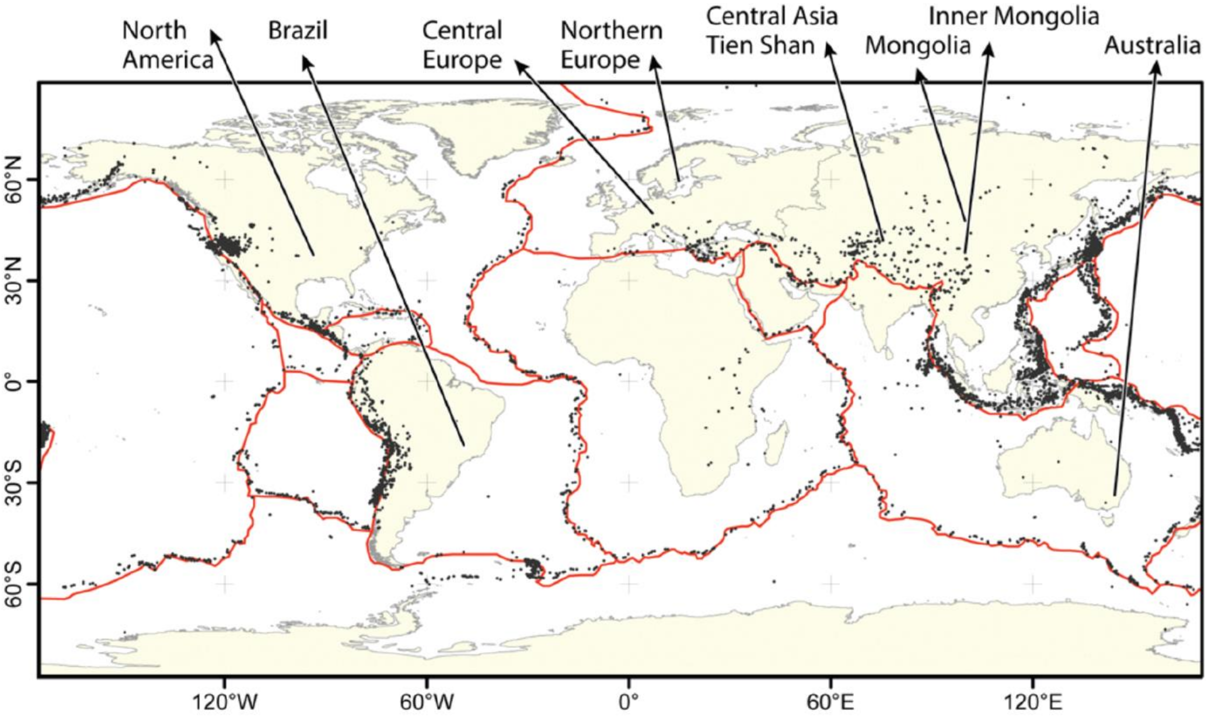

Figure 1. Intraplate earthquakes as indicated in Landgraf et al. (2017). Although several earthquakes have affected the intraplate regions (e.g., 1636, 1862, 1939 Ghana, 1809 South Africa; 1820 Congo-Angola; 1983 Guinea; 1932 South Africa, 1990 South Sudan), the African continent is not mentioned in this map.

Most of studies of earthquake-prone areas in intraplate domain and regions with low deformation rate (i.e., < 1 mm/yr) were focused primarily on historical or instrumental seismic events (Stein and Mazzoti, 2007). Field investigations coupled with mainshock and aftershock analysis using earthquake geology and seismotectonics applied to the New Madrid in 1811-

1812 (M ~8, USA)), the 1989 (Ms 6.3) Ungava - Quebec, 1957 Gobi-Altay M 8.3 earthquake (Mongolia), the 1988 Tenant Creek earthquake sequence (M 6.3 to 6.7, Central Australia) are striking examples of the intraplate seismic activity (Stein and Mazzoti, 2007;Landgraf et al., 2017).

1. Active and seismogenic faulting: The contribution of earthquake geology

Field investigations in earthquake geology made in regions with seismic activity in interplate and intraplate tectonic domains document the structural features linked to coseismic ruptures. Notions of fundamental seismogenic fault ruptures, inspired from past earthquakes, are decisive in building a methodology of investigation and analysis. Wells and Coppersmith (1994) derive regression between magnitude and surface rupture length, subsurface rupture length, downdip rupture width and rupture area. Aki and Richards (1980) derive seismic sources in relation to source function, station distance and wave speed. Hanks and Kanamori (1979) correlated moment magnitude from seismic moment relation to rupture length and rupture area. Johnston (1996a and b) established a procedure for determining seismic moment as well as moment magnitude for instrumental and intensity derived earthquake data in stable continental region.

Active faults can be determined and characterised through mapping their effects on Quaternary units with methods such as generating high-resolution DEM, tectonic geomorphology, paleoseismology, the contribution of InSAR in mapping surface rupture. Furthermore, to investigate the seismotectonics surrounding an earthquake area, we study tectonic geomorphology, which can indicate geological linear structures from past fault activities (Burbank and Anderson, 2009). Such studies can also be conducted using, for instance, GPS data, providing a rate of active deformation on the Earth’s surface such as the spatial deformation pattern caused by an earthquake to be compared with the neotectonic rate of deformation. The displacement field of the earthquake can be measured from the deformed ground surface, subsequently delineating the relationship between seismic characteristics, displacement gradient and rock properties.

Detailed investigations may be conducted in tectonic geomorphology and paleoseismology (Crone et al., 1997), with the objective of seismic and physical characterisation of active faults useful for the subsequent seismic hazard assessment (Camelbeeck and Meghraoui,1998; Goedhart and Booth, 2016a, 2016b; Meghraoui et al., 2016).

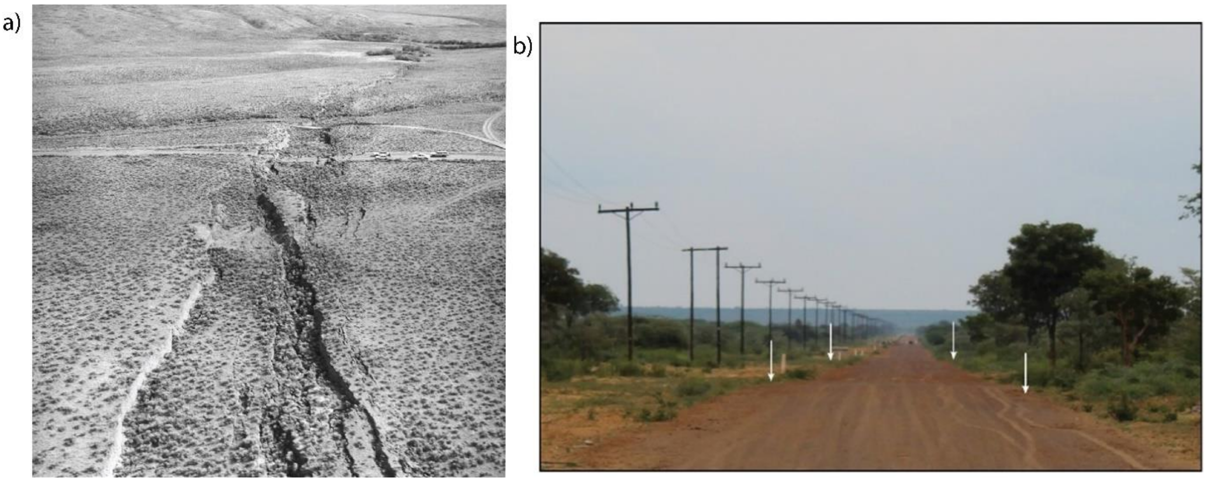

Figure 2. a) Surface faulting of 1983 Borah Peak earthquake in Basin and Range, Colorado (Crone et al., 1987). b) Escarpment of the Khurutse fault, located SE of the 2017 Moiyabana Earthquake (Mulabisana et al., 2021).

We also emphasize surface deformation and the use of radar images for InSAR before and after the 2017 mainshock obtained from the archives of the European Space Agency, and interferograms processes using GMTSAR (Sandwell et al., 2011). The SRTM Digital Elevation Model (30 m resolution) is used to remove the topographic phase component from the original interferogram (Farr et al., 2007). The spatial filter (Gaussian) is applied to obtain the interferogram, before proceeding with the unwrapped interferogram using the Snaphu software (Chen and Zebker, 2002). Finally, the unwrapped phase was converted into Line-Of-Sight (LOS) displacement. Rupture and slip models were developed using the ascending phase interferograms and the related coseismic deformation. InSAR study (from Sentinel-1 images) of the 2017 Moiyabana earthquake area provides the coseismic surface deformation, which is correlated with the 900-aftershock distribution recorded for three months post the event.

2. Thick crustal structure in intraplate tectonic domain

In intraplate regions, studies of earthquake surface deformation such as in eastern continental Canada by Bent (1994); Australia and North America by Crone et al. (1997); in the lower Rhine Graben of Europe by Camelbeeck and Meghraoui (1998); and Meghraoui et al. (2001); Australia by Clark et al. (2008); Botswana by Mulabisana et al. (2021) indicate the evidence of strong earthquakes seismic cycle. They have characterized their earthquake ruptures at depth,variable thickness of seismogenic layer, transition between brittle and ductile layers; crustal, lithospheric, and upper mantle layers and plate tectonic movement (strain rate).

Intraplate earthquakes occur differently as compared to interplate earthquakes. The tectonic loading within intraplate regions is shared by a complex system of interacting faults, whereas in interplate regions faults are loaded at constant rates by a relatively steady plate motion (Figure4) (Landgraf et al., 2017).

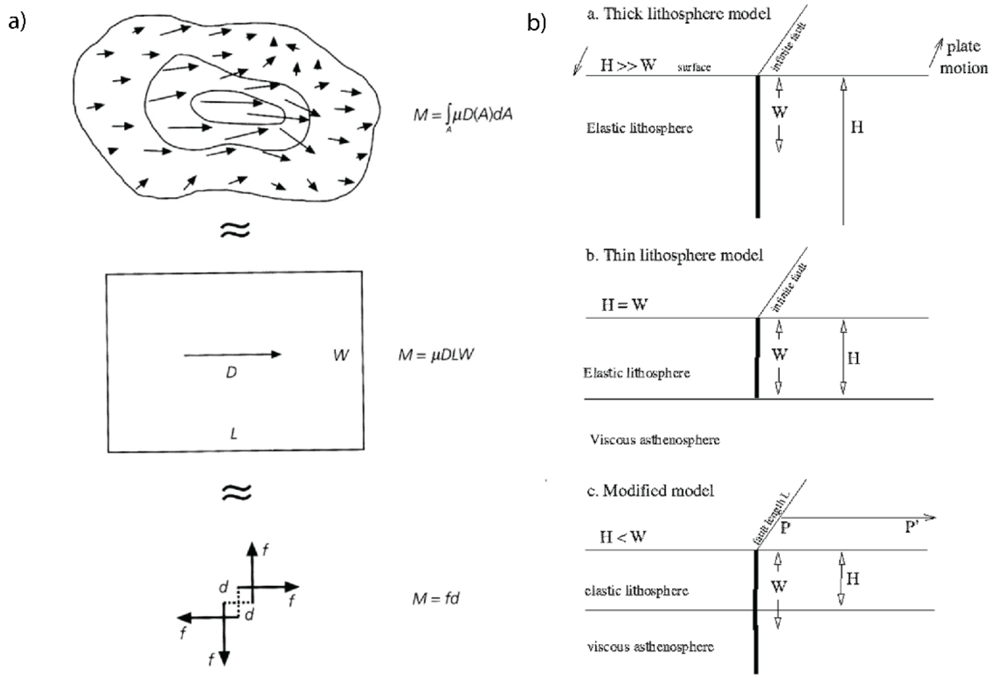

Figure 3. a) Physical parameters of an earthquake dislocation (Stein and Wysession, 2009). b) Three seismic cycle models for different elastic thicknesses (Chery et al., 2001).

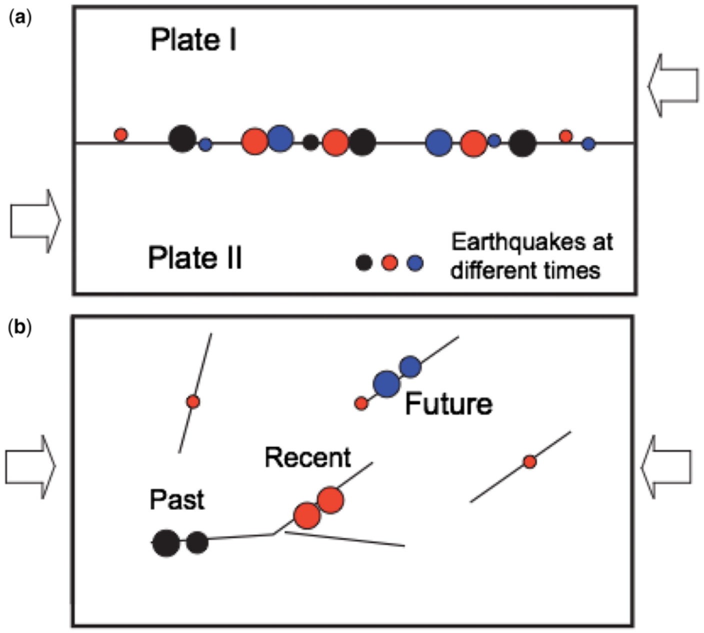

Figure 4. Conceptual models from Landgraf et al. (2017), indicating the difference between how earthquakes within intraplate (a) and interplate (b) regions occur over seismic cycle.

3. Investigation of seismicity distribution and stress field distribution (standard versus high-resolution location)

The determination of seismicity at depth using multidisciplinary approach such as investigating the record of an aftershock sequence has initial earthquake locations and depths obtained using the modified HYPOCENTER program (Lienert et al., 1986; Lienert and Havskov, 1995). Furthermore, the earthquake location has been improved initially in the SEISAN software package (Ottemöller et al., 2018) and later improved by relocating the events using a double difference approach as implemented in the HypoDD program (Waldhauser and Ellsworth, 2000). This was achieved by relocating the earthquake using the arrival times listed in the ISC bulletin, following the technique of Wysession et al. (1991).

Determining focal mechanism to indicate the maximum compressive horizontal and vertical stresses (Zoback and Zoback, 1989; Delvaux, 1993; Manzunzu et al., 2017) and utilise the obtained information on the kinematic of faulting through stress inversion. For this purpose, two methodologies were used to conduct the stress inversion of the focal mechanisms compiled in this study: the improved right dihedron method (Angelier and Mechler, 1977) and the iterative rotational optimisation method as applied in the WinTensor program (Delvaux 1993; Delvaux and Sperner, 2003).

4. Modelling of seismogenic structure

The modelling of a coseismic rupture is possible using forward modelling and an inverse method based on fault-rupture parameters for the dip slip and strike slip component of crustal brittle deformation. For this purpose, and among other methods, the use of Poly3D code considers triangulated surfaces as discontinuities in a linear, elastic, homogeneous, and isotropic half-space (Okada, 1985; Maerten et al., 2005).

Further investigations along those fault scarps using regional and ground geophysical methods such as Airborne Magnetics, Electrical Resistivity Tomography (ERT) and Reflection Seismic profiles attest to active deformation. The application of the first vertical derivative (FVD) filtering on total magnetic field intensity data enhances the narrower bodies and then supplement the results with ground geophysics data such as reflection seismics and resistivity to confirm the depth of the fault scarp displacement.

5. Assessing the SHA in intraplate tectonic domain

The other crucial part of assessing more accurate hazard is evaluating the contribution of the seismogenic layer in the analysis. We investigate the implication for the elastic thickness, which relates to the rheologically elastic layer of the lithosphere, discussed within the context of the seismic hazard assessment. We investigate the seismogenic layer thickness within specific study regions as derived from intraplate continental earthquake hypocentres and evaluate the difference with the crustal thickness. This is achieved by reviewing the available earthquake focal depths data to evaluate the depth distribution and determine the seismogenic layer thickness in intraplate continental southern Africa, using D90 by Tanaka (2004), and Tanaka and Ito (2002).

Seismic hazard assessment involves a multi-disciplinary approach of modelling the observed earthquakes, the characterization of potential future earthquakes and the processes that govern their generation and the propagation of their effects on the earth surface, focusing on geology, geophysics, seismology, paleoseismology, geodesy, physics, mathematics, and statistics (Figure 5; Reiter, 1990; Baker, 2008; McCalpin, 2009; Ares and Fatehi, 2013). In paleoseismology, intraplate continental tectonic domains have longer recurrence interval of large earthquakes (Table 1, Meghraoui and Crone, 2001). According to Bender and Perkins (1993), the SHA process is associated with many uncertainties due to unknown or inaccurate information about the location and characteristics of seismic sources, magnitude and recurrence times of earthquakes, the duration and characteristics of ground motion and the geological characteristics.

Table 1. Recurrence interval of large intraplate earthquakes from paleoseismology (Meghraoui and Crone, 2001).

Fault	**EQ magnitude**	**Rec. Int. (ka)**
Marryat C. (Aus)	5.8 (1986)	> 100 (Crone et al., 1997)
Tennant C. (Aus)	6.7 (1988)	> 50 (Crone et al., 1997)
El Camp (Spain)	6.1 (estimated)	> 30 (Massana et al., in press)
Killari (India)	6.4 (1993)	> 20 (Rajendran et al., 1993)
Bree (L. Rhine)	6.2 (estimated)	10 – 15 (Meghraoui et al., 1997)
Cheraw (Colorado)	7.0 (estimated)	~ 10 (Crone et al., 1997)
Basel (U. Rhine)	6.2 – 6.5	2.5 (Meghraoui et al., 2001)

Deterministic seismic hazard assessment (DSHA) approach develops one or more controlling earthquakes which are foreseen as the ones to produce the largest ground motion at the site. Based on the magnitude, distance and site characteristics, the ground motion at the site is predicted for each controlling earthquake. The basic principle of the DSHA approach is to try to identify the nearest active fault to a particular site and calculate the largest earthquake that could possibly occur on that fault (Kramer, 1996; McGuire, 2001; Bulajic and Manic, 2006). This fault is then used to calculate the largest possible ground shaking at the site.

The probabilistic seismic hazard analysis (PSHA) is based on the widely used classical methodology developed by Cornell (1968), McGuire (1974, 1976) and Der Kiureghian and Ang (1975, 1977). The technique uses the widest possible amount of data, combining seismological, geological, and geophysical data to build up a model of the earthquake-producing processes. Modern PSHA studies, following ideas proposed by Coppersmith and Youngs (1986), Reiter (1991) are usually able to deal with this problem by incorporating into the model what is known as a "logic tree", in which certain parameters are given a range of possible values with subjective assignment of the probability of each. The PSHA process generally consists of two key inputs: seismic source characterization, which involves a wide range of data types and scientific interpretations, and ground motion predictions. A seismic source model defines the seismogenic potential, location, size, and rate of occurrence of future earthquakes. We define unique seismic sources to account for distinct differences in the following criteria: 1. Earthquake recurrence rate and distribution 2. Maximum earthquake magnitude (M_{max}) 3. Expected future earthquake characteristics (e.g., style of faulting, rupture orientation, seismogenic thickness) 4. Probability that a fault is seismogenic and its location including orientation. We utilise available information from geological, paleoseismic, geodetic and seismological studies to determine recurrence parameters (slip rate and recurrence rates) from Youngs and Coppersmith (1985). The rupture area-based relations of Wells and Coppersmith (1994) was used to calculate the maximum earthquake magnitude (M_{max}). We also determine the b-value, which represents the slope of the Gutenberg-Richter relation and controls the relative frequency of occurrence of earthquakes of different magnitudes and the a–value, which is the intercept of the Gutenberg-Richter relation and represents the number of earthquakes with $M_W \geq 0$ occurring each year. The existing ground motion record dataset does not allow users to derive a local GMPE due to the lack of strong motion earthquakes. In this regard, models from other regions are carefully selected and tested if they fit appropriately to the local data.

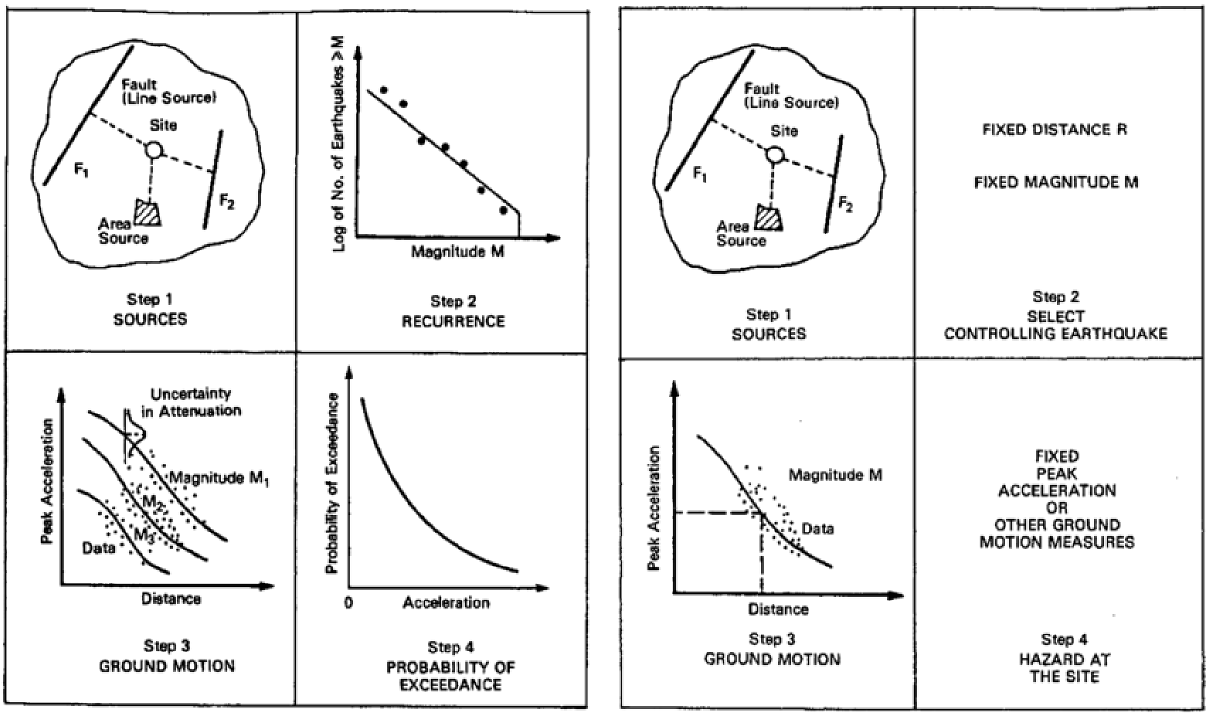

Figure 5. Probabilistic and Deterministic seismic hazard assessment as described by Reiter (1991)

In this thesis, combining the seismotectonics studies in Botswana and Kwazulu-Natal, and seismogenic depth studies, help us assessing a realistic seismic hazard at a regional scale. This methodology requires the building of a databank of reliable seismotectonic data which are used to prepare an accurate seismic source model. A multidisciplinary investigation of areas where large earthquakes have occurred in southern Africa in the past such as the 1932 M_W 6.9 St Lucia earthquake, 1969 M_W 6.3 Ceres earthquake and 2017 M_W 6.5 Moiyabana earthquake is utilised to produce a reliable seismic source model.

References

Aki K. and P. G. Richards, 1980. Quantitative Seismology, Theory and Methods. San Francisco: Freeman.

Angelier J. and P. Mechler, 1977. Sur une méthode graphique de recherche des contraintes principales également utilisable en tectonique et en séismologie: la méthode des dièdres droits, Bulletin de la Société géologique de France, 19, 1309 – 1318.

Ares A.F. and A. Fatehi, 2013. Development of probabilistic seismic hazard analysis for international sites, challenges and guidelines. Nuclear Engineering and Design, 259, pp.222-229.Baker, J.W., 2008. An introduction to probabilistic seismic hazard analysis (PSHA). White paper, version 1.

Bender, B.K. and D.M. Perkins, 1993. Treatment of parameter uncertainty and variability for a single seismic hazard map. Earthquake Spectra, 9(2), 165 – 195.

Bent, A.L., 1994. The 1989 (Ms 6.3) Ungava, Quebec, earthquake: A complex intraplate event. Bulletin of the Seismological Society of America, 84(4), pp.1075-1088.

Bulajic B. and M. Manic, 2006. Selection of the appropriate methodology for the deterministic seismic hazard assessment on the territory of the Republic of Serbia. Facta universitatis-series: Architecture and Civil Engineering, 4(1), 41 – 50.

Burbank, D. W. and R.S. Anderson, 2001. Tectonic geomorphology, Blackwell Science Ltd, Oxford, United Kingdom.

Camelbeeck, T. and M. Meghraoui, 1998. Geological and geophysical evidence for large paleoearthquakes with surface faulting in the Roer Graben (northwest Europe), Geophysics Journal International, 132, 347 – 362.

Chen C.W. and H.A. Zebker, 2002. Phase unwrapping for large SAR interferograms: Statistical segmentation and generalized network models. IEEE Transactions on Geoscience and Remote Sensing, 40(8), 1709 – 1719.

Chéry J., S. Merkel and S. Bouissou, 2001. A physical basis for time clustering of large earthquakes. Bulletin of the seismological society of America, 91(6), 1685 – 1693.

Clark, D., M. Dentith, K.H. Wyrwoll, L. Yanchou, V. Dent and W. Featherstone, 2008. The Hyden fault scarp, Western Australia: paleoseismic evidence for repeated Quaternary displacement in an intracratonic setting. Australian Journal of Earth Sciences, 55(3), 379 – 395.

Coppersmith K.J. and R.R. Youngs (1986). Capturing uncertainty in probabilistic seismic hazard assessments within intraplate tectonic environments, Proceedings of the Third U.S. National Conference on Earthquake Engineering, Charleston, 1, 301 – 312.

Cornell C.A. (1968). Engineering seismic risk analysis, Bulletin of the Seismological Society of America, 58, 1583 – 1606.

Crone A.J., M.N. Machette, M.G. Bonilla, J.J. Lienkaemper, K.L. Pierce, W.E. Scott and R.C. Bucknam, 1987. Surface faulting accompanying the Borah Peak earthquake and segmentation of the Lost River fault, central Idaho. Bulletin of the Seismological Society of America, 77(3), 739 – 770.

Crone A.J., M.N. Machette and J.R. Bowman, 1997. Episodic nature of earthquake activity in stable continental regions revealed by palaeoseismicity studies of Australian and North American Quaternary faults. Australian Journal of Earth Sciences, 44(2), pp.203-214.

Delvaux D., 1993. The TENSOR program for paleostress reconstruction: examples from the east African and the Baikal rift zones. EUG VII Strasbourg, France, 4–8 April 1993. Abstract supplement N°1 to Terra Nov. 5: 216.

Delvaux D. and B. Sperner, 2003. New aspects of tectonic stress inversion with reference to the TENSOR program. In: New Insights into Structural Interpretation and Modelling (D. Nieuwland Ed.). Geological Society, London, Special Publications 212: 75 – 100.

Der Kiureghian A. and A.H-S. Ang (1977). A fault-rupture model for seismic risk analysis, Bulletin of the Seismological Society of America, 67(4), 1173 – 1194.

Farr, T.G., P.A. Rosen, E. Caro, R. Crippen, R. Duren, S. Hensley, M. Kobrick, M. Paller, E. Rodriguez, L. Roth, D. Seal, S. Shaffer, J. Shimada, J. Umland, M. Werner, M. Oskin, D. Burbank, and D. Alsdorf (2007). The Shuttle Radar Topography Mission, Revision of Geophysics,45, RG2004, doi:10.1029/2005RG000183.

Goedhart, M.L. and Booth, P.W.K., 2016a. A palaeoseismic trench investigation of early Holocene neotectonic faulting along the Kango Fault, southern Cape Fold Belt, South Africa–Part I: Stratigraphic and structural features. South African Journal of Geology, 119(3), pp.545-568.

Goedhart, M.L. and P.W.K. Booth, 2016a. A palaeoseismic trench investigation of early Holocene neotectonic faulting along the Kango Fault, southern Cape Fold Belt, South Africa–Part II: Earthquake Parameters. South African Journal of Geology, 119(3), pp.569-582.

Hanks T.C. and H. Kanamori, 1979) A moment magnitude scale. Journal of Geophysical Research: Solid Earth, 84, 2348 – 2350.

Johnston, A.C., 1996a. Seismic moment assessment of earthquakes in stable continental regions—I. Instrumental seismicity, Geophysics Journal International, 124 (2), 381–414.

Johnston, A.C., 1996b. Seismic moment assessment of earthquakes in stable continental regions—II. Historical seismicity, Geophysics Journal International, 125 (3), 639 – 678.

Kramer S.L., 1996. Geotechnical earthquake engineering. In Prentice–Hall International series in Civil Engineering and Engineering Mechanics. Prentice-Hall, New Jersey.

Landgraf, A., Kübler, S., Hintersberger, E. and Stein, S., 2017. Active tectonics, earthquakes and palaeoseismicity in slowly deforming continents. In: Landgraf, A., Kuebler, S., Hintersberger, E. & Stein, S. (eds) Seismicity, Fault Rupture and Earthquake Hazards in Slowly Deforming Regions. Geological Society, London, Special Publications, 432, Geological Society, London, Special Publications, 432.

Lienert, B. R., E. Berg and L.N. Frazer, 1986. Hypocenter: an earthquake location method using centered, scaled, and adaptively damped least squares, Bulletin of Seismological Society of America, 76(3), 771 – 783.

Lienert, B. R., Havskov, J., 1995. A Computer Program for Locating Earthquakes Both Locally and Globally, Seismological Research Letters, 66 (5), 26 – 36.

Maerten, F., Resor, P., Pollard, D., Maerten, L., 2005. Inverting for slip on three-dimensional fault surfaces using angular dislocations, Bulletin of Seismological Society of America, 95 (5), 1654 – 1665.

Manzunzu B., V. Midzi, A. Mangongolo and F. Essrich, 2017. The aftershock sequence of the 5 August 2014 Orkney earthquake (ML 5.5), South Africa, Journal of Seismology, 21, 1323 – 1334.

McGuire R.K. (1974). Seismic structural response risk analysis, incorporating peak response regressions on earthquake magnitude and distance, Massachussets Technical, Department of Civil Engineering, Publication No. 399, p371.

McGuire R.K. (1976). FORTRAN computer program for seismic risk analysis, U.S Geological Survey Open-File Report 76-67, p90.

McGuire R. K., 2001. Deterministic vs. probabilistic earthquake hazards and risks. Soil Dynamics and Earthquake Engineering, 21(5), pp.377-384. doi: 10.1016/S0267-7261(01)00019-7.

Meghraoui, M., 2016. The seismotectonic map of Africa. Episodes, 39(1), pp.9-18.

Meghraoui, M. and Crone, A.J., 2001. Earthquakes and their preservation in the geological record. Journal of Seismology, 5(3), pp.281-285.

Meghraoui, M., B. Delouis, M. Ferry, D. Giardini, P. Huggenberger, I. Spottke and M. Granet, 2001. Active normal faulting in the upper Rhine graben and paleoseismic identification of the 1356 Basel earthquake. Science, 293(5537), 2070 – 2073.

Mulabisana, T., M. Meghraoui, V. Midzi, M. Saleh, O. Ntibinyane, T.Kwadiba, B. Manzunzu, O. Seiphemo, T. Pule and I. Saunders, 2021. Seismotectonic analysis of the 2017 moiyabana earthquake (MW 6.5; Botswana), insights from field investigations, aftershock and InSAR studies. Journal of African Earth Sciences, 182.

Njoroge M., R. Malservisi, D. Voytenko and M. Hackl, 2015. Is Nubia Plate Rigid? A geodetic study of the relative motion of different cratonic areas within Africa, International Association of Geodesy Symposia, p 1-9, doi:10.1007/1345_2015_212

Okada, Y., 1985. Surface deformation due to shear and tensile faults in a half-space, Bulletin of Seismological Society of America, 75 (4), 1135 – 1154.

Ottemöller L., P. Voss and J. Havskov, 2018. SEISAN Earthquake Analysis Software for Windows, Solaris, Linux and Macosx. Bergen.

Reiter L., 1990. Probabilistic seismic hazard analysis—lessons learned: a regulator's perspective. Nuclear Engineering and Design, 123(2–3), 123 – 128.

Reiter L., 1991. Earthquake hazard analysis: issues and insights. Columbia University Press.

Saria E., E. Calais, D.S. Stamps, S. Delvaux and C.J.H. Hartnady, 2014. Present-day kinematics of the East African Rift, Journal of Geophysical Research, 119, doi:10.1002/2013JB010901.

Stamps D.S., L.M. Flesch, E. Calais and A. Ghosh, 2014. Current kinematics and dynamics of Africa and the East African Rift System, Journal of Geophysical Research: Solid Earth, 119, 5161 – 5186, doi:10.1002/2013JB010717.

Stein S. and M. Wysession, 2009. An introduction to seismology, earthquakes, and earth structure. John Wiley & Sons.

Tanaka A., 2004. Geothermal gradient and heat flow data in and around Japan (II) Crustal thermal structure and its relationship to seismogenic layer. Earth, planets and space, 56(12), 1195 – 1199.

Tanaka A. and Y. Ishikawa (2002). Temperature distribution and focal depth in the crust of the northeastern Japan, Earth Planets Space, 54, 1 109 – 1 113.

Waldhauser F. and W.L. Ellsworth, 2000. A Double-Difference Earthquake Location Algorithm: Method and Application to the Northern Hayward Fault, California, Bulletin of Seismological Society of America, 90 (6), 1353 – 1368.

Wells D.L. and K.J. Coppersmith, 1994. New Empirical Relationships Among Magnitude, Rupture Length, Rupture Width, Rupture Area, and Surface Displacement, Bulletin of the Seismological Society of America, 84, 974-1002.

Wysession M.E., E.A. Okal and K.L. Miller, 1991. Intraplate seismicity of the Pacific Basin, 1913–1988. Pure and Applied Geophysics, 135(2), 261-359.

Youngs R.R. and K.J. Coppersmith, 1985. Implications of fault slip rates and earthquake recurrence models to probabilistic seismic hazard estimates. Bulletin of the Seismological society of America, 75(4), 939 – 964.

Zoback, M.L. and M.D. Zoback, 1989. Tectonic stress field of the continental United States: In Geological Society of America Memoir 172, Chapter 24, 523 – 539.

Chapter 2

Chapter 2: “Seismotectonic Analysis of the 2017 Moiyabana Earthquake (M_W 6.5; Botswana), Insights from field investigations, aftershock and InSAR studies” publication.

The tectonic and seismicity strain rates in intraplate southern Africa are low (about 1 nanostrain/yr.), however strong earthquakes do occur in areas with no known major historical earthquakes, surface deformation or strain accumulation, with their sources poorly known. In this chapter I investigate the 2017 Moiyabana M_W 6.5 earthquake, so as to add on the improvement of southern African seismotectonics for a realistic seismic hazard assessment. I combine several approaches (field and remote sensing investigations) in order to adopt a multidisciplinary strategy to understand the source of the Moiyabana earthquake. I consider the analysis of the mainshock, and aftershocks sequence based on a local seismic network and local seismotectonic characteristics; the earthquake rupture geometry, which is constrained from more than 900 aftershocks recorded over a period of three months and from the InSAR analysis of Sentinel-1 images (ascending orbit) and the focal mechanism solutions of the mainshock and aftershocks, that display a predominance of NW-SE trending and NE dipping normal faulting. The stress inversion of the focal mechanisms produced results that are compatible with a NE-SW extension under normal faulting regime.

Seismotectonic Analysis of the 2017 Moiyabana Earthquake (M_W 6.5; Botswana),

Insights from field investigations, aftershock and InSAR studies

Mulabisana, T. [1, 2,5], Meghraoui, M.[1], Midzi, V.[2], Saleh, M.[1,3], Ntibinyane O. [4]
Kwadiba T.[4], Manzunzu, B. [2], Seiphemo O. [4], Pule T.[2], Saunders I.[2]

[1] EOST- ITES, CNRS-UMR 7063, University of Strasbourg, France
[2] Council for Geoscience, 280 Pretoria Street, Silverton, Pretoria, South Africa
[3] NRIAG, Helwan, Egypt
[4] Botswana Geoscience Institute, Lobatse, Botswana
[5] Nelson Mandela University, Port Elizabeth, South Africa

3rd June 2021

Abstract

The 3 April 2017 M_W 6.5, Moiyabana (Botswana) earthquake occurred in the continental interior of the Nubian plate and in a seismogenic region previously considered as stable. Our objective is to combine several approaches (field and remote sensing investigations) in order to adopt a multidisciplinary strategy so as to enhance our understanding of earthquake occurrence in intraplate southern Africa. We analyse the mainshock and aftershocks sequence based on a local seismic network and local seismotectonic characteristics. The earthquake rupture geometry is constrained with more than 900 aftershocks recorded over a period of three months and from the InSAR analysis of Sentinel-1 images (ascending orbit). The mainshock (25.134 E, 22.565 S; depth 22 ± 3 km) was followed by more than 500 events of magnitude $M \geq 0.8$ recorded in April 2017 including the largest aftershock (M_W 4.6 on the 5 April 2017). Focal mechanism solutions of the mainshock and aftershocks display predominance of NW-SE trending and NE dipping normal faulting. Stress inversion of the focal mechanisms produced results that are compatible with a NE-SW extension under normal faulting regime. The InSAR study shows fringes (a pair of ascending images 2017-03-30 and 2017-04-11) with two lobes with 3.86 cm to 5.15 cm coseismic slip on a NW-SE elongated and 40-km-long surface deformation consistent with the mainshock location and normal faulting mechanism. The modelling of surface deformation provides the earthquake rupture dimension at depth with ~ 50 cm maximum slip on a fault plane striking 315°, dipping 45°, -80° rake and with M_o 3.68 x 10^{18} Nm. Although the seismic strain rate is of low level, the occurrence of the 2017 Moiyabana earthquake, followed by an aftershock sequence in the central Limpopo Mobile Belt classifies the intraplate region as an active plate interior.

Keywords: Seismotectonics, Earthquake, Fault, deformation, mainshock, aftershock

1 Introduction

Continental interiors are often considered as regions of low level of major earthquakes mostly because their earthquake catalogue is limited in time. Amid continental domains, intraplate southern Africa is classified as a Stable Continental Region (SCR) where the build-up of tectonic stresses is slow (e.g., < 8 nanostrain/yr.) and hence considered as among the Earth's least seismic active regions (Stamps et al., 2014; Njoroge et al., 2015; Saria et al., 2014; Johnston, 1996a, 1996b). Although the tectonic and seismicity strain rates are rather low (about 1 nanostrain/yr.) in intraplate southern Africa (the seismotectonic characteristics at the continental scale reveal the existence of active zones crossing the presumably stable African shields (Fig. 1; Hartnady, 1990; Meghraoui et al., 2016). Large earthquakes do occur in areas with no known major historical earthquakes, surface deformation or strain accumulation, but their sources are poorly known. The short record of instrumental and/or historical seismicity of these regions may preclude the full understanding of their seismogenic characteristics and occurrence rate of large earthquakes.

The 3 April 2017 Moiyabana earthquake with magnitude M_W 6.5 (Fig. 1) occurred in south-east Botswana, a region which is perceived as a stable continental tectonic domain with apparently no significant evidence of seismic strain release (Fig. 1). The main shock (25.134° E, 22.565° S, 26.5 ± 2.5 km depth according to the Council for Geoscience (CGS), Pretoria; Table 1) and aftershocks are located in a sparsely populated national park. Although the earthquake was widely felt in Botswana, South Africa and Zimbabwe, no severe damage was observed due to the low population density in the epicentral area (Midzi *et al.*, 2018). However, field investigations report slight structural damage with intensity of VI on the Modified Mercalli Intensity scale (MMI-56) observed at about 14 km, 40 km (in a mine) and 90 km mainly west of the epicentral location. In addition, Midzi *et al.* (2018) observed N-S trending clusters of aftershocks recorded during the first month with a spatial and temporal southward migration of seismic events. No strong seismic events have been reported in close proximity to the 2017 Moiyabana earthquake area, except for the 1952 Okavango and 2006 Machaze earthquakes (M_L6.7 and M_W7.0, respectively)

Studies on the earthquake activity of continental interiors have been mainly developed in the eastern United States and the New Madrid seismic zone (Hough and Page, 2011; Calais *et al.*, 2016), in eastern Canada (Bent, 1994), in Central Europe (Camelbeeck and Meghraoui, 1998), in intraplate India (Rajendran *et al.*, 1996), in Mongolia (Chéry *et al.*, 2001), and in Australia (Crone *et al.*, 1997; Clark *et al.*, 2008). Intraplate deformation can be assessed by the occurrence of strong earthquakes and identification of active tectonic structures in regions far from plate boundaries. The rigidity and stability of the southern Africa shield is questioned following the inferences from seismotectonic and geodetic studies that advocate the existence of incipient rifting south and southwest of the continental East African Rift (Fairhead and Henderson, 1977; Hartnady, 1990; Daly et al., 2020). Although GPS velocities are significantly lower than 1 mm/yr., (Fig. 1; Malservisi *et al.,* 2013; Saria *et al.,* 2014), different authors suggest that there might be a link between the 2017 Moiyabana earthquake sequence and the EARS (Fadel *et al.*, 2020; Chisenga et al., 2020). The invoked reasons are mainly the similarity between the normal faulting mechanism and related extensional tectonic stresses (Fadel *et al.,* 2020), the normal faulting activity of the EARS (e.g., the 22 February 2006 M_W 7.0 Machaze earthquake; Fenton and Bommer, 2006; Saunders et al., 2010) and the Okavango rift basin (e.g., the 11 October 1952 M_W 6.7 earthquake; Modisi *et al.,* 2000; Midzi *et al.,* 2018). Materna *et al.* (2019) imply that the occurrence of the 2017 event on the ancient tectonic zone of the Limpopo Mobile Belt may be responding to the stress field imposed by the EARS (Stamps et al, 2014).

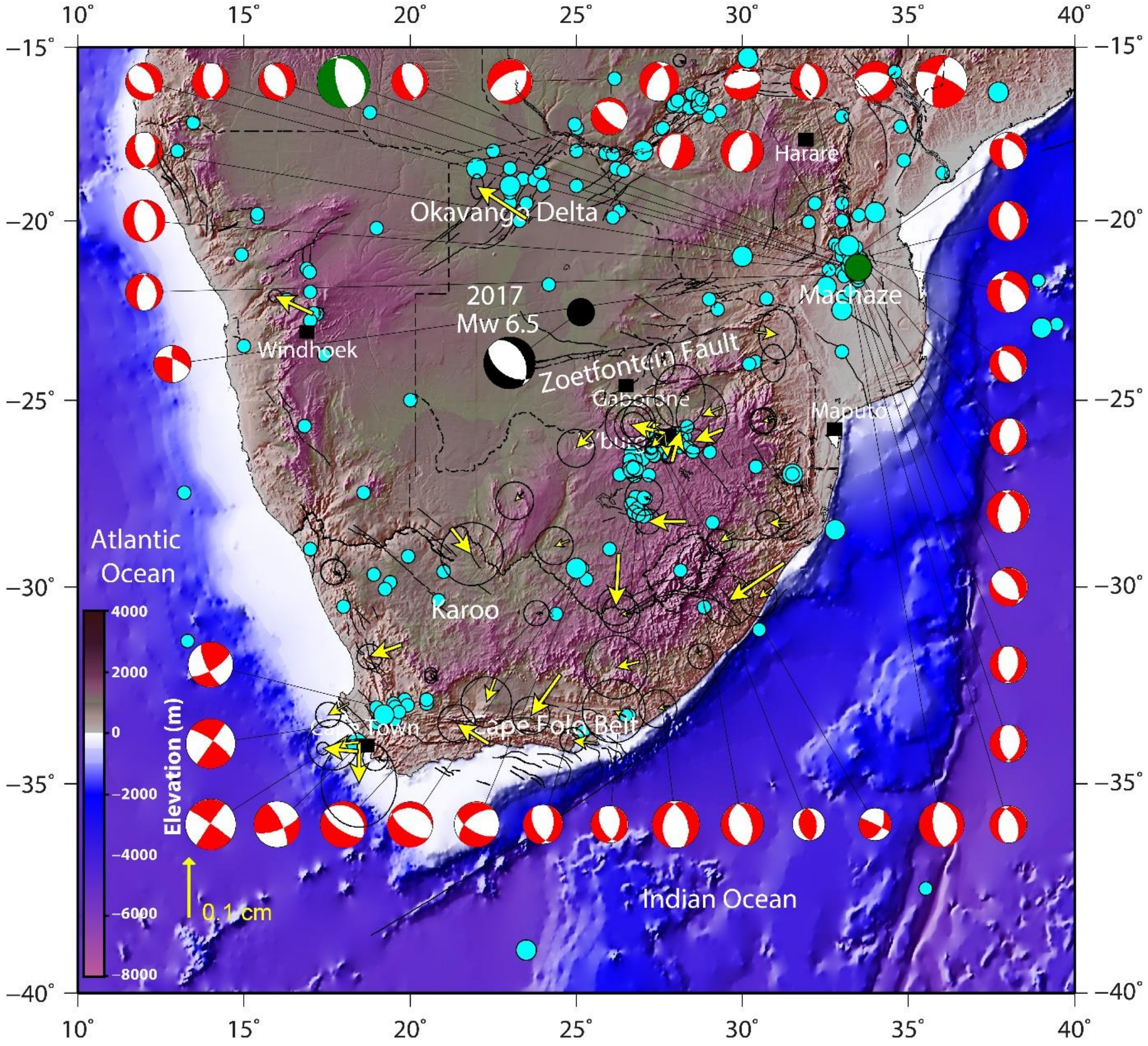

Figure 1: Seismotectonic background of southern Africa (light blue circles and red and white CMT focal mechanism solutions (SM1)), as updated from Meghraoui et al., (2016). Black circle is the location of the 3 April 2017 earthquake and its focal mechanism solution (black and white, CMT-Harvard, https://www.globalcmt.org/CMTsearch.html). The green and white focal mechanism is of the 23 February 2006 Machaze earthquake (Mw 7.0, Mozambique, green circle). GPS velocities (Nubia fixed, yellow arrow with 1σ error ellipse) are from Saria et al. (2014).

Table 1: Source parameters of the 3 April 2017 earthquake from various seismological centres.

Seismological Centre	Long. (°)	Lat. (°)	M_0 (Nm)	M_w	Depth (km)	Strike	Dip	Rake
USGS (Wpha)	25.15	-22.678	6.19×10^{18}	6.5	23.5	343	44	-62
GFZ	25.22	-22.66	6.3×10^{18}	6.5	27	331	37	-73
Geoscope	25.15	-22.678	5.86×10^{18}	6.4	29	333	36	-72
CMT Harvard	25.21	-22.54	7.01×10^{18}	6.5	30	332	41	-70
CGS (Pretoria) Midzi et al. (2018)	25.134	-22.565	-	6.5	26.5 ±2.5	340	46	-61
This study (InSAR)	25.134	-22.565	3.68×10^{18}	6.4	22 ±1.5	315	45	-80

In this paper, our objective is to better understand the earthquake generation processes in the 2017 Moiyabana earthquake area using near-field seismology and active tectonics coupled with remote sensing (geomorphic features and InSAR). Following the presentation of the seismotectonic context and a summary of previous works on the 2017 Moiyabana earthquake, we analyse the mainshock and aftershock sequence using the ~3-month records of portable stations supplemented by the seismograms of the permanent Botswana and South Africa seismic networks. The fault rupture geometry and focal mechanism solutions of the 2017 seismic sequence are determined along with the stress tensor distribution. Our InSAR study (from Sentinel-1 images) of the earthquake area provides the coseismic surface deformation, which coincides with the aftershock distribution and supports the inverse modelling of the fault-rupture parameters. The fault rupture geometry obtained from the seismic sequence and surface deformation is correlated with the composite fault escarpment identified SE of the earthquake area. We finally discuss the driving mechanisms and implications of the intraplate seismic activity and crustal deformation in southern Africa.

2 Seismotectonic setting and previous works

The collision of the Archean Kaapvaal and Zimbabwe Cratons between 2.7 and 2.6 Ga led to the formation of the Limpopo Mobile Belt, which constitute the site of the 2017 Moiyabana earthquake (Roering *et al.*, 1992; Brown *et al.*, 2008; Begg *et al.*, 2009). NW-SE trending shear zones within the Limpopo Mobile Belt are well identified by Bouguer anomalies (Ranganai *et al.*, 2002). The E-W trending Zoetfontein fault zone south of the earthquake location (Fig. 1.) developed in the lower Proterozoic era (Lekula *et al.*, 2018). Fourie *et al.* (2014) modelled the 380 m throw on the eastern part of the Zoetfontein zone and Lekula *et al.* (2018) attributed the western part to a 200 m graben structure. The crustal structure beneath cratons obtained from receiver functions and broadband seismic stations characterize the Moho average depth at 38 km, which is considered as the thinnest crust in the region (Nguuri *et al.*, 2001) and may explain the ~30 km thickness of the seismogenic layer (Midzi *et al.*, 2018).

The occurrence of the 2017 Moiyabana, Botswana earthquake prompted several works on its origin, driving mechanism, stress distribution and seismic strain accumulation. Kolawole *et al.* (2017) used high-resolution aeromagnetic, gravity data and InSAR analysis, and inverse modelling to investigate the Precambrian basement lithospheric structures and concluded that the fault rupture follows a distinct NW striking and NE dipping magnetic lineament within the Precambrian basement. Albano *et al.* (2017) show a model of the coseismic fault from InSAR results and infer a 20- km-long rupture plane, dipping 65° to the northeast, with a right-lateral component, and 2.7 m maximum slip at depth.

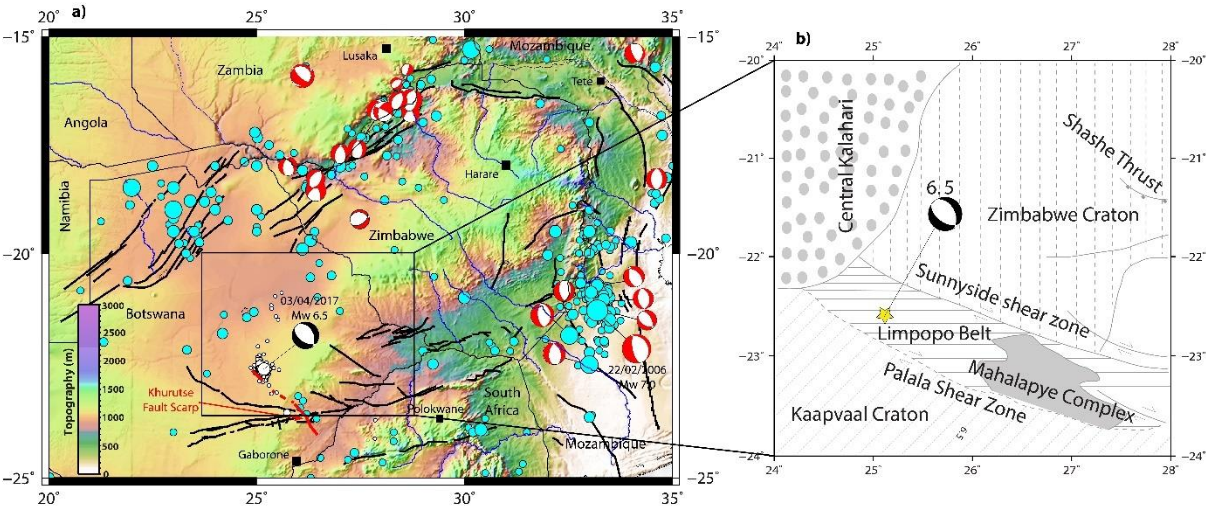

Figure 2. ***a)*** *Seismotectonic framework excerpt of the Seismotectonic Map of Africa (modified from Meghraoui et al., 2016) with focal mechanism (CMT-Harvard) of the 2017 Moiyabana mainshock. The red line is the inferred Khurutse fault scarp, cyan circles are background seismicity with magnitude 4.5 ≤ M ≤ 7.5;* ***b)*** *Structural geology background of the 2017 earthquake area (modified from Brown et al., 2008). The mainshock is indicated by a yellow star.*

Gardonio *et al.* (2018) provide a seismicity study coupled with InSAR results to infer 6 cm of subsidence, 10 km along the dip and 30 km along the strike of the fault and suggest that the pore fluids pressure from a deep source at 29 ± 4 km might be the cause of the 2017 event. Moorkamp *et al.* (2019) investigated the epicentral area with seismic velocity and resistivity profiles and showed the collocation of a weak upper mantle and weak crustal structure between strong Precambrian blocks. They also show that although the modelled resistivity may indicate fluid activation on conductive structures, there is no evidence of the fluid migrating upward or a tectonic structure presenting to be the source of the 2017 Moiyabana earthquake within the vicinity. Fadel *et al.* (2020) suggest a link with the EARS by modelling the 3D crustal and upper mantle shear wave velocity structure of Botswana and concluded that the rift can be the source of a fluid driven from ~150 km depth of the north-eastern tip of Botswana to migrate to the edge of the Kaapvaal Craton and the earthquake area. Chisenga et al. (2020) modelled the Bouguer gravity and produced a high-resolution crustal thickness map of Botswana which suggests a correlation of the earthquake activity with the thermal fluid and elevated heat flow from EARS. Thomas (2020) also used the analysis of Sentinel images and provided an interferogram that suggests 9 to 10 cm total coseismic slip at the surface. Finally, Olebetse *et al.* (2020) studied foreshock and aftershock events recorded by the Botswana seismic network and suggest a correlation with local geological structures of the Kaapvaal Craton and Limpopo mobile belt. Although no field investigations were conducted after the mainshock, most studies correlate the 2017 seismic sequence with the tectonic reactivation in the Limpopo Mobile Belt due to thermal fluids and elevated heat flow linked to the EARS.

3 Mainshock and Aftershock Analysis

The mainshock of 3 April 2017 with M_W 6.5 was reported by several international seismological centres (Table 1) but the South African National Seismograph Network (SANSN) provided the most accurate location, as their seismic stations are in close proximity to the source. The epicentre location of the SANSN (Council for Geoscience, Pretoria) also includes data from the Botswana seismic network (Fig. 3). The largest aftershock with magnitude M_W 4.6 occurred west of the mainshock on 5 April 2017 at a much shallower depth (~10 km) than the mainshock.

Following the mainshock, an aftershock sequence was recorded from 8 April to 29 June 2017 by a temporary network and shows more than 900 earthquake records. Aftershocks that occurred prior to 8 April 2017 (i.e., date of installation of the temporary network as presented in Figure 3) and recorded by the Council for Geoscience (CGS) together with the Botswana

Geological Institute (BGI) are excluded in our initial seismic sequence analysis (Figs. 5 a and b) due to fixed depth values (see figure in SM2). This early aftershocks-sequence consists of 65 events reaching M_L4.1 with a fixed constant 5-km-depth. The fixing of earthquake depths by the CGS is done in their routine seismic data analysis, as the sparse nature of the network makes it difficult to confidently determine depth values. The record of the seismic sequence (that benefited from the collaboration between seismic networks of the CGS and the BGI) includes seismic events with magnitude as low as M_L 0.8 with a decrease of daily occurrence rate from 101 to 20 seismic events within the first month of record (Midzi *et al.*, 2018). Following the mainshock, the seismicity decay obtained from the daily number of aftershocks conforms to the Omori's law (Fig. 4; Utsu et al., 1995).

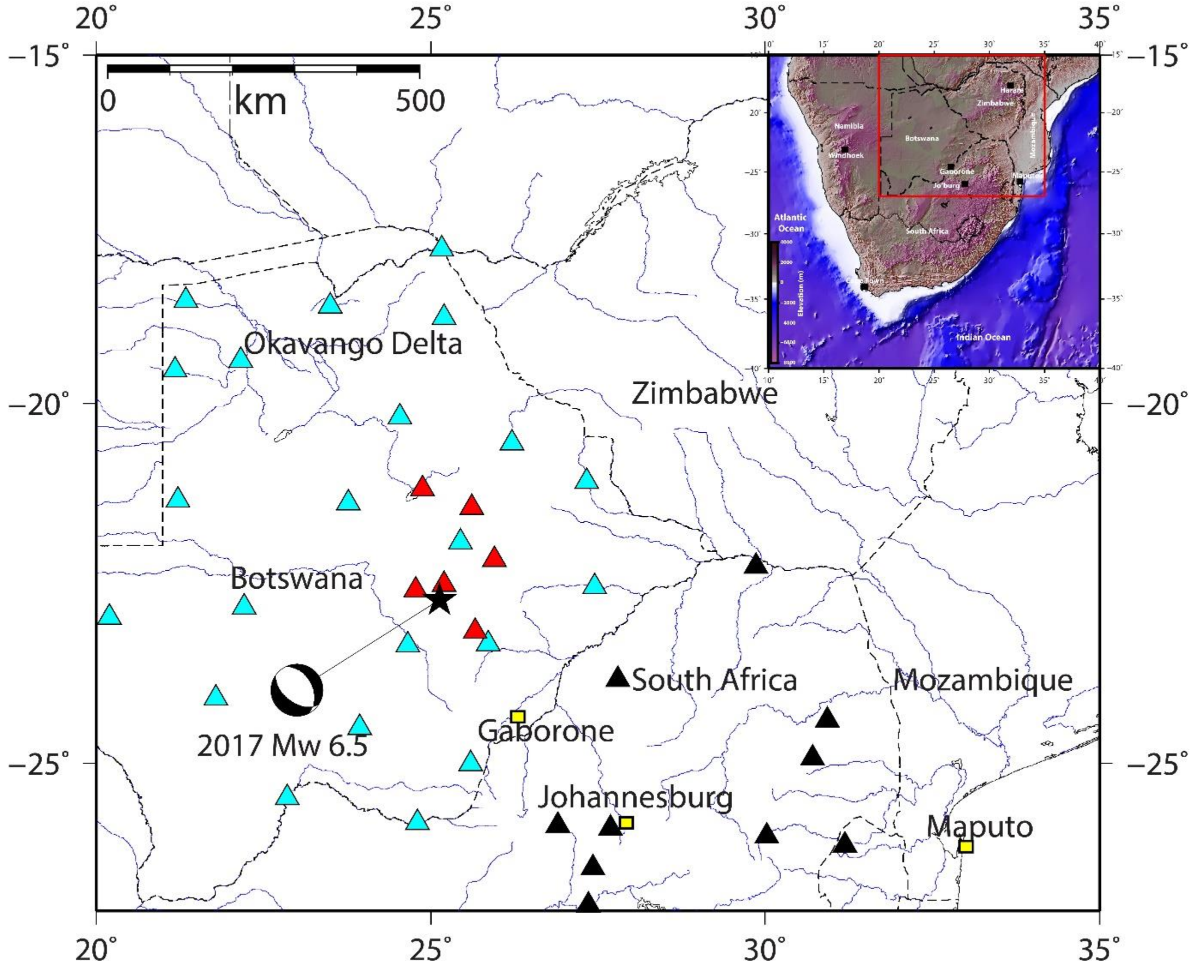

Figure 3. Seismic stations which recorded the mainshock (black star) and aftershocks. Focal mechanism is from Harvard CMT. The seismic stations in cyan triangles are managed by Botswana Geoscience Institute and black triangles by Council for Geoscience. Portable seismic stations (red triangles) were temporarily installed and recorded aftershocks from the 8th of April to the 29th of June 2017. The inset image shows the location of Figure 3 in red square.

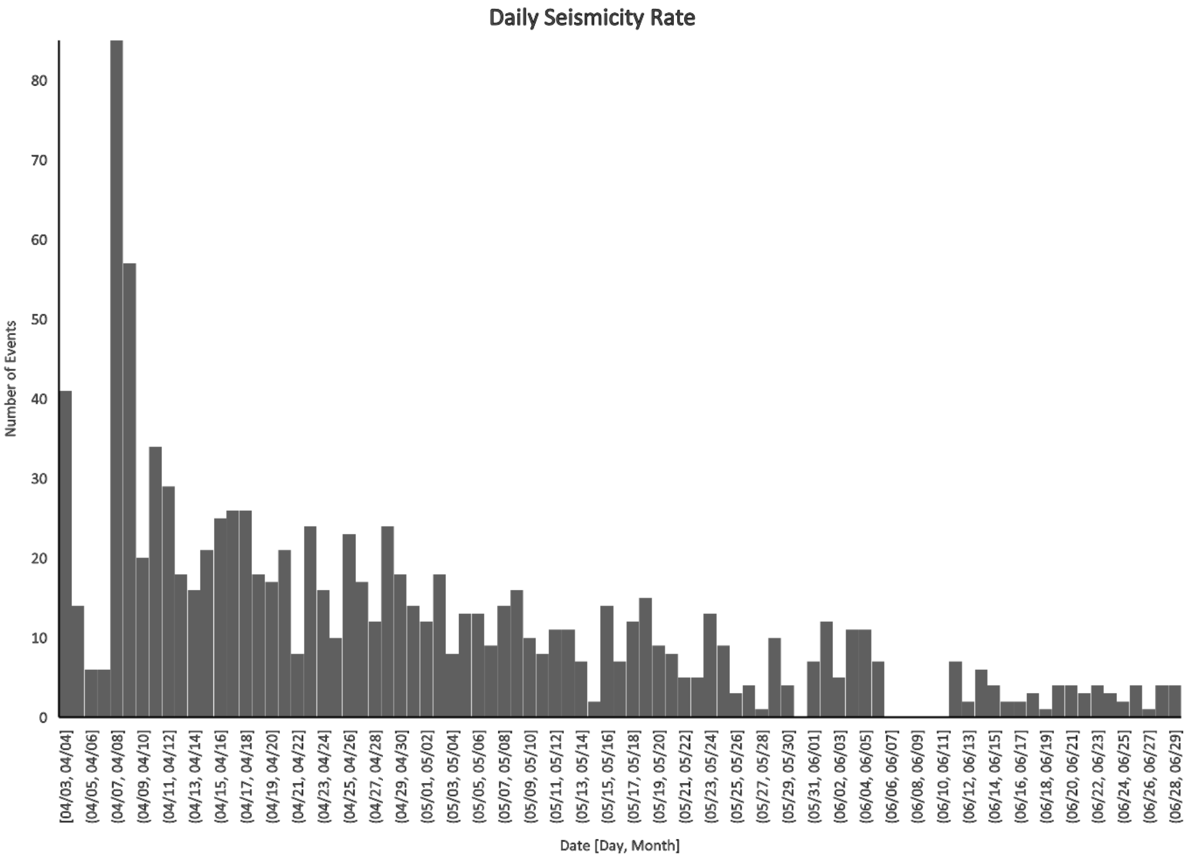

Figure 4. Daily number of seismicity recorded from the 3rd of April to the 29th of June 2017.

The initial earthquake locations were obtained using the modified HYPOCENTER program (Lienert *et al.*, 1986; Lienert and Havskov, 1995) in the SEISAN software package (Ottemöller *et al.*, 2018). This method utilises the interactive, least squares method to determine the location of the earthquake. The three-layer velocity model developed for South Africa (Midzi et al., 2010) was used in the location process (Table 2) resulting, on average, with epicentral and depth uncertainty of 1.5 km and 2.5 km, respectively.

Table 2: Velocity model used in aftershock locations (Midzi et al., 2010).

Modified depth to top of layer (km)	**P-wave velocity (km/s)**
0.00	5.80
20.00	6.50
38.00	8.04

The initial location of seismic sequence shows two clusters with a NNW-SSE trending western dense aftershock distribution and a N-S trending but sparse eastern aftershock sequence (Fig. 5a). The western aftershocks cluster includes the mainshock and largest aftershock whilst the eastern aftershock sequence, which is located about 20 km further east, includes one of the largest aftershocks with a magnitude M_L 4.2. The depth cross-section of the aftershocks shows the two clusters with a depth distribution of seismic events between 7 and 30 km for the western sequence, and between 4 and 12 km for the eastern aftershocks (Fig. 5b). The aftershocks also show a significant temporal eastern migration with the occurrence of the eastern seismic sequence mostly in June 2017 (Fig 6a). Fig. 6b illustrates the frequency of aftershocks versus the magnitude within the three months when temporary stations were deployed. The activity rate and b-value are 3.8 and 0.78, respectively, and we note the gap of earthquake magnitude between 4.6 and 6.5, implying that the M_W 6.5 event is a characteristic earthquake.

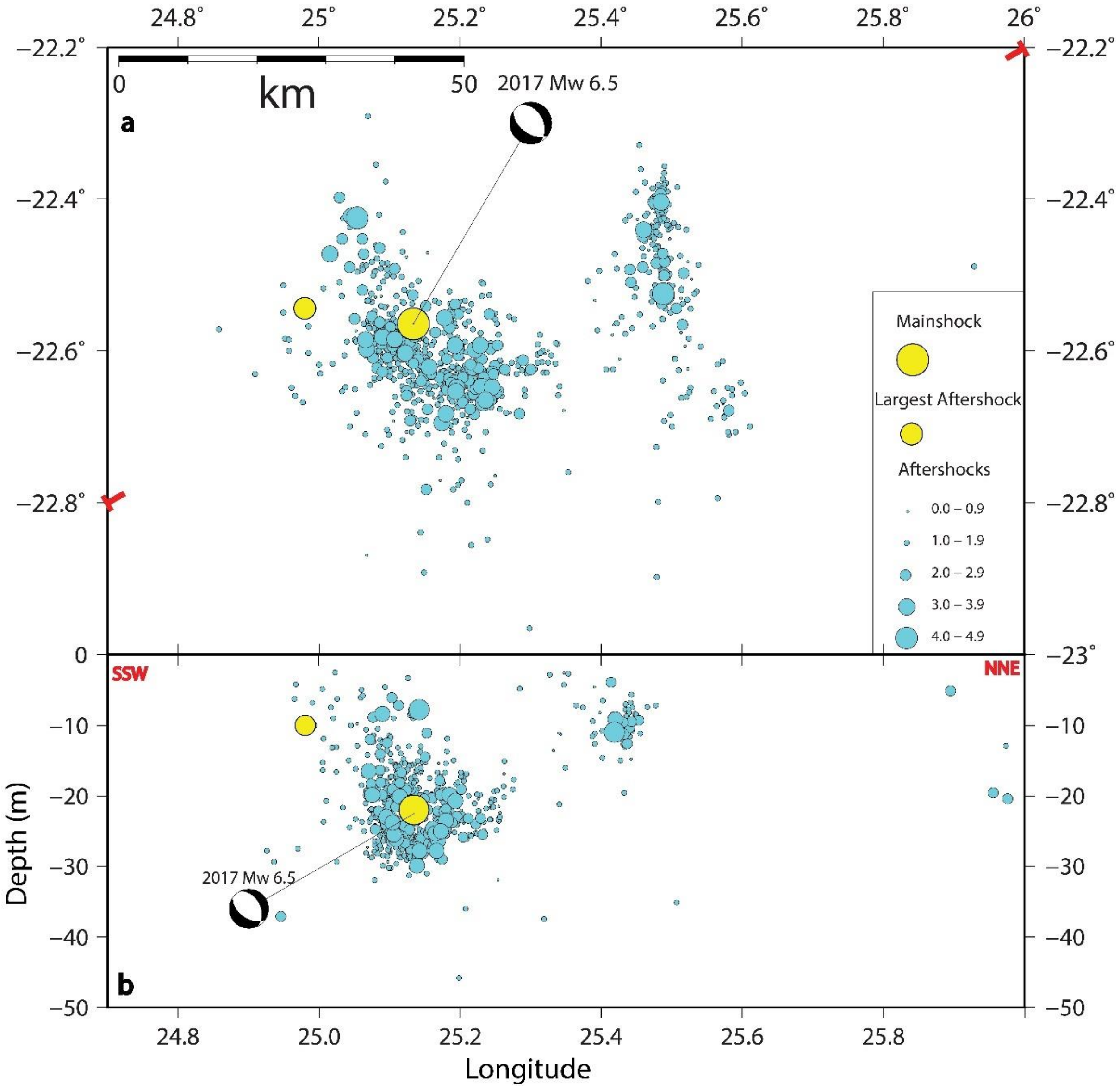

Figure 5. ***a)*** *Mainshock and the initial aftershocks sequence location of the 2017 Moiyabana earthquake with CMT-Harvard focal mechanism.* ***b)*** *Cross-section of the 2017 seismic sequence, as indicated by the T-symbols in Fig. 5(a), recorded by temporary network from 8 April to 29 June 2017 (cyan circles) following the mainshock.*

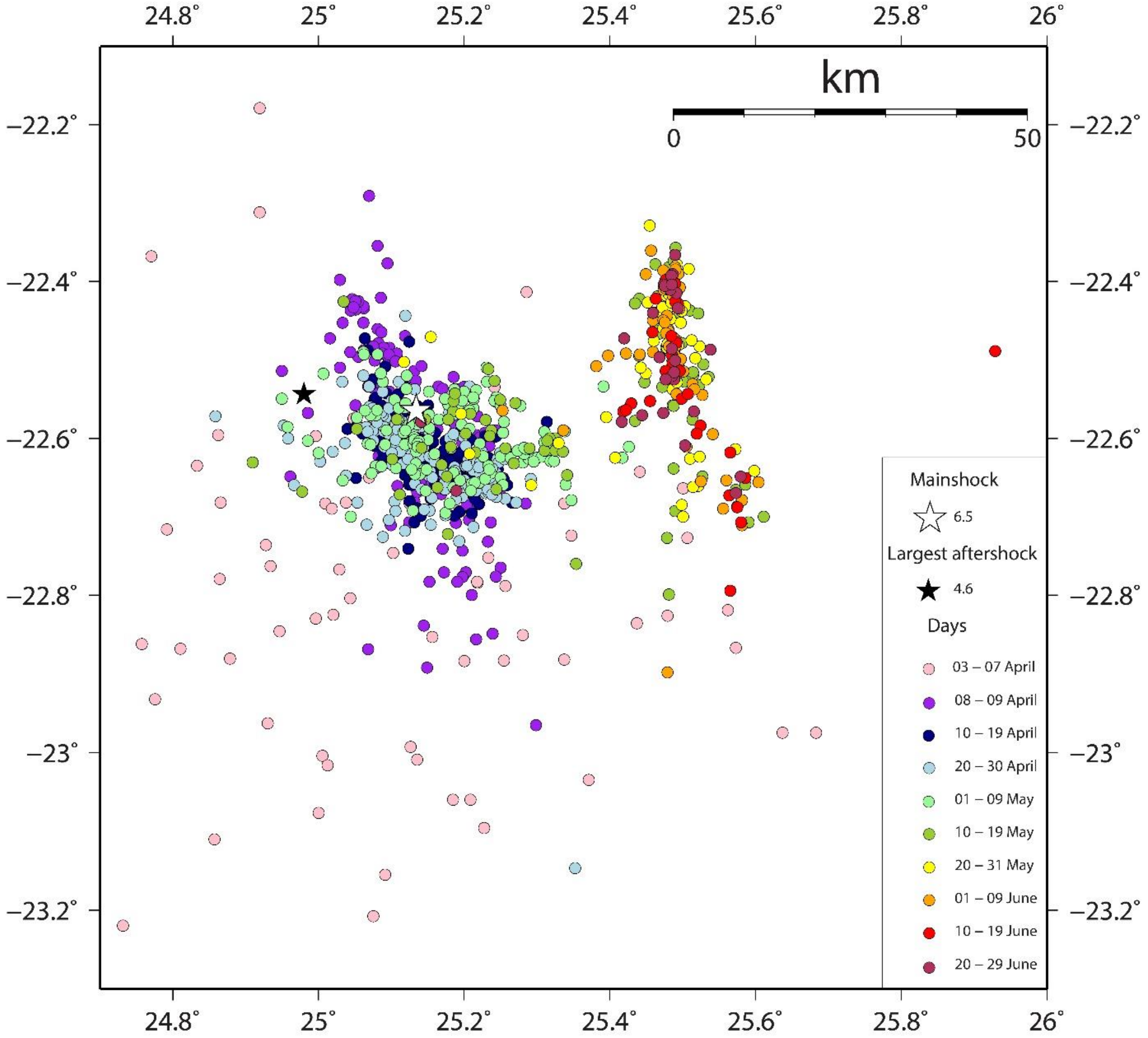

Figure 6. ***a)*** *Migration of more than 900 aftershocks (colour scale) recorded using the temporary network installed from 8 April to 29 June 2017 and 67 aftershocks (pink circles) recorded from 3 to 7 April 2017 by permanent stations. The eastern sequence occurred mostly in June 2017.*

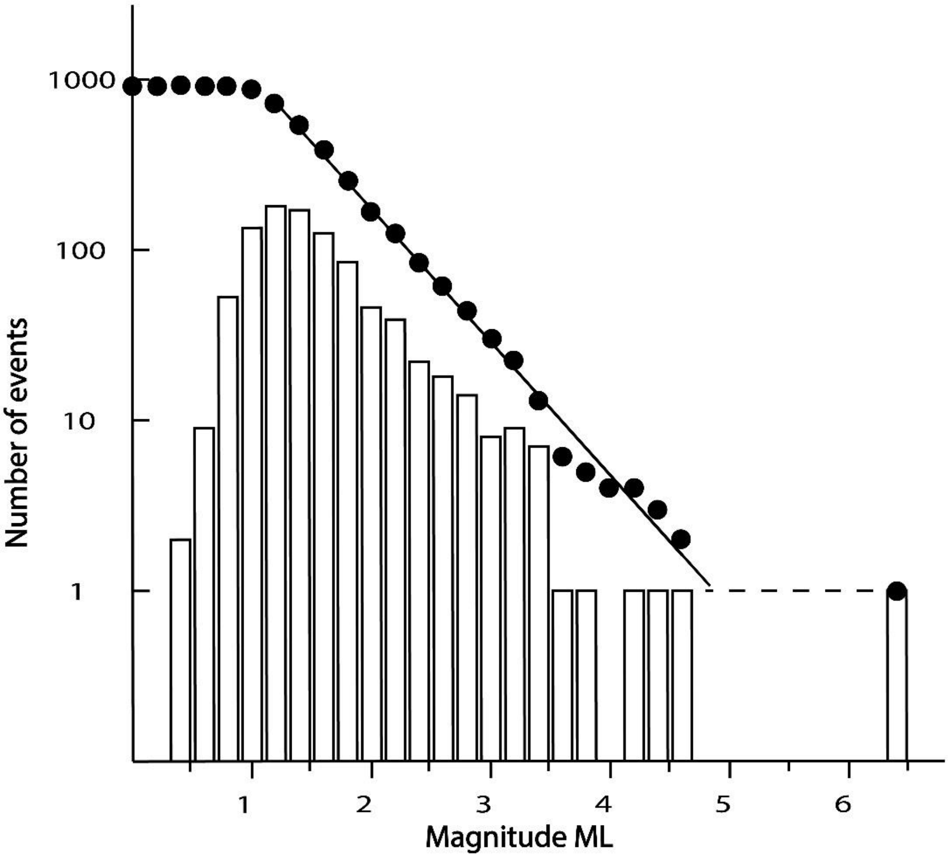

Figure 6. ***b)*** *Gutenberg-Richer relation Log N = 3.8-0.78*M_L *as applied to the 2017 earthquake sequence.*

In order to provide a complete description of aftershock distribution and improve their location and depth, the earthquakes were relocated using a double difference approach as implemented in the HypoDD program (Waldhauser and Ellsworth, 2000). In this seismicity analysis, we do not include aftershocks that occurred prior to the 8 April 2017 due to the distant location (> 150km) of seismic stations. The double difference approach uses cross-correlation between earthquake pairs to extract differential travel times from seismic stations. The cross correlation needs to occur from at least two seismic stations to further constraint the earthquake location. When a seismic station is not part of a pair, it does not contribute to further constrain the seismic source location. The computation reduces random noise in data by suppressing strong signatures of station geometry and allows a better location of the seismic source.

The HypoDD subprogram ***ph2dt*** is used to process first the seismic events into pairs, minimizing the RMS residuals between the observed and calculated travel time differences of P and S waves at same stations. 699 out of over 900 aftershocks were selected to be relocated considering the quality readings of P and S seismic waves, resulting in 1398 travel times. In this approach, we also consider the velocity model of Table 2, Vp/Vs ratio of 1.74. The aftershock analysis is made within the 50 km distance of the seismic sequence and at a maximum 170 km station distance, while previous studies of Midzi et al. (2010) provide the P-wave velocity 1-D model. The relocated earthquakes shown in Figs 7a and b are obtained from the double difference approach as implemented in the HypoDD program (Waldhauser and Ellsworth, 2000). The stability of the relocated solutions is satisfactory because six portable seismic stations are close to or within the aftershock sequence area and the P and S wave arrivals times allowed for an average 8500 iterations. Following the relocation process, the aftershocks distribution clearly shows the accurate concentration of seismic events in the seismogenic layer and upper crust (see figure in SM3). After relocation, most of the seismicity is located between 8 and 32 km depth, with most of arrival time RMS between 0.1 and 0.3 seconds (Fig. 7c). Taking into account the velocity model of Table 1, the depth uncertainties range between 0.7 and 2.1 km.

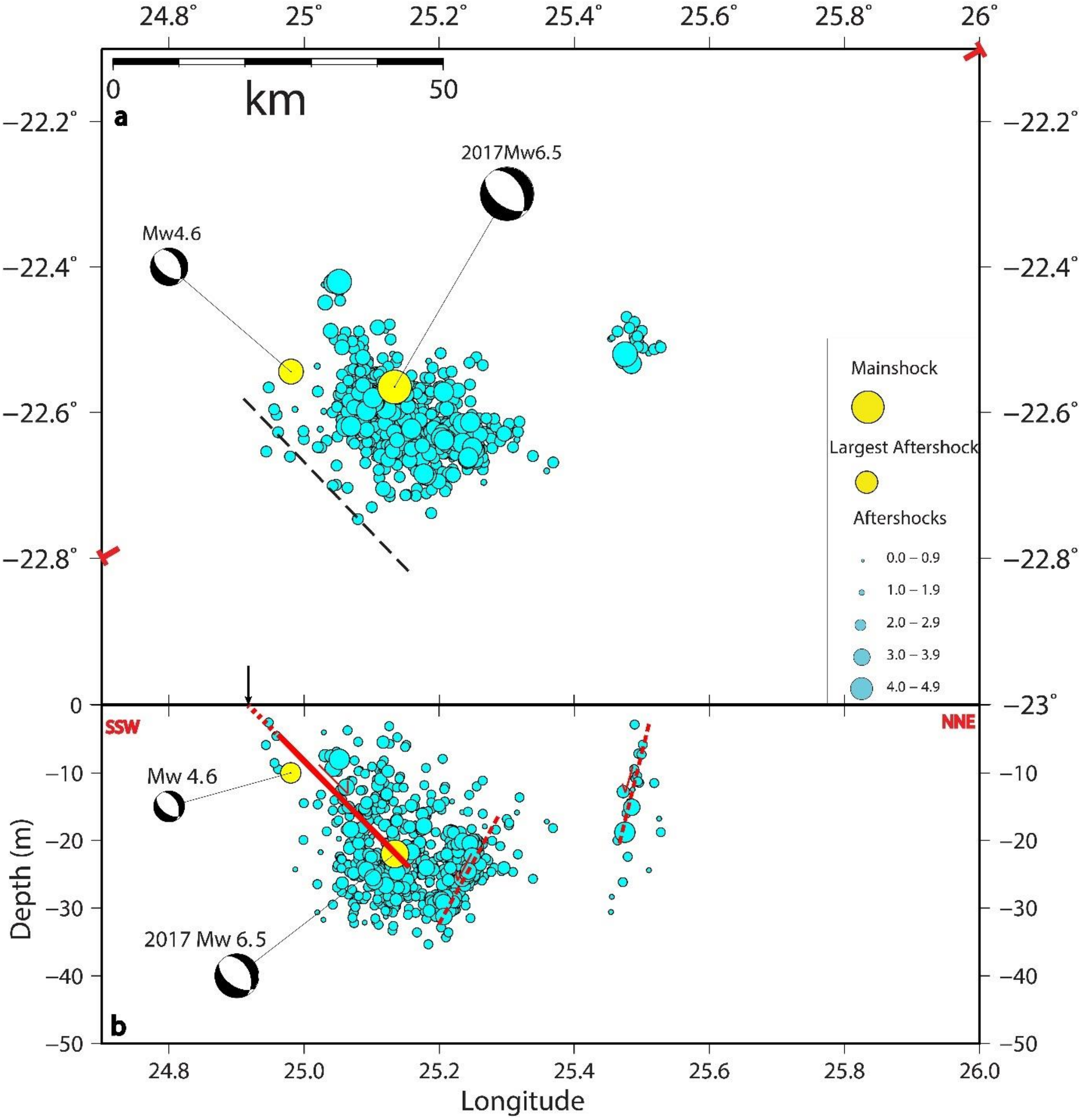

*Figure 7. **a)** Spatial distribution of aftershock locations obtained after relocation. Focal mechanism solutions of the mainshock and main aftershock are from CMT Harvard. The dashed line is the coseismic rupture tip inferred from the aftershocks at depth (Fig. 7b) and the analysis of InSAR fringes of coseismic surface deformation (see section on InSAR analysis). **b)** Aftershock sequence cross-section, as indicated by the T-symbols in Fig. 7(a), after relocation. Focal Red lines are the blind coseismic ruptures inferred from the mainshock and aftershocks sequence; the black arrow locates InSAR fringes of coseismic surface deformation (see section on InSAR analysis).*

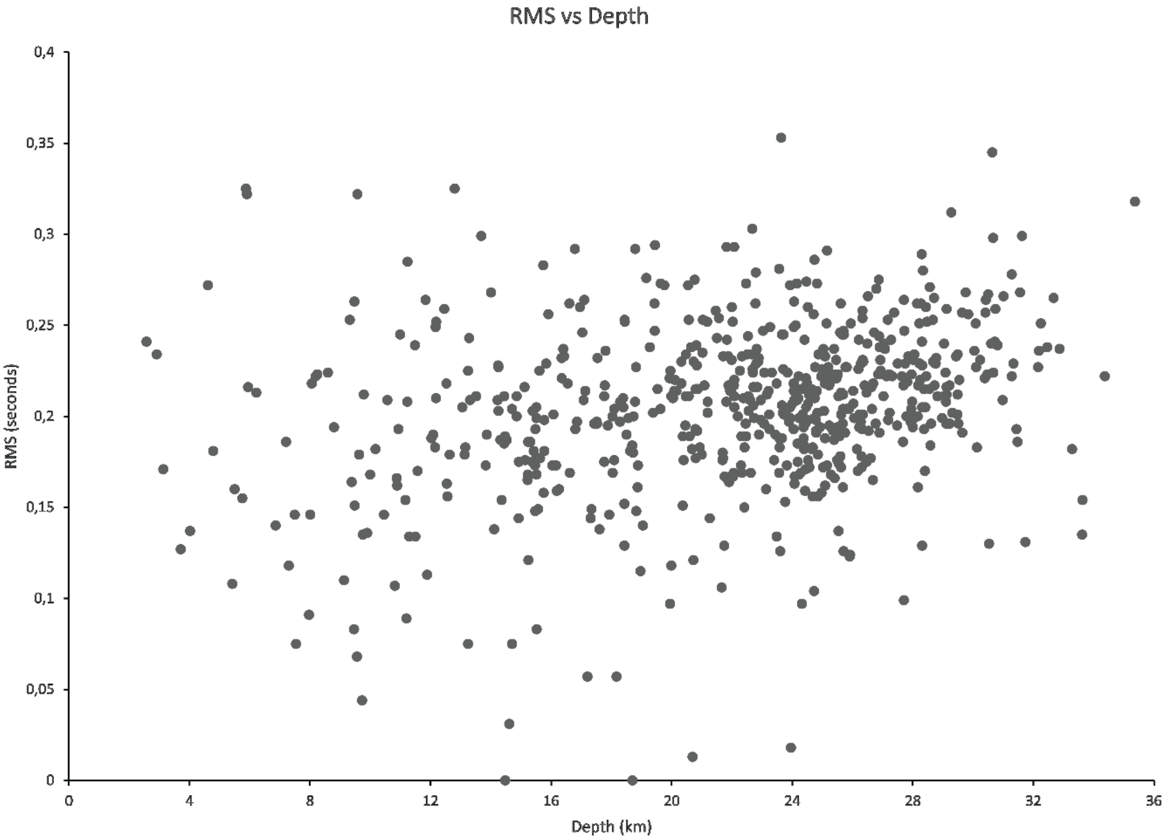

Figure 7. ***c)*** *RMS versus depth after relocating the aftershock sequence.*

Relocated events better show the clustering at depth (Fig. 7b). In the cross-section of Fig. 7(b), the western sequence of aftershocks shows sub-clusters between 10 and 30 km depth suggesting two conjugated fault ruptures. The eastern seismic cluster sequence appears at shallower depths (mostly between 5 and 15 km) and more clustered than in the SEISAN locations. They are well aligned marking a high angle west dipping rupture plane (Fig. 7b). The aftershock distribution and geometry of the inferred fault-ruptures at depth imply a graben-like tectonic structure within this part of the Limpopo Mobile Belt.

4 Focal Mechanism and Stress Inversion

The 2017 mainshock ruptured along a buried fault, which was not previously mapped. Therefore, any information on source geometry and stress orientation in the epicentral area is vital in understanding the driving mechanism. Focal mechanism solutions were calculated to indicate the maximum compressive horizontal and vertical stresses (Zoback and Zoback, 1989; Delvaux, 1993; Manzunzu *et al.*, 2017). The focal mechanism solutions for 46 selected aftershocks were computed based on first-motion polarities of P-wave (Ross *et al.*, 2018), using FOCMEC module in the SEISAN software package (Ottemöller et al., 2018). The degree of search varies from 2 to 20 degrees for different aftershocks. The focal mechanism solutions are shown in Fig. 8 and parameters are listed in SM4. The selected seismic events were those with signal to noise ratio above 2.0 and recorded by at least 5 stations with clear polarity readings.

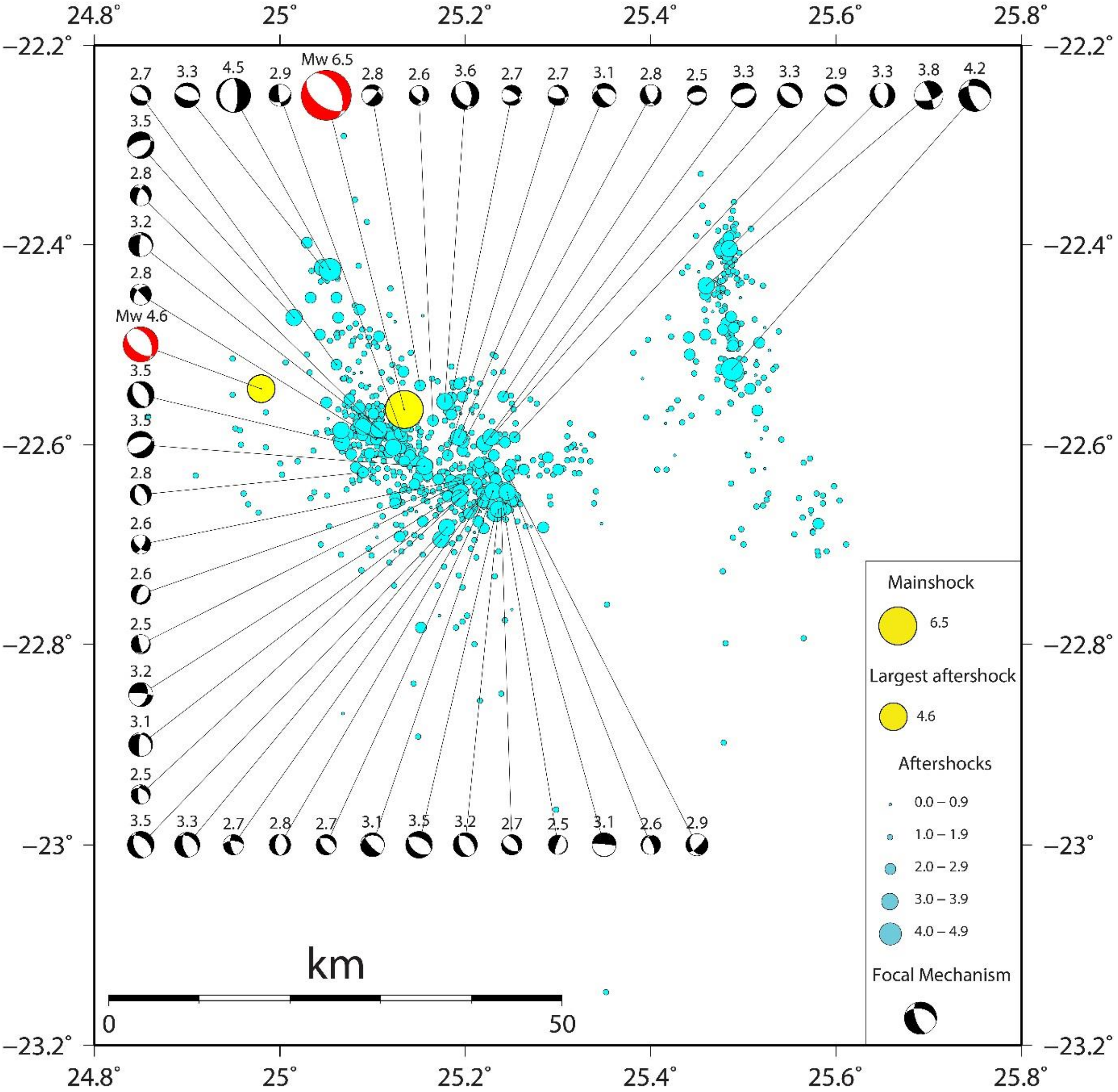

Figure 8. Focal mechanism solutions of 46 selected seismic events (see also Table SM4). Solutions are Schmidt lower hemisphere, the numbers above the solutions give the local magnitude. Aftershock locations are as in Fig. 5(a). Mechanism of mainshock (in red) is from Harvard CMT (https://www.globalcmt.org/CMTsearch.html).

Focal mechanisms of aftershocks show normal faulting and few oblique mechanisms (Fig. 8 and Table in SM4). The mainshock and largest aftershock show normal faulting mechanism, with roughly NE and SE dipping nodal planes at 41° and 42°, respectively. The 2017 Moiyabana earthquake sequence occurred in an area with no known seismic history, therefore the stress regime is also poorly known. Focal mechanisms of mainshock and 45 aftershocks provide the opportunity to obtain information on the kinematic of faulting through stress inversion. For this purpose, two methodologies were used to conduct the stress inversion of the focal mechanisms compiled in this study: the improved right dihedron method (Angelier and Mechler, 1977) and the iterative rotational optimisation method as applied in the WinTensor program (Delvaux 1993; Delvaux and Sperner, 2003).

The dihedron method provides an initial approximate stress tensor that is then used as the starting solution for the rotational optimisation method (Delvaux and Barth 2010). Delvaux and Sperner (2003) implemented the rotational optimisation method as an iterative method that can be applied to minimise the misfit between data and model function for each earthquake. During optimisation, only the solutions which are compatible with the lowest misfit are utilised for stress inversion. Out of the 46 focal mechanisms (92 nodal planes) from the database, 30 (60 nodal planes), as well as 14 (28 nodal planes) are compatible with a NE-SW extension under normal faulting regime (Fig. 9). The later analysis with 14 focal mechanisms is performed to test the results after optimising the dataset further for more compatibility.

The locations on a normal fault system along NW-SE trending shear zones of the Limpopo Mobile Belt show the influence of the geological background. Most of aftershocks are characterized by average NW (340°) striking with NE dipping fault planes, consistent with the stress distribution and NE-SW extension. The predominant normal faulting mechanism indicates an extensional neotectonic regime in the epicentral area.

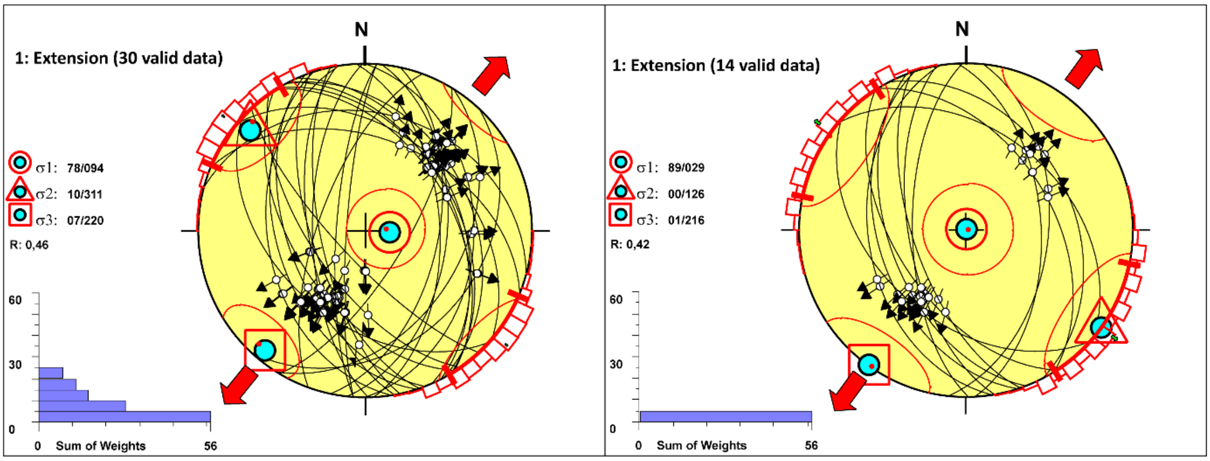

Figure 9. Stress inversion of 2017 earthquake aftershocks obtained from the WinTensor programme of Delvaux and Sperner (2003). Schmidt diagrams show nodal planes (black lines), with Left: Solution from 30 focal mechanisms taking into account all solutions, Right: Solution from 14 focal mechanisms with similar strike, dip of fault planes and slip vectors (black arrows). The stress tensor distribution (cyan circles) with σ1 in red circle, σ2 in triangle, σ3 in square, indicates 220°N and 216°N as the main extension directions (large red arrow). The ratio R (0.46 and 0.42) expresses the predominance of extensional stress state, and histograms sum of weights that verify the stress tensor.

As shown by the analysis of the 2017 Moiyabana earthquake data, its seismotectonic background and nearby geophysical studies such as magnetics and resistivity, the stress field confirms the large-scale extensional forces that may result from elevated heat flow, thermal fluid migration and SW extension of the EARS (Andreoli *et al.*, 1996; Delvaux and Barth, 2010; Meghraoui *et al.*, 2016; Materna *et al.*, 2019; Moorkamp *et al.*, 2019; Chisenga *et al.*, 2020). The active deformation across the Limpopo Mobile Belt and southern African intraplate domain shows N36E to N40E average extension direction with low level strain rate (~1 nanostrain/yr.; Malservisi *et al.*, 2013), and although the 2017 seismic source is relatively deep (> 20 km), the existence of thermal fluids and active tectonics with surface deformation suggests the presence of a seismic cycle and associated elastic strain release.

5 Surface deformation

5.1 InSAR Analysis

The SAR (Synthetic Aperture Radar) frames examined in this study are two pairs of ascending Sentinel-1A images that cover the earthquake area (Fig. 10). The used radar images before and after the 2017 mainshock were obtained from the archives of the European Space Agency, and interferograms are processed using GMTSAR (Sandwell *et al.*, 2011).

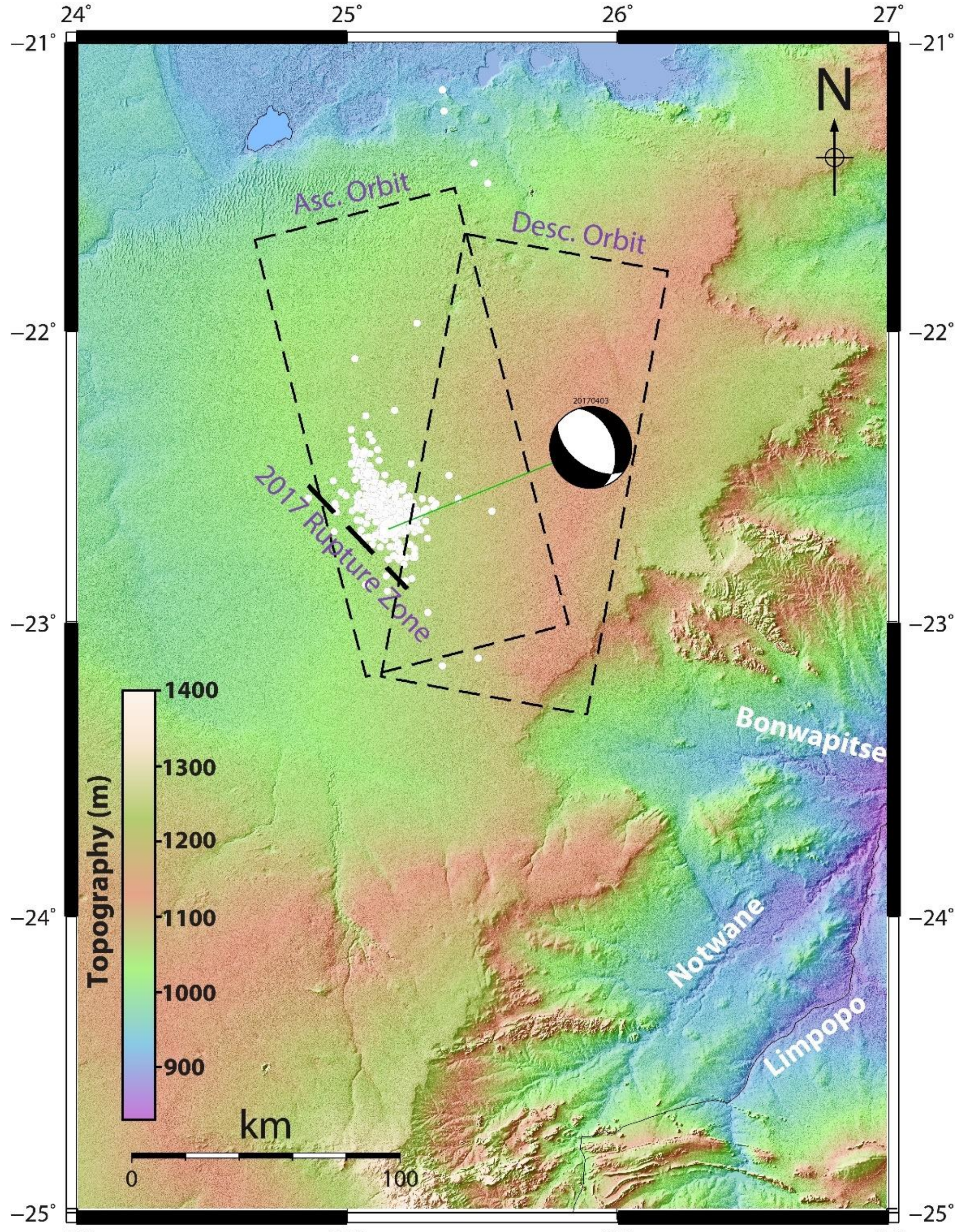

Figure 10. Frame of ascending and descending tracks of Sentinel-ESA-SAR images crossing the 2017 earthquake area. We observe that only the ascending track covers the whole 2017 earthquake area. Thick dashed line is the inferred 2017 Moiyabana earthquake rupture zone and small white circles show aftershock distribution. Focal mechanism of mainshock is from Harvard CMT. Background topography is from SRTM1'.

The SRTM Digital Elevation Model (30 m resolution) is used to remove the topographic phase component from the original interferogram (Farr et al., 2007). The spatial filter (Gaussian) is applied to obtain the interferogram (Fig. 11), before proceeding with the unwrapped interferogram using the Snaphu software (Chen and Zebker, 2002). Finally, the unwrapped phase was converted into Line-Of-Sight (LOS) displacement (Fig. 11). The obtained interferogram from a pair of ascending images (2017-03-30 and 2017-04-11; 1A/1A) shows clear lobes of LOS displacements (Fig. 11). The interferogram from ascending tracks show a consistent fringe distribution with ~40-km-long and ~20-km-wide NW-SE-trending lobes. The LOS measurements display ground displacement of the SW and NE blocks, respectively, indicating a clear straight limit between lobes that represents the fault zone on the SW edge of the lobe. For ascending tracks, the maximum and minimum values of the LOS displacement range from 4.2 cm to 5.6 cm for interferogram (Fig. 11) from which we estimate a total of 3.86 – 5.15 cm of vertical surface deformation across the fringes. The analysis of the Sentinel-1 interferogram shows a NW-SE elongated and 40-km-long surface deformation consistent with a blind fault rupture geometry. The interferogram also shows a surface deformation with subsidence coincident with the 2017 earthquake sequence location and normal faulting mechanism consistent with the source time function (http://geoscope.ipgp.fr/index.php/en/catalog/).

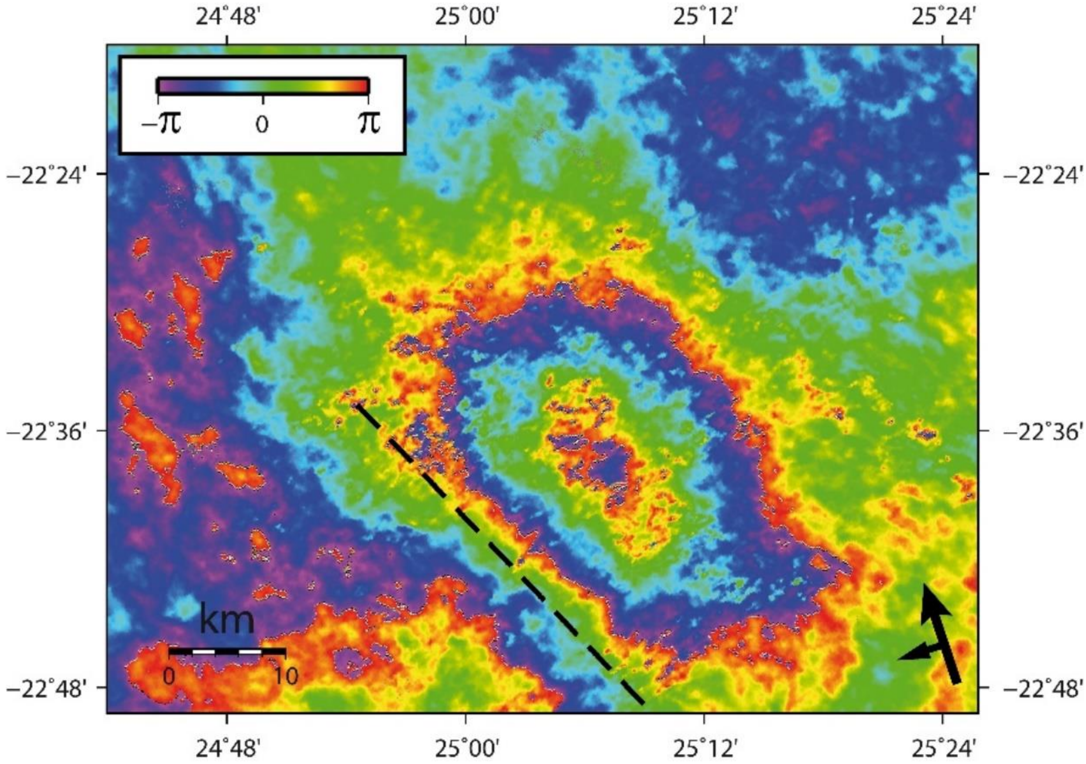

Figure 11. Fringes and lobes of interferogram of the 3rd of April 2017 Botswana earthquake. The dashed line is the projected fault rupture with respect to surface deformation with subsidence (~4.2 – 5.6 cm in LOS). The black arrow (small arrow) is the Sentinel satellite track with side look.

5.2 Earthquake Rupture Model

Rupture and slip models were developed using the ascending phase interferograms and the related coseismic deformation. To minimize the afterslip and/or postseismic effects, the modelling is based on interferograms obtained from the earliest coseismic pairs of Sentinel scenes (Figs 11, 12 a and b). In order to constrain the earthquake rupture geometry and slip distribution at depth, different solutions were tested using fault parameters for the inversion modelling that confirm the InSAR surface deformation.

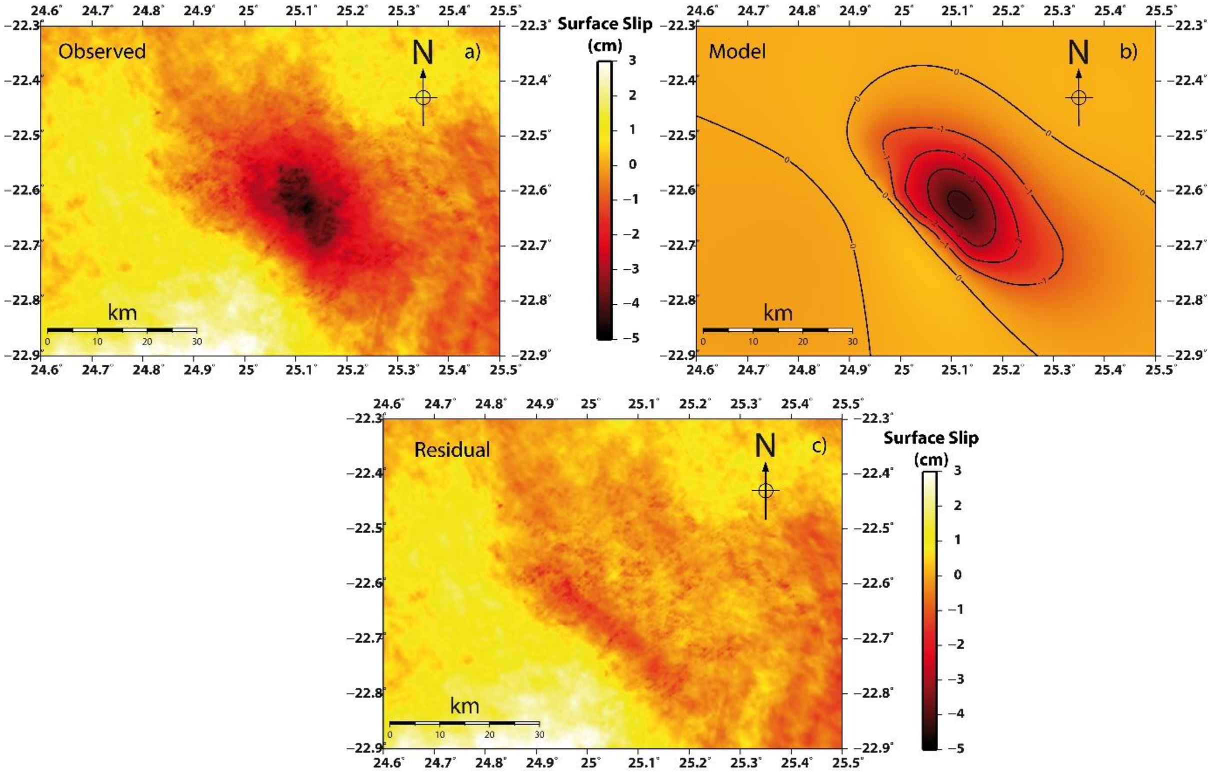

Figure 12 ***a)*** *Unwrapped SAR data interferogram with surface slip distribution.* ***b)*** *Modelling of surface deformation from the inversion of InSAR data.* ***c)*** *Residual of InSAR results versus model.*

The inversion modelling was performed for the dip slip and strike slip component of deformation using the Poly3D method considering triangulated surfaces as discontinuities in a linear, elastic, homogeneous, and isotropic half-space (Maerten *et al.*, 2005; see the details of the method in SM5). The blind coseismic fault coincides at the surface with the inflection area in between the uplift and subsidence lobes (see the fault tip trace in Figs 7b and 11). Considering different fault dimensions and dip angles, we performed a series of inversions that lead to the best fit (with 95% data variance) for the 3D surface slip obtained on the 315°, dipping 45°, -80° rake, ~40-km-long and ~22-km-wide fault geometry with a seismic moment of 3.68 x 10^{18} Nm (Table 1, Fig. 13).

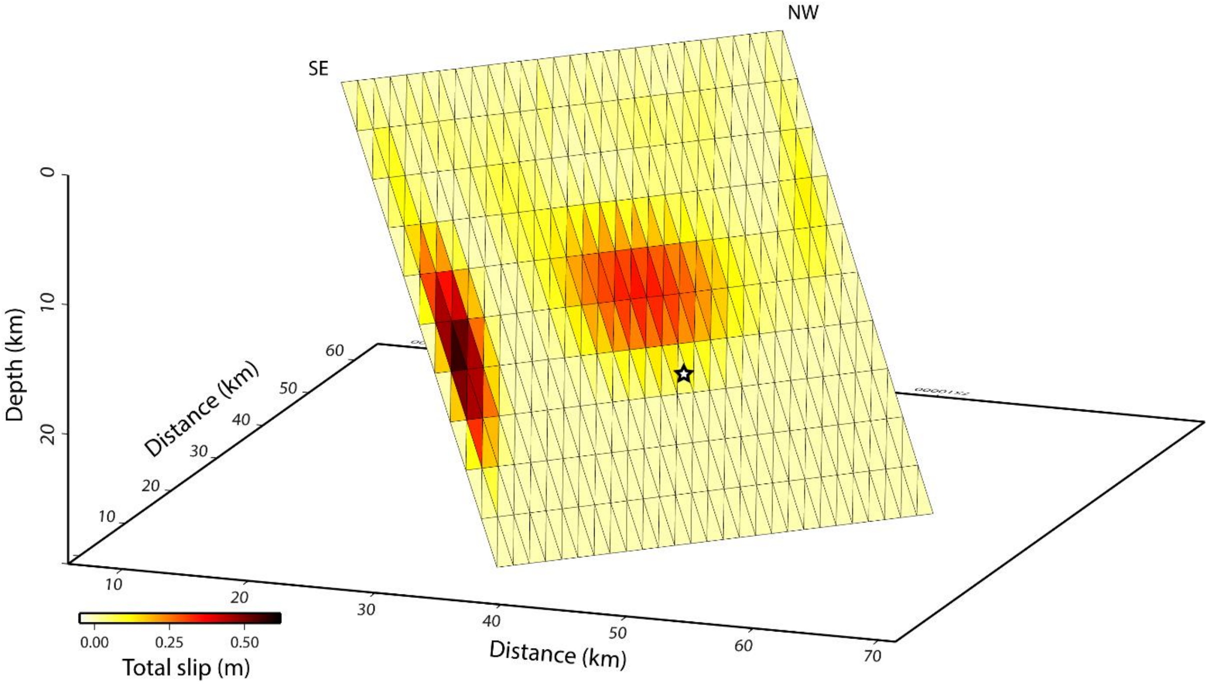

Figure 13. Model of fault rupture with slip distribution reaching 50 cm at depth, as inferred from the inversion of InSAR data and surface deformation. The star indicates the inferred 3rd *April 2017 earthquake hypocentre.*

The best fitting model shows a maximum slip of 50 cm at a depth of 22 ± 1.5 km and the existence of two asperities along the fault which agrees with the observed western seismic cluster (Figs 7a and b). Observed interferograms are compared to the inversion models in order to minimize the residual fringes with RMS misfit (Fig. 12c). The residual signals in Figure 12c (~1 cm) could be attributed to the atmospheric delay signal, the unwrapping error, and the surface motion caused by the post-seismic afterslip and aftershocks. As shown in Figure 14, the modelling allows to test the 0.744 cm RMS against the 0.4 smoothing and 0.23 roughness of the coseismic rupture. The location of the InSAR displacement and inferred blind fault rupture with NW-SE elongated lobes suggests a correlation with ~30-km-long buried fault that belongs to the Limpopo Mobile Tectonic Belt and can be correlated to the Khurutse fault scarp visible further southeast.

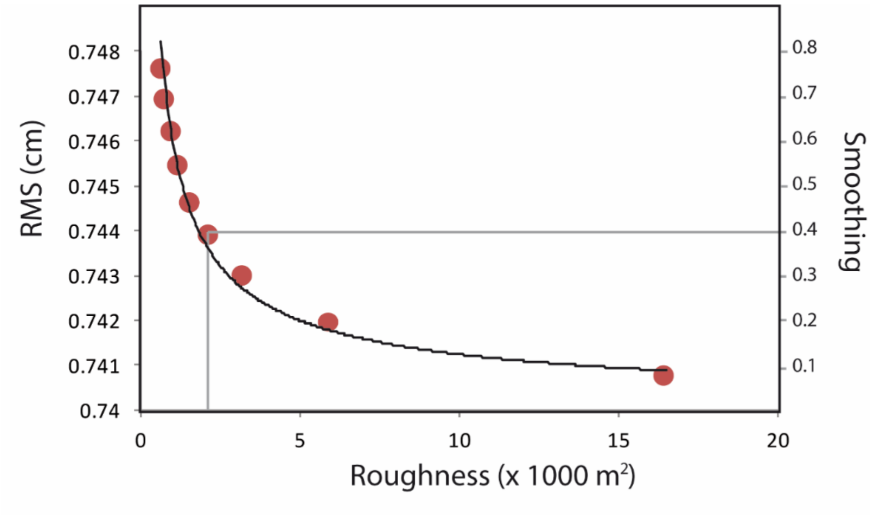

Figure 14. RMS misfit (minimize the residuals) obtained from the comparison between interferograms and inversion models of Figures 12a and b), residual of Figure 12c, and slip distribution of Figure 13. The 0.744 cm RMS and 0.4 smoothing (grey lines) correspond to the best compromise for the slip distribution on the fault plane.

6 Khurutse Fault Scarp and Long-term Seismic Cycle

The interplay between tectonic processes which build up topography and the surface processes which tear them down over time, in days to millions of years, are what defines tectonic geomorphology (Burbank and Anderson, 2001). Thus, the study of tectonic geomorphology can indicate geological linear structures from past fault activities. Such studies can be done using for instance GPS data, providing a rate of deformation on the Earth's surface such as the spatial deformation pattern caused by an earthquake. The displacement field of the earthquake can be measured from the deformed ground surface, subsequently delineating the relationship between seismic characteristics, displacement gradient and rock properties.

The Khurutse fault scarp is visible on topographic maps (both SRTM 90 m and 30 m resolution; Farr *et al.*, 2007) southeast of the 2017 M_W 6.5 earthquake (Figs 15, 16 and 17a). Four cross section profiles of the faults scarp (Fig. 17b) were plotted using the differential GPS data collected at sites indicated in (Fig. 17a).

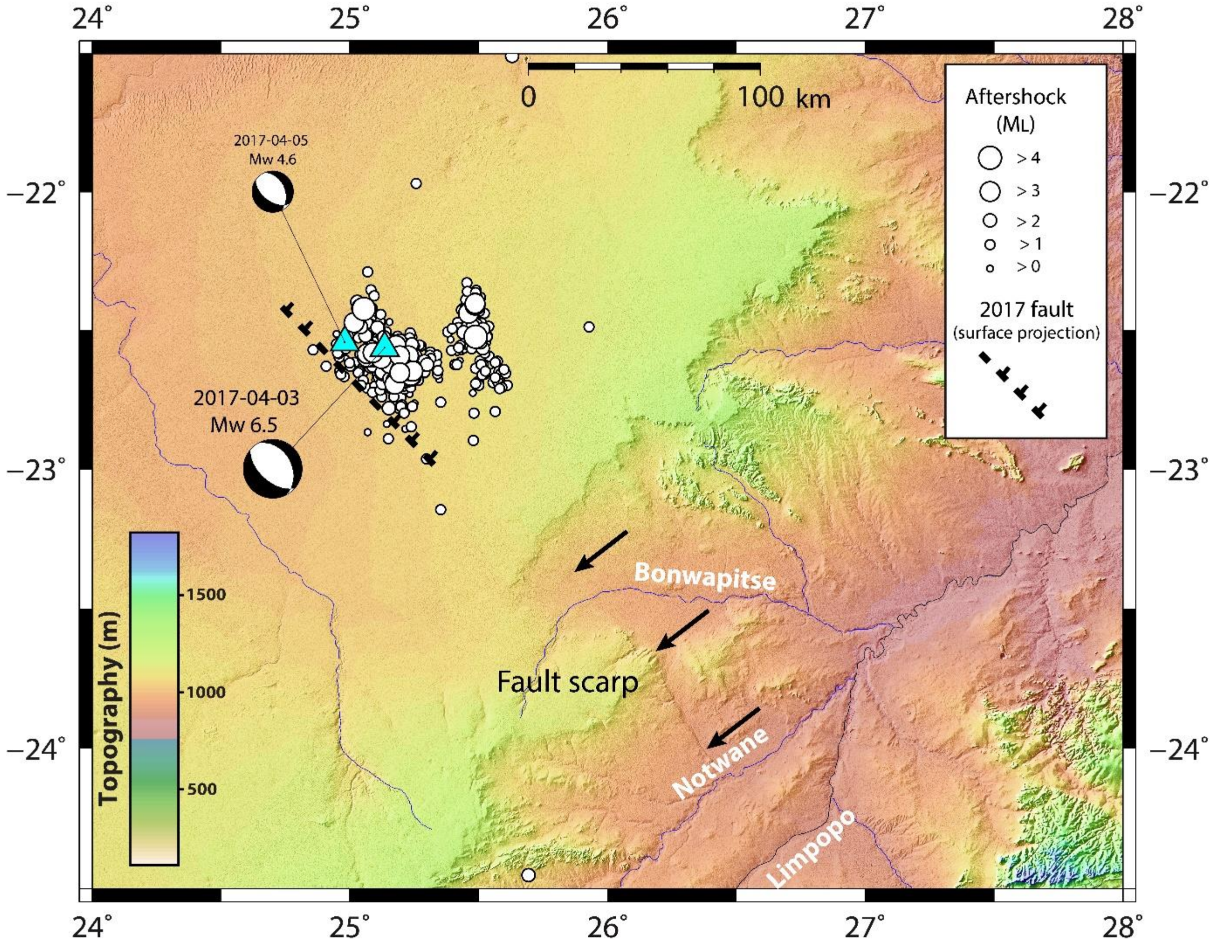

Figure 15: Identification of the Khurutse cumulative fault scarp (black arrows) southeast of the 2017 earthquake rupture indicated using a dashed line located from the projection of InSAR rupture (see Fig. 11). Also shown are the focal mechanisms of the mainshock and largest aftershock as presented in Tables 1 and SM4. Details of Khurutse fault scarp morphology are in landscape photos of Fig. 16 and map of Fig 17a. Background topography is from Shuttle Radar Topography Mission (SRTM) 1'' data.

Figure 16. Khurutse fault scarp with significant topographic offset. Left is fault scarp (view facing east) near profile A (24.004°S, 26.376°E) of Figs 17a and b; Right is fault scarp (view facing west) near profile B (23.967S, 26.350E) of Figs 17a and b. Fault scarps show composite and cumulative geomorphic structures that suggest repeated coseismic surface deformation.

The exposed NNW-SSE trending and ~80-km-long Khurutse fault scarp southeast of the 2017 epicentral area is aligned with the 2017 coseismic rupture and aftershock sequence (Fig 15). The escarpment is orthogonal to two main erosion valleys formed by different rivers and streams and crosses mainly Phanerozoic sediments. To the southeast, and although crossing an erosional valley, the fault scarp morphology is prominent and visible on left and right river channel banks (Fig. 17a) (Williamson, 1996). Differential GPS measurements of profiles across the fault scarp shows topographic offset ranging between 16.6 ± 1 m and 43.5 ± 1 m (Fig. 17b). All geomorphic profiles display a composite and sharp scarp morphology that reflects a cumulative surface deformation. The fault scarp height variation depends on the background geology and erosion effect and shows minimum and maximum topographic offsets in profiles A and D, respectively. That the linear morphology and scarp shape remain visible in the Limpopo Mobile Belt, is indicative of recent tectonic movement that may have resulted from incremental surface slip during past earthquakes.

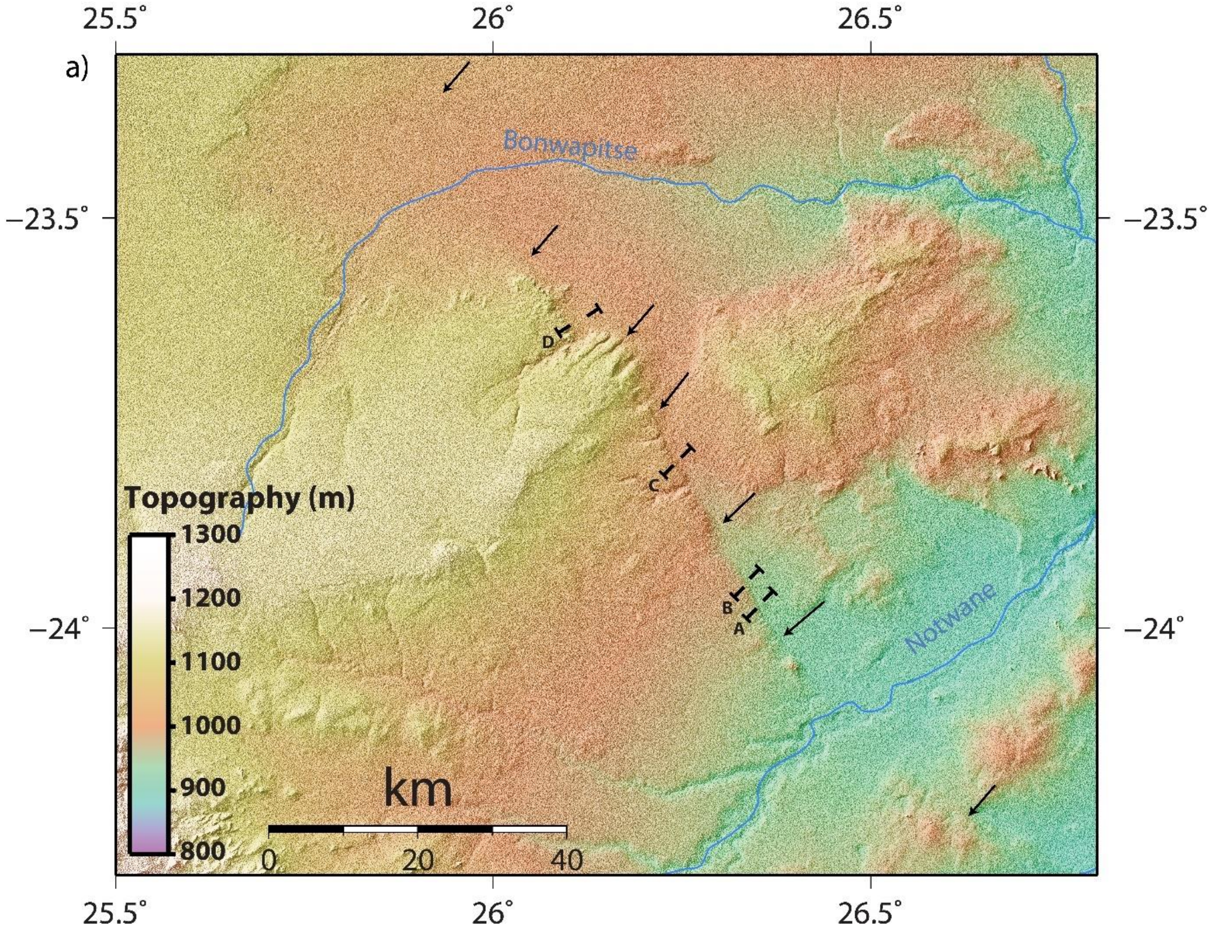

Figure 17. ***a)*** *Detail of the Khurutse fault scarps (arrows, see also arrows in Fig. 15) with location of the cross-section profiles of Fig. 17(b) denoted A to D (background topography from SRTM 1" data).*

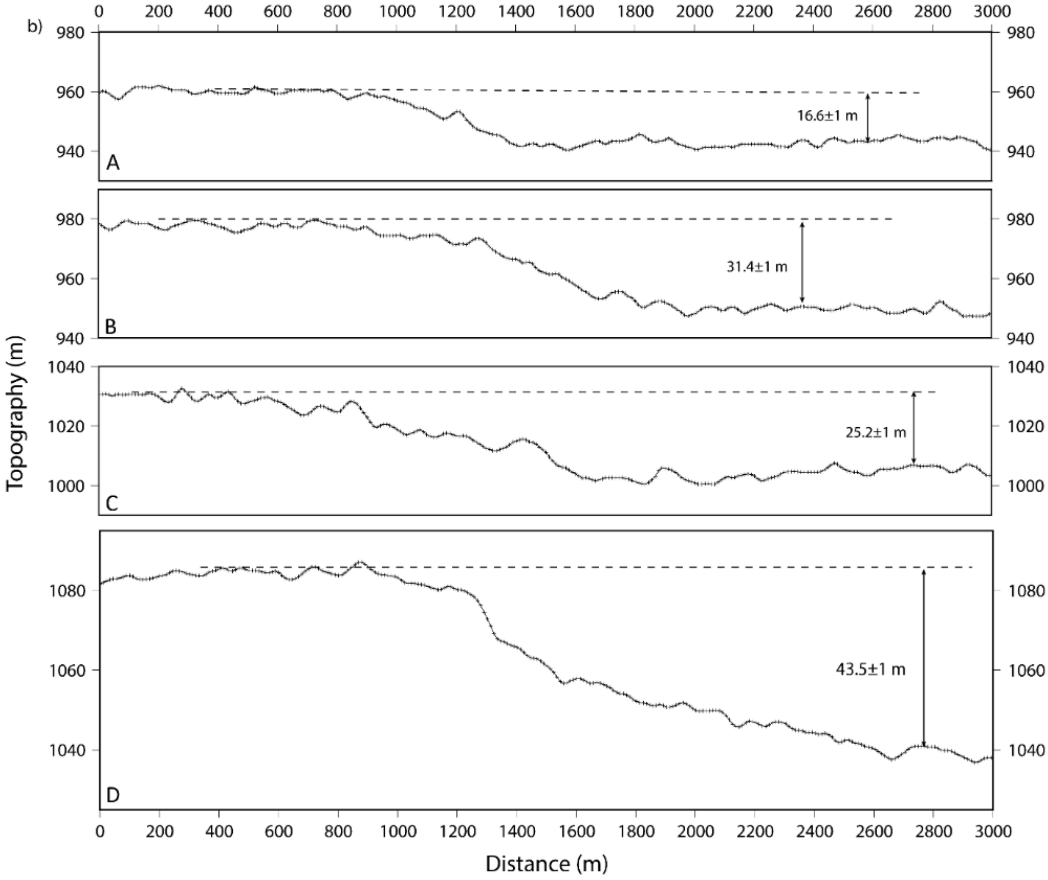

Figure 17. ***b)*** *Khurutse fault scarp cross-sections with measured geomorphic offsets, in meters.*

7 Discussion

Although previous studies using teleseismic data and InSAR provided initial results on the 2017 Moiyabana earthquake, our investigations present the integration of near field and remote sensing studies including seismology, seismotectonic and Radar satellite images. Field investigations using six portable seismic stations supplemented with data from nearby permanent broadband seismic stations and tectonic geomorphology combined with the study of InSAR data, brought new insights in the study of the 2017 Moiyabana earthquake (M_W 6.5). Focal mechanism solutions indicate that the mainshock ruptured on a NW-SE trending blind normal fault. More than 900 aftershocks shed light on the fault rupture geometry within ~30 km depth of the Limpopo Mobile Belt in Botswana. Two aftershock sequences range between 5 and 30 km depth and show the complexity of the active crustal structure that delineates a NW-SE trending, and 20 to 30 km wide graben structure. Most of the aftershocks are of normal faulting mechanism with a general NE-SW extension direction confirmed by the stress tensor inversion.

Interferograms obtained from the analysis of Sentinel 1A images display 2 to 3 fringes (from which we infer 3.86 to 5.15 cm vertical displacement) that form two lobes coincident with the mainshock and aftershock locations. The modelling of coseismic rupture and slip distribution obtained from the inversion of surface deformation suggests ~40-km-long and ~22-km-wide fault geometry with the fault striking 315°, dipping 45°, with -80° rake, with two asperities and a maximum 50 cm slip distribution. This is different from Albano *et al.* (2017) InSAR inferred coseismic model of 20- km-long rupture plane, dipping 65° to the northeast, with a right-lateral component, and 2.7 m maximum slip at depth. In the absence of near field seismicity data and using InSAR results with a Bayesian estimate of source parameters, Gardonio *et al*. (2018) suggest both ~17° and ~73° dipping fault planes and a poorly estimated hypocentre depth of 29 ± 4 km. From the inversion of InSAR results coupled with geophysical (aeromagnetic and gravity) data, Kolawole *et al.* (2017) test several fault patches and estimate 21 to 24 km hypocentre depth on a 53° NE dipping fault plane, comparable with our 22 ± 1.5 km depth and 45° NE dipping fault plane.

7.1 Rifting propagation within intraplate southern Africa

Large intraplate earthquakes ($M_W \geq 6$) in southern Africa may result from complex continental tectonics and elastic strain release with continuum deformation rather than movements of rigid blocks (Scholz *et al.*, 1976; Reeves *et al.*, 2004). The rifting of the Ghanzi-Chobe Proterozoic Belt, due to the extensional forces during the Kibaran Orogeny, gave rise to the beginning of the Okavango rifting (Leseane *et al.*, 2015). This is the area where a significant seismic sequence occurred on 11 September 1952 with M_L 6.1 and another of M_L 6.7 on 11 October 1952. The Zoetfontein fault is another active zone in Botswana which has been known to be seismically active, thus revealing a background seismicity associated with long-term deformation and faulting (Dorland *et al.*, 2006). Its boundary with the Zimbabwe Craton is on the Limpopo-Shashe Thrust Zone (Ranganai *et al.*, 2002). The 2017 Moiyabana earthquake reveals the existence of a NW-SE trending active normal fault zone within the Limpopo Mobile Belt in Botswana. Daly *et al.* (2020) investigated the Okavango normal fault system using SRTM1" and Pleaides images and identified NE to ENE trending faults with evidence of vertical displacement. At a larger scale, normal faulting mechanisms of Moiyabana, Okavango and Machaze active zones reflect the complex crustal deformation within the Nubian Plate (Kinabo *et al.*, 2008; Fenton and Bommer 2006; Fonseca *et al.*, 2014). As compared to the region where the 2017 Moiyabana earthquake is located, the EARS is much more seismically active, since it is a divergent plate boundary. Furthermore, the 2017 Moiyabana earthquake and Okavango active zones with related seismotectonic framework appear as an extension of the EARS to the west (Kinabo *et al.*, 2008). Hence, the Limpopo Mobile Belt and Okavango active zones mark the possible development of new rifting zones within Nubia active plate interior.

7.2 Seismotectonics of intraplate earthquakes in southern Africa

A detailed analysis of the mainshock and aftershocks of the 2017 Moiyabana earthquake sequence in Botswana and related surface deformation lead to a better understanding of the intraplate seismic activity in southern Africa. The coseismic fault has been documented by means of the two seismic sequences that illustrate the rupture geometry at depth. The use of two different software packages (SEISAN and HypoDD) for the earthquake locations provides an insight to the seismic sequence at depth that illustrates the fault rupture geometry. The coincidence in the location of mainshock, aftershocks, InSAR lobe results, and composite fault scarp reflects the long-term active deformation in the intraplate tectonic environment. Although the strain rate is rather low (~1 nanostrain/yr.), the occurrence of the 2017 Moiyabana earthquake constrains us to classify the Limpopo Mobile Belt as an active tectonic zone with a recurrent seismic strain release. These observations do not support the suggested hypothesis that the 2017 Moiyabana earthquake can be due to transient perturbations of local stresses due to pore fluid pressure (Gardonio *et al.*, 2018). The recurrence interval of large seismic events with surface deformation may reach several thousands of years that results from long-term but persistent seismic cycles (Camelbeeck and Meghraoui, 1998). In some regions such as Mongolia, major earthquakes in 1905 and 1957 with M_W 8 and 8.5, respectively, leave evidence of multiple rupture over the years (Chéry *et al.*, 2001). The study of recent earthquakes with near field investigations is crucial for a better understanding of the intraplate seismicity and active deformation in intraplate southern Africa.

8 Conclusion

The near field study of the 2017 Moiyabana earthquake (Mw 6.5) provides data and results on the crustal deformation of the intraplate tectonic domain of southern Africa. The detailed mainshock and aftershocks analysis shows a seismic sequence that suggests a fault-rupture geometry in agreement with normal focal mechanisms. The aftershocks analysis and focal mechanism solutions show predominately normal faulting that agrees with the NE-SW extensional stress regime in the region. Two distinct NW-SE to N-S trending aftershock sequences of more than 900 earthquakes processed using SEISAN, of which 699 aftershocks were relocated using the HypoDD program, are concentrated between 10 and 30 km depth. The distance between the two sequences being ~20 km, seismic events depict a graben-like structure where the mainshock and largest aftershock are located within the western sequence. The InSAR analysis shows the colocation of surface deformation with the western earthquake sequence and allows the modelling of a NW-SE trending fault rupture, dipping NE with an average 50 cm slip distribution and a seismic moment M_o 3.68 x 10^{18} Nm (Mw 6.4). SE of the epicentral area, we identified the NNW-SSE to NW-SE trending composite and sharp scarp morphology of the Khurutse fault scarp that aligns with the 2017 Moiyabana earthquake rupture. The active Okavango and Zoetfontein fault region, in the north and south of the Moiyabana earthquake location, respectively; indicate that the southern African continental region is active. In addition, the Khurutse fault scarp reflects a cumulative surface deformation, clearly highlighting the presence of a seismic cycle in this intraplate context.

Acknowledgements:

The work is supported by the Council of Geoscience (Pretoria), the Institut de la Terre et Environnement de Strasbourg (ITES) and UNESCO IGCP-659 project, and TM benefited from a Campus France scholarship of the French Embassy in Pretoria. The Council of Geoscience and Botswana Geoscience Institute provided field assistance for seismic stations deployment and for DGPS measurements of the Khurutse fault scarp. We are thankful to the European Space Agency for providing the Sentinel SAR images. We are indebted to Sophie Lambotte (ITE Strasbourg) for assistance in the relocation processing, Mohamed Khelif (CRAAG, Algiers) for assistance with SEISAN, Damien Delvaux for assistance with WinTensor program and Klaus Hinzen (University of Cologne) for discussion on an earlier version of manuscript. All figures have been produced using Generic Mapping Tools (Wessel & Smith 1998). We are also thankful to the Editor Mohamed G Abdelsalam and reviewer Sarah Stamps for their comments that improve the presentation of our manuscript.

References

Albano, M., Polcari, M., Bignami, C., Moro, M., Saroli, M., Stramondo, S., 2017. Did Anthropogenic Activities Trigger the 3 April 2017 Mw 6.5 Botswana Earthquake?, Remote Sens., 9 (10), 1028 – 1040.

Andreoli, M. A. G., Doucoure, M., Van Bever Donker, J., Brandt, D., Andersen, N. J. B., 1996. Neotectonics of southern Africa: A review, Afr. Geosci. Rev., 3(1), 1–16.

Angelier, J. Mechler, P., 1977. Sur une méthode graphique de recherche des contraintes principales également utilisable en tectonique et en séismologie: la méthode des dièdres droits, Bull. Soc. géol. Fr., 19, 1309 – 1318.

Begg, G. C., Griffin, W. L., Natapov, L. M., O’Reilly, S. Y., Grand, S. P., O’Neill, C. J., Hronsky, J. M. A., Poudjom Djomani, Y., Swain, C.J., Deen, T., Bowden, P., 2009. The Lithospheric Architecture of Africa: Seismic Tomography, Mantle Petrology, and Tectonic Evolution, Geosphere, 5, 23 – 50.

Bent, A. L., 1994. The 1989 (Ms 6.3) Ungava, Quebec, earthquake: A complex intraplate event, Bull. Seismol. Soc. Am., 84(4), 1075 – 1088.

Brown, R., Gernon, T., Stiefenhofer, J., Field, M., 2008. Geological constraints on the eruption of the Jwaneng Centre kimberlite pipe, Botswana. J. Volcanol. Geotherm. Res., 174 (1), 195 – 208.

Burbank, D. W., Anderson, R. S., 2001. Tectonic geomorphology, Blackwell Science Ltd, Oxford, United Kingdom.

Calais, E., T. Camelbeeck, Stein, S., Liu, M., Craig, T. J., 2016. A new paradigm for large earthquakes in stable continental plate interiors, Geophys. Res. Lett, 43(20), 10621 – 10637.

Camelbeeck, T., Meghraoui, M., 1998. Geological and geophysical evidence for large paleoearthquakes with surface faulting in the Roer Graben (northwest Europe), Geophys. J. Int., 132, 347 – 362.

Chéry, J., Carretier, S., Ritz, J.-F., 2001. Postseismic stress transfer explains time clustering of large earthquakes in Mongolia, Earth Planet. Sci. Lett., 194(1–2), 277–286, doi:10.1016/S0012-821X(01)00552-0.

Chisenga, C., Van der Meijde, M., Yan, J., Fadel, I., Atekwana, E. A., Steffen, R., Ramotoroko, C., 2020. Gravity derived crustal thickness model of Botswana: Its implication for the Mw 6.5 April 3, 2017, Botswana earthquake, Tectonophysics, 787. https://doi.org/10.1016/j.tecto.2020.228479

Clark, D., Dentith, M., Wyrwoll, K. H., Yanchoul, L., Dent, V., Featherstone, C., 2008. The Hyden fault scarp, Western Australia: paleoseismic evidence for repeated Quaternary displacement in an intracratonic setting, Aust. J. Earth Sci., 55, 379 – 395.

Crone, A. J., Machette, M. N., Bowman, J. R., 1997. Episodic nature of earthquake activity in stable continental regions revealed by palaeoseismicity studies of Australian and North American quaternary faults, Aust. J. Earth Sci., 44(2), 203–214.

Daly, M. C., Green, P., Watts, A. B., Davies, O., Chibesakunda, F., Walker, R., 2020. Tectonics and landscape of the Central African Plateau and their implications for a propagating Southwestern Rift in Africa, Geochemistry, Geophys. Geosystems, 21, 1 – 37, doi.org/10.1029/2019GC008746.

Delvaux, D., 1993. The TENSOR program for paleostress reconstruction: examples from the east African and the Baikal rift zones. EUG VII Strasbourg, France, 4–8 April 1993. Abstract supplement N°1 to Terra Nov. 5: 216.

Delvaux, D. B., Sperner, 2003. New aspects of tectonic stress inversion with reference to the TENSOR program. In: New Insights into Structural Interpretation and Modelling (D. Nieuwland Ed.). Geological Society, London, Special Publications 212: 75 – 100.

Delvaux, D., Barth, A., 2010. African stress pattern from formal inversion of focal mechanism data. Implications for rifting dynamics, Tectonophysics, 482, 105 – 128.

Dorland, H. C., Beukes, N. J., Gutzmer, J., Evans, D. A. D., Armstrong, R. A., 2006. Precise SHRIMP U-Pb zircon age constraints on the lower Waterberg and Soutpansberg Groups, South Africa, S Afr J Geol, 109, 139 – 156.

Fadel, I., Paulssen, H., van der Meijde, M., Kwadiba, M., Ntibinyane, O., Nyblade, A., Durrheim, R., 2020. Crustal and Upper Mantle Shear Wave Velocity Structure of Botswana: The 3 April 2017 Central Botswana Earthquake Linked to the East African Rift System, Geophys. Res. Lett, 47(4).

Farr, T. G., Rosen, P. A., Caro, E., Crippen, R., Duren, R., Hensley, S., Kobrick, M., Paller, M., Rodriguez, E., Roth, L., Seal, D., Shaffer, S., Shimada, J., Umland, J., Werner, M., Oskin, M., Burbank, D., Alsdorf, D., 2007. The Shuttle Radar Topography Mission, Rev. Geophys., 45, RG2004, doi:10.1029/2005RG000183.

Fairhead, J., Henderson, N., 1977. The seismicity of Southern Africa and incipient rifting, Tectonophysics, 41, 19–26.

Fenton, C., Bommer, J., 2006. The M_W 7 Machaze, Mozambique, earthquake of 23 February 2006, Seism. Res. Lett., 77, 426–439, doi:10.1785/gssrl.77.4.426.

Fonseca, J.F.B.D., Chamussa, J., Domingues, A., Helffrich, G., Antunes, E., van Aswegen, G., Pinto, L.V., Cust_odio, S., Manhiça, V.J., 2014. MOZART: a seismological investigation of the east African rift in Central Mozambique. Seismol Res. Lett. 85 (1), 108 – 116.

Fourie, C. J. S., Henry, G., Maré, L. P., 2014. The structure of the Karoo-age Ellisras Basin in Limpopo Province, South Africa in the light of new airborne geophysical data: a preliminary report, S Afr J Geol, 117 (2), 207 – 224.

Gardonio, B., Jolivet, R., Calais, E., Leclère, H., 2018. The April 2017 Mw6.5 Botswana Earthquake: An Intraplate Event Triggered by Deep Fluids, Geophys. Res. Lett, 45 (17), 8886 – 8896.

Hartnady, C., 1990. Seismicity and plate boundary evolution in Southeastern Africa, S. Afr. J. Geol., 93, 473–484.

Hough, S. E., Page, M., 2011. Toward a consistent model for strain accrual and release for the New Madrid Seismic Zone, central United States, J. Geophys. Res., 116, B03311, doi:10.1029/2010JB007783.

Johnston, A.C., 1996a. Seismic moment assessment of earthquakes in stable continental regions—I. Instrumental seismicity, Geophys. J. Int., 124 (2), 381– 414.

Johnston, A.C., 1996b. Seismic moment assessment of earthquakes in stable continental regions—II. Historical seismicity, Geophys. J. Int., 125 (3), 639 – 678.

Kinabo, B., Hogan, J., Atekwana, E., Abdel Salam, M. Modisi, M., 2008. Fault growth and propagation during incipient continental rifting: inside from a combined aeromagnetic and Shuttle Radar Topography Mission digital elevation model investigation of the Okavango Rift Zone, northwest Botswana, Tectonics, 27, doi:10.1029/2007TC002154.

Kolawole, F., Atekwana, E. A., Malloy, S., Stamps, D. S., Grandin, R., Abdelsalam, M. G., Leseane, K., Shemang E. M., 2017. Aeromagnetic, gravity, and Differential Interferometric Synthetic Aperture Radar (DInSAR) analyses reveal the causative fault of the 3 April 2017 Mw 6.5 Moiyabana, Botswana Earthquake, Geophys. Res. Lett, 44, 8837 – 8846.

Lekula, M., Lubczynskia, M. W., Shemang, E. M., 2018. Hydrogeological conceptual model of large and complex sedimentary aquifer systems – Central Kalahari Basin, Phys Chem Earth, 106, 47 – 62.

Leseane, K., Atekwana, E. A., Mickus, K. L., Abdelsalam, M. G., Shemang E. M., Atekwana, E. A., 2015. Thermal perturbations beneath the incipient Okavango Rift Zone, northwest Botswana, J. Geophys. Res. Solid Earth, 120 (2), 1210 – 1228.

Lienert, B. R., Berg, E., Frazer, L. N., 1986. Hypocenter: an earthquake location method using centered, scaled, and adaptively damped least squares, Bull. Seismol. Soc. Am., 76(3), 771 – 783.

Lienert, B. R., Havskov, J., 1995. A Computer Program for Locating Earthquakes Both Locally and Globally, Seismol. Res. Lett., 66 (5), 26 – 36.

Malservisi, R., Hugentobler, U., Wonnacott, R., Hackl, M., 2013. How rigid is a rigid plate? Geodetic constraint from the TrigNet CGPS network, South Africa, Geophys. J. Int., 192, 918 – 928.

Manzunzu, B., Midzi, V., Mangongolo, A., Essrich, F., 2017. The aftershock sequence of the 5 August 2014 Orkney earthquake (ML 5.5), South Africa, J. Seismol., 21, 1323 – 1334.

Maerten, F., Resor, P., Pollard, D., Maerten, L., 2005. Inverting for slip on three-dimensional fault surfaces using angular dislocations, Bull. Seismol. Soc. Am., 95 (5), 1654 – 1665.

Materna, K., Wei, S., Wang, X., Heng, L., Wang, T., Chen, W., Salman, R., Bürgmann, R., 2019. Source characteristics of the 2017 Mw6.4 Moijabana, Botswana earthquake, a rare lower-crustal event within an ancient zone of weakness, Earth Planet Sci Lett, 506, 348 – 359.

Meghraoui, M., Amponsah, P., Ayadi, A., Ayele, A., Ateba, B., Bensuleman, A., Delvaux, D., El Gabry, M., Fernandes, R., 2016. The Seismotectonic Map of Africa, Episodes, 39 (1), 9 – 18.

Midzi, V., Saunders, I., Brandt, M. B. C., Molea, T., 2010. 1-D velocity model for use by the SANSN in earthquake location, Seismol. Res. Lett., 81 (3), 460 – 466.

Midzi, V., Saunders, I., Manzunzu, B., Kwadiba, M. T., Jele, V., Mantsha, R., Marimira, K. T., Mulabisana, T. F., Ntibinyane, O., Pule, T., Rathod, G. W., Sitali, M., Tabane, L., van Aswegen, G., Zulu, B. S., 2018. The 03 April 2017 Botswana M6.5 earthquake: Preliminary results, J. African Earth Sci., 143, 187 – 194.

Modisi, M., Atekwana, E., Kampunzu, A., Ngwisanyi, 2000. Rift kinematics during the incipient stages of continental extension: evidence from the nascent Okavango Rift basin, northwest Botswana, Geology, 28, 939–942.

Moorkamp, M., Fishwick, S., Walker, R. J., Jones, A. G., 2019. Geophysical evidence for crustal and mantle weak zones controlling intra-plate seismicity – the 2017 Botswana earthquake sequence, Earth Planet Sci Lett, 506, 175 – 183.

Nguuri, T. K., Goree, J., James, D. E., Webb, S. J., Wright, C., Zengen, T. G., Gwavava, O., Snoke, J., A Kaapvaal Seismic Group, 2001. Crustal structure beneath southern Africa and its implications for the formation and evolution of the Kaapvaal and Zimbabwe cratons, Geophys. Res. Letters 28, 13, 2501-2504.

Njoroge, M., R. Malservisi, Voytenko, D., Hackl, M., 2015. Is Nubia Plate Rigid? A geodetic study of the relative motion of different cratonic areas within Africa, International Association of Geodesy Symposia, p 1-9, doi:10.1007/1345_2015_212

Okada, Y., 1985. Surface deformation due to shear and tensile faults in a half-space, Bull. Seismol. Soc. Am., 75 (4), 1135 – 1154.

Olebetse, T.A., Mmese, M.L., Simon, R.E., Maritinkole, J., 2020. Some Foreshocks and Aftershocks Associated with the Moiyabana Earthquake of 2017 in Botswana. Int. J. Geosci., 11, 238-250. https://doi.org/10.4236/ijg.2020.114013

Ottemöller, L., Voss, P., Havskov, J., 2018. SEISAN Earthquake Analysis Software for Windows, Solaris, Linux and Macosx. Bergen.

Rajendran, C. P., Rajendran, K., John, B., 1996. The 1993 Killari (Latur), central India, earthquake: An example of fault reactivation in the Precambrian crust, Geology 24, 651–654.

Ranganai, R. T., Kampunzu, A. B., Atekwana, E. A., Paya, B. K., King, J. G., Koosimile, D. I., Stettler, E. H., 2002. Gravity evidence for a larger Limpopo Belt in southern Africa and geodynamic implications, Geophys J Int., 149 (3), F9 – F14.

Reeves, C., de Wit, M. Sahu, B., 2004. Tight reassembly of Gondwana exposes phanerozoic shears in Africa as global tectonic players, Gondwana Res., 7, 7–19.

Roering, C., van Reenen, D. D., Smit, C. A., Barton, J. M., de Beer, J. H., de Wit, M. J., Stettler, E. H., van Schalkwyk, J. F., Stevens, G., Pretorius, S., 1992. Tectonic model for the evolution of the Limpopo Belt, Precambrian Res., 55, 539 – 552.

Ross, Z. E., Meier, M., Hauksson, E., 2018. P wave arrival picking and first-motion polarity determination with deep learning, J. Geophys. Res. Solid Earth, 123 (6), 5120 – 5129.

Sandwell, D., Mellors, R., Tong, X., Wei, M., Wessel, P., 2011. GMTSAR: An InSAR Processing System Based on Generic Mapping Tools. UC San Diego: Scripps Institution of Oceanography. Retrieved from: http://escholarship.org/uc/item/8zq2c02m.

Saria, E., Calais, E., Stamps, D.S., Delvaux, S. Hartnady, C.J.H., 2014. Present-day kinematics of the East African Rift, J. geophys. Res., 119, doi:10.1002/2013JB010901.

Saunders, I., Brandt, M.B.C., Molea, T.T., Akromah, L. Sutherland, B., 2010. Seismicity of Southern Africa during 2006 with special reference to the Mw 7 Machaze earthquake. S Afr J Geol, 113, 4, 369-380.

Scholz, C., Kocynski, T. Hutchins, D., 1976. Evidence for incipient rifting in Southern Africa, Geophys. J. R. astr. Soc., 44, 135–144.

Stamps, D. S., Flesch, L. M., Calais, E., Ghosh, A., 2014. Current kinematics and dynamics of Africa and the East African Rift System, J. Geophys. Res. Solid Earth, 119, 5161 – 5186, doi:10.1002/2013JB010717.

Stamps, D. S., Saria, E., Kreemer, C., 2018. A Geodetic Strain Rate Model for the East African Rift System, Sci. Rep., 8(1), 1 – 8.

Thomas, A., 2020. Mapping of Surface Deformation and Displacement Associated with the 6.5 Magnitude Botswana Earthquake of 3 April 2017 Using DInSAR Analysis, Geomat. Environ. Eng., 14, 4, https://doi.org/10.7494/geom.2020.14.4.81

Utsu T., Ogata, Y., Matsu'ura ; R.S., 1995. The centenary of the Omori formula for a decay law of aftershock activity, J. Phys. Earth, 43, 1-33.

Waldhauser, F., Ellsworth, W. L., 2000. A Double-Difference Earthquake Location Algorithm: Method and Application to the Northern Hayward Fault, California, Bull. Seismol. Soc. Am., 90 (6), 1353 – 1368.

Waldhauser, F., 2001. HypoDD: A computer program to compute double-difference earthquake locations, USGS Open File Rep., 01-113.

Wessel, P., Smith, H.F., 1998. New, improved version of the generic mapping tools released. EOS Trans. AGU 79, 579.

Williamson, I. T., 1996. The geology of the areas around Mmamabula and Dibete: including an account of the Greater Mmamabula Coalfield, Geological Survey Department: District Memoir 6, Chapter 1, pp 03.

Zoback, M. L., Zoback, M. D., 1989. Tectonic stress field of the continental United States: In Geological Society of America Memoir 172, Chapter 24, 523 – 539.

Tables

Seismological Centre	Long. (°)	Lat. (°)	M_0 (Nm)	M_w	Depth (km)	Strike	Dip	Rake
USGS (Wpha)	25.15	-22.678	$6.19\ 10^{18}$	6.5	23.5	343	44	-62
GFZ	25.22	-22.66	$6.3\ 10^{18}$	6.5	27	331	37	-73
Geoscope	25.15	-22.678	$5.86\ 10^{18}$	6.4	29	333	36	-72
CMT Harvard	25.21	-22.54	$7.01\ 10^{18}$	6.5	30	332	41	-70
CGS (Pretoria) Midzi et al. (2018)	25.134	-22.565	-	6.5	26.5 ±2.5	340	46	-61
This study (InSAR)	25.134	-22.565	$3.68\ 10^{18}$	6.4	22 ±1.5	315	45	-80

***Table 1**: Source parameters of the 3 April 2017 earthquake.*

Modified depth to top of layer (km)	**P-wave velocity (km/s)**
0.00	5.80
20.00	6.50
38.00	8.04

***Table 2**: Velocity model (Midzi et al., 2010) used in initial location of aftershocks using Seisan software as well as in the double difference relocation using the hypoDD software.*

Table Captions

Table 1: Source parameters of the 3 April 2017 earthquake.

Table 2: Velocity model (Midzi et al., 2010) used in initial location of aftershocks using Seisan software as well as in the double difference relocation using the hypoDD software.

Supporting Information

Supplementary Material:

- SM1: Table of Focal Mechanisms of Fig. 1.
- SM2: Spatial distribution and cross section of aftershock locations before and after the 8th of April 2017 (installation of temporary network).
- SM3: Spatial distribution of aftershock locations before and after DD relocation.
- SM4: Table of list of aftershocks and focal mechanisms.
- SM5: InSAR processing and modelling.

Resources

- Topography GEBCO: https://www.gebco.net/data_and_products/gridded_bathymetry_data/
- Topography SRTM 3" and 1": https://topex.ucsd.edu/gmtsar/demgen/
- Database of the Seismotectonic Map of Africa: Meghraoui et al., 2016
- ESA Sentinel images : https://sentinel.esa.int/web/sentinel/sentinel-data-access
- SEISAN package : ftp://ftp.geo.uib.no/pub/seismo/SOFTWARE/SEISAN/
- HypoDD: https://www.ldeo.columbia.edu/~felixw/hypoDD.html
- WinTensor software: http://damiendelvaux.be/Tensor/WinTensor/win-tensor_download.html

Supporting Information

Supplementary Material:

SM1: Table of Focal Mechanisms of Fig. 1.

Longitude	Latitude	Depth	Strike1	Dip1	Rake1	Strike2	Dip2	Rake2	Moment
26.07	-15.89	28.5	287	22	-116	135	70	-80	23
28.62	-15.77	10.0	215	13	-71	16	77	-94	23
26.88	-27.92	28.3	11	45	-61	153	52	-115	23
33.27	-21.25	12.6	254	30	-99	83	60	-85	23
33.15	-21.23	28.7	342	49	-77	142	42	-104	23
33.33	-21.09	22.9	352	40	-89	171	50	-91	23
33.12	-21.03	12.0	360	28	-69	157	64	-101	23
33.34	-21.01	12.0	305	44	-137	181	61	-54	23
33.36	-20.98	12.0	301	51	-139	182	60	-48	24
33.02	-20.98	10.0	187	45	-69	338	49	-110	23
33.40	-20.94	12.0	18	41	-73	176	51	-104	23
33.35	-20.93	12.0	166	50	-68	314	45	-114	23
33.15	-20.89	12.0	170	45	-106	12	47	-75	23
33.12	-20.88	12.0	14	39	-70	168	54	-106	23
33.09	-21.3	19.8	120	44	-116	333	52	-67	23
33.17	-21.39	12.0	17	42	-59	158	55	-115	23
33.19	-21.36	22.4	352	39	-90	172	51	-90	24
33.26	-21.51	15.0	345	35	-111	190	58	-76	23
33.37	-21.58	15.5	179	89	-31	290	67	-135	23
33.37	-21.32	12.0	326	24	-111	168	67	-81	26
33.58	-21.41	30.4	22	37	-61	167	59	-110	23
26.69	-28.05	28.3	11	45	-61	153	52	115	23
27.52	-26.37	2.0	354	49	86	167	41	-95	22
27.54	-26.35	1.0	296	88	144	28	54	3	22
33.18	-21.33	12.0	354	32	-89	172	58	-91	24
33.33	-21.09	22.9	352	40	-89	171	50	-91	23
33.59	-21.61	19.8	120	44	-116	333	52	-67	23

Longitude	Latitude	Depth	Strike	Dip	Rake	Magnitude
19.47	-33.17	10	154	74	20	5.6
19.32	-33.19	5	305	87	3	6.3
26.10	-15.92	30	36	34	-113	5.6
28.84	-30.53	15	168	37	-90	5.3
25.17	-29.51	8	120	63	-39	5.6
25.11	-29.56	8	126	64	-77	5.7
26.90	-27.90	2.3	190	45	-70	5.9
34.65	-15.63	17	47	50	236	5.1
33.49	-21.42	10	190	51	-70	5.3
36.00	-16.50	0	197	68	164	6.6
19.31	-33.34	15	305	78	-1.2	6.2
19.31	-33.34	10	334	74	160	5.8
28.72	-16.48	6	206.8	42.6	-75.5	5.3
27.90	-16.71	20	213.4	51.8	-59.2	5.0
25.17	-29.51	5.5	308	22	-86	5.8

SM2: Spatial distribution and cross section of aftershock locations before and after the 8th of April 2017 (installation of temporary network).

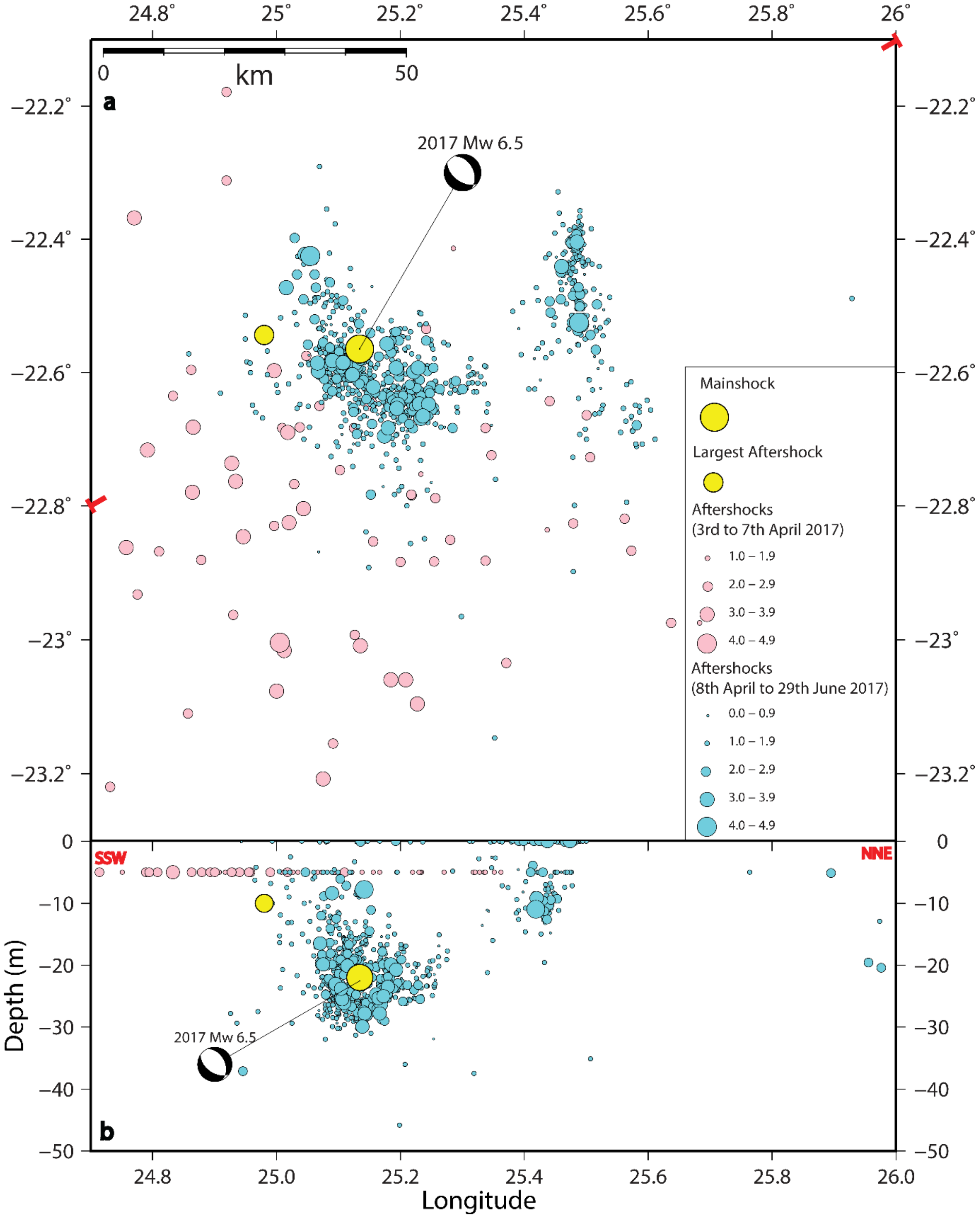

SM3: Spatial distribution of aftershock locations before and after DD relocation.

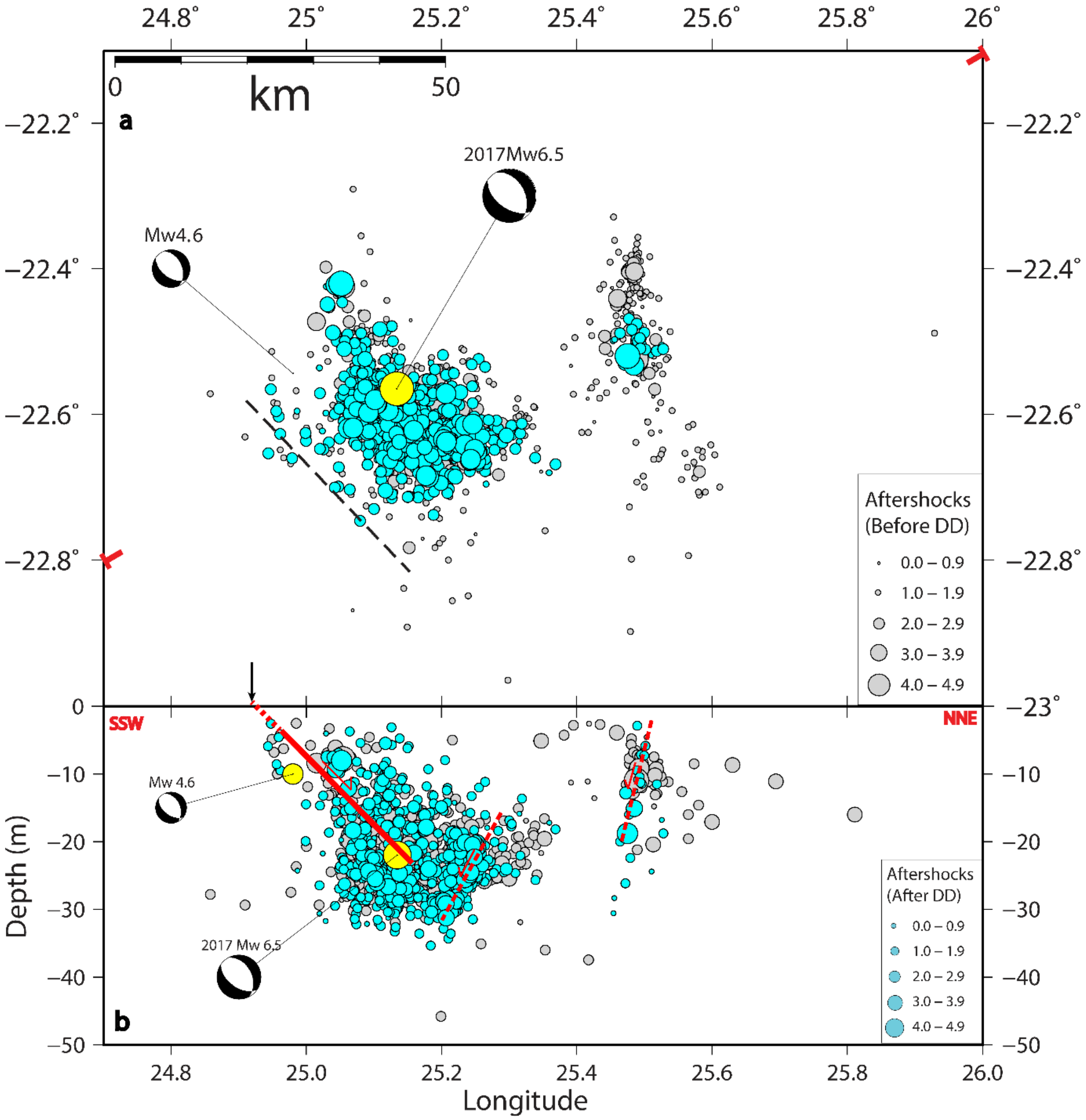

SM4: Table of list of aftershocks and focal mechanisms.

Focal mechanism solutions for the mainshock and 46 aftershocks of the 2017 earthquake sequence.

Year	Month	Day	Hour	Minutes	Seconds	Latitude	Longitude	Depth (km)	RMS (s)	Magnitude (M_L)	Strike	Dip	Rake
2017	4	3	17	40	13.40	-22.565	25.134	26.5	0.3	6.5 ($_W$)	332	41	-70
2017	4	5	0	55	48.60	-22.544	24.980	10.0	0.5	4.6 ($_W$)	336	42	-67
2017	4	8	16	22	24.10	-22.423	25.046	08.0	0.2	3.3	285	30	-90
2017	4	8	16	50	29.60	-22.599	25.221	19.9	0.2	3.3	250	50	-90
2017	4	8	17	31	30.70	-22.473	25.015	08.4	0.1	3.5	255	62	-67
2017	4	8	19	55	34.80	-22.425	25.054	07.8	0.1	4.5	180	20	-90
2017	4	9	1	30	16.50	-22.654	25.240	24.1	0.1	2.5	200	80	-90
2017	4	9	7	3	11.80	-22.593	25.228	20.7	0.2	3.3	310	40	-90
2017	4	10	2	51	03.50	-22.598	25.067	16.5	0.3	3.5	333	45	-90
2017	4	10	3	38	57.30	-22.664	25.239	25.7	0.3	2.7	328	47	-69
2017	4	10	19	28	12.60	-22.636	25.194	28.2	0.4	2.6	30	70	-30
2017	4	11	6	39	34.90	-22.588	25.111	24.7	0.4	2.8	200	68	-46
2017	4	11	7	40	13.00	-22.648	25.221	26.7	0.2	2.8	0	35	-90
2017	4	11	22	11	40.20	-22.647	25.230	26.3	0.4	3.1	137	76	-75
2017	4	13	3	43	18.50	-22.639	25.192	26.1	0.2	2.6	42	32	-71
2017	4	13	10	40	48.60	-22.653	25.254	22.2	0.3	2.6	206	24	-44
2017	4	13	18	41	22.20	-22.648	25.195	27.8	0.3	3.2	275	80	-44
2017	4	14	13	28	49.60	-22.628	25.090	18.3	0.3	2.8	171	41	-75
2017	4	16	5	41	12.10	-22.649	25.218	27.6	0.3	2.7	168	68	-35
2017	4	17	10	27	13.80	-22.658	25.219	26.7	0.2	2.7	147	55	-73
2017	4	18	7	42	10.00	-22.593	25.193	27.8	0.1	3.1	145	64	-56
2017	4	19	9	27	13.8	-22.622	25.156	22.4	0.2	3.5	264	42	-67
2017	4	20	9	34	16.30	-22.595	25.104	23.4	0.3	2.8	218	49	-11
2017	4	21	0	48	56.30	-22.598	25.198	22.2	0.2	2.8	32	41	-401
2017	4	21	18	27	39.60	-22.592	25.132	26.7	0.2	2.9	74	37	-11

2017	4	21	20	10	33.00	-22.639	25.212	25.6	0.3	2.5	179	64	-56
2017	4	22	6	28	10.70	-22.648	25.245	23.5	0.2	3.1	275	85	-90
2017	4	23	16	21	36.10	-22.631	25.247	20.8	0.2	2.9	46	74	-49
2017	4	24	9	4	23.90	-22.669	25.233	24.7	0.2	3.5	132	45	-79
2017	4	24	17	53	42.00	-22.665	25.236	25.3	0.2	3.2	159	52	-75
2017	4	25	13	21	20.10	-22.520	25.061	26.5	0.3	2.7	329	44	-61
2017	4	26	17	17	49.40	-22.635	25.204	25.4	0.2	2.5	52	23	-26
2017	4	27	5	34	35.60	-22.585	25.107	25.5	0.4	3.2	183	81	-70
2017	5	1	2	30	39.10	-22.695	25.174	23.8	0.2	3.3	170	62	-67
2017	5	1	8	44	01.90	-22.683	25.180	20.1	0.2	3.5	162	46	-68
2017	5	5	16	40	11.80	-22.654	25.194	29.9	0.1	3.1	184	76	-75
2017	5	6	14	37	59.50	-22.541	25.151	20.3	0.2	2.8	292	44	-22
2017	5	6	18	0	05.90	-22.557	25.178	25.0	0.1	3.6	357	53	-65
2017	5	7	12	37	18.40	-22.552	25.241	24.0	0.2	2.5	260	60	-90
2017	5	7	14	52	39.20	-22.593	25.253	23.2	0.2	2.9	292	44	-90
2017	5	10	4	39	20.90	-22.576	25.165	22.0	0.2	2.6	12	54	-37
2017	5	12	19	4	12.10	-22.553	25.185	21.9	0.2	2.7	304	64	-56
2017	5	13	5	54	31.00	-22.611	25.181	20.4	0.2	2.7	329	41	-40
2017	5	18	23	20	50.40	-22.441	25.460	04.5	1.1	3.8	340	81	-29
2017	6	21	7	10	32.30	-22.525	25.488	11.0	0.3	4.2	161	64	-56
2017	6	29	0	22	03.50	-22.404	25.485	00.1	0.4	3.3	6	49	-71

SM5: InSAR processing and modelling.

Modelling of fault rupture using Poly3Dinv

In order to model the earthquake rupture, we used the surface deformation (LOS) obtained from InSAR data. We invert the coseismic surface slip using planar surfaces constructed from triangular elements from the Poly3Dinv program (commercial) and a damped least square minimization. The method is based on the analytical solution for a triangular dislocation in a linear, elastic, homogeneous and isotropic half space, which uses triangular surfaces as discontinuities [Maerten et al, 2005]. The inversion allowed us to construct fault models that illustrate plate interface rupture planes with the corresponding slip distribution at depth.

We can describe the relationships between slip on the intraplate fault and ground displacements by the inversion formalism of Poly3DInv (Maerten et al., 2005):

$$d_i = \sum_{j=1}^{n} G_{ij} s_i + E$$

where ***G*** is the elastic response of the Earth (Green's functions), ***s*** is the fault slip and $\boldsymbol{d_i}$ is displacement observed at ground surface. Using the equation we invert the calculated surface displacement (coastal uplift and subsidence) to estimate the slip distribution along the fault.

The modelling procedure requires a rupture dislocation divided into fault surfaces meshed with triangles using MATLAB. To avoid unphysical oscillatory slip, the scale-dependant smoothing operator 0.3 and Poisson ratio 0.25 for Poly3Dinv are applied to the inverted slip distribution. In order to constrain the location, depth and geometry of the fault rupture at plate interface we run a series of inversions (see Fig. 13).

The following equation aims at minimizing the difference between the model (***Gs-d***) and the observed displacement (***Ds***)

$$\min\left[\left\|\mathbf{Gs} - d\right\|_2 + \varepsilon^{-2}\left\|\mathbf{Ds}\right\|_2\right]$$

We test the inversion results by the application of different parameters including the roughness and smoothing, and fault geometry (meshes) in order to reach the best fit solution

Main normal fault rupture parameters are strike = 315°, dipping 45°, -80° rake, ~40-km-long and ~22-km-wide fault geometry with a 3.68 10^{18} seismic moment. The coseismic maximum slip = 0.50 m on the fault plane.

References

Maerten F., Resor P., Pollard D., & Maerten L., 2005. Inverting for slip on three-dimensional fault surfaces using angular dislocations, *Bulletin of the Seismological Society of America*, **95 (5)**, 1654 – 1665.

Resources

- Topography GEBCO: https://www.gebco.net/data_and_products/gridded_bathymetry_data/
- Topography SRTM 3” and 1”: https://topex.ucsd.edu/gmtsar/demgen/
- Database of the Seismotectonic Map of Africa: Meghraoui et al., 2016
- ESA Sentinel images : https://sentinel.esa.int/web/sentinel/sentinel-data-access
- SEISAN package :
- HypoDD: https://www.ldeo.columbia.edu/~felixw/hypoDD.html
- WinTensor software: http://damiendelvaux.be/Tensor/WinTensor/win-tensor_download.html

Chapter 3

Chapter 3: “Tectonic Geomorphology in KwaZulu-Natal (KZN), South Africa: Active faulting background for the 31/12/1932, MW 6.9 earthquake” manuscript.

In this chapter I characterise faults in Kwazulu-Natal, with relation to the 1932 MW 6.9 St Lucia earthquake, to determine long time seismic cycle, for the benefit of improving seismic hazard assessment. The relatively low level of seismic activity and low deformation rate require an understanding of the long-term active tectonics and recurrence interval of large and damaging earthquakes. Hence, a detailed investigations in seismotectonics and tectonic geomorphology of the 1932 St Lucia earthquake area with the objective of characterising physical parameters of active faults is necessary for the improvement of seismic hazard assessment in the KwaZulu-Natal (KZN) region. I integrate studies such as tectonic geomorphology, geophysics, and geology to determine the fault characteristic along Tugela and Greytown fault scarp, alongside the reanalysis of the 1932 MW 6.9 St Lucia earthquake. This is done with the purpose of supplement the seismotectonics of southern Africa so as to improve the seismic hazard within this intraplate region.

Tectonic Geomorphology in KwaZulu-Natal (KZN), South Africa: Active faulting background for the 31/12/1932, M_W 6.9 earthquake

Mulabisana, T. [1, 2, 3 *], Meghraoui, M.[1], Okal, E.,[4], Chirenje, E. [2], Midzi, V.[2],
Sekiba, M.[2], Sebothoma, S. [2]

[1]EOST- ITES, CNRS-UMR 7063, University of Strasbourg, France
[2]Council for Geoscience, Pretoria, South Africa
[3]Nelson Mandela University, Port Elizabeth, South Africa
[4]Department of Earth & Planetary Sciences, Northwestern University, Illinois, USA
* Corresponding author

16th November 2022

Abstract

The characterisation of faults within intraplate regions, especially those with longer seismic cycles, is beneficial to the improvement of seismic hazard assessment. In southern Africa, the link between the instrumental, historical, and paleo-seismic activity with active faults is often difficult due to low seismic strain rate (< 1 mm/yr) and sparse distribution of seismic stations. The relatively low level of seismic activity and low deformation rate require an understanding of the long-term active tectonics and recurrence interval of large and damaging earthquakes. Here, we perform detailed investigations in seismotectonics and tectonic geomorphology of the 1932 St Lucia earthquake area with the objective of characterising physical parameters of active faults necessary for seismic hazard assessment in the KwaZulu-Natal (KZN) region. First, we delineate the seismic and tectonic characteristics of the E-W and ENE-WSW trending Tugela and Greytown fault scarps, respectively, as a structural background of past earthquakes. We proceed with the description of geomorphic markers of fault scarps using tectonic geomorphology. Airborne magnetics added with electrical resistivity tomography and seismic reflection profiles are used as ground geophysical methods to further investigate physical fault geometries. In addition, the intraplate activity within the KZN region is also explored using strain rate calculated from GPS data. The integration of these studies shows evidence of active faulting with right lateral offsets along the Tugela and Greytown fault scarps. The late Quaternary tectonic activity and characteristics of the Tugela fault suggest a possible correlation with 1932 earthquake. Field investigations along fault scarps combined with geophysical and seismotectonic studies will likely lead to a realistic seismic hazard assessment in the KZN region.

Keywords: Active faults, tectonic geomorphology, active deformation, geophysical profiles, seismic hazard assessment.

1 Introduction

The seismotectonic characteristics and identification of Quaternary surface faulting in many zones of stable continental regions have led to recent improvements in the seismic hazard studies (Johnston, 1996a, 1996b; Landgraf et al., 2017). In southern Africa, the link between the instrumental and historical seismic activity with active faults is often difficult due to low seismic strain rate (Andreaoli et al., 1996; Manzunzu et al., 2019). The relatively low level of seismic activity and low deformation rate (< 1 mm/yr; Hartnady, 1990; Malservisi et al., 2013) require an understanding of the long-term active tectonics and recurrence intervals of large and damaging earthquakes. Detailed investigations in tectonic geomorphology and paleoseismology with the objective of seismic and physical characterisation of active faults are pointed out as necessary for the subsequent seismic hazard assessment (Goedhart and Booth, 2016a, 2016b; Meghraoui et al., 2016). Goedhart and Booth (2016a, b) conducted palaeoseismic investigations along the Kango fault and determined a vertical displacement of 2 m with evidence of a paleo-earthquake of magnitude of $6.97 \leq M_W \leq 7.18$. The identification and characterisation of active and seismogenic faults for seismic hazard assessment in southern Africa has always been a challenge, as observed in Midzi et al. (1999) hazard assessment conducted with areal sources and Singh et al. (2011) conducting areal seismotectonics.

The interplay between active tectonics and surface processes contributes to the build-up of a topography with landforms and tectonic geomorphology over thousands to millions of years. Tectonic geomorphology can be used to investigate evidence of earthquake deformation with geomorphic markers due to coseismic surface faulting (Burbank and Anderson, 2009). In intraplate regions, studies of earthquake surface deformation such as in eastern continental Canada by Bent (1994); Australia and North America by Crone et al. (1997); in the lower Rhine Graben of Europe by Camelbeeck and Meghraoui (1998); and Meghraoui et al. (2001); Australia by Clark et al. (2008); Botswana by Mulabisana et al. (2021) indicate the evidence of strong earthquakes seismic cycle. Bent (1994) modelled long and short period seismograms of the 1989 M_S 6.3 Ungava earthquake to analyse the complexity of the fault orientation from source time function and field observations of surface rupture, concluding their compatibility with thrust and strike slip rupture. Camelbeeck and Meghraoui (1998) carried out paleoseismic investigations in the Roer Valley, giving evidence of seismogenic faults generated by large earthquakes in intraplate Europe. Meghraoui et al. (2001) also substantiate this hypothesis of large earthquakes occurring within intraplate Europe by identifying the 1356 Basel earthquake using palaeoseismic studies. Similarly, Clark et al. (2008) details the evidence of a seismic cycle along the Haiden region of Western Australia, concluding that the Haiden fault is prone to producing large earthquakes (Crone et al., 1997). The occurrence of the M_W 6.5 2017 Moiyabana (Botswana) earthquake further supports the existence of seismic cycles within continental regions in intraplate southern Africa (Mulabisana et al., 2021).

In this paper, we first delineate the seismic and tectonic characteristics of the KZN region, as a structural background of the 1932 St Lucia earthquake. We proceed with the description of geomorphic markers of the Tugela and Greytown fault scarps crossing Quaternary basins using tectonic geomorphology. Further investigations along those fault scarps using regional and ground geophysical methods such as Airborne Magnetics, Electrical Resistivity Tomography (ERT) and Reflection Seismic profiles attest to active deformation. Furthermore, the intraplate activity within the KZN region is explored using strain rate calculated from GPS data. We finally discuss the implications for the seismic hazard assessment.

2 Tectonic setting of KwaZulu-Natal

The KwaZulu-Natal region in South Africa consists of basement geology that is dominated by the Palaeo-Mesorchean Kaapvaal Craton welded together with the Mesoproterozoic Namaqua-Natal Belt. The Kaapvaal Craton which formed between 3.7 and 2.7 Ga covers approximately 1.2 million km^2 (de Wit et al., 1992) and represents the oldest tectonic region in southern Africa (Johnston et al., 1994). The Kaapvaal Craton can be subdivided into the Kimberley, Witwatersrand, Pietersburg, and Swaziland Terranes (Figure 1), which were assembled before the extrusion of the Ventersdorp lavas at 2.7 Ga (de Wit et al., 1992). The southern margin of the Kaapvaal Craton is bounded by the ~ 400 km Mesoproterozoic Namaqua-Natal Belt (Cornell et al., 2006). The Namaqua sector of the Namaqua-Natal Belt is bordered on its north-eastern boundary by the Paleoproterozoic Kheis Mobile belt (de Wit et al., 1992; Cornell et al., 2006; Adams and Nyblade, 2011). The Kheis Mobile Belt was described as a thin-skinned region with east-verging thrust belt characteristics (Cornell et al., 2011). The Pongola rift, situated near the eastern edge of the Kaapvaal Craton, later underwent reactivation as a compressional zone, probably in the late Proterozoic (Johnston et al., 1994).

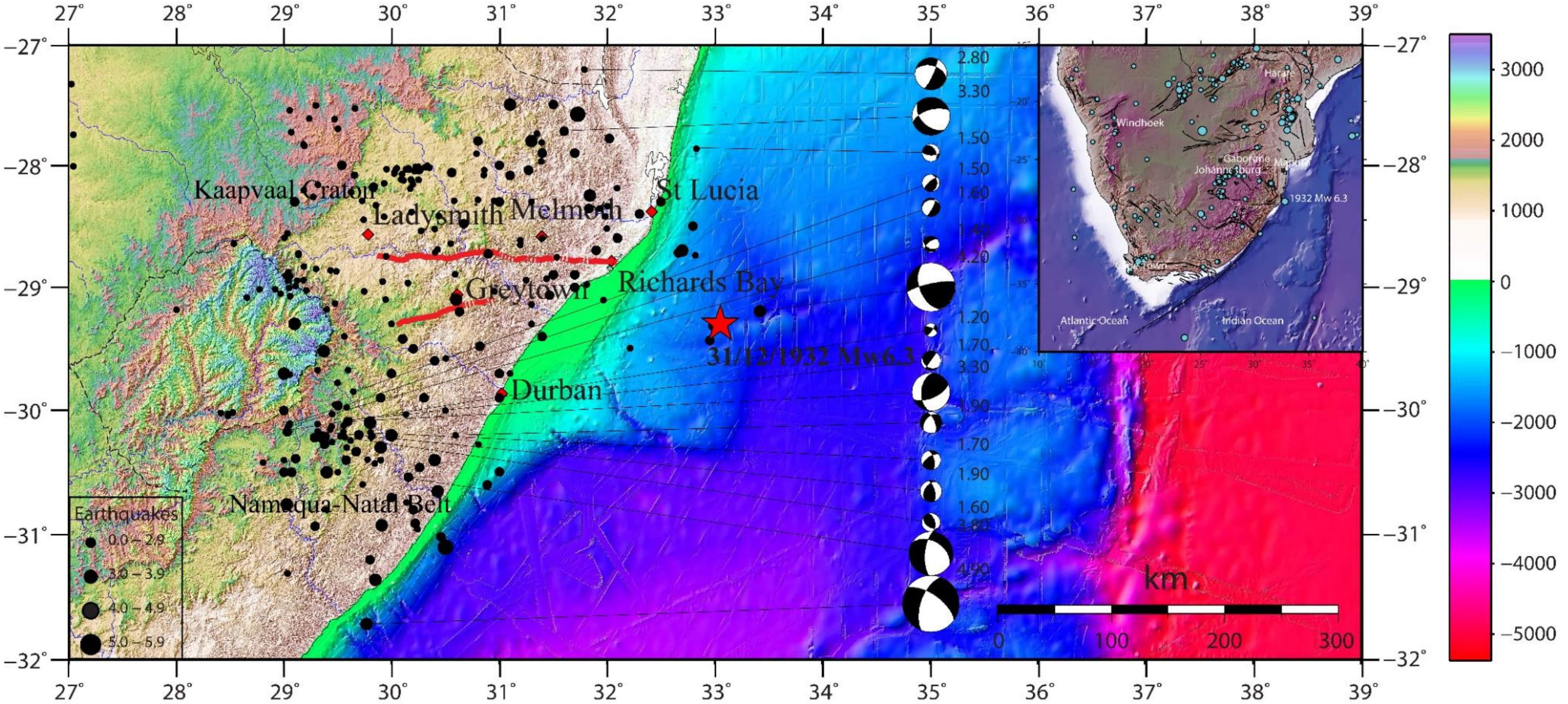

Figure 1: Tectonic Framework of KwaZulu-Natal showing Kaapvaal Craton and Namaqua-Natal Mobile Belt. Tugela and Greytown fault scarps are shown in red lines traced from SRTM1 (Farr et al., 2007), earthquakes in black circles with focal mechanism solutions from the South African National Seismic Network (SANSN) and offshore bathymetry from GEBCO Gridded Bathymetry Data Downloaded from https://download.gebco.net/. The red star shows this study's relocated epicentre of the 1932 M_W 6.9 St Lucia, KwaZulu-Natal. The southern African map inset shows seismicity in cyan circles and the 1932 M_W 6.9 St Lucia, KwaZulu-Natal, is labelled in white text.

3 The 1932 St Lucia Earthquake Revisited

The morning of 31 December 1932 at 06:31, an earthquake of magnitude M_W 6.9 shook the residents of KwaZulu-Natal, South Africa. Though effort was previously made to determine the location of this event, available solutions (Krige and Venter, 1933; Gutenberg and Richter, 1954) are uncertain. Thus, we considered reanalysing the event and collected 14 seismograms from seismic stations listed in the bulletin of the International Seismological Centre which enabled us to study the event waveforms in detail. However, there were not enough quality waveforms with good station distribution. Therefore, we relocated the earthquake using the arrival times listed in the ISC bulletin, following the technique of Wysession et al. (1991), which includes an estimate of an ellipse of confidence based on a Monte Carlo process consisting of injecting Gaussian noise into the dataset (Figure 3). The solution uses 45 P and S arrival times and converges to 29.30°S, 33.04 °E, approximately 100 km SSE of the historical locations, the ISC one (28.50°S, 32.80°E) being much closer to the shore, and Gutenberg and Richter (1954) (28.50°S, 32.75°E) possibly representing a simple transcription of the ISC epicentre to the nearest quarter degree. It is noteworthy that modern locations (29.08°S, 32.96°E, Centennial; and Engdahl and Villasenor (2002); 29.31°S, 33.09°E, ISC relocation) are only 26 km and 5 km, respectively from this study's location.

From the 14 collected waveforms we have four records of mantle waves; Love and Rayleigh at De Bilt, Netherlands (DBN); Rayleigh only at San Juan, Puerto Rico (SJG) and Sverdlovsk (SVE), now referred to as Yekaterinberg; and no usable body-wave records. Using the mantle magnitude M_m algorithm of Okal and Talandier (1989, 1990), with the absence of corrected magnitudes Mc as there is not any information on the focal mechanism of the earthquake, we recalculated the M_S 6.8 ISC magnitude of this event to M_W 6.9, resulting from a moment of the order of 3×10^{26} dyn*cm, in agreement with the conventional magnitudes reported for the event ($M_{PAS} = 6.75$; $M_S = 6.8 \pm 0.3$ as recomputed by the ISC).

The earthquake was felt as far as Pretoria, Ermelo, and Pilgrim's Rest (more than 500 km, 300 km and 400 km away, respectively) reporting intensity of III (Figure 4) on the MMI-scale. The shaking was much stronger at areas as far as Mbabane, Carolina, Pietermaritzburg and Kokstad reporting intensity IV (Krige and Venter, 1933). The highest intensity recorded was in St Lucia, particularly the Estuary, uMfolozi River mouth and seashore below the St Lucia lighthouse at VIII on MMI-scale. However, Krige and Venter (1933) suspect that the intensity along the seashore below the St Lucia lighthouse might have reached IX as there was evidence of ~2 cm wide cracks within the calcareous sandstone as far as ~ 1.5 km away. Along the St Lucia Estuary, located near the uMfolozi River mouth, a rumbling noise was observed for ~15 seconds, as well as an eruption of black clay mud up to a meter in height (Krige and Venter, 1933).

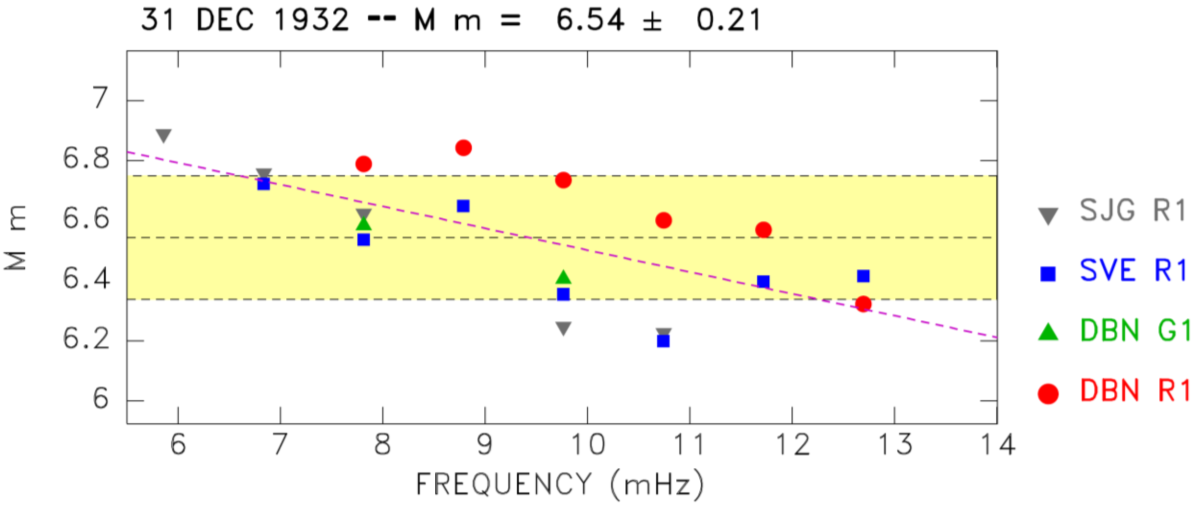

Figure 2. Mantle magnitude $M_m = \log_{10}M_0 - 20$ (Okal and Talandier, 1989), as a function of frequency.

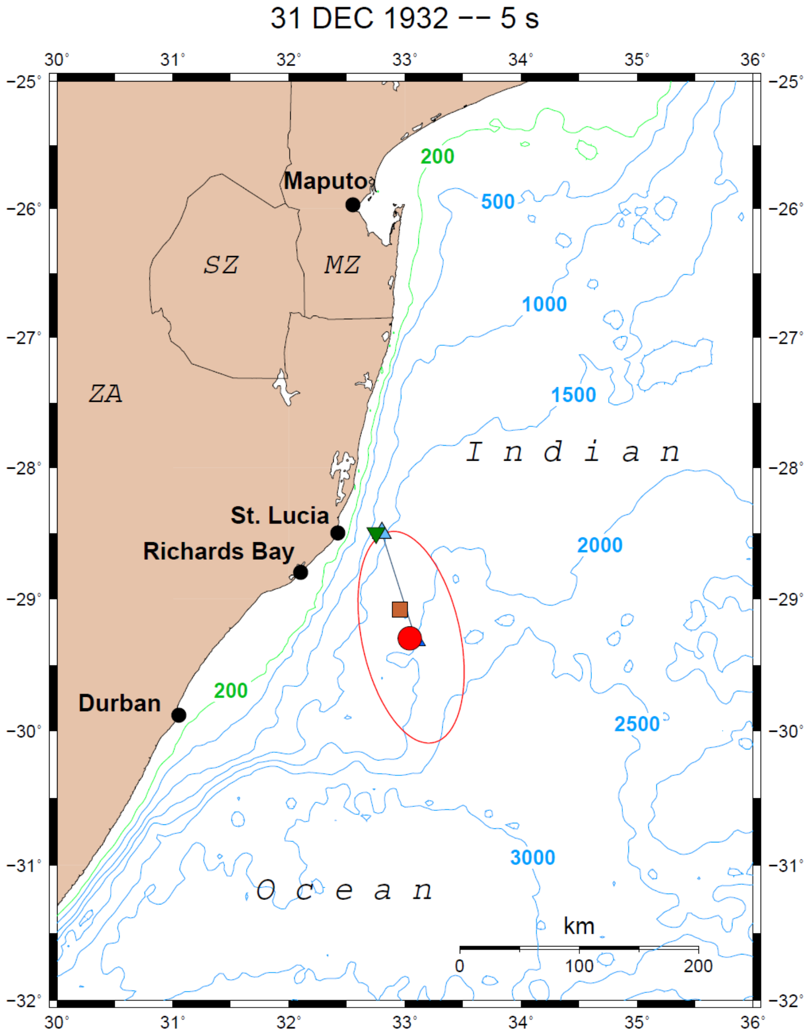

Figure 3. Relocations of the 1932 event: Red dot with ellipse: This study; Light blue triangle: Gutenberg and Richter (1954); Brown square: Centennial Catalogue (Engdahl and Villasenor, 2002). Isobaths in meters.

The seismic cycle of continental intraplate earthquakes exceeds tens to hundreds of thousands of years; this makes it challenging to assess seismic hazards accurately due to lack of records of strong earthquakes in the instrumental period. Therefore, it is important to understand the causative faults of these strong earthquakes for the improvement of seismic hazard assessment by inputting single active fault sources other than a statistical approach based on incomplete data sets. Thus, we investigated the causative fault of the 1932 M_W 6.9 St Lucia earthquake, for which we shall provide evidence showing that it is the Tugela fault.

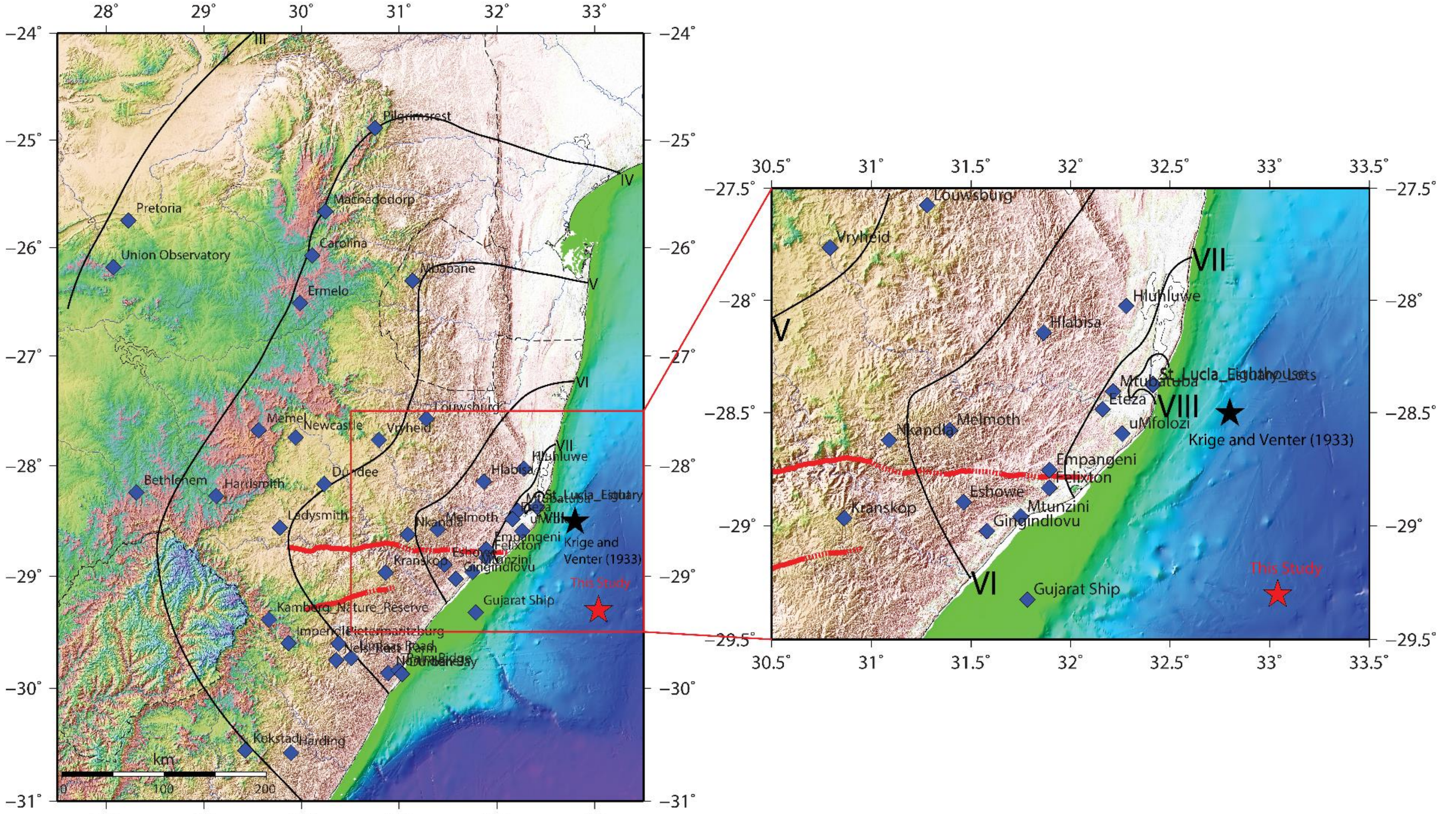

Figure 4: Intensity data (MMI31) of the 1932 M_W 6.9 St Lucia from Krige and Venter (1933), KwaZulu-Natal with a zoom into the area near the epicentre (from Krige and Venter (1933), black star) with highest reported intensity. The red star shows the epicentre location of the 1932 M_W 6.9 St Lucia earthquake from this study.

4 Tugela Fault Scarp

The study of tectonic geomorphology can indicate geological linear structures from past fault activities. Such studies are conducted using geodetic tools, which provide a rate of deformation on the Earth’s surface such as the spatial deformation pattern caused by an earthquake. The displacement field of the earthquake can be measured from the deformed ground surface, subsequently delineating the relationship between seismic characteristics, displacement gradient and rock properties. We apply tectonic geomorphology to the investigation of the Tugela fault scarp, to determine its characteristics and activity. The Tugela fault scarp is EW orientated scarp, stretching for ~230 km in KZN, South Africa (Figure 5).

There is clear evidence of a right-lateral movement, as seen from tectonic geomorphology and geological field investigations, visible with the displacement of river terraces at different sites along the fault.

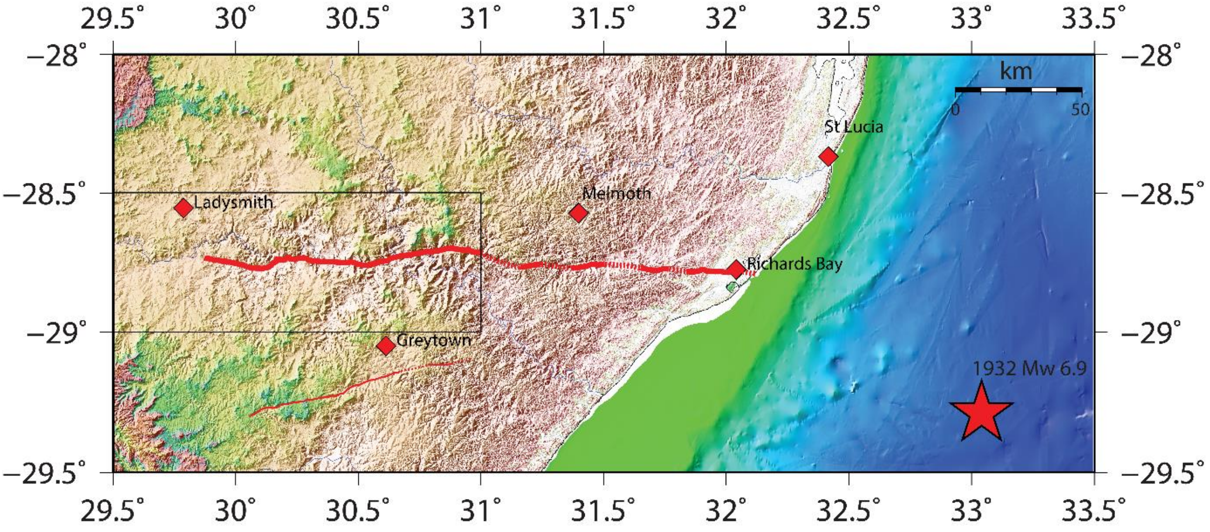

Figure 5: Tugela fault scarp highlighted with by a thick red line at areas where it is clearly visible, the red star shows the epicentre of the 1932 M_W 6.9 St Lucia earthquake (ISC Bulletin). The inset black block is the zoom in shown in Figure 4a.

Tectonic geomorphology investigations were conducted along the Tugela fault scarp using SRTM 1" (Farr et al., 2007) to identify geomorphic markers that have been affected by active deformation along the fault. The evidence of tectonic activity along the Tugela fault is clearly visible with right lateral movement displayed by the shift in river channels, at several places shown in Figure 4. We indicate the lateral movements along the fault from the eastern to the western margin, listed in

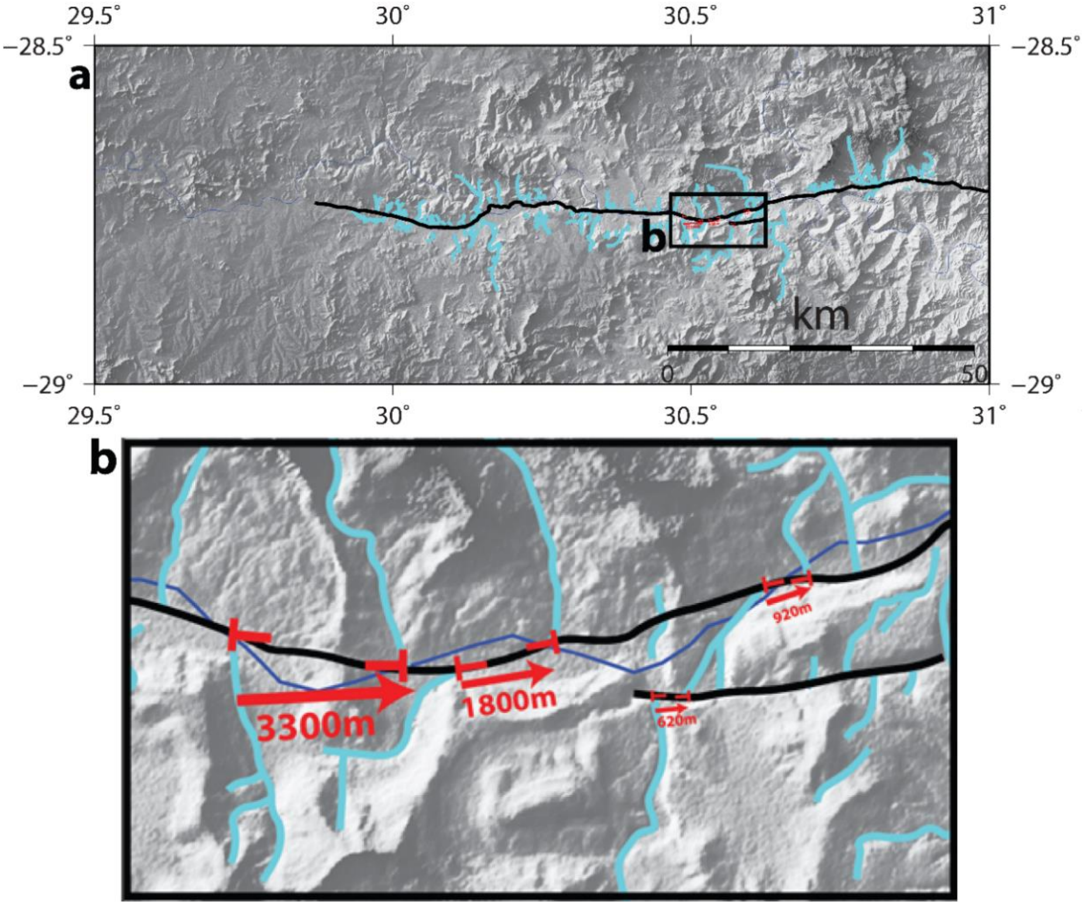

Figure 6: The right lateral movement (red arrows) on the western branch of the Tugela fault scarp, traced from SRTM1" (Farr et al., 2007). The red T shows the beginning and end of the right lateral movement of streams along the fault line with measurements in red text. The black line traces the Tugela fault scarp and blue lines stream terraces which are crosscut by the fault. Fault offsets are reported in Table 1.

Table 1. Right-lateral offsets as measured from Tugela fault scarp and stream terraces, mapped in SRTM1", with error bars estimated based on the thickness of the terraces along the Tugela fault scarp (see also Figure 6b).

Offset (m)	**Error (±m)**
920	180
620	100
1 800	200

3 300	200

5 Greytown Fault Scarp

The lack of strong earthquakes within intraplate continental regions challenges us to find other ways to investigate active faulting within these regions. To substantiate the hypothesis that this region has active faults that may generate earthquakes, we also investigate the Greytown fault scarp located about 50 km south of the Tugela fault (Figure 4and Figure 7). The fault scarp is ~80 km long, trending SW-NE, about 10 km south of Greytown city.

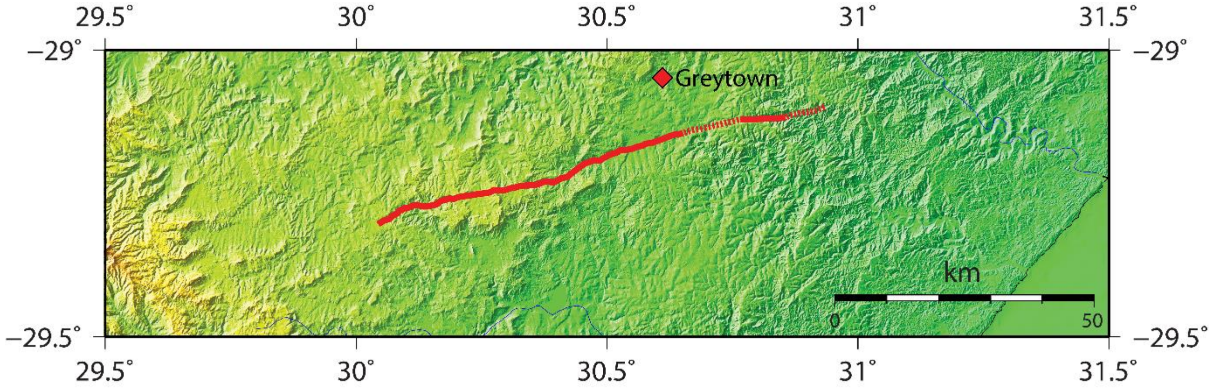

Figure 7: Greytown fault scarp, highlighted with a red line at areas where it is clearly visible.

Figure 8 shows right lateral offsets along the fault scarp, (Table *2*). There is also evidence of uplift towards the western part of the fault scarp (Figure 9) and a down throw with clear river channels cross-cut (Figure 10).

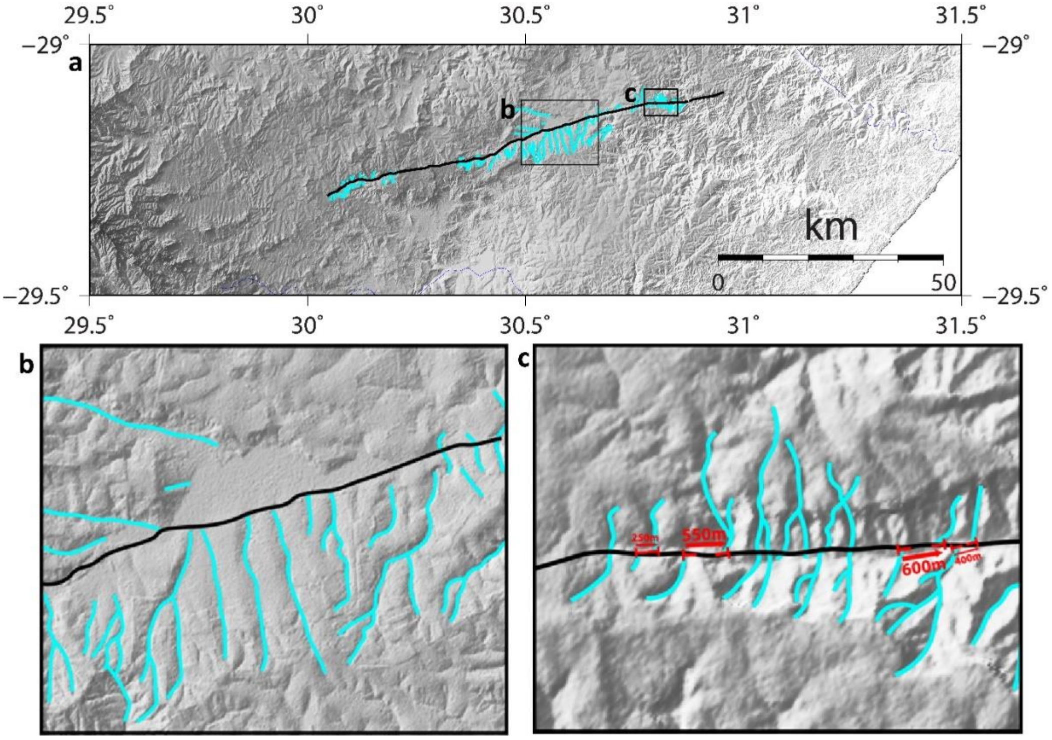

Figure 8: a) Terraces crosscut by the Greytown fault with detailed observations in boxes b and c obtained from SRTM 1'' data; b) Quaternary basin limited on its southern edge by the fault, and right lateral offset of streams located to the east; c) The fault crossing the dense hydrographic system. Fault offsets are reported in Table 2.

Table 2. Right-lateral offset as measured from Greytown fault scarp and terraces, mapped in SRTM1", with error bars estimated based on the thickness of the terraces along the Greytown fault scarp.

Offset (m)	**Error (± m)**
400	30
600	90
550	70
250	30

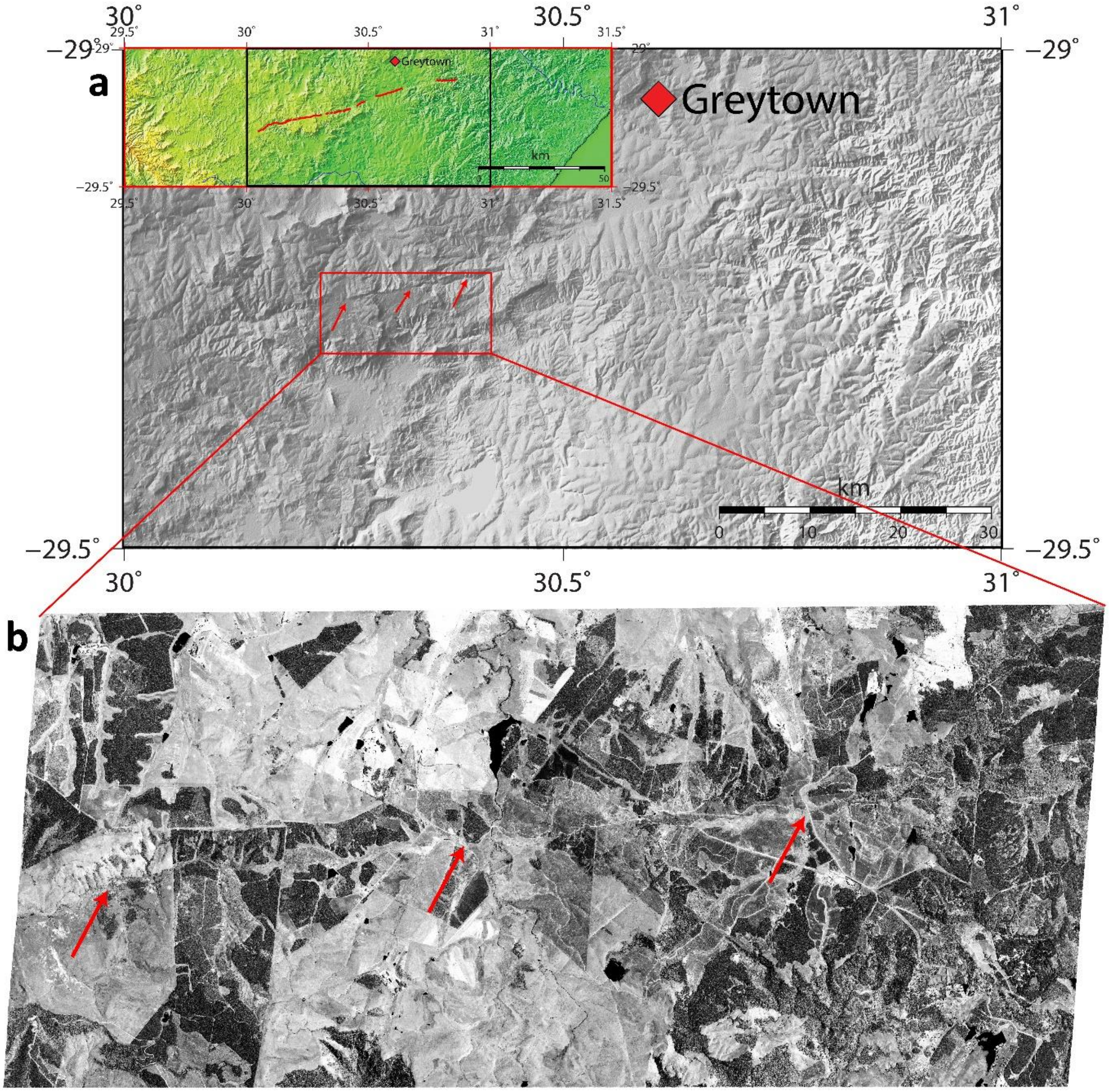

Figure 9: a) A zoomed section of the western branch of the Greytown fault scarp; b) Pleiades stereo image of western branch Greytown fault scarp; the red arrows show fault scarp visible on both a) SRTM1" and b) Pleiades stereo image.

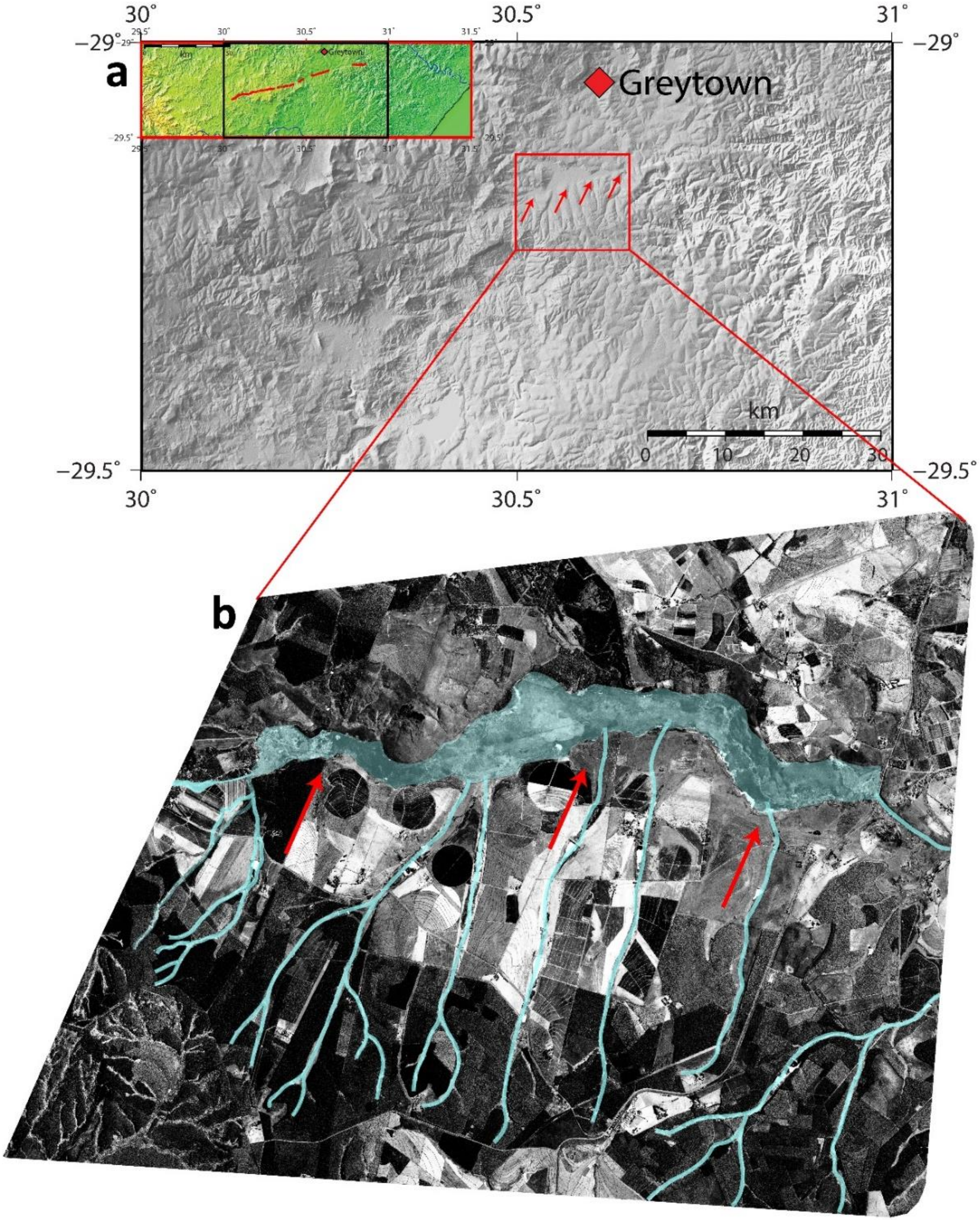

Figure 10: a) A zoomed section of the eastern branch of the Greytown fault scarp; b) Pleiades images of terraces crosscut by Greytown fault scarp (red arrows) visible on both a) SRTM1" and b) Pleiades image.

6 Geophysical Analysis of the Tugela and Greytown Fault Scarps

We apply the first vertical derivative (FVD) filtering on total magnetic field intensity data because it enhances the narrower bodies e.g., faults and or lineaments, though it may at times tends to enhance noise. Regional aeromagnetic data is interpreted (Figure 11(a)) and the narrow linear features, specifically the Tugela fault scarp interpretation is enhanced by the Vertical Derivative (Figure 11(b)).

Based on the qualitative evaluation of the existing data, lineaments are poorly resolved on the regional aeromagnetic data. This is expected since the data was acquired at 1 km line spacing increasing the chance of missing lineaments and other high frequency signals. Thus, ground geophysics data such as reflection seismics and resistivity were added to supplement and confirm the depth of the Tugela fault scarp displacement. The resistivity measurements are taken by injecting a current into the ground through 36 current electrodes with a 5 m spacing, resulting in a 180 m line and measuring the resulting voltage difference between those electrodes. The acquired electrical resistivity tomography (ERT) survey location and the position of the interpreted fault based on the observed low resistivity and high resistivity displacements are shown in Figure 12. Reflection seismic data acquisition was conducted using a standard asymmetric split spread seismic surveying technique. During the survey a total of 96 active channels were used spaced at 2 m intervals, with a minimal and maximum offset of 4 m and 194 m, respectively. These, yielded a minimal wavelength of ~1 m and a maximum wavelength of ~70 - 90 m. The shot was moved at 2 m intervals which allowed the recording of 99 shot locations along the survey spread giving a maximum of 48 nominal fold. The obtained stacked common midpoint section produced along the survey line displays six reflectors, R1, R2, R3, R4, R5 and R6 (Figure 12), visible between depths of ~4 m and ~28 m. Deformation offsets are mapped at positions D1, D2, D3 and D4 (Figure 12) dipping vertically and observed at distances of ~40 m, ~70 m, ~100m and ~110 m at depths from ~8 m to ~28 m.

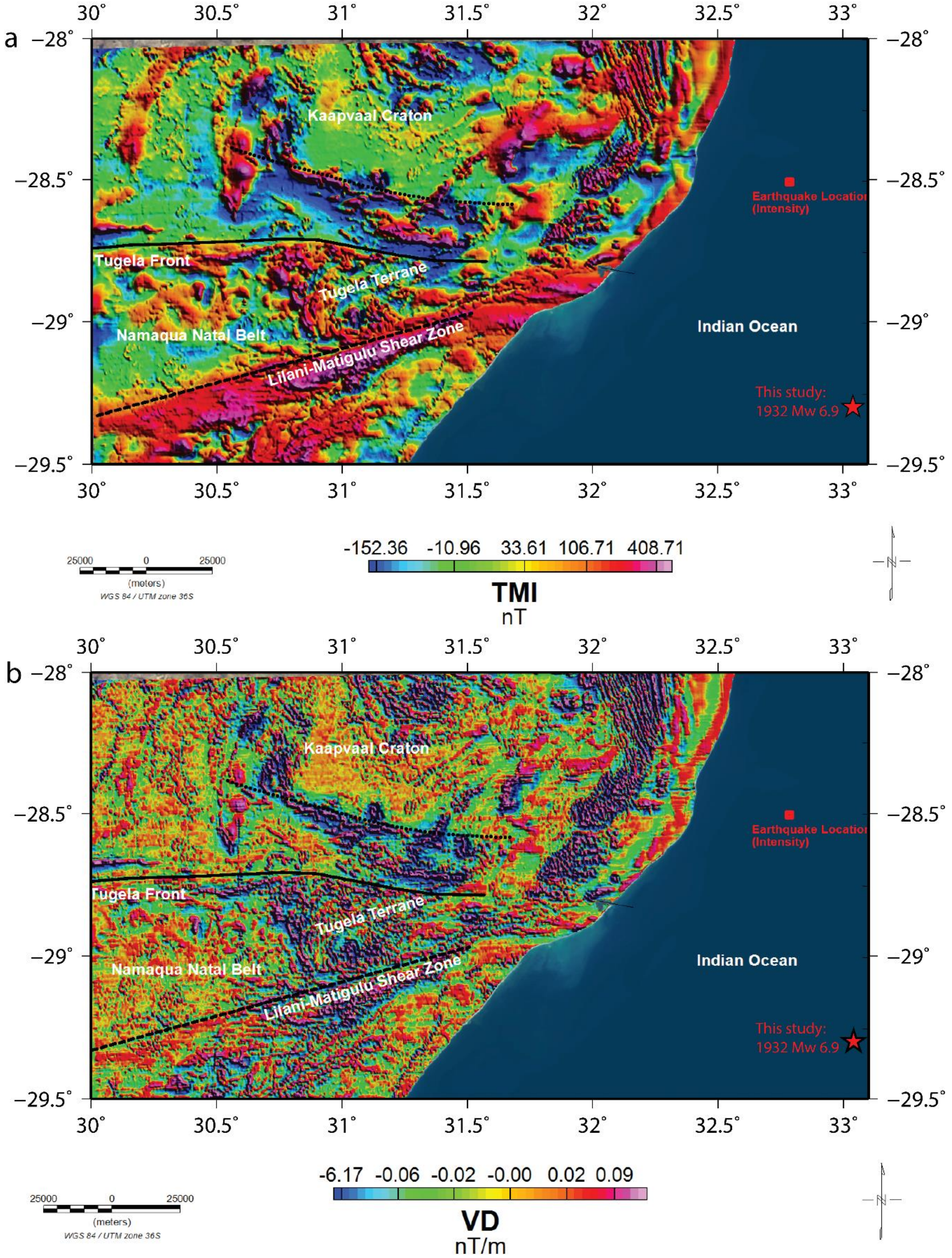

Figure 11: a) Interpreted total magnetic field with Tugela fault scarp as observed from tectonic geomorphology and b) interpreted first vertical derivative image with Tugela and Greytown fault scarps as observed from tectonic geomorphology.

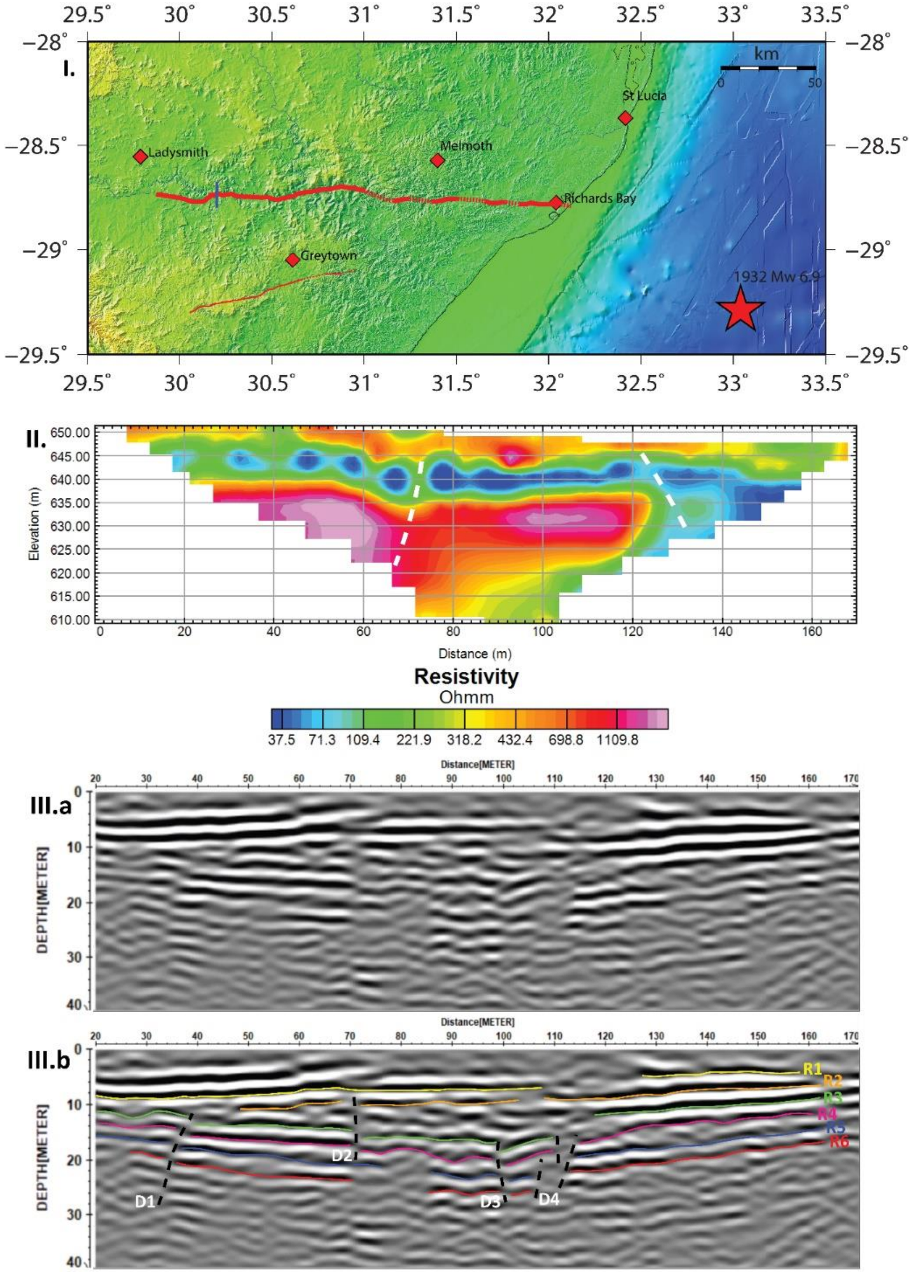

Figure 12: I. Survey location of 180 m-long profiles for resistivity and reflection seismics (blue line, exaggerated against the scale), the red star shows the epicentre of the 1932 M_W 6.9 St Lucia. II. Interpreted model (white dashed lines) resistivity at depth along the Tugela fault scarp. III.a) Common Midpoint (CMP) stacked reflection depth section displaying the sub-surface geology along Tugela fault scarp. III.b) indicates the CMP stacked section after the interpretations. R1, R2, R3, R4, R5 and R6 indicate the interpreted reflectors and D1, D2, D3 and D4 indicates fault offsets (black dashed lines). D2 and D4 are clearly visible on resistivity interpreted model at ~70 m and ~120 m, respectively.

7 GPS Slip Rate Analysis

Geographical Positioning System (GPS) data are widely used to determine crustal deformation and plate movement (e.g., Papanikolaou et al., 2005; Saria et al., 2014). In this study we also made use of GPS data for similar studies using data obtained from 14 GPS stations located in and around KwaZulu-Natal Province (Figure 11). The data were obtained from the Nevada Geodetic laboratory (http://*geodesy.unr.edu/)* and velocities calculated using Gamit-GlobK with Nubia fixed and ITRF 2014 (Altamimi et al., 2016).

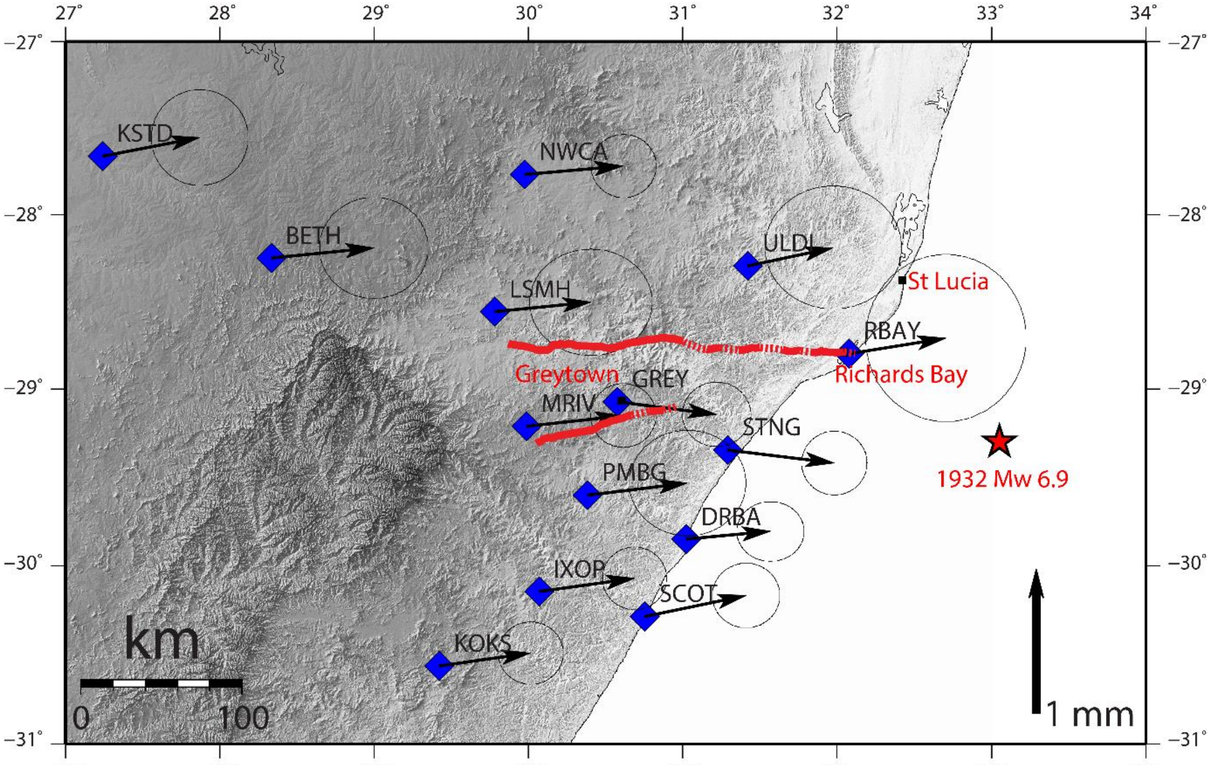

Figure 13: GPS velocities of stations in KwaZulu-Natal calculated using data from http://geodesy.unr.edu/. The ellipse errors are at 94.5 % confidence.

We consider the stations closest to the Tugela fault scarp to minimise the impact of other fault movements within the region. Thus, data from the following stations were used, LSMH and ULDI in the north, which were compared to data from MRIV, GREY and RBAY in the south (Figure 12). This comparison indicates evidence of right lateral movement along Tugela fault scarp as seen with the positive deformation difference of the southern block from that in the north of Tugela fault scarp Table *3*. The deformation rate difference between the north and south of Tugela fault scarp is small but perceptible (< 0.1 mm/yr), this is usual concerning deformation rate within continental intraplate domains.

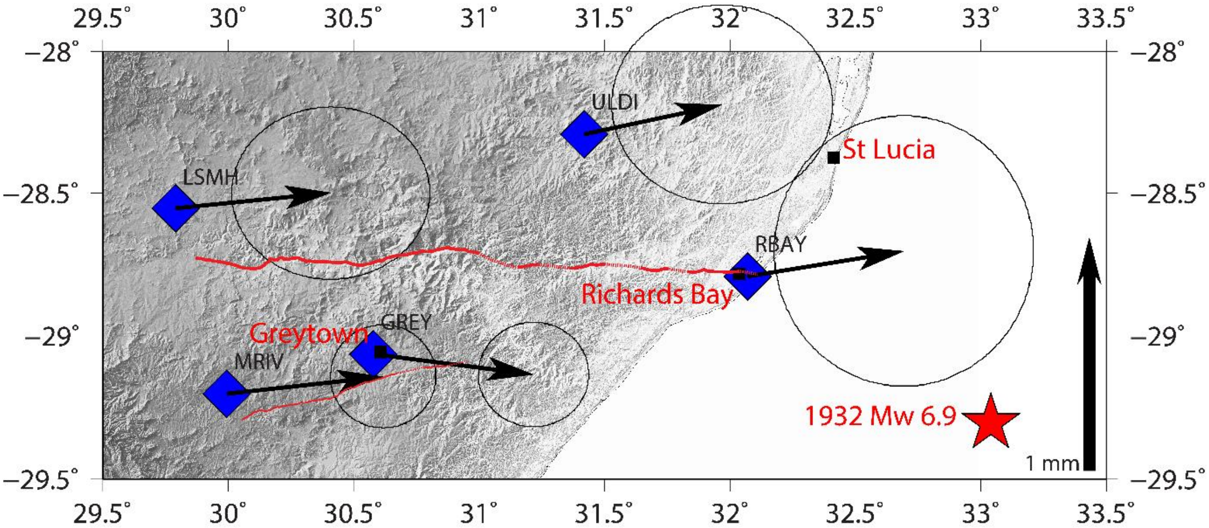

Figure 14. Focus on GPS velocities of stations around the Tugela fault scarp

Table 3. Deformation rate from stations north and south of Tugela fault scarp as per Figure 14.

	Station	V (mm/yr)	Avg. V (mm/yr)	Std Dev (mm/yr)	Difference V (mm/yr)
North	LSMH	0.754	0.962	0.218	0.120
	RBAY	1.016			
	ULDI	1.117			
South	GREY	0.888	0.842	0.105	
	MRIV	0.797			

8 Discussion and Prospective

The low seismic activity, seismic station distribution and low strain rate in the southern Africa intraplate continental region makes it challenging to characterise active faults. The short period of recording of historical seismicity also results in significant uncertainties when determining large possible earthquakes and their recurrence intervals. However, unavailability of maximum possible earthquake records is not indicative of the lack of a seismic cycle or inactivity of faults within intraplate continental region (Clark et al., 2011). According to Landgraf et al. (2017) epistemic uncertainties in seismic hazard can be reduced by better assessment of the spatiotemporal distribution of recorded moderate to large events within intraplate regions. Information on their fault sources would also be useful. Kubler et al. (2016) also illustrate the importance of assessing past earthquakes, slip rate and fault activity within intraplate regions using a multidisciplinary approach. Geomorphic and geophysical data, exploratory coring and paleoseismological investigations at Hemmerich and Untermaubach sites, in the Lower Rhine Graben, showed repeated normal faulting and a complex fault zone, respectively (Kubler et al., 2016). Salomon et al. (2022) investigate the Hebron fault, in Namibia, from pan-sharpened Worldview-3 satellite stereophotos high-resolution digital elevation model, discovering predominant normal faulting on a steeply west-dipping fault plane and evidence of a few events of magnitude $M_W \sim 7$.

Hence the need to assess the structural background of the 1932 St Lucia earthquake and GPS slip rate analysis in KwaZulu-Natal, South Africa, together with the detailed analysis on the Tugela and Greytown fault scarps to characterise and determine the evidence of a seismic cycle. The Tugela fault scarp is ~230 km long and clearly visible on the surface from southeast of Ladysmith extending EW until Richards Bay, which is 100 km NW of the 1932 M_W 6.9 St Lucia Earthquake. Tectonic geomorphology studies conducted along this fault scarp yielded evidence of several right lateral offsets from the hydrographic system indicating the existence of a seismic cycle within this intraplate continental region. Comparison of velocities obtained from GPS station data north and south the Tugela fault scarp also shows evidence of right lateral movement with the block north of the fault scarp moving faster than that in the south. The deformation rate in this intraplate continental region of southern Africa is low but perceptible. This is in support of conclusions from Johnston (1996a, 1996b) and Landgraf et al. (2017), that areas of slow strain rate are subject to seismic hazards.

Geophysical and tectonic geomorphology studies indicate evidence of a seismic cycle. The tectonic geomorphology together with geological and geophysical studies indicate that both fault scarps have evidence of strike slip faulting as well as dip-slip. Paleoseismological studies, to determine long-term (late Quaternary) slip rate by isotopic or fossil dating of Quaternary units, must be conducted to conclude with certainty that the Tugela and Greytown fault scarp are active.

References

Adams, A. and Nyblade, A., 2011. Shear wave velocity structure of the southern African upper mantle with implications for the uplift of southern Africa. Geophysical Journal International, 186(2), pp.808-824.

Andreoli, M.A.G., Doucoure, M., Van Bever Donker, J., Brandt, D., Andersen, N.J.B., 1996. Neotectonics of southern Africa-a review. Africa Geoscience Review, 3(1), pp.1-16.

Altamimi, Z., Rebischung, P., Métivier, L., and Collilieux, X., 2016. ITRF2014: A new release of the International Terrestrial Reference Frame modeling nonlinear station motions, Journal of Geophysical Research: Solid Earth, 121, 6109 – 6131.

Bent, A.L., 1994. The 1989 (Ms 6.3) Ungava, Quebec, earthquake: A complex intraplate event. Bulletin of the Seismological Society of America, 84(4), pp.1075-1088.

Burbank, D.W. and Anderson, R.S., 2009. Tectonic geomorphology. John Wiley & Sons.

Camelbeeck, T. and Meghraoui, M., 1998. Geological and geophysical evidence for large palaeo-earthquakes with surface faulting in the Roer Graben (northwest Europe). Geophysical Journal International, 132(2), pp.347-362.

Clark, D., Dentith, M., Wyrwoll, K.H., Yanchou, L., Dent, V. and Featherstone, W., 2008. The Hyden fault scarp, Western Australia: paleoseismic evidence for repeated Quaternary displacement in an intracratonic setting. Australian Journal of Earth Sciences, 55(3), pp.379-395.

Clark, D., McPherson, A. and Collins, C., 2011. Australia's seismogenic neotectonic record, Geoscience Australia Record, 11, 1 – 95.

Cornell, D.H., Thomas, R.J., Gibson, R., Moen, H.F.G., Reid, D.L., Moore, J.M. and Gibson, R.L., 2006. The Namaqua-Natal Province. Geological Society of South Africa.

Cornell, D.H., Van Schijndel, V., Ingolfsson, O., Scherstén, A., Karlsson, L., Wojtyla, J. and Karlsson, K., 2011. Evidence from Dwyka tillite cobbles of Archaean basement beneath the Kalahari sands of southern Africa. Lithos, 125(1-2), pp.482-502.

Crone, A.J., Machette, M.N. and Bowman, J.R., 1997. Episodic nature of earthquake activity in stable continental regions revealed by palaeoseismicity studies of Australian and North American Quaternary faults. Australian Journal of Earth Sciences, 44(2), pp.203-214.

De Wit, M.J., de Ronde, C.E., Tredoux, M., Roering, C., Hart, R.J., Armstrong, R.A., Green, R.W., Peberdy, E. and Hart, R.A., 1992. Formation of an Archaean continent. Nature, 357(6379), pp.553-562.

Engdahl, E. R., and A. Villasenor, 2002. Global Seismicity: 1900−1999, in: International Earthquake and Engineering Seismology Part A, pp. 665−690, Elsevier, New York.

Farr, T.G., P.A. Rosen, E. Caro, R. Crippen, R. Duren, S. Hensley, M. Kobrick, M. Paller, E. Rodriguez, L. Roth, D. Seal, S. Shaffer, J. Shimada, J. Umland, M. Werner, M. Oskin, D. Burbank, and D. Alsdorf (2007). The Shuttle Radar Topography Mission, Revision of Geophysics,45, RG2004, doi:10.1029/2005RG000183.

Goedhart, M.L. and Booth, P.W.K., 2016a. A palaeoseismic trench investigation of early Holocene neotectonic faulting along the Kango Fault, southern Cape Fold Belt, South Africa–Part I: Stratigraphic and structural features. South African Journal of Geology, 119(3), pp.545-568.

Goedhart, M.L. and Booth, P.W.K., 2016a. A palaeoseismic trench investigation of early Holocene neotectonic faulting along the Kango Fault, southern Cape Fold Belt, South Africa–Part II: Earthquake Parameters. South African Journal of Geology, 119(3), pp.569-582.

Gutenberg, B., and C.F., 1954. Richter, Seismicity of the Earth and associated phenomena, Princeton University Press, 310 p.

Hartnady, C.J., 1990. Seismicity and plate boundary evolution in southeastern Africa. South African Journal of Geology, 93(3), pp.473-484.

Johnston, A.C., Kanter, L.R., Coppersmith, K.J. and Cornell, C.A., 1994. The earthquakes of stable continental regions. Volume 3: Seismicity data sheets (part 1). Final report (No. EPRI-TR-102261-V3). Electric Power Research Inst.(EPRI), Palo Alto, CA (United States); Memphis State Univ., TN (United States). Center for Earthquake Research and Information; Geomatrix Consultants, Inc., San Francisco, CA (United States); CAC, Inc., Portola Valley, CA (United States).

Johnston, A.C., 1996a. Seismic moment assessment of earthquakes in stable continental regions—I. Instrumental seismicity. Geophysical Journal International, 124(2), pp.381-414.

Johnston, A.C., 1996b. Seismic moment assessment of earthquakes in stable continental regions—II. Historical seismicity. Geophysical Journal International, 125(3), pp.639-678.

Krige, F.A. and Venter, L.J., 1933. The Zululand earthquake of 31st December 1932. Transactions of the Geological Society of South Africa, 37, 101–112.

Kuebler S., R. Streich, E. Luck, M. Hoffmann, A. M. Friedrich, and M. R. Strecker, 2016. Active Faulting in a Populated Low-Strain Setting (Lower Rhine Graben, Central

Europe) Identified by Geomorphic, Geophysical, and Geological Analysis. In: Landgraf, A., S., Kubler, E., Hintersberger, and S. Stein, (eds), Seismicity, Fault Rupture and Earthquake Hazards in Slowly Deforming Regions. Geological Society, London, Special Publications, 432.

Landgraf A., S. Kübler, E. Hintersberger and S. Stein, 2017. Active tectonics, earthquakes and palaeoseismicityin slowly deforming continents, In: Geological Society Special Publication, 432, 1, pp. 1-12.

Malservisi, R., Hugentobler, U., Wonnacott, R. and Hackl, M., 2013. How rigid is a rigid plate? Geodetic constraint from the TrigNet CGPS network, South Africa. Geophysical Journal International, 192(3), pp.918-928.

Manzunzu, B., Midzi, V., Mulabisana, T.F., Zulu, B., Pule, T., Myendeki, S. and Rathod, G.W., 2019. Seismotectonics of South Africa. Journal of African Earth Sciences, 149, pp.271-279.

Meghraoui, M., Delouis, B., Ferry, M., Giardini, D., Huggenberger, P., Spottke, I. and Granet, M., 2001. Active normal faulting in the upper Rhine graben and paleoseismic identification of the 1356 Basel earthquake. Science, 293(5537), pp.2070-2073.

Meghraoui, M., 2016. The seismotectonic map of Africa. Episodes, 39(1), pp.9-18.

Midzi, V., Hlatywayo, D.J., Chapola, L.S., Kebede, F., Atakan, K., Lombe, D.K., Turyomurugyendo, G. and Tugume, F.A., 1999. Seismic hazard assessment in Eastern and Southern Africa. Annals of Geophysics, 42(6).

Mulabisana, T., Meghraoui, M., Midzi, V., Saleh, M., Ntibinyane, O., Kwadiba, T., Manzunzu, B., Seiphemo, O., Pule, T. and Saunders, I., 2021. Seismotectonic analysis of the 2017 moiyabana earthquake (MW 6.5; Botswana), insights from field investigations, aftershock and InSAR studies. Journal of African Earth Sciences, 182, pp.104297.

Okal, E.A., and J. Talandier, 1989. Mm: A variable period mantle magnitude, Journal of Geophysical Research, 94, 4169 – 4193.

Okal, E.A., and J. Talandier, 1990. Mm: Extension to Love waves of the concept of a variable-period mantle magnitude, Pure Applied Geophysics, 134, 355 – 384.

Papanikolaou I.D., G. P. Roberts, and A. M. Michetti, 2005. Fault scarps and deformation rates in Lazio–Abruzzo, Central Italy: Comparison between geological fault slip-rate and GPS data, Tectonophysics 408, 147 – 176.

Salomon G. W., T. New, R. A. Muir, B. Whitehead, S. Scheiber-Enslin, J. Smit, V. Stevens, B. Kahle, R. Kahle, F. D. Eckardt and R. Alastair Sloan, 2022. Geomorphological and geophysical analyses of the Hebron Fault, SW Namibia: implications for stable continental region seismic hazard, Geophysics Journal International, 229, 235 – 254.

Saria E., E. Calais, D. S. Stamps, D. Delvaux, and C. J. H. Hartnady, 2014. Present-day kinematics of the East African Rift, Journal of Geophysical Research: Solid Earth, 119, 3584 – 3600.

Singh, M., Kijko, A. and Durrheim, R., 2011. First-order regional seismotectonic model for South Africa. Natural Hazards, 59(1), pp.383-400.

Wysession, M.E., E.A. Okal and K.L. Miller, 1991. Intraplate seismicity of the Pacific Basin, 1913−1988, Pure Applied Geophysics, 135, 261-359.

Chapter 4

Chapter 4: Contribution of seismogenic layer thickness to the seismotectonics of southern Africa

1 Introduction

The previous chapters focused on seismotectonics within the Moiyabana region in Botswana, as well as Tugela and Greytown regions of Kwazulu-Natal, South Africa, as this is an important aspect to improving seismic hazard assessment. The other crucial part of assessing more accurate hazard is evaluating the contribution of the seismogenic layer in the analysis. Thus, we look in this chapter at the southern Africa seismogenic layer thickness to complete the achievement of the aim of this project. Seismogenic layer is the part of the crust where earthquakes are generated and its thickness (Maggi et al., 2000) is different from that of the crust in continental areas (Watts and Burov, 2003). The continental crust is thus characterised by multi-layer rheology with elastic layers that include the seismogenic layer.

We investigate the seismogenic layer thickness within southern Africa as derived from intraplate continental earthquake hypocentres and evaluate the difference with the crustal thickness. The implication for the elastic thickness, which relates to the rheologically elastic layer of the lithosphere, is discussed within the context of the seismic hazard assessment.

We present some of the major tectonic structures that may have affected the crustal composition within southern Africa. The Archaean Congo, Kaapvaal and Zimbabwe Cratons, formed between 2.0 and 3.6 Ga are bounded by younger mobile belts (2 Ga – 300 Ma), Damara-Katanga, Kheis, Limpopo, Namaqua-Natal, and Cape Fold Belt (Naydenov et al., 2015). The southern tip of the Congo Craton forms part of the northwestern part of southern African shield and comprises of an under-explored region of Archean rocks that are mostly exposed within the Congo basin (Alessio et al., 2019).

2 Tectonic Framework

The Kaapvaal Craton is the largest block within the study region and Johnston et al. (1994) categorise it, together with the Zimbabwe Craton as the oldest tectonic regions formed between 2.7 and 3.7 Ga and covering an area of about 1.2 million km^2 (Adams and Nyblade, 2011) in southern Africa (Figure 1).

De Wit and Ransome (1992) state that the Kaapvaal Craton collided with the Zimbabwe Craton forming the Limpopo Mobile Belt during the late Archean, which caused dominant foliation in the Zimbabwe Craton. Located to the northwest of the Kaapvaal Craton is the Kheis oregenic Belt (~1800 Ma) and a northern branch of the Namaqua-Natal Belt (~1200 Ma) (Cornell et al., 2011), which is described as a thin-skinned region with east-verging thrust belt characteristics. The Neoproterozoic Namaqua-Natal and Damara-Katanga Belts bound the southern and the north-western margin of the Kaapvaal Craton, respectively (Johnston et al., 1994; Adams and Nyblade, 2011). The late Palaeozoic compression formed the Cape Fold Belt, a dominant structural domain along the southern coastal region of Africa (Hälbich, 1983), which extends southwards offshore as far as the Agulhas Bank along the strike slip margin of south-eastern Africa (Tucholke et al., 1981).

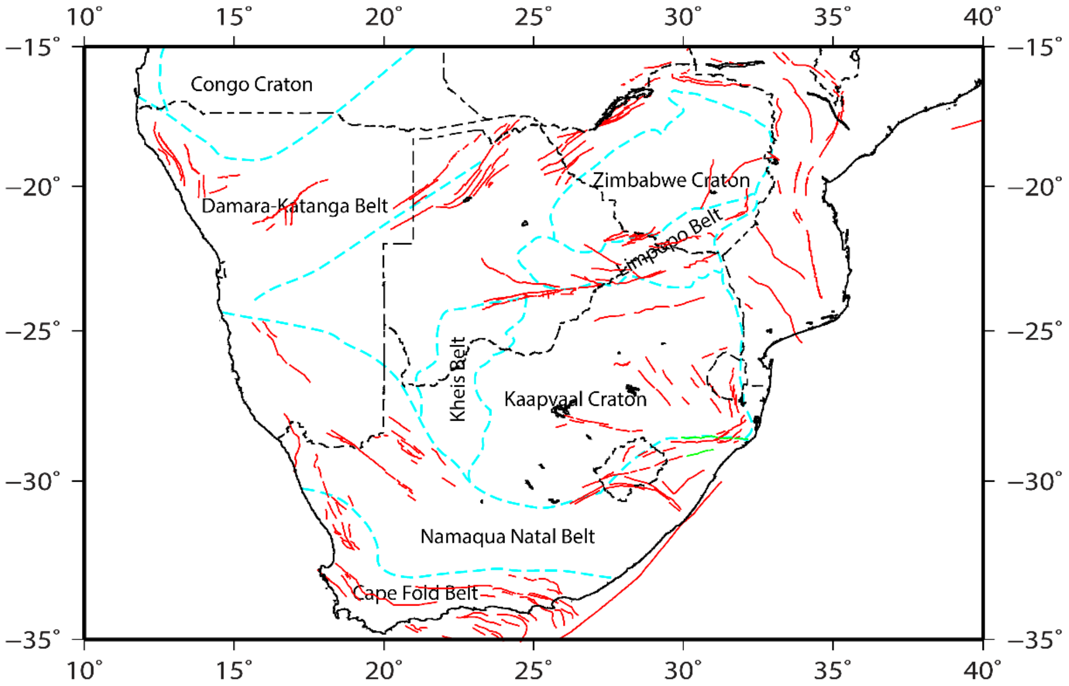

Figure 1. Southern African tectonic framework (Faults obtained from Meghraoui et al., 2016)

3 Crustal Thickness

Southern Africa crustal structure thickness and composition investigations such as those by Nguuri et al. (2001), Doucouré and de Wit (2002), Nair et al. (2006), Yang et al. (2008) and Youssof et al. (2013), show the crustal thickness range of 26 – 56 km. Nguuri et al. (2001) analysed the crustal structure using receiver functions from 81 Broadband stations, yielding a clear contrast of crustal thickness between Archean cratons and mobile belts. The former being the thinner part of the southern African crust. Doucouré and de Wit (2002) consolidated Nguuri et al. (2001) receiver functions analysis with Harvey et al. (2002) surface-wave inversions to estimate the southern African crustal thickness. Nair et al. (2006) conclude, from stacking receiver functions recorded at 80 broadband stations, that the crustal composition of southern African Archean cratonic regions is felsic and thinner than the mobile belts. Yang et al. (2008) used Rayleigh wave phase velocity maps in southern Africa, combined with Li and Burke (2006) two plane wave method phase velocity maps, to produce a 3D structure of the crust, concluding that the shear wave velocity is low in Archean regions, with less mafic lower crust, than that in Proterozoic terranes. Youssof et al. (2013) produced a high-resolution crustal structure model beneath the southern African continental region using 6 300 receiver functions from 85 seismic stations. The model shows short wavelength crustal thickness and composition of high heterogeneity with mid-crustal discontinuity within cratons.

Tugume et al. (2013) modelled the crustal thickness in areas where there are no seismic stations to constraint the Moho depth from receiver functions. This was conducted based on a Parker–Oldenburg iterative inversion method, which is independent of point constraint data. They utilised the global gravity model EIGEN-6c at a grid spacing of 0.1° from Forster et al. (2011), yielding a two-layer model with Moho-topography as the interface, assuming the entire gravity signal as the Moho topography, as well as removing the effect of surface topography by Bouguer correction and sedimentary basins correction. The gravity derived crustal thickness ranges from 30 km along crustal regions to 40 km in central parts of southern Africa, of which agrees to receiver function inversion derived crustal thickness to within 6 km (Tugume et al. 2013).

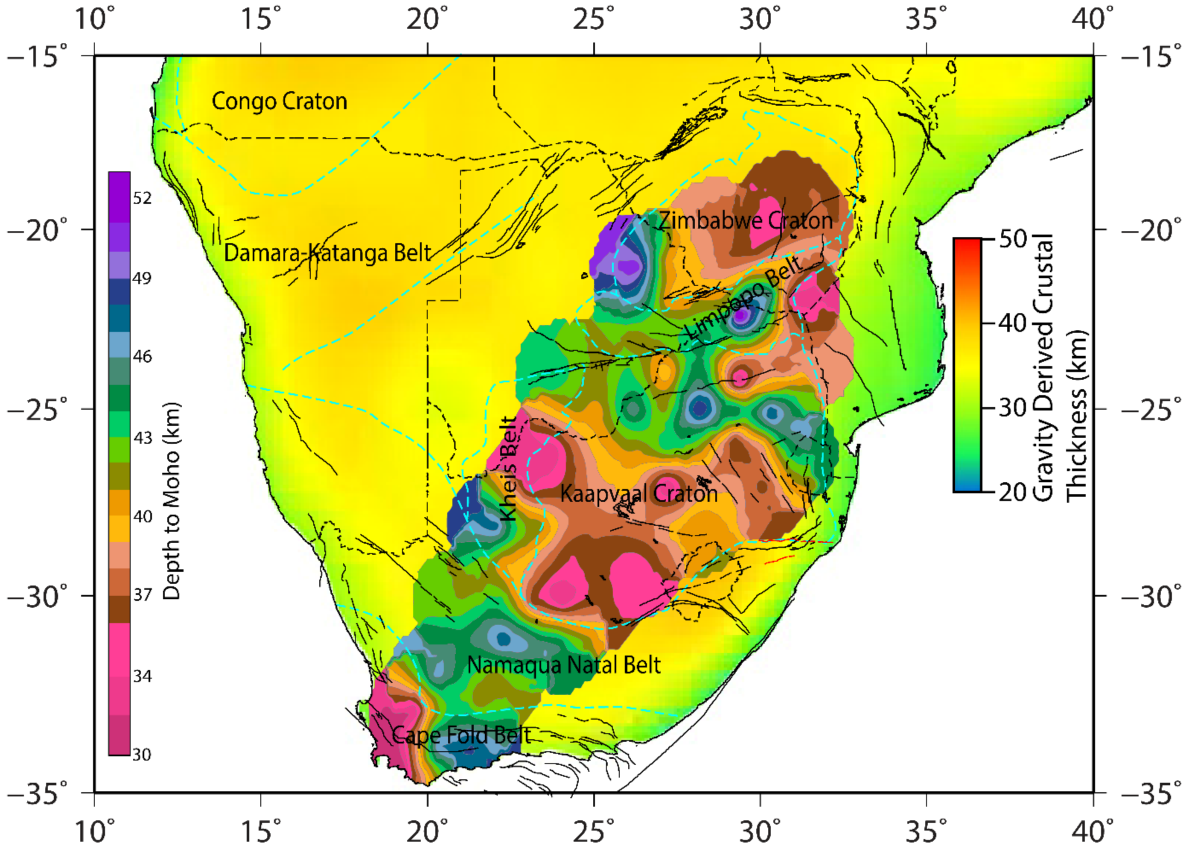

Figure 2. Depth to Moho (Youssof et al., 2013) and gravity derived crustal thickness (Tugume et al., 2013).

4 Earthquake Depths

The sparse 2D seismic station distribution in southern Africa is the greatest impediment to determining earthquake focal depths, though still paramount in assessing seismic hazard accurately. Thus, we review the available earthquake focal depths data to evaluate the depth distribution and determine the seismogenic layer thickness in intraplate continental southern Africa. The catalogue of the depth values used in this study were obtained from different published depth values (Midzi et al., 2010; Brandt, 2014; Shudofsky, 1985; Dziewonski et al., 1991; Bowers, 1997; Fan and Wallace, 1995; Foster and Jackson, 1998; Brandt and Saunders, 2011; Brandt, 2014; Mangongolo et al., 2017; Mulabisana et al., 2021; Sitali et al., 2022). Most focal depths in southern Africa have been calculated using the advanced techniques of moment tensor inversion and waveform fitting (Midzi et al., 2010; Brandt, 2014). The techniques are implemented using 1D velocity models in southern Africa (e.g., Midzi et al., 2010), which does not account for crustal lateral heterogeneity, thus yielding significant uncertainties. Shudofsky (1985) studied the source mechanism and focal depths of a few selected events in East Africa with an inclusion of few events in southern Africa using Rayleigh-wave inversion and body-wave modelling. Dziewonski et al. (1991) investigated global seismicity parameters using centroid moment tensor technique. Bowers (1997) concludes that the 1994 mb 5.6 is a shallow event, at 2 km, which is contradictory to Fan and Wallace (1995)'s conclusion, stating that the earthquake epicentre is at 12 km. However, the event has since been reanalysed to a magnitude of M_L 4.7 and 5.8 km depth as part of the South African National Seismic Network earthquake analysis (SANSN). Foster and Jackson (1998) assessed earthquake depths in Africa using P and SH body-wave inversion from analogue and digital waveform data. Brandt and Saunders (2011) calculated regional moment tensor for 3 events in South Africa and thus contributing to the depth database of southern Africa. Brandt (2014) studied focal depths of the Augrabies swarm using minimum root mean square for the differences between measured and velocity model predicted travel times, thus confirming the hypothesis of shallow events in South Africa. Mangongolo et al. (2017) conducted three studies to review earthquake hypocentral depths in South Africa with only synthetic waveform modelling and use of multiple phase arrivals yielding favourable results. They indicate that the depth distribution in southern Africa is of shallow unimodal nature due to lack of known tectonic events occurring in the lower crust. Mulabisana et al. (2021) analysed the Moiyabana M_W 6.5 earthquake aftershocks' depths from focal mechanism solutions computed from first-motion polarities of P-wave. Sitali et al. (2022) analysed an Anker earthquake swarm, reporting events < M_L 3.6 with depths up to 15 km. Routine analysis of seismic events data from the gold mine mining regions of South Africa also yields reliable depths of the events in those regions.

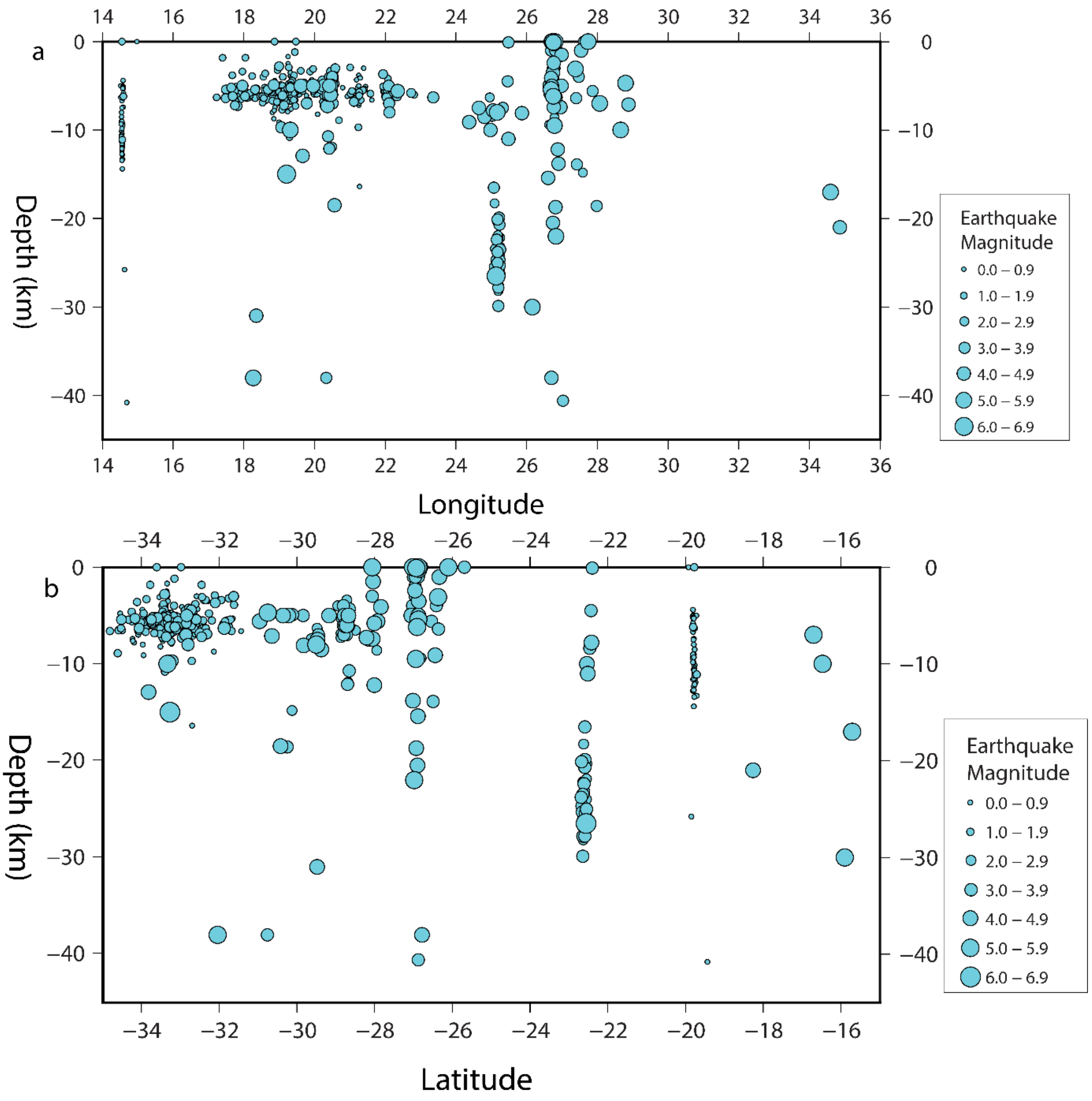

Figure 3. Earthquake depth values in southern Africa: a) EW cross section and b) NS cross section.

5 Seismogenic layer

Seismogenic layer thickness is defined by the earthquake depths within the crust or lithosphere. Earthquakes occurring within continents are confined in the crust, thus the seismogenic layer thickness is restricted to the thickness of the crust (Maggi et al., 2000). We look at the depth to Moho from Youssof et al. (2013), together with the southern Africa earthquake depths and confirm that in this region, the earthquake depths are restricted within the crust, mostly in the upper crust (Figure 4).

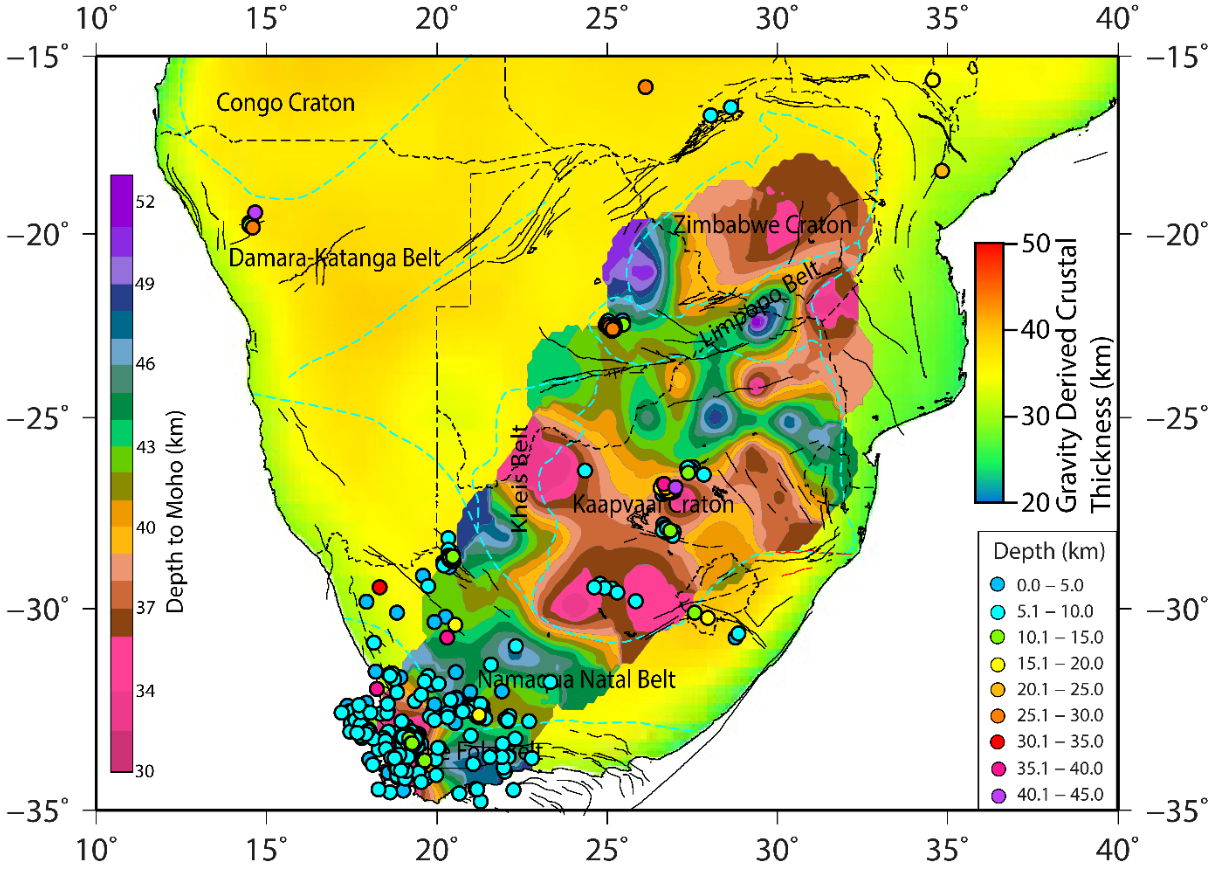

Figure 4. The depth to Moho (Youssof et al., 2013) and gravity derived crustal thickness (Tugume et al., 2013) with earthquake depths in southern Africa.

The seismogenic crust is assumed to extend from the surface down to the base of the seismogenic crustal layer and is defined for the hazard analysis as the zone within which moderate-to-large earthquakes will occur. Typically, in continental crust this is in the uppermost 15 km. The lower limit of the seismogenic thickness layer is defined as the depth of the lower limit of earthquake rupture. It is said to be the depth at which the rock at the fault becomes ductile because of high temperature or composition and again does not resist slip or sliding. Thus, the depth is generally associated with the maximum depths of seismicity in each region. Typically, direct evidence for the seismogenic crust and the focal depth distribution in a region comes from a consideration of the depths of well-determined instrumental earthquake hypocentres.

In their study, Tanaka (2004), and Tanaka and Ito (2002) compare high-quality thermal measurements and seismicity depth data to examine the concept that temperature is a fundamental parameter for determining the thickness of the seismogenic zone. They compare high-quality gridded heat flow or geothermal gradient and D90, the depth above which 90% of earthquakes occur, to conclude that these are correlated well with each other. According to Nazareth and Hauksson (2004) the seismogenic thickness is determined using the depth distribution of the seismic moment release of approximately 19 years of seismicity. Thus, considering the arguments above, D90 is assumed to be a reasonable indicator of the maximum thickness of the seismogenic crust.

We therefore decided to investigate the seismogenic layer in this study through the evaluation of D90. In section 4 above, we assessed earthquake depths in southern Africa, from which we estimated D90 values for various sub-regions for which depths values were available. Thus, we considered D90 at the following geological provinces: a) NW Damara-Katanga Belt, b) central Botswana, c) central Kaapvaal Craton, d) south Kaapvaal Craton, e) NW Namaqua-

Natal belt, f) SW Namaqua-Natal belt, g) east Cape Fold Belt and h) west Cape Fold Belt, for both longitude and latitude cross sections as in

Figure 5. The seismogenic thickness values are observed to range from 6.5 km in the eastern branch of the Cape Fold Belt to 26.7 km in central Botswana (Table 1).

The deepest seismogenic zone is situated in west Limpopo belt. However, it is important to point out that the events utilised to derive the D90 in this region were from the aftershocks of 2017 Moiyabana Earthquake. Thus, we cannot conclude with certainty that this is indeed the D90 of the region when including other events which are not aftershocks of the 2017 Moiyabana Earthquake. Therefore, we consider all the other seven regions as indicated in Figure 5 and Table 1. The central and south Kaapvaal Craton regions have thicker seismogenic layer compared to the other remaining five regions, with both regions in the Cape Fold belt consisting of the thin seismogenic zone. The Cambrian-Ordovician Cape Fold Belt is the youngest geological region within this study and mostly comprised of crustal thickness of 25 – 35 km and seismogenic thickness of 6.5 – 7.4 km.

Table 1: Seismogenic layer thickness values obtained for various geological provinces in southern Africa.

Geological Province	**Seismogenic Depth (km)**
a) NW Damara-Katanga Belt	13.3
b) West Limpopo Belt	26.7
c) Central Kaapvaal Craton	15.4
d) South Kaapvaal Craton	14.8
e) NW Namaqua-Natal belt	12.1
f) SW Namaqua-Natal belt	7.0
g) East Cape Fold Belt	6.5
h) West Cape Fold Belt	7.4

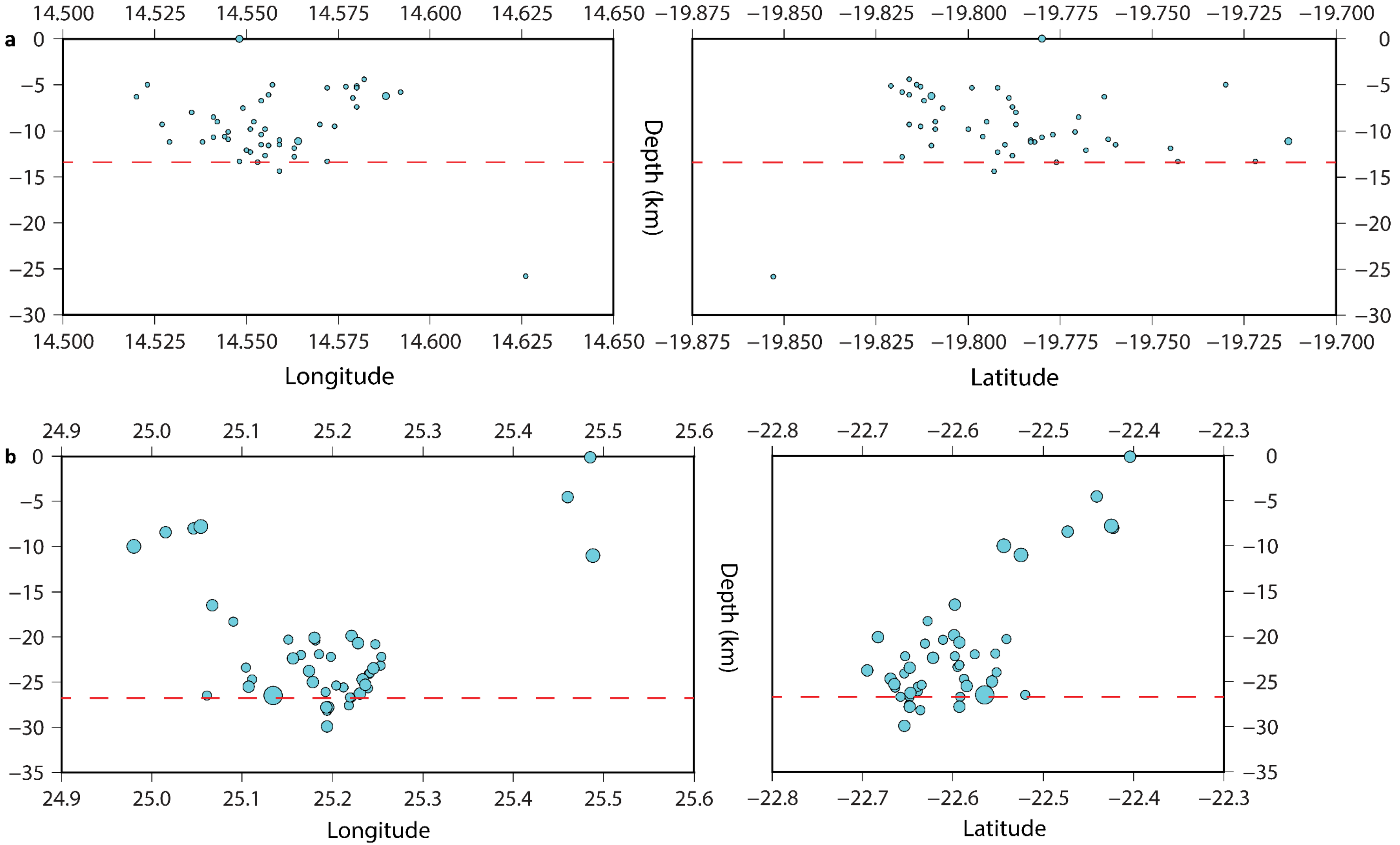
a
b
14.500
14.525
14.550
14.575
14.600
14.625
14.650
Longitude
−19.875
−19.850
−19.825
−19.800
−19.775
−19.750
−19.725
−19.700
Latitude
Depth (km)
0
−5
−10
−15
−20
−25
−30
−35
24.9
25.0
25.1
25.2
25.3
25.4
25.5
25.6
−22.8
−22.7
−22.6
−22.5
−22.4
−22.3

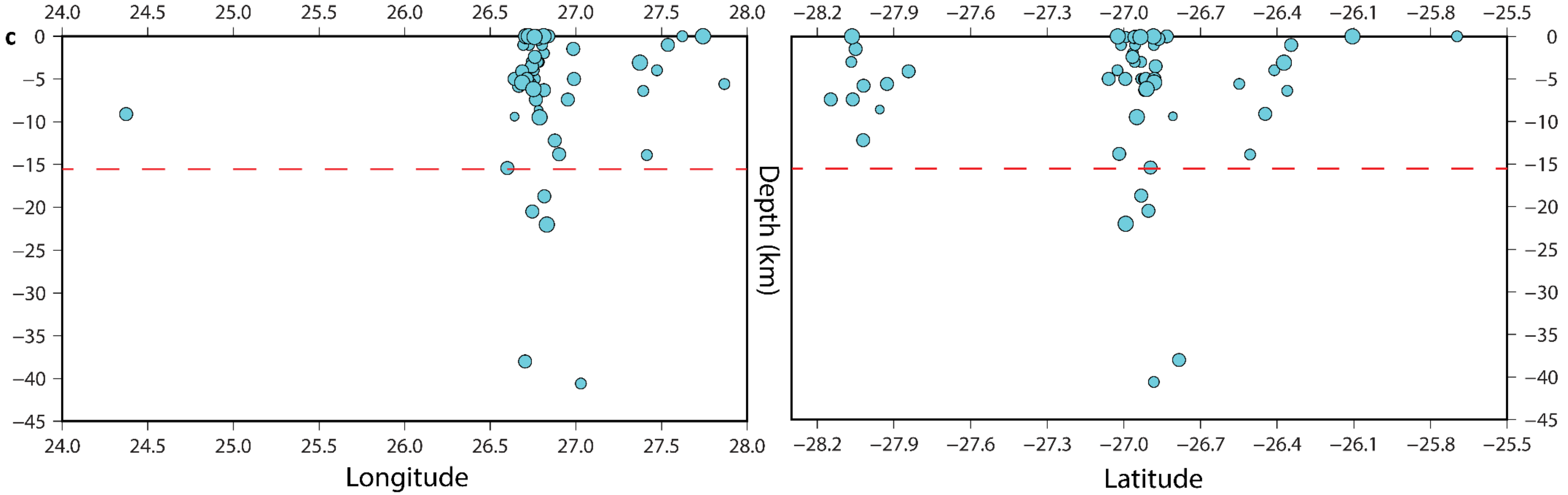
c
24.0 24.5 25.0 25.5 26.0 26.5 27.0 27.5 28.0
0 −5 −10 −15 −20 −25 −30 −35 −40 −45
Longitude
−28.2 −27.9 −27.6 −27.3 −27.0 −26.7 −26.4 −26.1 −25.8 −25.5
Latitude
Depth (km)

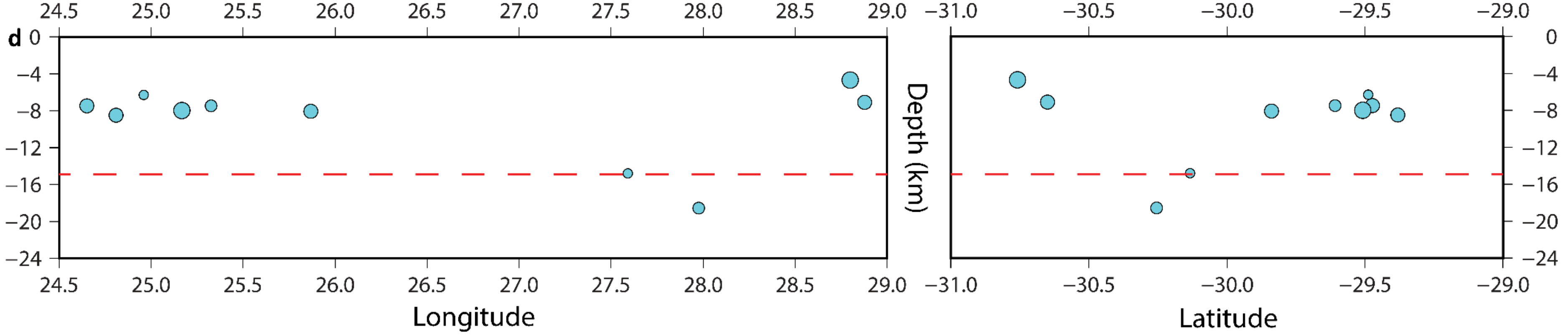
d
24.5 25.0 25.5 26.0 26.5 27.0 27.5 28.0 28.5 29.0
0 −4 −8 −12 −16 −20 −24
Longitude
−31.0 −30.5 −30.0 −29.5 −29.0
Latitude
Depth (km)

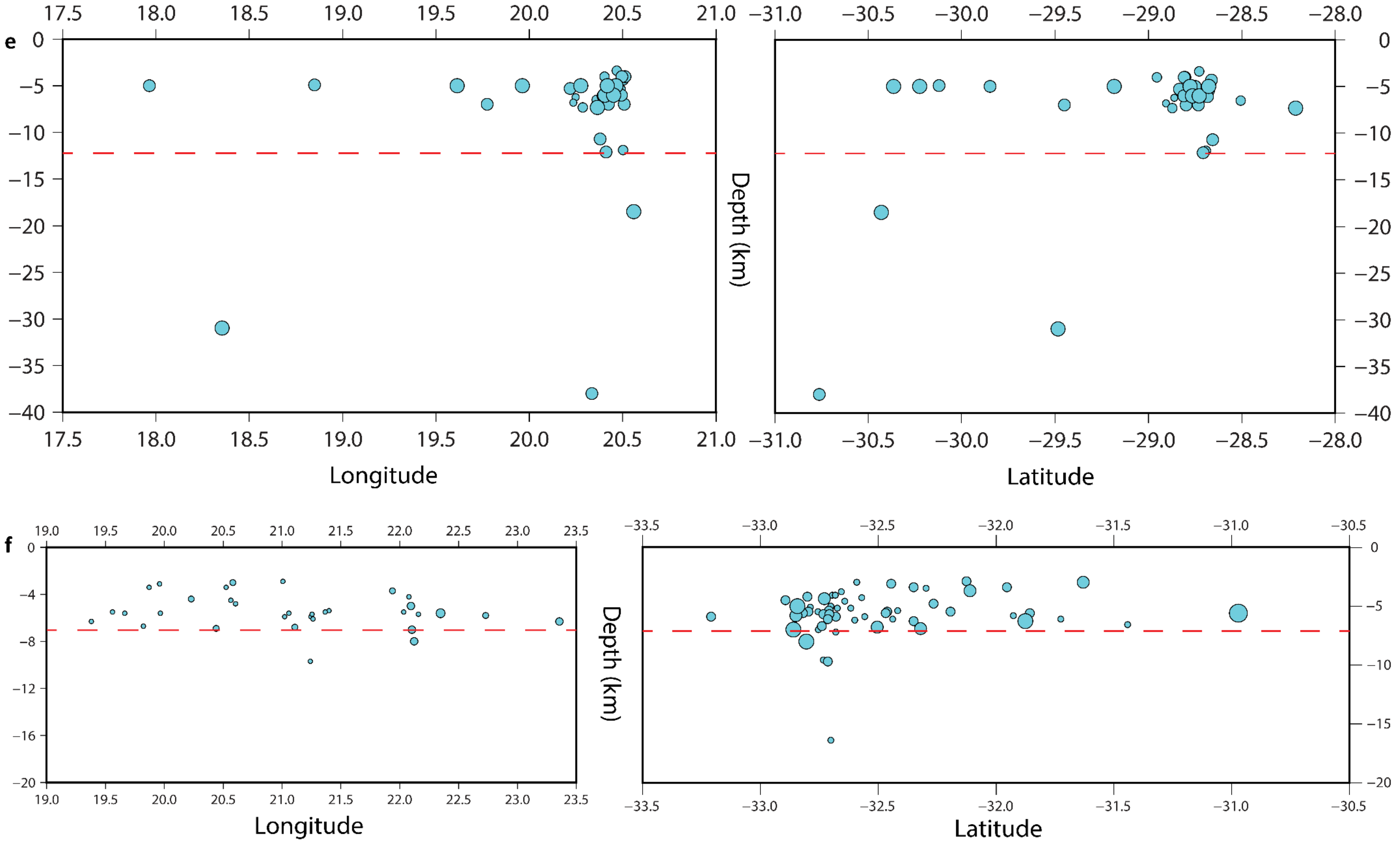
e
17.5
18.0
18.5
19.0
19.5
20.0
20.5
21.0
0
−5
−10
−15
−20
−25
−30
−35
−40
Longitude
−31.0
−30.5
−30.0
−29.5
−29.0
−28.5
−28.0
Latitude
Depth (km)
f
19.0
19.5
20.0
20.5
21.0
21.5
22.0
22.5
23.0
23.5
0
−4
−8
−12
−16
−20
Longitude
−33.5
−33.0
−32.5
−32.0
−31.5
−31.0
−30.5
0
−5
−10
−15
−20
Latitude
Depth (km)

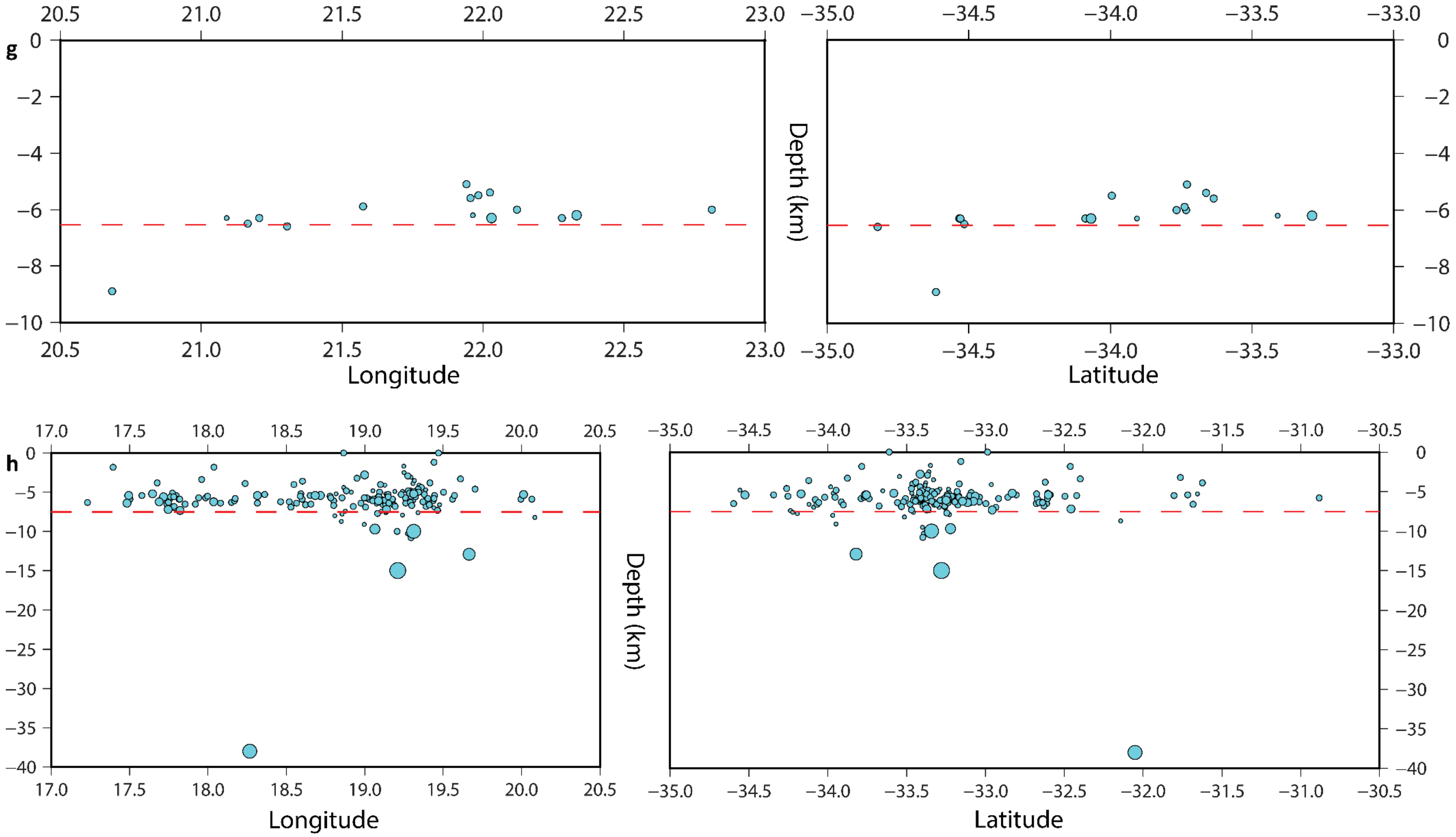

Figure 5. Seismogenic layer assessed using D90 of events located at a) NW Damara-Katanga Belt, b) west Limpopo belt, c) central Kaapvaal Craton, d) south Kaapvaal Craton, e) NW Namaqua-Natal belt, f) SW Namaqua-Natal belt, g) east Cape Fold Belt and h) west Cape Fold Belt. The layer thickness value is marked by the red broken line.

6 Discussion and Conclusion

The seismogenic thickness in southern Africa ranges between 6.5 to 15.4 km, with the exclusion of the West Limpopo Belt region as the only available data was aftershocks of the 2017 Moiyabana earthquake. The crustal thickness ranges between 30 to 52 km, thus only about the upper 30% of the southern African crust generate 90% of the earthquakes. The Archean Kaapvaal Craton, oldest region within the study area, has a relatively thinner crust ranging from 34 – 42 km in the south with small pockets of up to 49 km in the north. The seismogenic layer in this region is however thicker compared to the younger geological regions. The Namaqua-Natal and Cape Fold belts, younger geological regions have a more heterogenous crustal thickness, ranging from 25 – 50 km with a thinner seismogenic layer of ≤ 12 km.

The seismogenic layer thickness values obtained in this study are indication that the upper crust is where elastic stress release occurs in South(ern) Africa, given that the elastic thickness values are greater or equal to the crustal thickness (Doucoure and De Wit, 2002).

The unimodal nature of the shallow seismogenic layer thickness values obtained in this study support the occurrence of shallow fault ruptures and may thus significantly influence the seismic hazard of southern Africa. This will be explored in the following chapter.

References

Alessio B. L., A. S. Collins, P. Siegfried, S. Glorie, B. De Waele, J. Payne and D. B. Archibald, 2019. Neoproterozoic tectonic geography of the south-east Congo Craton in Zambia as deduced from the age and composition of detrital zircons, Geoscience Frontiers, 10, 2045 – 2061.

Bowers D. (1997). The October 30, 1994, seismic disturbance in South Africa: Earthquake or large rock burst?, Journal of Geophysical Research, 102, 9 843 – 9 857.

Brandt M. B. C. (2014). Focal depths of South African earthquakes and mine events, The Journal of The Southern African Institute of Mining and Metallurgy, 114.

Brandt M. B. C. and I. Saunders (2011). New Regional Moment Tensors in South Africa, Seismological Research Letters, 82 (1), 69 – 80.

Craig T. J. and J. A. Jackson (2021). Variations in the Seismogenic Thickness of East Africa, Journal of Geophysical Research: Solid Earth, 12.

Doucouré C. M., M. J. de Wit (2002). Temporal variation in rigidity and mechanical behaviour of old thick continental lithosphere, South African Journal of Geology, 105, 39 – 50.

Dziewonski A.M., G. Ekström, J.H. Woodhous and G. Zwart (1991). Centroid-moment tensor solutions for July – September, 1990, Physics of the Earth and Planetary Interiors, 67, 211 – 220.

Fan G. and T. Wallace (1995). Focal Mechanism of a Recent Event in South Africa: A Study Using a Sparse Very Broadband Network, Seismological Research Letters, 66 (5), 13 – 18.

Förste, C., S.L. Bruinsma, R. Shako, O. Abrikosov, F. Flechtner, J.-C. Marty, J.-M. Lemoine, C. Dahle, H. Neumeyer, F. Barthelmes, R. Biancale, G. Balmino and R. König (2011). A new release of EIGEN-6: The latest combined global gravity field model including

LAGEOS, GRACE and GOCE data from the collaboration of GFZ Potsdam and GRGS Toulouse. EGU General Assembly, abstract volume, Vienna, Austria.

Foster A. N. and J. A. Jackson (1998). Source parameters of large African earthquakes: implications for crustal rheology and regional kinematics, Geophysical Journal International, 134 (2), 422 – 448.

Harvey J. D., M. J. de Wit, J. Stankiewicz and C. M. Doucoure (2002). Structural variations of the crust in the Southwestern Cape, deduced from seismic receiver functions, South African Journal of Geology, 104, 231 – 242.

Hauksson E. (2011). Crustal geophysics and seismicity in southern California, Geophysical Journal International, 186, 82 – 98.

Johnston, A.C., Kanter, L.R., Coppersmith, K.J. and Cornell, C.A., 1994. The earthquakes of stable continental regions. Volume 3: Seismicity data sheets (part 1). Final report (No. EPRI-TR-102261-V3). Electric Power Research Inst.(EPRI), Palo Alto, CA (United States); Memphis State Univ., TN (United States). Center for Earthquake Research and Information; Geomatrix Consultants, Inc., San Francisco, CA (United States); CAC, Inc., Portola Valley, CA (United States).

Li A. and K. Burke (2006). Upper mantle structure of southern Africa from Rayleigh wave tomography, Journal of Geophysical Research, 111.

Maggi A., J. A. Jackson, D. McKenzie, and K. Priestley (2000). Earthquake focal depths, effective elastic thickness, and the strength of the continental lithosphere, Geology, 28 (6), 495 – 498.

Mangongolo A., F.O. Strasser, I. Saunders and G.W. Rathod (2017). Depths of Earthquakes in South Africa, Seismological Research Letters, 88 (4).

Meghraoui, M., 2016. The seismotectonic map of Africa. Episodes, 39(1), pp.9-18.

Mulabisana T., M. Meghraoui, V. Midzi, M. Saleh, O. Ntibinyane, T. Kwadiba, B. Manzunzu, O. Seiphemo, T. Pule, I. Saunders (2021). Seismotectonic analysis of the 2017 moiyabana earthquake (MW 6.5; Botswana), insights from field investigations, aftershock and InSAR studies, Journal of African Earth Sciences, 182.

Nagar M., G. Pavankumar, P. Mahesh, N. Rakesh, A.K. Chouhan, D. Nagarjuna, S. Chopra, M.R. Kumar, (2021). Magnetotelluric evidence for trapped fluids beneath the seismogenic zone of the Mw6.0 Anjar earthquake, Kachchh intraplate region, Northwest India, Tectonophysics, 814.

Nair S. K., S. S. Gao, K. H. Liu, and P. G. Silver (2006). Southern African crustal evolution and composition: Constraints from receiver function studies, Journal of Geophysical Research, 111.

Nguuri T. K., J. Gore, D. E. James, S. J. Webb, C. Wright, T. G. Zengeni, Gwavava, J. A. Snoke, and Kaapvaal Seismic Group (2001). Crustal structure beneath southern Africa and its implications for the formation and evolution of the Kaapvaal and Zimbabwe cratons, Geophysical Research Letters, 28 (13), 2501 – 2504.

Shudofsky G. N. (1985). Source mechanisms and focal depths of East African earthquakes using Rayleigh-wave inversion and bodywave modelling, Geophysical Journal International, Volume 83, Issue 3, December 1985, Pages 563 – 614.

Sitali M., B. Manzunzu, V. Midzi, S. Shipena and B. Lushetile (2022). Seismotectonic analysis of the Anker area, Kunene region north-western Namibia, Journal of Seismology, 26, 319–331.

Tanaka A. and Y. Ishikawa (2002). Temperature distribution and focal depth in the crust of the northeastern Japan, Earth Planets Space, 54, 1 109 – 1 113.

Yang Y., A. Li, and M. H. Ritzwoller (2008). Crustal and uppermost mantle structure in southern Africa revealed from ambient noise and teleseismic tomography, Geophysical Journal International, 174, 235 – 248.

Youssof M., H. Thybo, I. M. Artemieva, A. Levander (2013). Moho depth and crustal composition in Southern Africa, Tectonophysics, 609, 267 – 287.

Chapter 5

Chapter 5: Improved seismotectonic model on seismic hazard assessment in southern Africa

1 Introduction

The aim of this project is to determine the impact of improved seismotectonic model on seismic hazard assessment in southern Africa. A realistic assessment of seismic hazard at a regional scale requires the building of a databank of reliable seismotectonic data, which are used to prepare an accurate seismic source model. This involves multidisciplinary investigations of areas where large earthquakes have occurred in southern Africa in the past. The areas where such investigations are being conducted include the Koffiefontein region, St Lucia area in KwaZulu-Natal (KZN), the Ceres area in the Western Cape Province, the Kango and Baviaanskloof region in the Eastern Cape and Central Botswana where the 3 April 2017 M6.5 earthquake occurred. We review several seismic hazard studies from Fernández and Guzman (1979); Shapira and Fernández (1989); Midzi et al. (1999); Kijko et al. (2003) and Midzi et al. (2020) along the hazard assessment conducted using a new seismotectonic mode from this study.

The probabilistic seismic hazard analysis is based on the widely used classical methodology developed by Cornell (1968), McGuire (1974, 1976) and Der Kiureghian and Ang (1975, 1977). The technique uses the widest possible amount of data, combining seismological, geological, and geophysical data to build up a model of the earthquake-producing processes. The aim is to understand the nature of the features in the earth's crust that are causing earthquakes in a region, and to be able to produce a numerical model of these features. The PSHA process generally consists of two key inputs: seismic source characterization and ground motion predictions. Early use of the PSHA method suffered from one important drawback, it required perfect information on all parameters of the earthquake process, which was usually not available. Considering the few hundred years for which earthquake data are available, there is insufficient information to calculate some of the parameters required precisely. There is therefore an element of uncertainty in what is known about the properties of any seismic source zone, which really needs to be factored in the calculations of hazard. Modern PSHA studies, following ideas proposed by Coppersmith and Youngs (1986) are usually able to deal with this problem by incorporating into the model what is known as a "logic tree", in which certain parameters are given a range of possible values with subjective assignment of the probability of each.

2 Seismic Source Model

Accurate seismic hazard assessment at a regional scale requires the identification and characterization of major seismic sources. Seismic source models required for carrying out seismic hazard assessment include a reliable seismic source model and ground motion model. The identification of seismic sources is a critical part of seismic hazard analysis and involves a wide range of data types and scientific interpretations. The technique uses the widest possible amount of data, combining seismological, geological, and geophysical data to build up a model of the earthquake-producing processes. The aim is to understand the nature of the features in the earth's crust that are actually causing earthquakes in a region, and to be able to produce a numerical model of these features. A seismic source model for southern Africa was previously defined and published by Midzi et al. (2020) in their assessment of the seismic hazard of South Africa. We consider new input data from Tugela and Greytown faults in KwaZulu-Nata, and Khurutse fault scarp in Botswana, to determine the impact addition of linear sources will have on Seismic Hazard in southern Africa.

A seismic source model defines the seismogenic potential, location, size, and rate of occurrence of future earthquakes. Ideally the model gives a clear definition of the causative faults that give rise to the observed seismicity. However, there’s few characterised active faults in South Africa, therefore in addition we create a source model made up of characterised area source zones that encompass the possible sources of earthquakes likely to contribute towards the seismic hazard of the region. Though limited in quantity and usefulness, available geological, geodetic, seismic, and geophysical data are useful in demarcating the zones and in assisting with the evaluation of seismic source characteristics. Unique seismic sources are usually defined to account for distinct differences in the following criteria: 1. Earthquake recurrence rate and distribution 2. Maximum earthquake magnitude (M_{max}) 3. Expected future earthquake characteristics (e.g., style of faulting, rupture orientation, seismogenic thickness) 4. Probability that a fault is seismogenic and its location including orientation. These differences are accounted for by drawing a source boundary between the regions. Further, because the historical record of observed earthquakes is short relative to the recurrence intervals for large-magnitude earthquakes, there is an assumption that the spatial distribution of observed smaller-magnitude earthquakes constrains the spatial distribution of larger-magnitude earthquakes. In this study, the integration and interpretation of compiled data (Table 1) resulted in the generation of 26 area source zones and seven fault sources (Kango and Hebron / Dreylingen, Tshipise and Bosbokpoort, Tugela, Greytown and Khurutse faults) whose boundaries are shown in Figure 1.

Table 1: The list of identified and delineated seismic sources with the type of data used to identify them.

Source Name	Source Type
CEDAR – Cedarville fault area	Concentrated Area Zone
CENTRAL – Province in Botswana	Concentrated Area Zone
CFBE – Eastern Cape fold belt	Regional Area Zone
CFBW – Western Cape fold belt	Concentrated Area Zone
CRAND – Central Rand goldfields	Concentrated Area Zone
EMALAHLENI- eMalahleni coal mines	Concentrated Area Zone
ERAND – East Rand goldfields	Concentrated Area Zone
FWRAND – Far west Rand goldfields	Concentrated Area Zone
KARAS – Northern branch of Namaqualand belt in Karas Province, Namibia	Concentrated Area Zone
KAROO_LOW	Regional Area Zone
KGALAGADI – Province of Botswana	Regional Area Zone
KHEIS – Kheis mobile belt	Regional Area Zone
KOFFIE – Koffiefontein region	Concentrated Area Zone
KOSH – Klerksdorp –Orkney-Stilfontein-Hartbeesfontein goldfields	Concentrated Area Zone
KVAAL – Kaapvaal craton	Background Area Zone
LESOTHO – Lesotho & part of KZN	Concentrated Area Zone
LIMPOPO – Limpopo mobile belt	Concentrated Area Zone
MB – Mozambique Belt	Concentrated Area Zone
MOZCHAN – Mozambique Channel	Regional Area Zone
MPUMA – Mpumalanga Province in South Africa	Concentrated Area Zone
NAM_WEST – Western Namaqualand belt	Concentrated Area Zone
NWEST – Platinum mine region in Northwest Province, South Africa	Concentrated Area Zone
SNAM – southern Namaqualand	Concentrated Area Zone
TUGELA – Tugela fault area	Concentrated Area Zone
WELKOM – Welkom goldfields	Concentrated Area Zone
WRAND – West Rand goldfields	Concentrated Area Zone
ZEBEDIELA – Zebediela fault area	Concentrated Area Zone
Bosbokpoort fault	Fault Zone
Hebron / Dreylingen fault	Fault Zone
Kango fault	Fault Zone
Tshipise fault	Fault Zone
Tugela fault	Fault Zone
Greytown fault	Fault Zone
Khurutse faults	Fault Zone

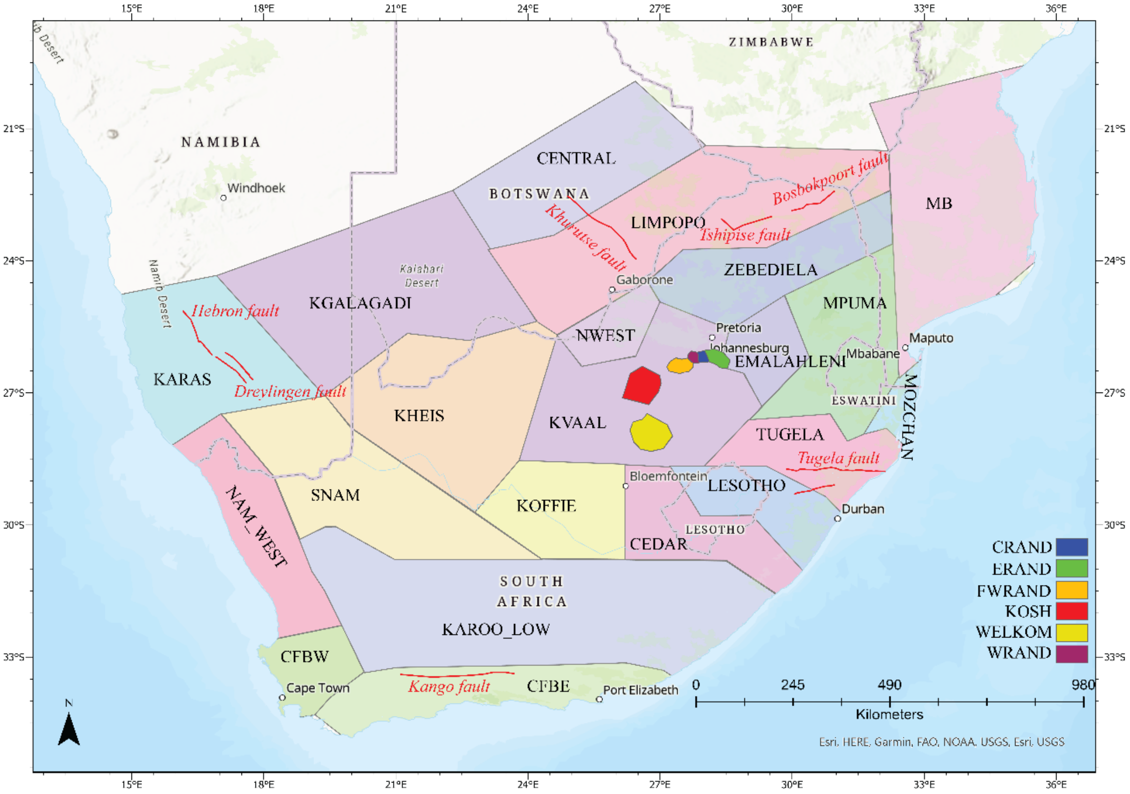

Figure 1. Identification of the individual area and fault source zones delineated in this study.

3 Rupture Size and Aspect Ratio

The rupture area- and surface rupture length-based relations of Wells and Coppersmith (1994) was judged to be suitable for use in this study. Since Wells and Coppersmith (1994) provided regression coefficients for all-slip-type relationships, relations for normal and strike-slip faulting were selected:

Strike-slip: $M = 3.98(\pm 0.07) + 1.02(\pm 0.03) \log_{10} RA$

Normal faulting $M = 3.93(\pm 0.23) + 1.02(\pm 0.1) \log_{10} RA$

Strike-slip: $M = 5.16(\pm 0.13) + 1.12(\pm 0.08) \log_{10} SRL$

Where M = moment magnitude, RA = Rupture area and SRL = Surface rupture length, which is obtained by linking Rupture length and Rupture width related through the rupture aspect ratio. The aspect ratio (length: width) of ruptures for small magnitudes is assessed to be 1:1.

With increasing magnitude and rupture length/area, the rupture width will eventually reach the bottom or the top of the seismogenic crust. Once the entire seismogenic width has ruptured, the aspect ratio will increase with increasing magnitude to conserve the proper rupture length.

4 Rupture Strike and Dip, and Style of Faulting

Assessments in relation to future rupture parameters that relate to the multiple seismic sources are discussed in Table 2. Discussed for each of the seismic source zones are the characteristics of each zone in relation to the rupture parameters.

Table 2. The source zone–specific assessments of the future rupture parameters, where S – Strike in degrees, D – dip in degrees, DD – Dip Direction and R – Rake or slip direction in degrees.

Zones	Tectonic Regime (Stress Regime)	Earthquake Focal Mechanisms		
		S	D	R
CEDAR	Normal faulting	173	40	-90
CENTRAL	Normal faulting	254	45	-75
CFBE	Normal faulting (60%)	336	62	-65
	Strike-slip faulting (40%)	90	90	-10
CFBW	Strike slip Faulting	320	76	-1.6
CRAND	Normal faulting (70%)	90	60	-90
	Strike Slip faulting (30%)	330	80	-5
EMALAHLENI	Normal faulting.	132	60	-62
ERAND	Normal faulting	185	45	-57
FWRAND	Normal faulting (70%)	221	53	-74
	strike-slip faulting (30%)	2	82	-18
KARAS	Normal faulting	320	60	-80
KAROO_LOW	Normal faulting (50%)	111	56	-53
	Strike Slip faulting (50%)	109	71	-2
KGALAGADI	Normal faulting (50%)	5	80	-80
	Strike-slip (50%)	60	80	-20
KHEIS	Normal faulting	350	75 -80	-70
KOFFIE	Normal fault (60%)	205	41	-90
	Strike Slip (40%)	250	56	-9
KOSH	Normal faulting 70%)	228	57	-84
	Strike-slip faulting (30%)	145	65	-10
KVAAL	Normal faulting	294	44	-73
LESOTHO	Normal faulting	185	68	-52
LIMPOPO	Normal faulting	241	30	-90
MB	Normal faulting	171	41	-90
MOZCHAN	Normal faulting	213	40	-69
MPUMA	Normal faulting	128	52	-51
NAM_WEST	Normal faulting (50%)	160	80	-70
	Strike-slip faulting (50%)	160	80	-10
NWEST	Normal faulting	125	48	-76
SNAM	Strike slip faulting	110	67	-15
TUGELA	Normal faulting	158	69	-49
WELKOM	Normal faulting	178	47	-50
WRAND	Normal faulting.	240	55	-73
ZEBEDIELA	Normal faulting.	125	48	-76

5 Area Source Recurrence Parameters

The following parameters were calculated and are included in Table 3:

- The b-value, which represents the slope of the Gutenberg-Richter relation and controls the relative frequency of occurrence of earthquakes of different magnitudes.
- The a–value, which is the intercept of the Gutenberg-Richter relation and represents the number of earthquakes with $M_W \geq 0$ occurring each year. Note that for some zones alternative values for a and b-value were obtained using the two techniques, maximum likelihood, and least squares technique. These were done were there was higher uncertainty due to lack of sufficient data.
- The maximum expected earthquake magnitude (Mmax) for each value. Given that there is much uncertainty associated with the determination of this parameter, alternative approaches were used resulting in more than one weighted value determined for each source zone.

Table 3. Updated recurrence parameters calculated for source zones considered in the present study. Included are obtained Mmax values and their weights. Note: ML refers to Mmax values obtained using the Maximum likelihood technique, K-S-B to the Kijko-Sellevol-Bayes technique and WC94 – refers to Mmax values obtained using an equation from Wells and Coppersmith (1994), MINE - refers to value assigned based on largest observed magnitude in the gold mining region.

Zone	b-value	a-value (M≥0)	Mmax	Mmax weight	Technique
CEDAR	1.08	3.69	5.8 6.3 8.0	0.3 0.5 0.2	Mobs+0.5 K-S-B WC94
CENTRAL	0.76	2.04	7.0 6.76 7.8	0.3 0.5 0.2	Mobs+0.5 ML WC94
CFBE	1.17	3.70	5.9 5.66 7.9	0.3 0.5 0.2	Mobs+0.5 ML WC94
CFBW	0.72 0.76	1.91 (0.5) 2.33 (0.5)	6.7 7.07 7.6	0.3 0.5 0.2	Mobs+0.5 K-S-B WC94
CRAND	1.69	5.61	5.1 5.5 6.5	0.2 0.6 0.2	Mobs+0.8 MINE WC94
EMALAHLENI	1.50	4.51	5.1 6.28 6.7	0.3 0.5 0.2	Mobs+0.5 K-S-B WC94
ERAND	1.47	5.41	5.2	0.3	Mobs+0.5

			5.5	0.5	MINE
			6.8	0.2	WC94
FWRAND	1.59	6.58	5.1	0.6	K-S-B
			6.8	0.4	WC94
KARAS	1.01	3.45	5.2	0.6	K-S-B
			7.6	0.4	WC94
KAROO_LOW	0.97	3.37 (0.5)	5.7	0.4	Mobs+0.5
	1.13	4.04 (0.5)	5.45	0.6	K-S-B
KGALAGADI	1.02	2.85 (0.5)	5.5	0.3	Mobs+0.5
	0.82	1.91 (0.5)	6.66	0.5	K-S-B
			7.6	0.2	WC94
KHEIS	1.56	3.63 (0.5)	5.1	0.3	Mobs+1.3
	1.09	2.08 (0.5)	5.34	0.5	K-S-B
			7.9	0.2	WC94
KOFFIE	0.79	3.06	6.7	0.3	Mobs+0.5
			7.67	0.5	K-S-B
			7.0	0.2	WC94
KOSH	1.44	6.07	6.0	0.3	Mobs+0.5
			5.8	0.5	K-S-B
			6.8	0.2	WC94
KVAAL	1.04	3.14	5.1	0.6	K-S-B
			7.3	0.4	WC94
LESOTHO	0.96	2.80	5.8	0.3	Mobs+0.5
			6.33	0.5	K-S-B
			7.6	0.2	WC94
LIMPOPO	0.83	2.15	5.8	0.3	Mobs+0.5
			6.05	0.5	K-S-B
			7.8	0.2	WC94
MB	0.80	3.47	7.5	0.3	Mobs+0.5
			8.03	0.5	K-S-B
			7.7	0.2	WC94
MOZCHAN	1.17	4.09 (0.5)	6.2	0.3	Mobs+0.5
	1.32	4.68 (0.5)	7.92	0.5	K-S-B
			7.7	0.2	WC94
MPUMA	0.76	2.25	5.3	0.3	Mobs+0.5
			5.04	0.5	K-S-B
			7.5	0.2	WC94
NAM_WEST	0.72	1.87	6.0	0.3	Mobs+0.5
			6.45	0.5	K-S-B
			7.6	0.2	WC94
NWEST	1.09	2.54	5.1	0.2	Mobs+0.9
			5.62	0.6	K-S-B
			6.9	0.2	WC94
SNAM	0.87	3.04	6.0	0.3	Mobs+0.5
			5.69	0.5	K-S-B
			7.6	0.2	WC94
TUGELA	0.99	2.87	6.5	0.3	Mobs+0.5
			6.25	0.5	ML
			7.9	0.2	WC94
WELKOM	1.35	5.33	5.4	0.3	Mobs+0.5
			5.1	0.5	K-S-B
			7.1	0.2	WC94

WRAND	1.44	4.68	5.1 5.5 6.8	0.2 0.6 0.2	Mobs+1.2 MINE WC94
ZEBEDIELA	1.02	3.03	5.3 5.1 7.7	0.3 0.5 0.2	Mobs+0.5 K-S-B WC94

6 Characteristics of Identified Fault Sources

Using available information from geological, paleoseismic, geodetic and seismological studies, various parameters including recurrence parameters (slip rate and recurrence rates from Youngs and Coppersmith (1985)) and M_{max} values (Wells and Coppersmith, 1994) were determined for the four faults assumed to have reliable evidence of their capability. The parameters obtained are all included in Table 4. Long-term (late Quaternary) slip rate cannot be assessed as yet by isotopic or fossil dating of Quaternary units, therefore, the long-term slip rate determination could not be assessed. However, the short-term geodetic slip rate is available from GPS measurements across the KZN area as detailed in Chapter 3. The right-lateral slip rate 0.12 - 0.113 mm/yr of Tugela Fault is quite consistent with most of intraplate strike-slip faults worldwide.

Table 4. Characteristics of identified fault sources. In brackets are proposed weights of parameters

Fault source	Seismogenic Probability p[S]	Style of faulting	M_{max} (weight)	Recurrence Rates (events/year)	Slip rate (mm/ year)	b value	Direction of fault dip	Dip angle, °
Hebron / Dreylingen fault	Evidence from geological and paleoseismic investigations. Thus p[S] = 1	Normal faulting	6.80 (0.4) 7.17 (0.3) 7.28 (0.2) 7.42 (0.1)	0.000011 (0.9) 0.0025 (0.1)	0.004 (0.9) 5.0 (0.1)	1.01	West	60 - 80
Kango fault	Direct evidence from paleoseismic investigations. Thus p[S] = 1	Normal faulting	6.75 (0.1) 7.00 (0.4) 7.25 (0.4) 7.50 (0.1)	0.000125 (0.8) 0.000167 (0.2)	0.1 (0.2) 0.2 (0.6) 0.3 (0.2)	1.17	South	50 - 67
Tshipise and Bosbokpoort fault	Some direct paleoseismic evidence, evidence, presence of hot springs and association with seismicity. Thus p[S] = 1	Normal faulting	6.6 (0.4) 7.6 (0.3) 8.0 (0.3)	0.01 (0.7) 0.00041 (0.3) For $M \geq 5.0$	0.125 (0.7) 0.625 (0.3)	1.0 (0.2) 0.83 (0.8)	South	80
Tugela fault	Direct tectonic geomorphology, geology, and geophysical evidence	Strike slip faulting	7.8 (0.4) 7.5 (0.3) 8.1 (0.3)	0.00001 (0.9) 0.0001 (0.1) For $M \geq 7.0$	0.12 (0.9) 0.113 (0.1)	0.83	South	69

7 Identification of suitable ground motion prediction equations

GMPEs are used to relate a ground-motion parameter (e.g., peak ground acceleration) to a set of variables describing the earthquake source, wave propagation path and local site conditions (Douglas, 2003). These independent variables invariably include magnitude, source-to-site distance, and local site conditions, and often style-of-faulting (mechanism). Some recent models go further to account for other factors affecting earthquake ground motions (e.g., hanging wall effects). Given that hundreds of GMPEs have been published in recent times, it is a daunting task to identify suitable models for a given project.

The alternatives to developing a ground motion model can be grouped into three general categories:

1. Use of a set of available ground motion models and to assign a probability weight to each model
2. Develop a new attenuation relation from data and seismological source models
3. Develop a composite ground motion model

Since there are no GMPEs that have previously been derived specifically for South Africa, it is necessary to develop a model / s based on one of the categories mentioned above. Accelerometers were only installed in South Africa in the gold mining regions of the country from 2010. However, the existing ground motion record dataset does not allow users to derive a local GMPE due to the lack of strong motion earthquakes. In this regard, models from other regions are carefully selected and tested if they fit appropriately to the local data. In previous work, Grobbelaar et al. (2020) followed a modified version of the first alternative procedure to identify and select a set of GMPEs suitable for use in seismic hazard studies in southern Africa. In this procedure, predictions of pre-selected GMPEs were compared to observed seismic data following the procedure by Scherbaum et al. (2009) to test if the selected models capture the observed ground motions. Models derived for both stable continental regions (SCR) and active shallow crustal regions were selected and tested. South Africa is generally considered to be a SCR, mainly because of its position relative to plate boundaries, relatively low number of large earthquake activity and the slow rates of crustal deformation. However, the current tectonic regime of the southern African region shows evidence of extensional tectonic stresses with dominant normal faulting (Manzunzu et al., 2019; Midzi et al., 2020; Stamps et al., 2018). Johnston et al. (1994) showed that extensional tectonic stresses are uncommon within SCRs and thus for this reason alternative GMPEs from active shallows crust were also selected and tested.

Of the six models identified by Grobbelaar et al. (2020) to cover the South African observed earthquake ground motion, three were assumed to cover the epistemic uncertainty associated with the predicted ground motion and thus were finally selected for use in the seismic hazard assessment. Of the three models, two that were previously derived for active shallow crust (Boore and Atkinson, 2008 and Akkar et al., 2014) were found to be suitable. Both equations have the advantage of specifically including the average shear-wave velocity over the uppermost 30m of ground, VS30, as a predictive parameter as well as being able to predict ground motion at long periods. A clear advantage of the Akkar et al. (2014) GMPE is the ability to explicitly select an appropriate style of faulting.

We cannot also avoid the clear evidence that strain rates are very low as well as the intraplate position of southern Africa. Thus, one other equation, which was previously determined for a SCR, was also selected (Atkinson and Boore, 2006). The three models are implemented in the hazard calculation with the Akkar et al. (2014) GMPE given a high weight of 0.5, Boore and Atkinson (2008) a weight of 0.3 and Atkinson and Boore (2006) a weight of 0.2 for all the sources (Table 5).

Table 5. The three GMPEs selected for use in the PSHA of South Africa

GMPE	Region	Weight	Remarks
Akkar et al. (2014)	Europe and Middle East	0.5	Active shallow crust. Mostly events of normal faulting used.
Boore and Atkinson (2008)	Western North America	0.3	Active shallow crust. Data used had a mixture of focal mechanisms.
Atkinson and Boore (2006)	Eastern North America	0.2	Stochastic finite-fault approach with small to moderate earthquake data from ENA also used to provide region specific underlying parameters.

8 Seismic Hazard Assessment

In this study, classical probabilistic seismic hazard calculations were carried out using the OPENQUAKE software developed by the Global Earthquake Model Foundation. A comprehensive manual (Crowley et al., 2015) on the use of the software is available for free on the GEM website. The probabilistic seismic hazard analysis applied in this study is based on the widely used classical methodology developed by Cornell (1968), McGuire (1974, 1976) and Der Kiureghian and Ang (1975, 1977). The hazard calculations were made for the following conditions, using a characterized seismic source model as described in sections above:

- All calculations were made for 10% probability of exceedance in 50 years (or return period of 475 years).
- The minimum magnitude adopted is M_{min} = 5.0, which is consistent with the practice of excluding frequent, small events of little engineering significance.

Calculations were performed at three target response periods, PGA, 0.15s and 2.0s. This was done to ensure a full description of the predicted hazard for southern Africa. In this study, the classical probabilistic approach as originally defined by Cornell (1968) was applied to obtain new realistic southern African seismic hazard maps. In this application, a seismic source model comprising 27 area source zones and four fault sources was used. Given the inadequacies associated with the data used, such as short earthquake catalogue and limited geological information on active faults, both epistemic and aleatory uncertainties were considered and applied in the hazard calculation through the use of logic trees. Seismic hazard maps for return periods of 475 years (i.e., 10% probability of exceedance in 50 years) for three spectral ordinates (PGA, 0.15s, 0.2s) were produced (Figure 2). All spectral periods show high hazard values at the gold mining, Koffiefontein and Cape town regions. The former is mainly influenced by levels of seismicity and two later regions most likely due to past strong earthquakes recorded within the region and continuous high level of seismicity. There is also a clear influence of the MB zone source, which has a record of large earthquakes on the hazard for the north-eastern part of the country, as well as the SNAM zone sources, mostly due to the Augrabies swarm. The high acceleration observed in the KOSH region at lower periods could be a result of the shallow moderate earthquakes in that area as well as the high activity rates associated with the mining related earthquakes. The influence of large events in the southwestern part of the country in the Western Cape Province is also clear, mainly because the moderate to strong events and longer earthquake records.

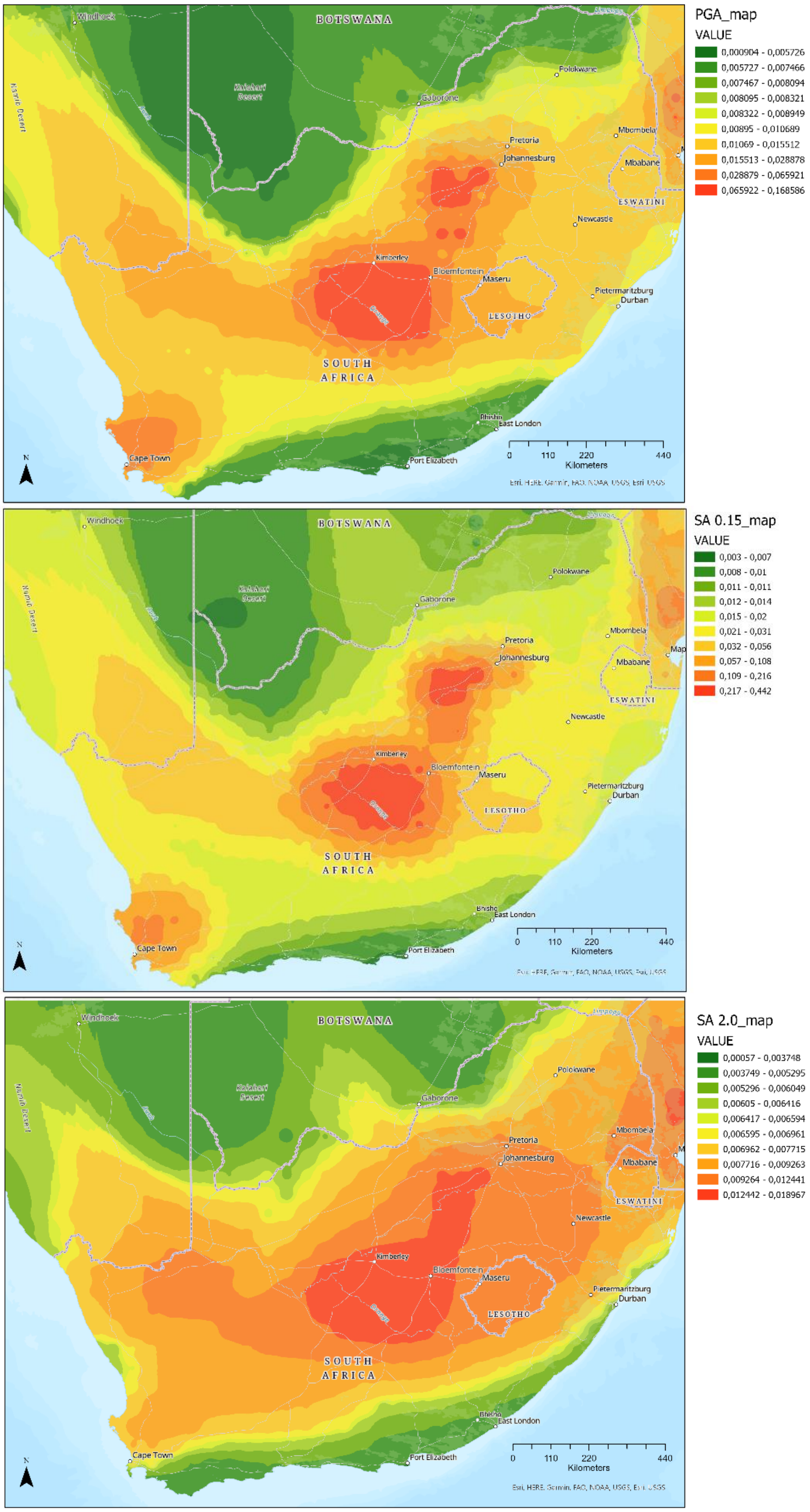

Figure 2. New PGA, 0.15s and 0.2s seismic hazard maps for southern Africa prepared at return period of 475 years.

The hazard results from Midzi et al. (2020) shows highest values of 0.2184 in the mining regions, as well as the Augrabies and Koffiefontein regions with 0.0659. The Cape Town and Kwazulu-Natal regions show low values of 0.0293.

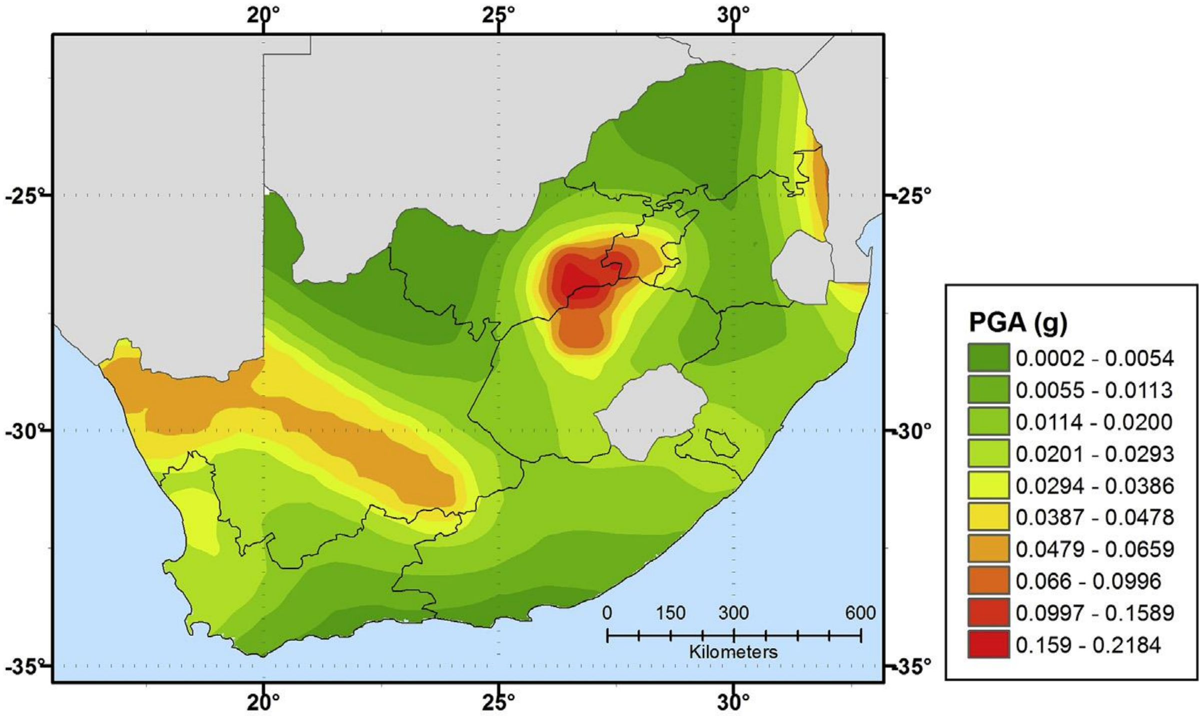

Figure 3. Midzi et al. (2020) PGA seismic hazard maps for southern Africa prepared at return period of 475 years.

9 Discussion

To analyse the effect of the new seismotectonic model of southern Africa, the seismic hazard results from this study are compared to those from Midzi et al. (2020) since they are the first hazard maps produced for South Africa using a probabilistic seismic hazard assessment approach where seismic source zones were utilised. When comparing the hazard results obtained from this study to those from Midzi et al. (2020) study, the maximum PGA values are observed in the mining region from both studies. However, the maximum values from this study are lower than those from Midzi et al. (2020). This could be due to the contribution of the seismogenic depth utilised in the hazard input model. There are also differences in the Cape

Town and Kwazulu-Natal regions which shows high hazard values from this study as compared to the previous study of Midzi et al. (2020).

10 Conclusion

The work presented on the seismic hazard assessment shows the importance of having a reliable seismic source model, which was derived from the new seismotectonic model of southern Africa. The contribution from the seismotectonics of Moiyabana earthquake as well as the Kwazulu-Natal; and the seismogenic depth of southern Africa, resulted in a more realistic seismic hazard of southern Africa. The changes done in this new SSC model compared to what was published in the previous map (Midzi et al., 2020) are quite significant. This proves the importance of seismotectonics within intraplate southern Africa region. In addition, GMPEs are also crucial in this work. Unfortunately, the lack of strong motion data in the country makes it impossible to derive a model specifically for South Africa. However, investigations should continue to assess and implement published models for this region.

References

Akkar S., M.A. Sandıkkaya and J.J. Bommer (2014). Empirical ground-motion models for point-and extended-source crustal earthquake scenarios in Europe and the Middle East, Bulletin of earthquake engineering, 12(1), 359-387.

Atkinson G.M. and D.M. Boore (2006). Earthquake ground-motion prediction equations for eastern North America, Bulletin of the Seismological Society of America, 96(6), 2181–2205, doi: 10.1785/0120050245.

Boore D.M. and G.M. Atkinson (2008). Ground-motion prediction equations for the average horizontal component of PGA, PGV, and 5%-damped PSA at spectral periods between 0.01 s and 10.0 s, Earthquake Spectra, 24(1), 99-138.

Coppersmith K.J. and R.R. Youngs (1986). Capturing uncertainty in probabilistic seismic hazard assessments within intraplate tectonic environments, Proceedings of the Third U.S. National Conference on Earthquake Engineering, Charleston, 1, 301-312.

Cornell C.A. (1968). Engineering seismic risk analysis, Bulletin of the Seismological Society of America, 58, 1583-1606.

Der Kiureghian A. and A.H-S. Ang (1977). A fault-rupture model for seismic risk analysis, Bulletin of the Seismological Society of America, 67(4), 1173-1194.

Douglas J. (2003). Earthquake ground motion estimation using strong-motion records: a review of equations for the estimation of peak ground acceleration and response spectral ordinates, Earth-Science Reviews, 61(1-2), 43-104.

Fernandez L.M. and J.A. Guzman (1979). Seismic History of Southern Africa, Geological Survey of South Africa, Seismologic Series 9, 1-38.

Grobbelaar M., V. Midzi, J. Bunk, N. Flint, B. Manzunzu, T. Mulabisana, S. Myendeki, T. Pule and W. Meintjes (2020). 2019/2020 Report: Seismic Hazard and Risk Related Studies, CGS report number 2020-0030.

Johnston A.C., L.R. Kanter, K.J. Coppersmith and C.A. Cornell (1994). The stable continental region earthquake database, In: The Earthquakes of Stable Continental Regions: Assessment of Large Earthquake Potential, EPRI Report TR-102261-V1

Kijko A., S.J.P. Retief and G. Graham (2003). Seismic hazard and risk assessment for Tulbagh, South Africa: part II–assessment of seismic risk, Natural Hazards, 30(1), 25-41.

Manzunzu B., V. Midzi, T.F. Mulabisana, B. Zulu, T. Pule, S. Myendeki and G.W. Rathod (2019). Seismotectonics of South Africa. Journal of African Earth Sciences, 149, 271-279.

McGuire R.K. (1974). Seismic structural response risk analysis, incorporating peak response regressions on earthquake magnitude and distance, Massachussets Technical, Department of Civil Engineering, Publication No. 399, p371.

McGuire R.K. (1976). FORTRAN computer program for seismic risk analysis, U.S Geological Survey Open-File Report 76-67, p90.

Midzi V., B. Manzunzu, T. Mulabisana, B.S. Zulu, T. Pule and S. Myendeki (2020). Probabilistic seismic hazard maps for South Africa, Journal of African Earth Sciences, 162.

Midzi V., D.J. Hlatywayo, L.S. Chapola, F. Kebede, K. Atakan, D.K. Lombe, G. Turyomurugyendo and Tugume F.A. (1999). Seismic hazard assessment in Eastern and Southern Africa, Annals of Geophysics, 42(6).

Scherbaum F., E. Delavaud and C. Riggelsen (2009). Model selection in seismic hazard analysis: an information-theory perspective, Bulletin of the Seismological Society of America, 99, 3234-3247.

Shapira A. and L.M. Fernandez (1989). Probabilities of exceedance for prescribed peak ground accelerations (PGA) at selected southern African locations, Tectonophysics, 167(2-4), 253-260.

Stamps D.S., E. Saria and C. Kreemer (2018). A Geodetic Strain Rate Model for the East African Rift System, Scientific Reports, 8.

Wells D.L. and K.J. Coppersmith (1994). New Empirical Relationships Among Magnitude, Rupture Length, Rupture Width, Rupture Area, and Surface Displacement, Bulletin of the Seismological Society of America, 84, 974-1002.

Chapter 6

Chapter 6: Conclusion

Throughout the historical period, Southern Africa experienced several infrequent but destructive earthquakes with M > 6 (Meghraoui et al., 2016). In this thesis, seismicity data analysis and field investigations related with these earthquake sources became necessary in the perspective of a realistic seismic hazard assessment. A new seismotectonic model including reliable seismic sources derived from tectonic geomorphology and earthquake geology provides a basis for a new seismic hazard evaluation. This was achieved through a thorough study of the seismotectonic characteristics of each region, which was emphasized by the study of the 2017 Moiyabana and 1932 St Lucia earthquakes in southern Africa.

The near field study of the 2017 Moiyabana earthquake (Mw 6.5) provides data and results on the crustal deformation of the intraplate tectonic domain of southern Africa. The detailed mainshock and aftershocks analysis shows a seismic sequence that suggests a fault-rupture geometry in agreement with normal focal mechanisms. The aftershocks analysis and focal mechanism solutions show predominately normal faulting that agrees with the NE-SW extensional stress regime in the region. The InSAR analysis shows the colocation of surface deformation with the western earthquake sequence and allows the modelling of a NW-SE trending fault rupture, dipping NE with an average 50 cm slip distribution and a seismic moment M_o 3.68 x 10^{18} Nm (Mw 6.4). SE of the epicentral area, we identified the NNW-SSE to NW-SE trending composite and sharp scarp morphology of the Khurutse fault scarp that aligns with the 2017 Moiyabana earthquake rupture. The active Okavango and Zoetfontein fault region, in the north and south of the Moiyabana earthquake location, respectively; indicate that the southern African continental region is active. In addition, the Khurutse fault scarp reflects a cumulative surface deformation, clearly highlighting the presence of a seismic cycle in this intraplate context.

The assessment of the structural background of the 1932 St Lucia earthquake and GPS slip rate analysis in KwaZulu-Natal, South Africa, together with the tectonic geomorphology along the Tugela and Greytown fault scarps characterise and determine the evidence of a seismic cycle in southern Africa. The Tugela fault scarp is ~230 km long and clearly visible on the surface from southeast of Ladysmith extending EW until Richards Bay, which is located ~100 km SE of the 1932 M_W 6.9 St Lucia Earthquake. Tectonic geomorphology studies conducted along this fault scarp yielded evidence of several right lateral offsets from the hydrographic system indicating the existence of a seismic cycle within this intraplate continental region.

Comparison of velocities obtained from GPS station data north and south the Tugela fault scarp also shows evidence of right lateral movement with the block north of the fault scarp moving faster than that in the south. The deformation rate in this intraplate continental region of southern Africa is low but perceptible. This is in support of conclusions from Johnston (1996a, 1996b) and Landgraf et al. (2017), that areas of slow strain rate are subject to seismic hazards. Paleoseismological studies, to determine long-term (late Quaternary) slip rate by isotopic or fossil dating of Quaternary units, must be conducted to conclude with certainty that the Tugela and Greytown fault scarp are active.

There is evidence of the upper 30% of the southern African crust producing most of the earthquakes. The Archean Kaapvaal Craton, oldest region within the study area, has a relatively thinner crust with a thicker seismogenic layer compared to the younger geological regions. The Namaqua-Natal and Cape Fold belts, younger geological regions have a more heterogenous crustal thickness with a thinner seismogenic layer. The seismogenic layer thickness, the part of the crust where anelastic deformation occurs, within intraplate southern Africa differs from the elastic thickness, as well as the crustal thickness. The shallow seismogenic depth, of a unimodal nature may have an influence on the seismic hazard of southern Africa due as it is indicative of shallow fault ruptures.

Limitations and Perspectives

The contribution from the active faulting and seismotectonics of Moiyabana earthquake as well as the Kwazulu-Natal; and the seismogenic depth of southern Africa, resulted in a more realistic seismic hazard of southern Africa. Although significant, the changes done in this new seismic source characteristic model compared to what was published in the previous map (Midzi et al., 2020) may not be sufficient. Indeed, further field investigations on the identification of active faults and the study of their ability in generating large earthquakes are needed in South Africa. An inventory of active faults affecting late Quaternary deposits (units younger than 150 ka) is recommendable in South Africa. Although field investigations have been initiated along the Kango fault along the Cape folding belt region (Goedhart and Booth, 2016a), paleoseismic studies using trenching across faults in KZN are missing. Trenching through fault scarps and subsequent dating of faulting events represent a necessary step in the characterisation of past earthquakes. The cumulative right-lateral offset along the Tugela and Greytown fault zones denotes of a rather continuous and successive coseismic faulting activity likely associated with large earthquakes (with Mw > 6). The strain rate being relatively low in

South Africa (< 8 ηstrain/yr; Malservisi et al., 2013), the active deformation and related seismic cycle do not favour a short return period of earthquake generation on a single fault segment. This limitation should not rule out the occurrence of large earthquakes and associated risk across the south African seismotectonic zones.

References

Adams, A. and Nyblade, A., 2011. Shear wave velocity structure of the southern African upper mantle with implications for the uplift of southern Africa. Geophysical Journal International, 186(2), pp.808-824.

Andreoli, M.A.G., Doucoure, M., Van Bever Donker, J., Brandt, D., Andersen, N.J.B., 1996. Neotectonics of southern Africa-a review. Africa Geoscience Review, 3(1), pp.1-16.

Begg, G. C., Griffin, W. L., Natapov, L. M., O'Reilly, S. Y., Grand, S. P., O'Neill, C. J., Hronsky, J. M. A., Poudjom Djomani, Y., Swain, C.J., Deen, T., Bowden, P., 2009. The Lithospheric Architecture of Africa: Seismic Tomography, Mantle Petrology, and Tectonic Evolution, Geosphere, 5, 23 – 50.

Bent, A.L., 1994. The 1989 (Ms 6.3) Ungava, Quebec, earthquake: A complex intraplate event. Bulletin of the Seismological Society of America, 84(4), pp.1075-1088.

Boschi, E., Gasperini, P. and Mulargia, F., 1995. Forecasting where larger crustal earthquakes are likely to occur in Italy in the near future. Bulletin of the Seismological Society of America, 85(5), pp.1475-1482.

Brown, R., Gernon, T., Stiefenhofer, J., Field, M., 2008. Geological constraints on the eruption of the Jwaneng Centre kimberlite pipe, Botswana. J. Volcanol. Geotherm. Res., 174 (1), 195 – 208.

Calais, E., T. Camelbeeck, Stein, S., Liu, M., Craig, T. J., 2016. A new paradigm for large earthquakes in stable continental plate interiors, Geophys. Res. Lett, 43(20), 10621 – 10637.

Camelbeeck, T. and Meghraoui, M., 1998. Geological and geophysical evidence for large palaeo-earthquakes with surface faulting in the Roer Graben (northwest Europe). Geophysical Journal International, 132(2), pp.347-362.

Chéry, J., Carretier, S., Ritz, J.-F., 2001. Postseismic stress transfer explains time clustering of large earthquakes in Mongolia, Earth Planet. Sci. Lett., 194(1–2), 277–286, doi:10.1016/S0012-821X(01)00552-0.

Clark, D., Dentith, M., Wyrwoll, K. H., Yanchoul, L., Dent, V., Featherstone, C., 2008. The Hyden fault scarp, Western Australia: paleoseismic evidence for repeated Quaternary displacement in an intracratonic setting, Aust. J. Earth Sci., 55, 379 – 395.

Cornell, D.H., Thomas, R.J., Gibson, R., Moen, H.F.G., Reid, D.L., Moore, J.M. and Gibson, R.L., 2006. The Namaqua-Natal Province. Geological Society of South Africa.

Cornell, D.H., Van Schijndel, V., Ingolfsson, O., Scherstén, A., Karlsson, L., Wojtyla, J. and Karlsson, K., 2011. Evidence from Dwyka tillite cobbles of Archaean basement beneath the Kalahari sands of southern Africa. Lithos, 125(1-2), pp.482-502.

Crone, A. J., Machette, M. N., Bowman, J. R., 1997. Episodic nature of earthquake activity in stable continental regions revealed by palaeoseismicity studies of Australian and North American quaternary faults, Aust. J. Earth Sci., 44(2), 203–214.

De Wit, M.J., de Ronde, C.E., Tredoux, M., Roering, C., Hart, R.J., Armstrong, R.A., Green, R.W., Peberdy, E. and Hart, R.A., 1992. Formation of an Archaean continent. Nature, 357(6379), pp.553-562.

Fernandez, L.M. and Guzman, J.A., 1979. Seismic history of Southern Africa, Seismological Series Geological Survey of South Africa 9, p.38.

Goedhart, M.L. and Booth, P.W.K., 2016a. A palaeoseismic trench investigation of early Holocene neotectonic faulting along the Kango Fault, southern Cape Fold Belt, South Africa–Part I: Stratigraphic and structural features. South African Journal of Geology, 119(3), pp.545-568.

Goedhart, M.L. and Booth, P.W.K., 2016a. A palaeoseismic trench investigation of early Holocene neotectonic faulting along the Kango Fault, southern Cape Fold Belt, South Africa–Part II: Earthquake Parameters. South African Journal of Geology, 119(3), pp.569-582.

Hälbich, I.W., 1983. Geodynamics of the Cape Fold Belt in the Republic of South Africa, a summary. Profile of Orogenic Belts, 10, pp.21-29.

Hartnady, C., 1990. Seismicity and plate boundary evolution in Southeastern Africa, S. Afr. J. Geol., 93, 473–484.

Hough, S.E. and Page, M., 2011. Toward a consistent model for strain accrual and release for the New Madrid seismic zone, central United States. Journal of Geophysical Research: Solid Earth, 116(B3).

Johnston, A.C., Kanter, L.R., Coppersmith, K.J. and Cornell, C.A., 1994. The earthquakes of stable continental regions. Volume 3: Seismicity data sheets (part 1). Final report (No. EPRI-TR-102261-V3). Electric Power Research Inst.(EPRI), Palo Alto, CA (United States); Memphis State Univ., TN (United States). Center for Earthquake Research and Information; Geomatrix Consultants, Inc., San Francisco, CA (United States); CAC, Inc., Portola Valley, CA (United States).

Johnston, A.C., 1996a. Seismic moment assessment of earthquakes in stable continental regions—I. Instrumental seismicity, *Geophys. J. Int.*, 124 (2), 381– 414.

Johnston, A.C., 1996b. Seismic moment assessment of earthquakes in stable continental regions—II. Historical seismicity, Geophys. J. Int., 125 (3), 639 – 678.

Kijko A., S.J.P. Retief and G. Graham (2003). Seismic hazard and risk assessment for Tulbagh, South Africa: part II–assessment of seismic risk, Natural Hazards, 30(1), 25-41.

Landgraf A., S. Kübler, E. Hintersberger and S. Stein, 2017. Active tectonics, earthquakes and palaeoseismicityin slowly deforming continents, In: Geological Society Special Publication, 432, 1, pp. 1-12.

Malservisi, R., Hugentobler, U., Wonnacott, R. and Hackl, M., 2013. How rigid is a rigid plate? Geodetic constraint from the TrigNet CGPS network, South Africa. Geophysical Journal International, 192(3), 918 – 928.

Manzunzu, B., Midzi, V., Mulabisana, T.F., Zulu, B., Pule, T., Myendeki, S. and Rathod, G.W., 2019. Seismotectonics of South Africa. Journal of African Earth Sciences, 149, pp.271-279.

Meghraoui, M., Amponsah, P., Ayadi, A., Ayele, A., Ateba, B., Bensuleman, A., Delvaux, D., El Gabry, M., Fernandes, R., 2016. The Seismotectonic Map of Africa, Episodes, 39 (1), 9 – 18.

Midzi, V., Hlatywayo, D.J., Chapola, L.S., Kebede, F., Atakan, K., Lombe, D.K., Turyomurugyendo, G. and Tugume, F.A., 1999. Seismic hazard assessment in Eastern and Southern Africa. Annals of Geophysics, 42(6). Njoroge, M., R. Malservisi, Voytenko, D., Hackl, M., 2015. Is Nubia Plate Rigid? A geodetic study of the relative motion of different cratonic areas within Africa, International Association of Geodesy Symposia, p 1-9, doi:10.1007/1345_2015_212.

Midzi V., B. Manzunzu, T. Mulabisana, B.S. Zulu, T. Pule and S. Myendeki (2020). Probabilistic seismic hazard maps for South Africa, Journal of African Earth Sciences, 162.

Rajendran, C. P., Rajendran, K., John, B., 1996. The 1993 Killari (Latur), central India, earthquake: An example of fault reactivation in the Precambrian crust, Geology 24, 651–654.

Ranganai, R. T., Kampunzu, A. B., Atekwana, E. A., Paya, B. K., King, J. G., Koosimile, D. I., Stettler, E. H., 2002. Gravity evidence for a larger Limpopo Belt in southern Africa and geodynamic implications, Geophys J Int., 149 (3), F9 – F14.Roering, C., van Reenen, D. D., Smit, C. A., Barton, J. M., de Beer, J. H., de Wit, M. J., Stettler, E. H., van

Schalkwyk, J. F., Stevens, G., Pretorius, S., 1992. Tectonic model for the evolution of the Limpopo Belt, Precambrian Res., 55, 539 – 552.

Saria, E., Calais, E., Stamps, D.S., Delvaux, S. Hartnady, C.J.H., 2014. Present-day kinematics of the East African Rift, J. geophys. Res., 119, doi:10.1002/2013JB010901.

Singh, M., Kijko, A. and Durrheim, R., 2011. First-order regional seismotectonic model for South Africa. Natural Hazards, 59(1), pp.383-400.

Shapira A. and L.M. Fernandez (1989). Probabilities of exceedance for prescribed peak ground accelerations (PGA) at selected southern African locations, Tectonophysics, 167(2-4), 253-260.

Stamps, D. S., Saria, E., Kreemer, C., 2018. A Geodetic Strain Rate Model for the East African Rift System, Sci. Rep., 8(1), 1 – 8.

Tucholke BE, Houtz RE, Barrett DM. Continental crust beneath the Agulhas plateau, southwest Indian Ocean. Journal of Geophysical Research: Solid Earth. 1981 May 10;86(B5):3791-806.

Annex 1

List of Publications

1. Mulabisana T., M. Meghraoui, V. Midzi, M. Saleh, O. Ntibinyane, T. Kwadiba, B. Manzunzu, O. Seiphemo, T. Pule, I. Saunders (2021). Seismotectonic analysis of the 2017 moiyabana earthquake (MW 6.5; Botswana), insights from field investigations, aftershock and InSAR studies, Journal of African Earth Sciences, 182, 1 – 17.
2. Manzunzu B., M.B.C. Brandt, V. Midzi, R.J. Durrheim, I. Saunders, T.F. Mulabisana (2021). Towards a homogeneous moment magnitude determination for earthquakes in South Africa: Reduction of associated uncertainties, Journal of African Earth Sciences, 173, 1-11.
3. Midzi V., T. pule, T. Mulabisana, B. Zulu and B. Manzunzu (2020). Reassessment of source parameters of 'major' southern African earthquakes, South African Journal of Geology, 123 (1), 59 – 74.
4. Midzi V., T. Pule, B. Manzunzu, T. Mulabisana, B.S. Zulu and S. Myendeki (2020). Improved earthquake location in the gold mining regions of South Africa using new velocity models, South African Journal of Geology, 123 (1), 35 – 38.
5. Midzi V, B. Manzunzu, T.F. Mulabisana, B.S. Zulu, T. Pule, S. Myendeki and G. Rathod (2020). The Probabilistic Seismic Hazard Maps of South Africa. Journal of African Earth Sciences, 162, 1 – 14.
6. Manzunzu B., V. Midzi, T. Mulabisana, B. Zulu, T. Pule, S. Myendeki and G.W. Rathod (2020). Seismotectonics of South Africa, Journal of African Earth Sciences, 149, 271 – 279.
7. Midzi V., I. Saunders, B. Manzunzu, M.T. Kwadiba, V. Jele, R. Mantsha, K.T. Marimira, T.F. Mulabisana, O. Ntibinyane, T. Pule, G.W. Rathod, M. Sitali, L. Tabane, G. van Aswegen, B.S. Zulu (2018). The 03 April 2017 Botswana M6.5 earthquake: Preliminary results. Journal of African Earth Sciences, 143, 187 – 194.
8. Mulabisana T., V. Midzi and B. Manzunzu (2018). Local site effects during the Orkney earthquake of 5 August 2014, Pure and Applied Geophysics, 176, 147 – 164.

List of Conferences

1. IPGS PhD student congress 28 November 2018.

2. The Council for Geoscience annual conference 11 – 12 February 2019.
3. South African Geophysical Association's 16th Biennial Conference & Exhibition 06 – 09 October 2019.
4. 2nd Conference of the Arabian Journal of Geosciences 25 – 28 November 2019.
5. IPGS PhD student congress 2021.
6. Geoscience: the fulcrum of human development Council for Geoscience Annual Conference 4th – 5th March 2021
7. EGU General Assembly 19 – 30 April 2021.
8. IAGA-IASPEI 21 – 27 August 2021.

List of Presentations

1. T. Mulabisana, E. Chirenje, V. Midzi, October 2019. Seismotectonics and seismic history of the Koffiefontein region, SAGA 2019.
2. T. Mulabisana, Mustapha M. and V. Midzi, November 2019. Seismotectonics of the Khurutse Region, Botswana, 2nd CAJG 2019.
3. T. Mulabisana. Active Tectonics, Crustal Deformation and Seismotectonic background for a realistic Seismic Hazard Assessment in southern Africa. IPGS PhD student congress 2021.
4. T. Mulabisana, M. Meghraoui, V. Midzi and B. Manzunzu. The impact of aftershocks on the seismotectonics of the 2017 Moiyabana, Botswana earthquake (Keynote). Geoscience: the fulcrum of human development Council for Geoscience Annual Conference 4th – 5th March 2021.
5. Thifhelimbilu Mulabisana, Mustapha Meghraoui, Vunganai Midzi, Mohamed Saleh, Onkgopotse Ntibinyane, Motsamai Tarzan Kwadiba, Brassnavy Manzunzu, Oarabile Seiphemo, Tebogo Pule, and Ian Saunders. Seismotectonic Analysis of the 2017 Moiyabana Earthquake (MW 6.5; Botswana. EGU General Assembly 19 – 30 April 2021.
6. Thifhelimbilu Mulabisana, Mustapha Meghraoui, Vunganai Midzi, Mohamed Saleh, Onkgopotse Ntibinyane, Motsamai Tarzan Kwadiba, Brassnavy Manzunzu, Oarabile Seiphemo, Tebogo Pule and Ian Saunders. The impact of aftershocks on seismotectonics of 2017 Moiyabana, Botswana earthquake. IAGA-IASPEI 21 – 27 August 2021.

Résumé

L'objectif de cette thèse est de déterminer l'impact d'un modèle sismotectonique amélioré sur l'évaluation des risques sismiques en Afrique australe. Cet objectif est atteint par la combinaison de plusieurs approches afin d'adopter une stratégie multidisciplinaire permettant d'améliorer notre compréhension de l'occurrence des tremblements de terre dans l'Afrique australe intraplaque. La caractérisation des forts tremblements de terre et des failles dans les régions intraplaques par des études géologiques, géophysiques et de géomorphologie tectonique est bénéfique pour l'amélioration de l'évaluation de l'aléa sismique.

Le premier chapitre décrit la méthodologie de recherche et les étapes suivies pour évaluer la tectonique active, la déformation de l'écorce terrestre et la sismotectonique en Afrique australe afin d'améliorer l'évaluation des risques sismiques. L'Afrique australe appartient au domaine tectonique intraplaque caractérisé par un faible niveau de sismicité et un faible taux de déformation (Stamps et al., 2014 ; Njoroge et al., 2015 ; Saria et al., 2014 ; Johnston, 1996a, 1996b). Cependant, deux tremblements de terre majeurs se sont produits en Afrique australe et ont été choisis comme centre d'intérêt, à savoir les tremblements de terre de Moiyabana en 2017 et de Sainte-Lucie en 1932.

Notre objectif est de mieux comprendre les processus de génération des séismes en Afrique australe intraplaque en utilisant la sismologie en champ proche, la tectonique active, la télédétection (caractéristiques géomorphologiques et InSAR) et l'impact d'une sismotectonique améliorée sur l'évaluation de l'aléa. Wells et Coppersmith (1994) établissent une régression entre la magnitude et la longueur de la rupture en surface, la longueur de la rupture en subsurface, la largeur de la rupture en aval-pendage et la zone de rupture. Aki et Richards (1980) calculent les sources sismiques en fonction de la fonction de la source, de la distance de la station et de la vitesse de l'onde. Hanks et Kanamori (1979) ont corrélé l'ampleur

du moment à partir de la relation entre le moment sismique et la longueur et la zone de la rupture. Johnston (1996a et b) a établi une procédure pour déterminer le moment sismique ainsi que la magnitude du moment pour les données sismiques instrumentales et dérivées de l'intensité dans une région continentale stable.

Les failles actives peuvent être déterminées et caractérisées en cartographiant leurs effets sur les unités quaternaires à l'aide de méthodes telles que la génération de MNE à haute résolution, la géomorphologie tectonique, la paléosismologie, la contribution de l'InSAR à la cartographie des ruptures de surface. Wells et Coppersmith (1994) établissent une régression entre la magnitude et la longueur de la rupture en surface, la longueur de la rupture en subsurface, la largeur de la rupture en aval-pendage et la zone de rupture. Aki et Richards (1980) calculent les sources sismiques en fonction de la fonction de la source, de la distance de la station et de la vitesse de l'onde. Hanks et Kanamori (1979) ont corrélé l'ampleur du moment à partir de la relation entre le moment sismique et la longueur et la zone de la rupture. Johnston (1996a et b) a établi une procédure pour déterminer le moment sismique ainsi que la magnitude du moment pour les données sismiques instrumentales et celles dérivées de l'intensité dans une région continentale stable. La détermination du mécanisme focal pour indiquer les contraintes horizontales et verticales maximales de compression (Zoback et Zoback, 1989 ; Delvaux, 1993 ; Manzunzu et al., 2017) et l'utilisation des informations obtenues sur la cinématique de la faille par l'inversion des contraintes.

La modélisation d'une rupture cosismique est possible à l'aide d'une modélisation prospective et d'une méthode inverse basée sur les paramètres de la rupture de faille pour la composante de glissement de pendage et de glissement de direction de la déformation fragile de l'écorce terrestre. À cette fin, et entre autres méthodes, l'utilisation du code Poly3D considère les surfaces triangulées comme des discontinuités dans un demi-espace linéaire, élastique, homogène et isotrope (Okada, 1985 ; Maerten et al., 2005). D'autres études menées le long de ces failles à l'aide de méthodes géophysiques régionales et terrestres telles que le magnétisme aéroporté, la tomographie de résistivité électrique (ERT) et les profils sismiques de réflexion attestent d'une déformation active. L'application du filtrage de la première dérivée verticale (FVD) sur les données d'intensité du champ magnétique total permet de mettre en évidence les corps les plus étroits, puis de compléter les résultats par des données géophysiques au sol telles que la sismique réflexion et la résistivité pour confirmer la profondeur du déplacement de l'escarpement de la faille.

L'approche de l'évaluation déterministe de l'aléa sismique (DSHA) développe un ou plusieurs séismes de contrôle qui sont prévus comme étant ceux qui produiront le mouvement du sol le plus important sur le site. L'analyse probabiliste des risques sismiques (PSHA) est basée sur la méthodologie classique largement utilisée développée par Cornell (1968), McGuire (1974, 1976) et Der Kiureghian et Ang (1977). Cette technique utilise la plus grande quantité possible de données, combinant des données sismologiques, géologiques et géophysiques pour construire un modèle des processus de production des tremblements de terre. Les études PSHA modernes, qui suivent les idées proposées par Coppersmith et Youngs (1986), Reiter (1991) sont généralement en mesure de traiter ce problème en incorporant dans le modèle ce que l'on appelle un "arbre logique", dans lequel certains paramètres reçoivent une gamme de valeurs possibles avec une attribution subjective de la probabilité de chacune d'entre elles.

Le deuxième chapitre se concentre sur le séisme de Moiyabana (Botswana) de MW 6,5 du 3 avril 2017, qui s'est produit à l'intérieur du continent de la plaque africaine et dans une région sismogénique précédemment considérée comme stable. Notre objectif est de combiner plusieurs approches (enquêtes de terrain et de télédétection) afin d'adopter une stratégie multidisciplinaire pour améliorer notre compréhension de l'occurrence des tremblements de terre dans l'Afrique australe intraplaque.

Le choc principal (25,134 E, 22,565 S ; profondeur 22 ± 3 km) a été suivi par plus de 500 événements de magnitude $M \geq 0,8$ enregistrés en avril 2017, y compris la plus grande réplique (MW 4,6 le 5 avril 2017). La structure crustale sous les cratons obtenue à partir des fonctions réceptrices et des stations sismiques à large bande caractérise la profondeur moyenne du Moho à 38 km, ce qui est considéré comme la croûte la plus mince de la région (Nguuri et al., 2001) et peut expliquer l'épaisseur de ~30 km de la couche sismogénique (Midzi et al., 2018). La collision des cratons archéens du Kaapvaal et du Zimbabwe entre 2,7 et 2,6 Ga a conduit à la formation de la ceinture mobile du Limpopo, qui constitue le site du séisme de Moiyabana de 2017 (Roering et al., 1992 ; Brown et al., 2008 ; Begg et al., 2009).

Nous analysons la séquence de la secousse principale et de la réplique sur la base d'un réseau sismique local et des caractéristiques sismotectoniques locales. La plus grande réplique de magnitude MW 4,6 s'est produite à l'ouest de la secousse principale le 5 avril 2017 à une profondeur beaucoup plus faible (~10 km) que la secousse principale. Après la secousse principale, une séquence de répliques a été enregistrée du 8 avril au 29 juin 2017 par un réseau temporaire et montre plus de 900 enregistrements de tremblements de terre. L'enregistrement de la séquence sismique comprend des événements sismiques d'une magnitude aussi faible que ML 0,8 avec une diminution du taux d'occurrence quotidien de 101 à 20 événements sismiques au cours du premier mois d'enregistrement (Midzi et al., 2018). Après le choc principal, la décroissance de la sismicité obtenue à partir du nombre quotidien de répliques est conforme à la loi d'Omori (Utsu et al., 1995). La localisation initiale de la séquence sismique obtenue à l'aide du programme HYPOCENTER modifié (Lienert et al., 1986 ; Lienert et Havskov, 1995) dans le progiciel SEISAN (Ottemöller et al., 2018), montre deux groupes avec une distribution de répliques denses occidentales orientées NNW-SSE et une séquence de répliques orientales orientées N-S mais clairsemées. Afin de fournir une description complète de la distribution des répliques et d'améliorer leur localisation et leur profondeur, les tremblements de terre ont été relocalisés en utilisant une approche de double différence telle que mise en œuvre dans le programme HypoDD (Waldhauser et Ellsworth, 2000).

Les solutions de mécanismes focaux pour 46 répliques sélectionnées ont été calculées sur la base des polarités de premier mouvement de l'onde P (Ross et al., 2018), en utilisant le module FOCMEC dans le progiciel SEISAN (Ottemöller et al., 2018). Les mécanismes focaux des répliques montrent des failles normales et quelques mécanismes obliques (figure 8 et tableau dans SM4). Le choc principal et la plus grande réplique montrent un mécanisme de faille normal, avec des plans nodaux plongeant grossièrement vers le NE et le SE à 41° et 42°, respectivement. Les mécanismes focaux du choc principal et des 45 répliques permettent d'obtenir des informations sur la cinématique des failles grâce à l'inversion des contraintes. Sur les 46 mécanismes focaux (92 plans nodaux) de la base de données, 30 (60 plans nodaux), ainsi que 14 (28 plans nodaux) sont compatibles avec une extension NE-SW en régime de faille normale. L'analyse ultérieure avec 14 mécanismes focaux est effectuée pour tester les résultats après avoir optimisé l'ensemble des données pour une meilleure compatibilité. La plupart des répliques sont caractérisées par un impact moyen NW (340°) avec des plans de faille plongeant vers le NE, ce qui est cohérent avec la distribution des contraintes et l'extension NE-SW. Le mécanisme de faille normale prédominant indique un régime néotectonique en extension dans la zone épicentrale.

La géométrie de la rupture du séisme est contrainte par plus de 900 répliques enregistrées sur une période de trois mois et par l'analyse InSAR des images de Sentinel-1 (orbite ascendante). L'étude InSAR montre des franges avec deux lobes avec un glissement cosismique de 3,86 cm à 5,15 cm sur une déformation de surface allongée NW-SE et longue de 40 km, cohérente avec la localisation du choc principal et le mécanisme de faille normale. La modélisation de la déformation de surface fournit la dimension de la rupture du séisme en profondeur avec un glissement maximal de ~ 50 cm sur un plan de faille orienté à 315°, avec un pendage de 45°, une inclinaison de -80° et avec un Mo de 3,68 x 1018 Nm. Bien que le taux de déformation sismique soit faible, l'occurrence du séisme de Moiyabana en 2017, suivi d'une séquence de répliques dans la ceinture mobile centrale du Limpopo, classe la région intraplaque comme un intérieur de plaque actif.

Le troisième chapitre présente les failles de Tugela et de Greytown dans le Kwazulu-Natal en Afrique du Sud-Est, ainsi que la réévaluation du tremblement de terre de St Lucia MW 6,9 de 1932. Nous effectuons des recherches détaillées sur la sismotectonique et la géomorphologie tectonique de la zone du tremblement de terre de 1932 à St Lucia, dans le but de caractériser les paramètres physiques de la faille sismogénique nécessaires à l'évaluation des risques sismiques dans la région du KwaZulu-Natal (KZN). Le matin du 31 décembre 1932 à 06:31, un tremblement de terre de magnitude MW 6.9 a secoué les habitants du KwaZulu-Natal, en Afrique du Sud. Nous avons relocalisé le tremblement de terre en utilisant les temps d'arrivée répertoriés dans le bulletin du CSI, en suivant la technique de Wysession et al. (1991), qui comprend une estimation d'une ellipse de confiance basée sur un processus de Monte Carlo consistant à injecter un bruit gaussien dans l'ensemble des données. La solution utilise 45 temps d'arrivée P et S et converge vers 29,30°S, 33,04°E, à environ 100 km au SSE des localisations historiques, celle de l'ISC (28,50°S, 32,80°E) étant beaucoup plus proche de la côte, et celle de Gutenberg et Richter (1954) (28,50°S, 32,75°E) représentant peut-être une simple transcription de l'épicentre de l'ISC au quart de degré le plus proche.

Tout d'abord, nous définissons les caractéristiques sismiques et tectoniques des escarpements de faille de Tugela et de Greytown, respectivement orientés E-W et ENE-WSW. L'escarpement de la faille de Tugela est un escarpement orienté EW, qui s'étend sur ~230 km dans le KZN, en Afrique du Sud, et à environ 50 km au sud se trouve l'escarpement de la faille de Greytown, qui mesure ~80 km de long et qui est orienté SW-NE. Nous procédons à la description des marqueurs géomorphologiques des escarpements de faille à l'aide de la géomorphologie tectonique. Des études géomorphologiques tectoniques ont été menées le long de l'escarpement de la faille de Tugela en utilisant le SRTM 1" (Farr et al., 2007) pour identifier les marqueurs géomorphologiques qui ont été affectés par la déformation active le long de la faille. Les preuves de l'activité tectonique le long des failles de Tugela et de Greytown sont clairement visibles avec un mouvement latéral droit illustré par le déplacement des chenaux fluviaux sur plusieurs sites.

D'autres études sur les géométries physiques des failles ont été réalisées à l'aide d'un système de magnétisme aéroporté, de la tomographie de résistivité électrique et de profils de réflexion sismique. D'après l'évaluation qualitative des données existantes, les linéaments sont mal résolus sur les données aéromagnétiques régionales. Des données géophysiques au sol, telles que la sismique réflexion et la résistivité, ont donc été ajoutées pour compléter et confirmer la profondeur du déplacement de l'escarpement de la faille de Tugela. La coupe empilée du point médian commun obtenue le long de la ligne de levé montre six réflecteurs, visibles entre des profondeurs de ~4 m et ~28 m. Les décalages de déformation sont cartographiés à des positions, plongeant verticalement et observés à des distances de ~40 m, ~70 m, ~100 m et ~110 m à des profondeurs de ~8 m à ~28 m.

En outre, nous explorons également l'utilisation du taux de déformation calculé à partir des données GPS obtenues à partir de 14 stations GPS situées dans et autour de la province du KwaZulu-Natal. Nous considérons les stations les plus proches de l'escarpement de la faille de Tugela afin de minimiser l'impact des autres mouvements de faille dans la région. Ainsi, les données des deux stations suivantes au nord et des trois stations au sud de l'escarpement de la faille de Tugela ont été comparées. Cette comparaison indique un mouvement latéral droit le long de l'escarpement de la faille de Tugela, comme le montre la différence de déformation positive du bloc sud par rapport au bloc nord de l'escarpement de la faille de Tugela. La différence de vitesse de déformation entre le nord et le sud de l'escarpement de la faille de Tugela est faible mais perceptible (< 0,1 mm/an), ce qui est habituel en ce qui concerne la vitesse de déformation dans les domaines intraplaques continentaux. Les études de terrain le long des failles, combinées aux études géophysiques et sismotectoniques, conduiront probablement à une réévaluation de l'évaluation des risques sismiques dans la région de KZN.

L'autre partie cruciale de l'évaluation précise de l'aléa sismique est l'évaluation de la contribution de la couche sismogénique dans l'analyse des failles actives. Ainsi, nous profitons ici des résultats des deuxième et troisième chapitres pour déterminer l'épaisseur de la couche sismogénique en Afrique australe afin de compléter notre étude de la couche sismogénique par l'évaluation du D90. L'épaisseur de la couche sismogénique en Afrique australe est dérivée des hypocentres des séismes continentaux intraplaques, combinés à l'analyse des données gravimétriques et magnétiques, et corrélée à l'épaisseur de la croûte. Nous présentons quelques-unes des principales structures tectoniques qui ont pu affecter la composition de la croûte terrestre en Afrique australe. Dans cette étude, nous examinons la couche sismogénique en évaluant la profondeur à laquelle se produisent 90 % des tremblements de terre (D90), en tenant compte des valeurs de profondeur disponibles dans le catalogue de sismicité de l'Afrique australe. La zone sismogénique la plus profonde est située dans la ceinture du Limpopo occidental. Cependant, il est important de souligner que les événements utilisés pour calculer le D90 dans cette région étaient des répliques du tremblement de terre de Moiyabana de 2017. Nous ne pouvons donc pas conclure avec certitude qu'il s'agit bien du D90 de la région si l'on inclut d'autres événements qui ne sont pas des répliques du séisme de Moiyabana de 2017. Par conséquent, nous considérons toutes les sept autres régions comme indiqué dans la figure 5 et le tableau 1. Les régions centrales et méridionales du craton de Kaapvaal ont une couche sismogénique plus épaisse que les cinq autres régions, les deux régions de la ceinture de plissement du Cap étant constituées d'une zone sismogénique mince. La ceinture de plissement du Cap du Cambrien-Ordovicien est la région géologique la plus jeune de cette étude et comprend principalement une épaisseur crustale de 25 à 35 km et une épaisseur sismogénique de 6,5 à 7,4 km.

L'épaisseur de la croûte varie entre 30 et 52 km, de sorte que seuls les 30 % supérieurs de la croûte de l'Afrique australe génèrent 90 % des tremblements de terre. Le craton archéen de Kaapvaal, la région la plus ancienne de la zone d'étude, possède une croûte relativement plus fine, allant de 34 à 42 km au sud, avec de petites poches allant jusqu'à 49 km au nord. La couche sismogénique dans cette région est cependant plus épaisse que dans les régions géologiques plus jeunes. Les ceintures de Namaqua-Natal et de Cape Fold, régions géologiques plus jeunes, ont une épaisseur crustale plus hétérogène, allant de 25 à 50 km, avec une couche sismogénique plus fine de ≤ 12 km. Les valeurs d'épaisseur de la couche sismogénique obtenues dans cette étude indiquent que la croûte supérieure est l'endroit où se produit la libération des contraintes élastiques en Afrique du Sud (de l'Ouest), étant donné que les valeurs d'épaisseur élastique sont supérieures ou égales à l'épaisseur de la croûte (Doucoure et De Wit, 2002). La nature unimodale des valeurs d'épaisseur de la couche sismogénique peu profonde obtenues dans cette étude soutient l'occurrence de ruptures de failles peu profondes et peut donc influencer de manière significative l'aléa sismique de l'Afrique australe.

Le cinquième et dernier chapitre de cette thèse combine des études multidisciplinaires des zones où de grands tremblements de terre se sont produits en Afrique australe, comme discuté dans les chapitres précédents, ainsi que la profondeur sismogénique déterminée dans le quatrième chapitre pour évaluer un risque sismique réaliste à l'échelle régionale. Ceci permet d'atteindre l'objectif de cette thèse qui est de déterminer l'impact d'un modèle sismotectonique amélioré sur l'évaluation de l'aléa sismique en Afrique australe. Nous incluons également des données sur les failles actives et les paramètres sismiques de zones précédemment étudiées telles que la zone active de Ceres dans la province du Cap Occidental (1969, MW 6.3), la région de Kango et Baviaanskloof dans le Cap Oriental, la faille d'Hebron / Dreylingen en Namibie et les failles de Tshipise et Bosbokpoort dans la province de Limpopo. L'intégration et l'interprétation des données compilées ont permis de générer un modèle sismique avec 26 zones sources et sept sources de failles (failles de Kango et Hebron / Dreylingen, Tshipise et Bosbokpoort, Tugela, Greytown et Khurutse). En utilisant les informations disponibles provenant d'études géologiques, paléosismiques, géodésiques et sismologiques, divers paramètres, y compris les paramètres de récurrence (taux de glissement et taux de récurrence de Youngs et Coppersmith (1985)) et les valeurs de Mmax (Wells et Coppersmith, 1994) ont été déterminés pour les quatre failles supposées avoir des preuves fiables de leur capacité.

Comme il n'y a pas de GMPEs qui ont été dérivées spécifiquement pour l'Afrique du Sud, il est nécessaire de développer un modèle / s basé sur l'une des catégories, à savoir :

1. Utilisation d'un ensemble de modèles de mouvement du sol disponibles et attribution d'un poids de probabilité à chaque modèle,

2. Développer une nouvelle relation d'atténuation à partir de données et de modèles de sources sismologiques,

3. Développement d'un modèle composite de mouvement du sol.

Cependant, les accéléromètres n'ont été installés en Afrique du Sud dans les régions aurifères du pays qu'à partir de 2010. Ainsi, le jeu de données existant sur les mouvements du sol ne permet pas aux utilisateurs de dériver un GMPE local en raison du manque de tremblements de terre à fort mouvement. À cet égard, les modèles provenant d'autres régions sont soigneusement sélectionnés et testés pour déterminer s'ils s'adaptent correctement aux données locales.

Des calculs probabilistes classiques de l'aléa sismique ont été effectués à l'aide du logiciel OPENQUAKE développé par la Global Earthquake Model Foundation. Les calculs de l'aléa ont été effectués pour les conditions suivantes, en utilisant un modèle de source sismique caractérisé comme décrit dans les sections ci-dessus :

- Tous les calculs ont été effectués pour une probabilité de dépassement de 10 % en 50 ans (ou une période de retour de 475 ans).
- La magnitude minimale adoptée est Mmin = 5,0, ce qui est cohérent avec la pratique consistant à exclure les événements fréquents et de faible ampleur ayant peu d'importance du point de vue technique.

Les calculs ont été effectués pour trois périodes de réponse cibles, PGA, 0,15s et 2,0s. Toutes les périodes spectrales montrent des valeurs de danger élevées dans les régions des mines d'or, de Koffiefontein et du Cap. La première est principalement influencée par les niveaux de sismicité et les deux dernières régions sont très probablement dues aux forts tremblements de terre enregistrés dans la région et au niveau élevé et continu de la sismicité. Il y a également une influence évidente de la source de la zone MB, qui a enregistré de grands tremblements de terre sur l'aléa pour la partie nord-est du pays, ainsi que des sources de la zone SNAM, principalement en raison de l'essaim d'Augrabies. La forte accélération observée dans la région de KOSH à des périodes plus faibles pourrait être le résultat de séismes modérés peu profonds dans cette zone ainsi que de taux d'activité élevés associés aux séismes liés à l'exploitation minière. L'influence des grands événements dans la partie sud-ouest du pays, dans la province du Cap occidental, est également évidente, principalement en raison des événements modérés à forts et des enregistrements de tremblements de terre plus longs.

La contribution de la sismotectonique du tremblement de terre de Moiyabana et du Kwazulu-Natal, ainsi que la profondeur sismogénique de l'Afrique australe, ont permis

d'obtenir un aléa sismique plus réaliste pour l'Afrique australe. Les changements apportés dans ce nouveau modèle SSC par rapport à la carte précédente (Midzi et al., 2020) sont très importants. Cela prouve l'importance de la sismotectonique dans la région intraplaque de l'Afrique australe. En outre, les GMPE sont également essentiels dans ce travail. Malheureusement, le manque de données sur les mouvements forts dans le pays rend impossible la dérivation d'un modèle spécifique pour l'Afrique du Sud.

Mots-clés : Sismotectonique, tremblement de terre, faille, déformation, choc principal, réplique, failles actives, géomorphologie tectonique, déformation active, profils géophysiques, évaluation des risques sismiques.

Références

Aki K. and P. G. Richards, 1980. Quantitative Seismology, Theory and Methods. San Francisco: Freeman.

Begg G. C., W. L. Griffin, L. M. Natapov, S. Y. O’Reilly, S. P. Grand, C. J. O’Neill, J. M. A. Hronsky, Y. Poudjom Djomani, C.J. Swain, T. Deen & P. Bowden, 2009. The Lithospheric Architecture of Africa: Seismic Tomography, Mantle Petrology, and Tectonic Evolution, Geosphere, 5, 23 – 50.

Brown, R., Gernon, T., Stiefenhofer, J., & Field, M., 2008. Geological constraints on the eruption of the Jwaneng Centre kimberlite pipe, Botswana. J. Volcanol. Geotherm. Res.174 (1), 195–208.

Coppersmith K.J. and R.R. Youngs (1986). Capturing uncertainty in probabilistic seismic hazard assessments within intraplate tectonic environments, Proceedings of the Third U.S. National Conference on Earthquake Engineering, Charleston, 1, 301 – 312.

Cornell C.A. (1968). Engineering seismic risk analysis, Bulletin of the Seismological Society of America, 58, 1583 – 1606.

Delvaux D., 1993. The TENSOR program for paleostress reconstruction: examples from the east African and the Baikal rift zones. EUG VII Strasbourg, France, 4–8 April 1993. Abstract supplement N°1 to Terra Nov. 5: 216.

Der Kiureghian A. and A.H-S. Ang (1977). A fault-rupture model for seismic risk analysis, Bulletin of the Seismological Society of America, 67(4), 1173 – 1194.

Doucouré C. M., M. J. de Wit (2002). Temporal variation in rigidity and mechanical behaviour of old thick continental lithosphere, South African Journal of Geology, 105, 39 – 50.

Farr, T.G., P.A. Rosen, E. Caro, R. Crippen, R. Duren, S. Hensley, M. Kobrick, M. Paller, E. Rodriguez, L. Roth, D. Seal, S. Shaffer, J. Shimada, J. Umland, M. Werner, M. Oskin, D. Burbank, and D. Alsdorf, 2007. The Shuttle Radar Topography Mission, Revision of Geophysics,45, RG2004, doi:10.1029/2005RG000183.

Gutenberg, B., and Richter, C.F., 1954. Seismicity of the Earth and associated phenomena, Princeton University Press, 310 p.

Hanks T.C. and H. Kanamori, 1979. A moment magnitude scale. Journal of Geophysical Research: Solid Earth, 84, 2348 – 2350.

Johnston, A.C., 1996a. Seismic moment assessment of earthquakes in stable continental regions—I. Instrumental seismicity, Geophysics Journal International, 124 (2), 381–414.

Johnston, A.C., 1996b. Seismic moment assessment of earthquakes in stable continental regions—II. Historical seismicity, Geophysics Journal International, 125 (3), 639 – 678.

Lienert B. R., E. Berg & L. N. Frazer, 1986. Hypocenter: an earthquake location method using centered, scaled, and adaptively damped least squares, Bulletin of the Seismological Society of America, 76(3), 771 – 783.

Lienert B. R. and J. Havskov, 1995. A Computer Program for Locating Earthquakes Both Locally and Globally, Seismological Research Letters, 66 (5), 26 – 36.

Maerten, F., Resor, P., Pollard, D., Maerten, L., 2005. Inverting for slip on three-dimensional fault surfaces using angular dislocations, Bulletin of Seismological Society of America, 95 (5), 1654 – 1665.

Manzunzu B., V. Midzi, A. Mangongolo and F. Essrich, 2017. The aftershock sequence of the 5 August 2014 Orkney earthquake (ML 5.5), South Africa, Journal of Seismology, 21, 1323 – 1334.

McGuire R.K. (1974). Seismic structural response risk analysis, incorporating peak response regressions on earthquake magnitude and distance, Massachussets Technical, Department of Civil Engineering, Publication No. 399, p371.

McGuire R.K. (1976). FORTRAN computer program for seismic risk analysis, U.S Geological Survey Open-File Report 76-67, p90.

Midzi V., B. Manzunzu, T. Mulabisana, B.S. Zulu, T. Pule and S. Myendeki (2020). Probabilistic seismic hazard maps for South Africa, Journal of African Earth Sciences, 162.

Midzi V., I. Saunders, B. Manzunzu, M. T. Kwadiba, V. Jele, R. Mantsha , K. T. Marimira, T. F. Mulabisana, O. Ntibinyane, T. Pule, G. W. Rathod, M. Sitali, L. Tabane, G. van Aswegen, & B. S. Zulu, 2018. The 03 April 2017 Botswana M6.5 earthquake: Preliminary results, Journal of African Earth Sciences, 143, 187 – 194.

Nguuri, T. K., Goree, J., James, D. E., Webb, S. J., Wright, C., Zengen, T. G., Gwavava, 0., Snoke, J. A. & Kaapvaal Seismic Group, 2001. Crustal structure beneath southern Africa and its implications for the formation and evolution of the Kaapvaal and Zimbabwe cratons, Geophys. Res. Letters 28, 13, 2501-2504.

Njoroge M., R. Malservisi, D. Voytenko and M. Hackl, 2015. Is Nubia Plate Rigid? A geodetic study of the relative motion of different cratonic areas within Africa, International Association of Geodesy Symposia, p 1-9, doi:10.1007/1345_2015_212.

Okada, Y., 1985. Surface deformation due to shear and tensile faults in a half-space, Bulletin of Seismological Society of America, 75 (4), 1135 – 1154.

Ottemöller, L., Voss, P., Havskov, J., 2018. SEISAN Earthquake Analysis Software for Windows, Solaris, Linux and Macosx. Bergen.

Reiter L., 1991. Earthquake hazard analysis: issues and insights. Columbia University Press.

Roering C., D. D. van Reenen, C. A. Smit, J. M. Barton, J. H. de Beer, M. J. de Wit, E. H. Stettler, J. F. van Schalkwyk, G. Stevens & S. Pretorius, 1992. Tectonic model for the evolution of the Limpopo Belt, Precambrian Research, 55, 539 – 552.

Ross Z. E., M. Meier, & E. Hauksson, 2018. P wave arrival picking and first-motion polarity determination with deep learning, Journal of Geophysical Research: Solid Earth, 123 (6), 5120 – 5129.

Saria E., E. Calais, D.S. Stamps, S. Delvaux and C.J.H. Hartnady, 2014. Present-day kinematics of the East African Rift, Journal of Geophysical Research, 119, doi:10.1002/2013JB010901.

Stamps D.S., L.M. Flesch, E. Calais and A. Ghosh, 2014. Current kinematics and dynamics of Africa and the East African Rift System, Journal of Geophysical Research: Solid Earth, 119, 5161 – 5186, doi:10.1002/2013JB010717.

Utsu T., Ogata, Y., Matsu'ura ; R.S., 1995. The centenary of the Omori formula for a decay law of aftershock activity, J. Phys. Earth, 43, 1-33.

Waldhauser F. & W. L. Ellsworth, 2000. A Double-Difference Earthquake Location Algorithm: Method and Application to the Northern Hayward Fault, California, Bulletin of the Seismological Society of America, 90 (6), 1353 – 1368.

Wells D.L. and K.J. Coppersmith, 1994. New Empirical Relationships Among Magnitude, Rupture Length, Rupture Width, Rupture Area, and Surface Displacement, Bulletin of the Seismological Society of America, 84, 974-1002.

Wysession, M.E., E.A. Okal and K.L. Miller, 1991. Intraplate seismicity of the Pacific Basin, 1913−1988, Pure Applied Geophysics, 135, 261-359.

Youngs R.R. and K.J. Coppersmith, 1985. Implications of fault slip rates and earthquake recurrence models to probabilistic seismic hazard estimates. Bulletin of the Seismological society of America, 75(4), 939 – 964.

Zoback, M.L. and M.D. Zoback, 1989. Tectonic stress field of the continental United States: In Geological Society of America Memoir 172, Chapter 24, 523 – 539.